JACOBS
UNIVERSITY

Fraunhofer
MEVIS

Software Assistance for Preoperative Risk Assessment and Intraoperative Support in Liver Resection Surgery

by Christian Hansen

A PhD thesis submitted in partial fulfillment of the requirements for the degree of Doctor of Philosophy in Computer Science at the School of Engineering and Science, Jacobs University Bremen.

Dissertation Committee:

Prof. Dr.-Ing. Horst K. Hahn (Dissertation Advisor)
School of Engineering and Science, Jacobs University Bremen, Germany

Prof. Dr.-Ing. Lars Linsen
School of Engineering and Science, Jacobs University Bremen, Germany

Prof. Dr.-Ing. Bernhard Preim
Department of Computer Science, University of Magdeburg, Germany

Date of Defense: May 10, 2012

Hansen, Christian (Dipl.-Ing.):
Software Assistance for Preoperative Risk Assessment and Intraoperative Support in Liver Resection Surgery
Dissertation, Jacobs University Bremen, Germany
Bremen, June 22, 2012.

Notes on Reading this Work

Expressions in **bold** are important for understanding the subsequent sections and chapters. In addition, this emphasizes comparisons or helps explain terms. A list of abbreviations and symbols is provided in the appendix.

This thesis has been written independently, except where sources and collaborations are acknowledged, and has not been submitted at another university for the conferral of a degree. Parts of this thesis are based on previously published material or material that is prepared for publication at the time of this writing. Previous publications are mentioned at the end of each chapter and a complete list can be found in the appendix.

Abstract

THIS THESIS contributes to the field of computer-assisted liver surgery with a focus on surgical planning and intraoperative support. Resection planning for liver surgery has become an essential tool in the clinical routine. Based on 3D reconstructions from radiologic images of the patient, different resection plans can be simulated and assessed before an intervention. During an intervention, surgical navigation systems align the planning information with the patient's liver and thus support the realization of a preoperative plan.

New techniques for **preoperative risk assessment** in liver surgery are presented in this work. Thereby, the determination of safety margins around tumors is addressed which is a challenging task for surgeons. The spatial relation of tumors to the intrahepatic vascular anatomy and the amount of remnant liver volume are important factors when deciding whether a tumor-free safety margin can be achieved. Besides a method to define safety margins with uniform width, a method to define non-uniform safety margins is proposed while considering robustness and sensitivity of vascular risk.

In addition, techniques for **intraoperative support** of liver interventions are introduced. First, the intraoperative adaptation of surgical planning data is focused. A software assistant to quickly adapt risk analyses and resection proposals in case of intraoperatively detected findings is presented. In this context, appropriate interfaces for surgeon-computer interaction and an approach for automatic generation of virtual resection surfaces are proposed. Second, new visualization techniques designed for intraoperative use are addressed. Intraoperative visualizations have to follow specific requirements such as the workflow and cognitive load of the surgeon, which together call for a context-driven reduction of complexity and a focus on critical areas. Therefore, surgical risk maps and an approach for illustrative augmented reality are presented. The developed visualization techniques provide a new and objective basis for the assessment of risks during liver surgery. Third, new techniques for auditory support for navigated liver surgery are introduced. Auditory support has the potential to reduce the dependency on visual presentations and freeing the surgeon to focus attention on the situs rather than on a monitor.

The transfer of these methods from academic research to applicability in clinical routine was an important goal of this dissertation project. A great value was set on including clinicians in the development process by using their feedback to define design requirements, creating new concepts, and finally evaluating the developed methods in a clinical environment. Therefore, the development was accompanied by a number of clinically oriented tests.

Table of Contents

1 Introduction

Curiosity is always the starting point for solutions to a problem.

(Galileo Galilei)

For thousands of years, humans tried to understand the anatomy and function of the human liver. The introduction of radiological imaging in the 20th century provided completely new insights into anatomy. This led to significant improvements in many surgical procedures. In liver surgery, 3D models can now be produced from scan data, allowing surgeons to see the position of tumors and their relation to vascular structures. Based on these patient-individual models, this thesis introduces novel techniques for preoperative risk assessment and intraoperative support in liver surgery.

1.1 Medical Background

The liver (gr. hepar) is an essential organ with a complex vascular anatomy. Unfortunately, it is also an organ frequently affected by tumors. If tumors in the liver are removed by a surgeon, the vascular anatomy must be preserved as much as possible while ensuring an adequate safety margin around tumors. This becomes difficult if a liver contains multiple tumors or if tumors are located centrally or close to major vessels.

Physicians employ x-ray computed tomography (CT) or magnetic resonance (MR) imaging to gain information about the patient's liver anatomy and pathology. Based on these images, surgical planning software provides 3D models of a patient. This additional information assists radiologists and surgeons in choosing a resection strategy [Lang et al., 2005]. Once the planning is performed, surgeons would like to utilize the planning data during an intervention. Therefore, surgical navigation systems align the planning information with the patient's liver and thus support the realization of a preoperative plan. Based on preoperative planning models, these navigation systems have the potential to support intraoperative decision making during liver resection.

1.2 Challenges and Contributions

A great challenge in liver surgery is the optimal planning of resection strategies. This involves the definition of a virtual resection surface, which divides the liver in a remnant part and a part to be resected. Due to better outcomes in metastasis treatment using modern chemotherapy, surgical trends have recently changed towards smaller resection volumes [Lang et al., 2010]. For this reason, the **determination of optimal safety margins** around tumors has become increasingly important. This is particularly true for patients with potentially insufficient postoperative liver volume. A software assistant to quickly determine safety margins based on the risk distribution of vascular supply and drainage is therefore presented in this work.

Once a surgeon has defined a resection strategy with the planning software, it seems to be obvious to use this plan in the operating room during surgery. However, using intraoperative ultrasound (**IOUS**) during oncological interventions, between 19% and 33% of patients with primary liver malignancies or metastases show additional tumors [Ellsmere et al., 2007; Sietses et al., 2010; Shah et al., 2010]. Intraoperative changes to the resection strategy may be necessary, especially if the new tumors are adjoined to hepatic vessels. Therefore, techniques for the **adaptation of preoperative planning data** in case of additional intraoperative findings would be beneficial. Besides a fast and reliable adaptation method, the design of surgeon-computer interfaces should allow usage in the sterile area of an operating room. This functionalities are provided by a software assistant for intraoperative planning adaptation which is introduced in this thesis. In addition, techniques for automatic adaptation of resection proposals are proposed.

Another challenge in liver surgery is the **appropriate presentation of planning models in the operating room**. Although software assistants for surgical planning are utilized before an intervention, the intraoperative presentation of planning models has thus far been limited. One reason is that these models were not developed to provide information in complex workspaces like the operating room. In this thesis, different means of intraoperative representation (visual and auditive) are introduced, analyzed, and evaluated. The proposed intraoperative representations reduce the complexity of planning data by simultaneously enhancing surgically relevant information.

The methods proposed in this thesis have investigated in collaboration with the University of Lübeck (Institute for Robotics and Cognitive Systems), the Technical University of Munich (Institute of Micro Technology and Medical Device Technology), and the University of Bern (Center for Biomedical Engineering Research). While the work in Munich and Bern focuses on the development of a navigation system for open liver surgery, the group from the University of Lübeck is developing a system for navigated laparoscopic liver surgery. The methods implemented in the context of this dissertation project are embedded in clinical software prototypes with a direct interface to the navigation systems mentioned above.

In addition, clinicians were included in the development and evaluation process. Their feedback was used to define and to refine design requirements, improve concepts, and verify the methods in a clinical environment. The developed techniques were evaluated in collaboration with the surgical departments of General Hospital Celle, Asklepios Clinic Barmbek, University Hospital Lübeck, and Robert-Bosch Hospital Stuttgart.

1.3 Structure of this Thesis

This thesis is structured as follows. After a report of fundamentals (**Chapter 2**), new techniques for preoperative risk assessment and intraoperative support are introduced. The proposed techniques are described with examples in liver resection surgery.

- **Chapter 3** introduces techniques for interactive determination of safety margins around tumors based on patient-individual vascular risk distribution. Thereby, the determination of both uniform and non-uniform margins is addressed.

- **Chapter 4** describes new methods for intraoperative adaptation of the surgical planning data. A tool to quickly adapt risk analyses and resection plans in case of intraoperatively detected tumors is proposed. In this context, appropriate interfaces for surgeon-computer interaction are discussed.

- **Chapter 5** introduces a new visual representation of surgical planning data, called risk maps. The technique is based on an analysis of critical structures

in the proximity of a planned resection surface. Distances and depth cues are visually enhanced while model complexity is reduced.

- **Chapter 6** presents visualization methods for augmented reality (AR) in surgery. To improve the understanding of spatial relations and depth, illustrative visualization methods for 3D planning models are proposed.

- **Chapter 7** proposes methods for auditory support in navigated liver surgery. An auditory display system for open liver surgery is introduced for providing support in guiding the tracked instrument towards and remaining on a predefined resection surface.

Clinically oriented test and evaluations are reported in respective chapters. Finally, conclusions with respect to the objectives of this thesis are drawn, and suggestions for further research are provided (**Chapter 8**).

2 Fundamentals

> I never told anyone about my work; I told my wife that when people found out what I was doing, they would think I went crazy.
>
> *(Wilhelm Conrad Röntgen)*

The discovery of radiological imaging by Wilhelm Conrad Röntgen in the year 1895 opened completely new possibilities for medicine. More than one hundred years later, medical diagnosis and treatment without the support of radiologic imaging is unimaginable. The invention of CT scanners by Godfrey Hounsfield and colleagues in 1971 enabled physicians to examine the internal structures of the liver in detail without the loss of blood. Based on these images, anatomist such as Claude Couinaud created a new understanding of liver surgery. Computer-assisted liver surgery performed today is based on modern radiologic imaging, advanced surgical instruments, navigation technology, and complex 3D models of patient livers.

This chapter provides fundamentals that are essential to understand and classify the new techniques described in the subsequent chapters. It starts with an overview of the human liver. In addition to liver anatomy and function, cancer diseases and their medical treatment are addressed. Subsequently, an overview of the state of the art in computer-assisted liver surgery is given. In this context, a surgical decision pipeline with regard to computer-assisted liver surgery is outlined and discussed. Finally, the chapter is summarized and conclusions are drawn.

2.1 Clinical Background: The Human Liver

2.1.1 Anatomy and Function

The liver (gr. hepar) is the largest gland in the human body located in the right-upper quadrant of the abdominal cavity below the diaphragm and right of the stomach. It has a complex vascular anatomy with a dual blood supply and systems to drain bile and blood:

- The **portal vein** (PV) caries nutrient-rich blood from the abdominal organs into the liver. Unfortunately, tumor cells can also spread from these organs through the portal vein into the liver parenchyma, which makes the liver a frequent site of metastatic cancer.
- The **hepatic artery** (HA) delivers blood from the aorta. Oxygen is provided from both sources. Approximately half of the liver's oxygen is provided by the portal vein, and half is provided by the hepatic artery [Kleinman et al., 2008].

In addition, the liver contains two drainage systems.

- The **hepatic vein** (HV) drains blood into the vena cava, which connects with the right atrium of the heart. It is divided in three main branches the right hepatic vein (RHV), the middle hepatic vein (MHV), and the left hepatic vein (LHV).
- The **biliary duct** (BD) is responsible for draining bile, which is produced by the liver cells and flows into the main bile duct and the gallbladder.

All vessels are organized in a finely branched, interwoven system inside the liver parenchyma. Based on this vascular anatomy, a numbering system developed by Couinaud [1954] is nowadays applied internationally and provides standardized identification of liver segments. It divides the liver into eight segments by three longitudinal planes (through the right, middle, and left hepatic veins) and one transverse plane (cf. Figure 2.1). The Couinaud model assumes that these segments have vascular inflow, outflow, and biliary drainage and can each be resected without damaging the remaining segments [Brant et al., 1999]. However, studies based on CT imaging have shown that number, volume, and shape of liver segments show significant variation between patients [Fasel et al., 1998; Fischer et al., 2002].

The human liver performs a variety of very important functions. It synthesizes, processes, and stores substances that are essential for normal body function. Main liver functions include:

- metabolism of carbohydrates, proteins, fats
- bile production and excretion

- storage of glycogen, vitamins, iron
- formation and destruction of certain blood components
- detoxification and excretion of harmful substances
- heat production [Walsh et al., 2007]

Most of the functions are controlled on a cellular level by the liver cells, called hepatocytes. Hepatocytes account for approximately 80% of the liver mass and exhibit unrivaled complexity and diversity of functions [Maurel, 2010]. Another interesting type of cell in the liver is the Kupffer cell. Kupffer cells are specialized macrophages responsible for cleaning the blood of products of metabolism, bacterias, and overaged erythrocytes. For further information about liver histology, refer to the books of Amenta [1997] and Maurel [2010].

2.1.2 Liver Cancer

The human liver is an organ frequently affected by tumors. An essential distinction is made between benign and malignant tumors. While **benign** liver tumors such as cysts or hemangiomas are often asymptomatic and do not require medical treatment, **malignant** liver tumors can be life-threatening. Malignant tumors are subdivided into primary and secondary tumors. **Primary** tumors grows at the organ where tumor progression began, whereas **secondary** tumors (also called metastases) are the spread of tumor cells from one organ to another.

The **hepatocellular carcinoma (HCC)**, a primary malignant liver tumor, is the third most common cause of death from cancer worldwide [Ferlay et al., 2010]. According to the most recently published GLOBOCAN global analysis, the regions of highest incidence are Eastern and Southeastern Asia as well as Middle and Western Africa. Low rates are reported in developed regions, with the exception of Southern Europe [Ferlay et al., 2010]. Besides primary liver cancer, **liver metastases** are the second most common tumor type in Germany [Neumann et al., 2010]. Although untreated patients with liver metastases have poor prognoses (median time to death ≈ 6.9 month [Scheele et al., 1990]), the 5-year survival rates for patients who have undergone surgical resection is reported between 23 and 51% in recent studies [Vigano et al., 2008; Brouquet et al., 2011; Swan et al., 2011] depending on the number and diameter of metastases as well as the amount of infiltration into other organs. However, 5-year survial does not mean that the cancer is healed because approximately one-third of actual 5-year survivors suffer cancer-related death [Pulitano et al., 2010].

2.1.3 Treatment of Liver Cancer

A potential curative treatment of liver cancer is the surgical resection of tumors. The optimal prognosis of the patient is the complete resection of the tumor including a

tumor-free safety margin (called **R0 resection**). There are two kinds of resection types in oncologic liver surgery:

(1) Anatomical Resections

(2) Non-Anatomical Resections

Whereas resection surfaces for anatomical resection are based on the boundaries the liver segments defined by the portal vein (cf. Fig. 2.1), resection surfaces for non-anatomical resection, e.g., wedge resections, do not consider these anatomical boundaries. Anatomical resections can be further divided into following types:

- Single-Segment Resection
- Bi-Segment Resection
  - Right Posterior Sectionectomy (Segments VII, VIII)
  - Left Posterior Sectionectomy (Segments II, III)
- Hemihepatectomy
  - Right Hemihepatectomy (Segments V-VII ±I without MHV)
  - Extended Right Hemihepatectomy (Segments V-VII ±I with MHV)
  - Left Hemihepatectomy (Segments II-IV ±I without MHV)
  - Extended Left Hemihepatectomy (Segments II-IV ±I with MHV)
- Trisectionectomy
  - Right Trisectionectomy (Segments I, IV-VIII)
  - Left Trisectionectomy (Segments I-VI)
- Central Resection (Segments IV,V,VIII ±I)

The decision about the resection of segment I often has to be decided individually, depending on the location and type of tumor. The described classification is similar to the nomenclature reported in Lang et al. [2005] and the *IHPBA Brisbane 2000 Terminology of Liver Anatomy and Resections* [IHPBA, 2000]. The main differences lie in the definition of extended hemihepatectomies. Clinical feedback concerning virtual resection proposals revealed that many surgeons desire a consideration of the MHV [Wendt, 2011]. Existing nomenclatures do not cover this aspect. Therefore, these nomenclatures are slightly changed and extended within the scope of this thesis.

Although recent studies report that only 10 to 20% of patients are candidates for surgical resection [Neumann et al., 2010], the number of patients with resectable tumors can be expanded significantly by increasing hepatic reserve (e.g., portal vein embolization, two-stage hepatectomy), combining resection with ablation, and decreasing tumor size (preoperative chemotherapy) [Pawlik et al., 2008]. Besides

the aforementioned therapies, liver transplantation is a curative surgical option for patients with cirrhosis and/or HCC. However, due to donor shortages and the high medical expense of this therapy, liver transplantation is not an option for many patients.

Beside these two curative liver cancer therapies, several palliative therapies exist. Brachytherapy, for instance, is based on the precise placement of radiation sources in the tumor area. In addition, a wide range of ablation techniques, such as radio-frequency ablation, laser ablation, or microwave ablation, are applied to destroy tumor cells locally. However, incomplete ablation of liver tumors due to insufficient technology of ablation needles, tissue cooling by the neighboring blood vessels, large tumor masses, and ablation of tumors in close vicinity to heat sensitive organs remain difficult tasks in this context [Kunzli et al., 2011]. Nevertheless, with the development of preoperative simulations for heat propagation [Kröger et al., 2010], intraoperative imaging and navigation support [Bale et al., 2010], ablation therapies have significantly improved and are candidates for curative liver cancer treatment.

According to interviewed surgeons, the selection of an optimal cancer therapy for a specific patient is often difficult. A recent study by Nathan et al. [2011] showed that the choice of cancer therapy in the liver (liver resection, liver transplantation, and tumor ablation) depends more heavily on the surgeon's specialty than on clinical factors.

2.2 Computer-Assisted Liver Surgery

Computer-assisted liver surgery represents a set of methods which use computer technology to support preoperative planning, the actual surgery, and postoperative assessment (cf. Fig. 2.2). This section reviews the state of the art in computer-assisted liver surgery while focusing on preoperative and intraoperative support. Before each section concerning the state of the art, the decision pipelines for both preoperative planning and intraoperative realization are described.

Methods in the field of computer-assisted liver surgery can be divided into two groups. The first group represents methods that are already part of current software assistants and have been successfully used in clinical routines (e.g., semi-automatic segmentation of anatomical structures). Clinical feedback concerning these methods has led to further improvements and constructive research (e.g., fully automatic segmentation methods). The second group represents methods that are nowadays only available in a small number of specialized clinics (e.g., intraoperative adaptation of planning data) and represent a new field of research in computer-assisted liver surgery.

2.2.1 Preoperative Decision Pipeline

When a patient is diagnosed with a malignant tumor, a wide range of essential decisions has to be made by the physicians involved. For the design of surgial

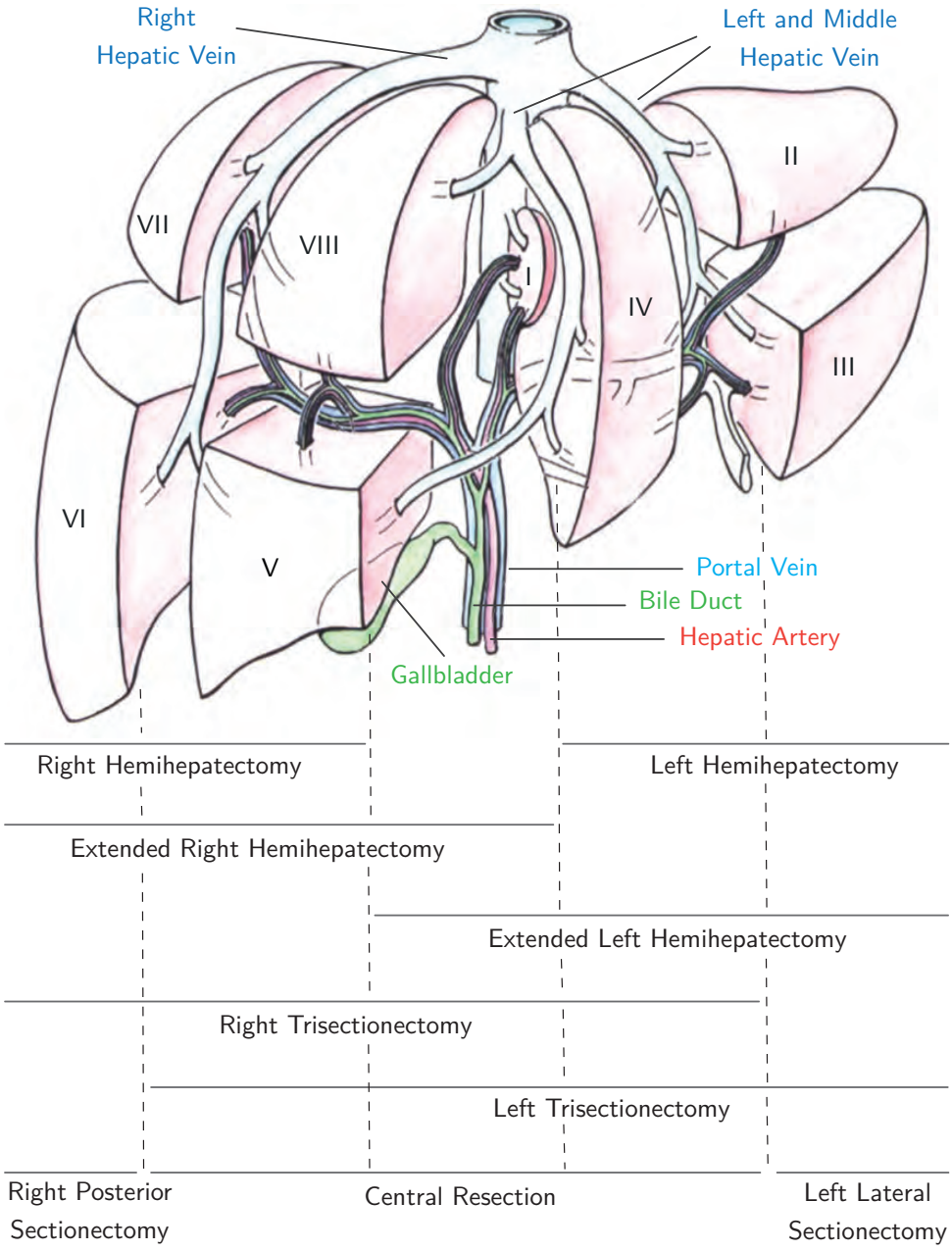

Figure 2.1: Illustration of the human liver with its vascular systems, i.e, portal vein, hepatic vein, hepatic artery, and bile duct (Image adapted from Karaliotas et al. [2007]). The liver segments are labeled with roman numbers according to Couinaud [1954]. Associated anatomical resections types are indicated at the bottom.

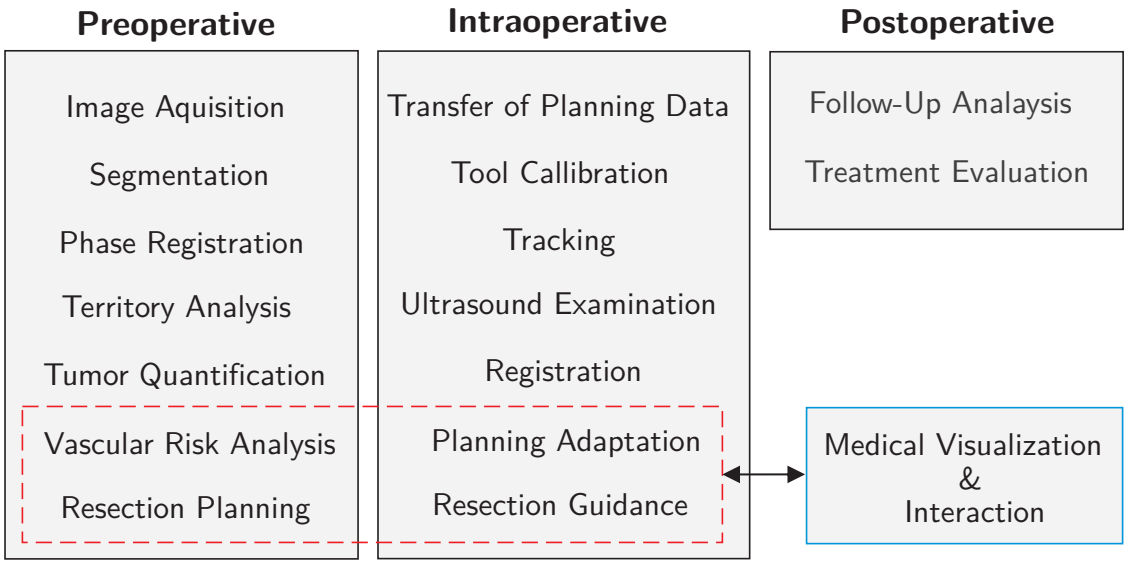

Figure 2.2: Research topics in the field of computer-assisted liver surgery. The dashed rectangle enhances the area that is addressed within the scope of this thesis and exhibits a strong relation to the research field of medical visualization and surgeon-computer interaction.

planning systems it is essential to understand which decisons need to be made and which information is required to support decison making. One of the first decisions is the choice of the therapy. If surgical resection is possible, this therapy is nowadays often the method of choice, because clinical studies indicate the best long-term survival rates [Neumann et al., 2010]. According to a review of Grundmann et al. [2008], the decision about surgical resection should be determined using the following parameters:

(1) General operability of the patient

(2) Achievability of an **R0 situation** (if necessary, in combination with other cancer therapies such as ablation or chemotherapy)

(3) Sufficient estimated **postoperative liver volume** (if necessary, in combination with portal vein embolization or two-stage hepatectomy)

(4) The feasibility of preserving **two contiguous hepatic segments** with adequate vascular **inflow and outflow** as well as biliary drainage

(5) Biological aspects of the tumor

In addition, they considered the experience of the surgeon and the hospital as important parameters for deciding about the resection. While the general operability (1) of liver resections depends mainly on patient anamnesis and the presence of

additional diseases, biological aspects of the tumor (5) depend on the results of biopsy. Support with medical software assistants is limited in these cases. However, decisions (2-4) address aspects that often require extensive anatomical analysis as accessible by 3D computation.

A technical view of steps performed during preoperative decision making is illustrated in Fig. 2.3. After the preoperative image acquisition, a decision about the need for a computer-assisted planning needs to be taken. This decision depends on many factors. Besides clinical factors such as the location of tumors and the complexity of the planned intervention the decision often depends on personnel or financial resources of the hospital.

When a decision has been made in favour of computer-assisted planning, a number of image-processing steps have to be performed. These tasks include phase registration, segmentation and volumetry of liver and lesions, vessel segmentation and labeling of vessels. These tasks are usually performed by radiologic technicians. Contributions of surgeons are not required in most cases.

The surgical decision pipeline starts with a preoperative risk analysis. A risk analysis includes the determination of proper safety margins around tumors. Based on the widths of safety margins, affected vascular branches and vascular territories are calculated. This procedure is called **vascular risk analysis**. The following workflow steps for vascular risk analysis are described by Preim et al. [2002]:

(1) The user selects a lesion and specifies its **safety margin**.

(2) The system visualizes the margin and all **vessels at risk**.

(3) The system estimates the affected region of the liver, called **territory at risk**.

(4) The user defines a **resection surface** based on vessels and territories at risk.

(5) The system calculates the percentage of remaining functional liver volume.

If insufficient remaining functional liver volume is calculated in step 5, the user may return to step 1 to decrease the margin size and perform steps 2-5 again. According to Preim et al. [2002], this may increase the chance of recurrence but could be better than a palliative treatment in selected cases. For a clinical discussion concerning the optimal width of safety margins, refer to Sect. 3.1 on page 38. The width of a surgical margin is an important decision in the preoperative planning stage because it is related to the achievability of an R0 situation.

Once the vascular risk analysis has been performed, the determination of a virtual resection surface is necessary to estimate the postoperative liver volume and to determine the cutting direction. However, the definition of an optimal resection surface through a liver is not trivial. From the mathematical point of view, this can be considered a multi-parameter optimization problem. Based on a clinical survey of liver surgeons, Demedts et al. [2010] defined the following parameters as important for the evaluation of virtual resection surfaces:

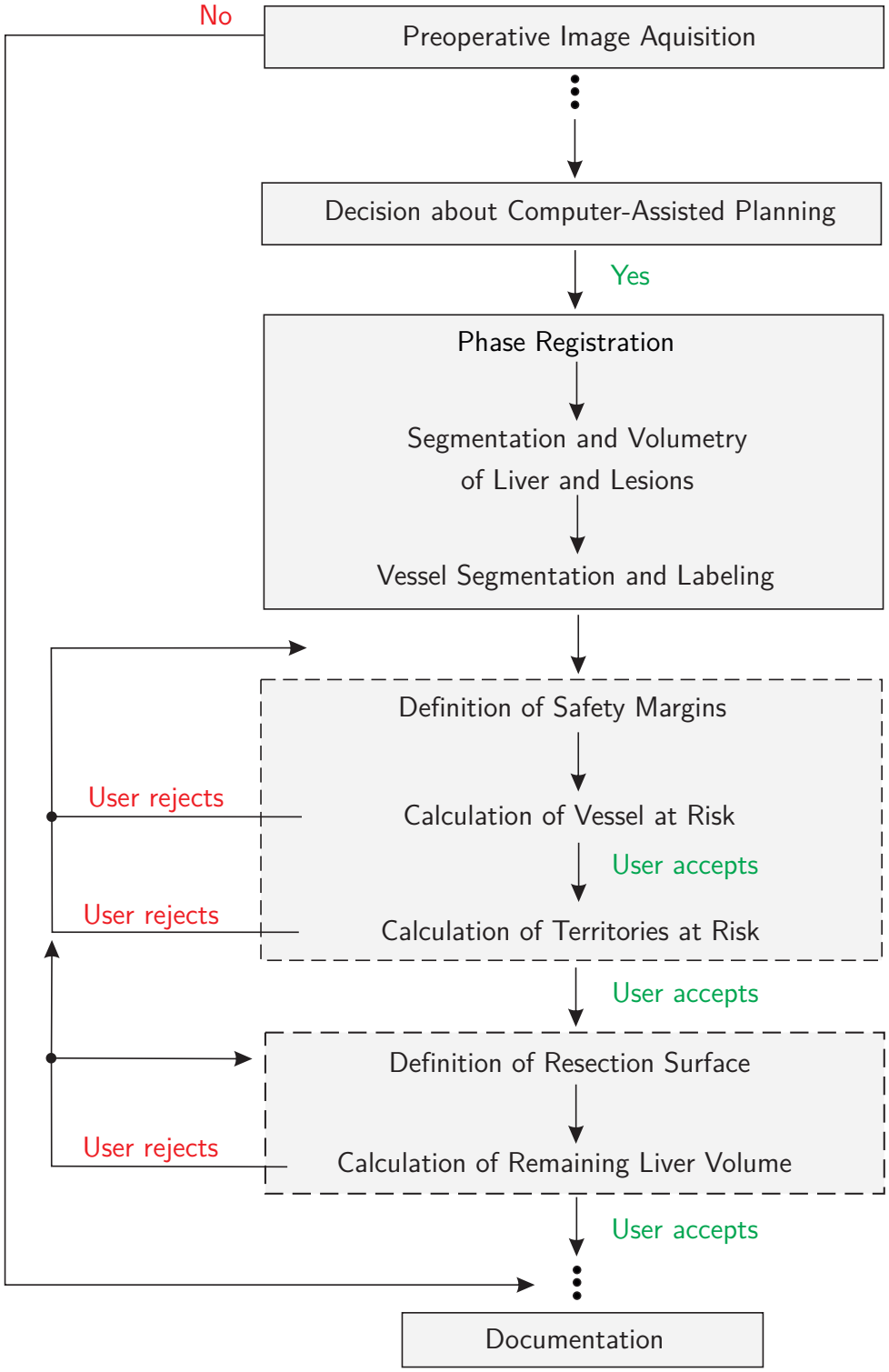

Figure 2.3: Part of the preoperative decision pipeline for liver surgery from a technical point of view. The dashed rectangles represent workflow steps that are focused in this thesis.

- Remnant volume in ml
- Safety margin around tumors in mm
- Supplied volume of the remnant liver in %
- Drained volume of the remnant liver in %
- Completely perfused remnant liver in %
- Resection area in cm^2
- Curvature of resection surface

These physical values are of interest when defining a virtual resection surface. However, not all parameters are weighted equally. The weights depend on factors such as tumor type or surgical preference. In most cases, the amount of remnant liver volume and the safety margins around tumors are the most meaningful and essential parameters.

In surgery, the amount of risk for the patient normally increases with the complexity of the surgical procedure [Zachow et al., 2010]. Therefore, the number of surgical decisions to be made and their difficulties vary from patient to patient. Computer-aided surgical planning can provide additional information which may support surgeons, especially in complex cases for which a decision is not easily made.

2.2.2 Surgical Planning for Liver Surgery

Which tools are necessary to support preoperative decision making in oncologic liver surgery? In the context of a large national survey [Oldhafer et al., 2002], 92 % of participating surgeons requested a 3D visualization that illustrates the spatial relations between tumors and vessels, 64% requested tools that allow a simulation of different resection strategies, and 55 % requested that measurements such as volume, diameter, and distances are included in the visualization. With an optimal integration of such tools in a clinical workflow, participating surgeons expected a better assessment of operability (87 %) and an increase of patient safety during the intervention (55%).

Lang et al. [2010] defined two main requirements for planning applications in oncologic liver surgery: The visualization of patient-individual anatomy and the assessment of resectability. The visualization of patient-individual anatomy includes the illustration of hepatic vessels (PV, HV, HA, BD) and associated vascular territories. The assessment of resectability includes the determination of tumor-free safety margins and the estimation of remaining liver volume. These two basic requirements imply many functions that need to be available in planning software. This section gives an overview of key components for computer-aided liver surgery planning. It covers image acquisition and phase registration, segmentation of anatomical and pathological structures, approximation of vascular territories, risk analysis, and virtual resection planning.

Preoperative Image Acquisition

Preoperative imaging is applied several days before surgery for diagnosis and surgical planning. Ultrasound is often used for diagnosis. For liver surgery planning, CT or MR imaging is applied. These images build the basis for 3D planning models and for model-based risk analysis.

Special contrast agents injected into the patient provide a better visual contrast between vascular structures and liver tissue (cf. Fig. 2.4). Wide availability and established contrast agents are reasons to prefer a preoperative liver imaging based on CT. A recent study by Hata et al. [2011] reports a sensitivity of CT to detect liver metastasis around 72 % which decreases to 35% for small lesions with a diameter below 1 cm. Consequently, small tumors are often detected only intraoperatively through palpation by the surgeon or by using IOUS. Refer to Sect. 4.1 on page 70 for more details on intraoperatively detected lesions.

Besides preoperative CT imaging, MR imaging has been increasingly employed in recent years due to the introduction of new liver-specific contrast agents such as Gadoxetic acid. Several clinical studies report that MR imaging using liver-specific contrast agents has a greater sensitivity in visualizing liver tumors than contrast-enhanced CT imaging [Hammerstingl et al., 2008; Motosugi et al., 2011; Baek et al., 2011]. This was found to be particularly true for small liver lesions. Ongoing clinical trials will further evaluate advantages and disadvantages of liver-specific contrast agents.

CT or MRI data are acquired in different time phases of contrast propagation. First, the contrast agent reaches arteries, then the portal vein, and finally the hepatic vein. A good contrast-timing is essential to receive an adequate image quality for diagnostic purposes. The following four phases are common for liver imaging: non-contrast, arterial phase, venous phase, and late phase. Liver arteries are enhanced in the arterial phase, while veins are not. In addition, portal vein and hepatic vein are enhanced in the venous phase. The visual enhancement of lesions in the image data varies over all phases depending on the type of lesion and the amount of supplying blood vessels.

Phase Registration

Due to different respiration states and patient movement during the acquisition phases, the datasets have to be aligned. This is necessary for an exact spatial assessment of intrahepatic vessels in relation to tumors. In most cases, rigid registration approaches provide adequate accuracy for surgical planning. The accuracy can be improved by also utilizing non-rigid registration methods [Lange et al., 2005; Huang et al., 2009].

Segmentation of the Liver

The segmentation of the liver is of utmost importance for preoperative planning. It provides the basis for estimating the postoperative liver volume. In combination with vessel segmentation, it allows the approximation of vascular territories. However,

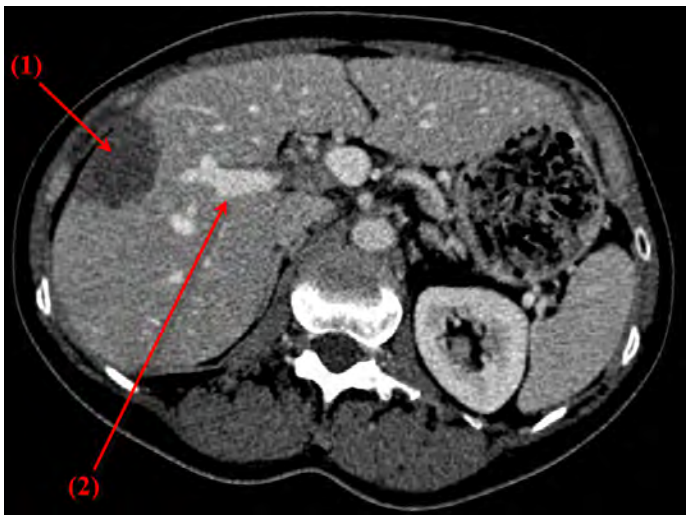

Figure 2.4: Contrast-enhanced CT slice (venous phase) containing a peripheral liver metastasis (1). The injected contrast agent provides good distinction between vascular structures (2) and liver parenchyma.

liver segmentation is challenging because of varying image qualities and low contrast between neighboring organs of the liver.

Automatic and interactive liver segmentation algorithms are investigated. For **interactive** segmentation of the liver, live wire algorithms in combination with a shape-based interpolation [Schenk et al., 2000] proved to be efficient in the clinical routine. A review and comparison of CT-based liver segmentation methods entered in the liver segmentation competition at MICCAI 2007 can be found in [Heimann et al., 2009]. According to their review, interactive segmentation methods achieved better results than automatic approaches. The best **automatic** methods [Heimann et al., 2006; Kainmueller et al., 2007; Wimmer et al., 2009] use model-based assumptions about the liver shape and achieved acceptable results in the majority of selected cases. Current research in this field focuses on the improvement of automatic approaches concerning accuracy and robustness and their application on MR images [Gloger et al., 2010; Rusko et al., 2011].

Segmentation of Tumors

Segmentation and volumetry of tumors is an essential task in planning software for oncologic liver surgery. Important decisions like the resection strategy or the choice of further treatments rely on a determination of the diameter and volume of tumors. Although liver tumors are often hard to visually delimit from adjacent structures in preoperative images, a range of advanced liver tumor segmentation techniques is described. Segmentation techniques can be divided in three groups: interactive segmentation methods, methods with minimal user interaction, and fully automatic methods.

A wide range of **interactive** segmentation algorithms for liver tumors has been described. To name a few, active contour models [Lu et al., 2005], graph cuts [Stawiaski et al., 2008], or energy-minimizing implicit functions [Heckel et al., 2011] (cf. Fig. 2.5) were found to be effective for surgical planning. Although interactive segmentation consumes time in clinical routines, the methods are essential in current software for surgical planning applications due to highly varying quality of clinical image data.

The second group attempts to require only **minimal user interaction** by focusing on the analysis of the acquired image data. Therefore, a region of interest is defined (e.g., by drawing a stroke) which provides parameters for the algorithm initialization. In simple cases, threshold-based approaches that automatically learn a threshold, e.g., based on the voxel distribution of the region of interest, are sufficient for tumor segmentation. However, threshold-based approaches fail if tumors are of low contrast or inhomogeneous and are often combined with advanced image processing such as model-based morphological processing [Moltz et al., 2009] or random-walk segmentation [Jolly et al., 2008]. Li et al. [2008] propose to segment tumors using optimization methods by minimizing a function that incorporates tumor boundary, local, and elasticity constraints. Other promising segmentation approaches with minimal user interaction are based on level sets [Smeets et al., 2010] or enhanced region growing techniques [Zhou et al., 2010].

The third group includes tumor segmentations that are performed completely **automatically**. This is a challenging task because of the high diversity of liver lesions. The literature describes methods that work well for tumors with high contrast, such as hypodense tumors in contrast-enhanced late-phase CT images [Pescia et al., 2008; Massoptier et al., 2008; Militzer et al., 2010; Schwier et al., 2011]. These methods generally consist of a detection phase followed by a dedicated segmentation step for each detected finding. Recent research in this field focuses on the detection of arbitrary lesions types and the automatic detection and segmentation of tumors in MR images.

Results from segmentation algorithms are not acceptable in all cases. Therefore, tools for semi-automatic adaptation of segmentation results in 3D are meaningful. Such correction tools need to handle user inputs in real time. Low-level tools for editing contours or removing pixels are described [Olabarriaga et al., 2001; Kang et al., 2004] and can be found in radiologic applications. Such interaction techniques are often time-consuming and require endurance of the user. High-level correction tools for tumor segmentations are rarely available. A promising idea is to request only minimal user interaction such as drawing a partial contour in a single slice and perform the correction in neighboring slices by using image information. For a description of such image-based correction techniques refer to the work of Grady et al. [2006] and Heckel et al. [2009].

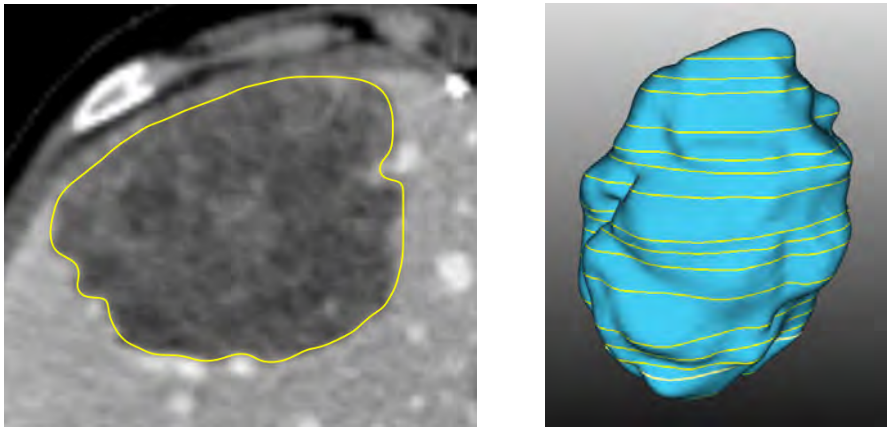

(a) (b)

Figure 2.5: Contour-based interactive segmentation of tumors. Image Courtesy Frank Heckel, Fraunhofer MEVIS.

Segmentation and Analysis of Vascular Structures

The segmentation of vascular structures in the liver is important for an adequate visualization of vessels in order to explore the patient-individual branching pattern. In combination with tumor segmentation, spatial relations between vessels and tumors can be analyzed. Therefore, the segmentation of vessels builds the basis for vascular risk analyses. In addition, vessel segmentations provide important landmarks for intraoperative navigation.

According to Friman et al. [2010], all current vessel segmentation methods are based on a growth process emanating from either an automatically defined or user-defined starting point. The differences lie in the growth process. A common approach is to use the region-growing algorithm [Adams et al., 1994] in combination with an appropriate shape analysis, e.g., curve evolution and front propagation. To detect small vessels in low contrast regions, a range of vessel tracking methods is described (refer to Friman et al. [2010]). For overviews of vessels segmentation procedures, refer to Kirbas et al. [2004] and Lesage et al. [2009].

For the visualization and exploration of vascular structures in the liver, the segmentation is often enhanced by a mathematical model description. The following computational steps, described by Selle et al. [2002], are common when calculating a vascular model of the liver. First, skeletonization with a topology-preserving thinning algorithm yields an exact centerline and vessel radii at each voxel of the skeleton. Second, a graph analysis transforms the vessel skeleton into a directed, acyclic graph for which nodes represent furcations. Third, a 3D representation based on a geometric surface description is generated [Hahn et al., 2001; Oeltze et al., 2005] to provide an abstract visualization of vascular structures (cf. Fig. 2.7).

Approximation of Vascular Territories

Once a segmentation of vascular structures in the liver is available, the issue of shape and extent of the associated liver segments arises. Segments of the liver, as introduced in Sect. 2.1.1, are supplied or drained by specific liver vessels. Their location and volume are important for preoperative risk analysis and resection planning. When liver segments were introduced by Couinaud [1954], modern radiological 3D imaging did not exist. Thus, the Couinaud segments can only be considered a rough, schematic guideline for liver resection planning. With the use of radiological imaging and vessel segmentation algorithms, a more accurate model of the liver segments, called vascular territories, is provided.

Thorn et al. [1999] introduced a tool for interactive determination of portal venous territories based on radiologic images. Therefore, three vertical and four horizontal planes are initialized based on user-defined landmarks (e.g., vena cava) and subsequently modified to define eight territories. However, the tool assumes planar borders between territories as proposed by Couinaud [1954]. Anatomical studies show that the assumption of the planar border does not hold [Fasel et al., 1998]. Furthermore, the number of portal venous liver territories may vary in cases of vascular anomalies or large tumors.

In order to predict the location and volume of territories based on the structure and characteristics of liver vessels, different computational models were developed. The models can be distinguished by their distance metric. Selle et al. [2002] introduced a model that is based on potential fields. In addition, they developed a model based on a Euclidean distance metric using a Voronoi decomposition. Both models were evaluated with vascular corrosion casts of the human liver. Therefore, the portal and hepatic veins were injected with resin. Afterwards, the liver was corroded which left the detailed branching structure of the vessel systems [Selle et al., 2002]. While the portal venous structures of the corrosion casts could be reconstructed up to the sixth branching order, clinical datasets acquired with present imaging technologies only allow a reconstruction up to the third branching order [Preim et al., 2007]. In order to test the robustness of the methods and their clinical applicability, the portal veins of eight datasets were generated using three different pruning levels (levels of detail). For each vascular model, vascular territories were calculated (cf. Fig. 2.6). The comparison between the approximated and the authentic territories showed a volumetric overlap between 80% and 90% depending on the pruning level [Selle et al., 2002]. Although the Voronoi decomposition exhibits a different formulation and a significantly lower computational complexity than the potential field method, the resulting territories showed very similar results. For a detailed presentation of the results, refer to the thesis of Selle [1999].

In conclusion, the approximation of vascular territories in the liver using a Voronoi decomposition based on a Euclidean distance metric has revealed to be efficient and showed sufficient accuracy for liver surgery planning. The methods for the approximation of vascular territories are part of the planning software HepaVision [Bourquain et al., 2002], an FDA-approved tool for preoperative planning in oncologic

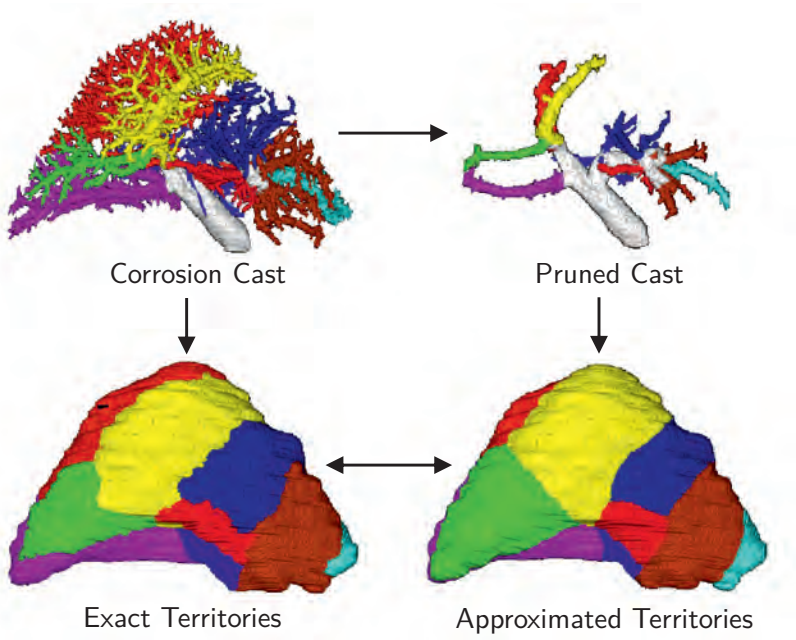

Figure 2.6: Segmented portal vein from a corrosion cast of the human liver (upper right) and the associated pruned vascular tree (upper left). Vascular territories are shown for the corrosion cast (lover right) and the pruned representation (lower left). Image adapted from Selle et al. [2002].

liver surgery, which has been tested in several evaluations [Schenk et al., 2008] and more than 6500 clinical cases since 2002.

Risk Analysis

In the treatment of liver diseases, surgical risk can be measured using **functional tests** like scintigraphy [Graaf et al., 2010] or the LiMax test [Stockmann et al., 2010], which is meaningful for cases with uncertain liver parenchyma quality. Furthermore, **scoring systems** such as the POSSUM test [Chandra et al., 2009] or the MELD score rank patients depending on physiological and operative parameters. However, both functional test and scoring systems assist surgeons in the choice of an optimal course of therapy, but support resection planning only to a limited extent. Spatial information (e.g., distances between risk structures or the optimal course of a trajectory) and possible damages (e.g., areas of risk) cannot be evaluated using the aforementioned methods. Nevertheless, Asakuma et al. [2007] and Stockmann et al. [2010] showed within clinical studies that functional tests in combination with virtual resection planning based on CT images [Bourquain et al., 2002] facilitate the prediction of postoperative functional liver volume. Therefore, algorithms are proposed that provide a quantitative measure in order to classify patients.

When removing a part of the liver in case of a tumor resection, surgeons usually aim to preserve as much perfused liver tissue as possible. By considering that the

liver contains a complex, interwoven vessel structure with two supply systems (PV, HA) and two drainage systems (HV, BD) a computer-assisted vascular risk analysis can support important surgical decisions (e.g., about the width of the safety margin) in critical cases. Preim et al. [2002] introduced a method to detect and visualize vessels at risk in oncologic liver surgery. The method assumes a limited number of safety margins around tumors. Standard widths were set to 5, 10, and 15 mm or alternatively to 2, 5, and 10 mm, depending on the type of tumor (cf. Fig. 2.7a). By default, red is employed for the smallest margin, which is assumed to be resected; yellow and green are used for larger margins. To determine the vascular branches within a certain safety margin around the tumor, the border voxels are detected by calculating the difference of the tumor and an eroded mask using a structuring element for erosion. Distance transformation is applied to all border voxels, and affected vessels are identified by means of a graph analysis. A similar approach is presented by Schwaiger et al. [2010], although they visualize only the minimal distance between tumor and vessels using three standard distances (5, 10, and 15 mm). Hierarchical dependencies of vessel branches, as described by Preim et al. [2002], are not taken into account.

Based on the work of Selle et al. [2002], who evaluated different approaches for the estimation of liver territories, Preim et al. [2002] proposed approximating the affected parenchyma using a nearest-neighbor distance model of the liver volume according to the centerline voxels of segmented vascular structures. These calculated volumes are called **territories at risk**. For each of the three safety margins, the territories at risk are quantitatively analyzed. Finally, an iso-surface renderer generates separate triangular meshes and sets vertex colors that correspond to the colors of associated vessels at risk (cf. Fig. 2.7b). Within a subsequent clinical study [Lang et al., 2005], the results of computer-assisted risk analysis led to a change of operation planning (compared to the examination of normal CT images) with regard to the extent of resection or the need for vascular reconstruction in selected cases (7 of 21 patients).

In the field of living donor liver transplantation (LDLT), risk analyses introduced in Preim et al. [2002] and Selle et al. [2002] assist surgeons in selecting the graft type, e.g., preserving or resecting the middle hepatic vein of donors when transplanting the right liver lobe. Therefore, the potential congestion volume can be calculated by detecting affected hepatic vessels and estimating the associated regional hepatic venous volumetry [Asakuma et al., 2007]. Model-based risk analyses for LDLT are therefore an important tool in the clinical routine [Radtke et al., 2007; Asakuma et al., 2007].

In order to find a standardized, comparable value for the vascular risk of a patient, Beller et al. [2009a] presented a measure to assess **surgical difficulty** of tumor resection. First, the volumes of territories at risk with safety margins from 1 to 30 mm are determined for the portal vein and hepatic vein. All volumes are stated as a percentage of the total liver. Second, the normalized integral of all risk volumes is calculated and defines a risk coefficient for the tumor. A performed surgical user study which compared the proposed risk coefficient with the opinion of surgical experts revealed that the risk coefficient is best illustrated by the territories at risk of

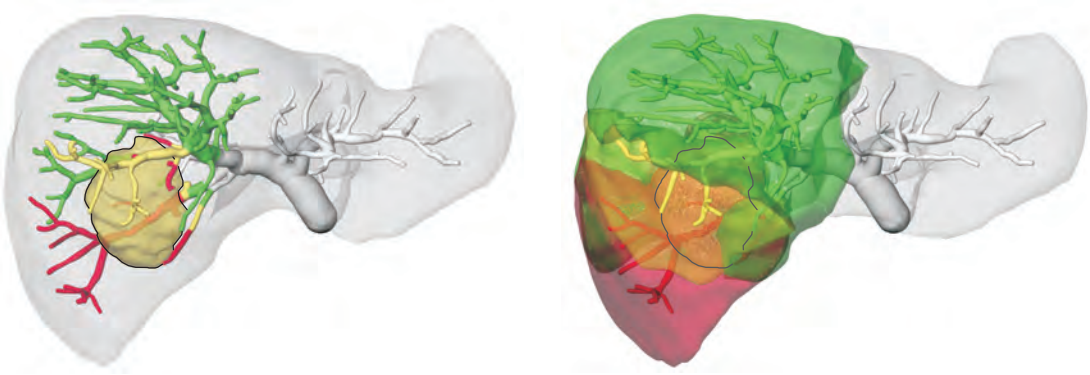

(a) (b)

Figure 2.7: Risk analysis for the portal vein with adjacent metastases as described in [Preim et al., 2002]. (a) The visualization of vessels at risk simulates affected branches when using a safety margin of 2 mm (red), 5 mm (yellow), or 10 mm (green). (b) Based on the analysis of vessels at risk, dedicated territories at risk are computed.

the hepatic vein, or alternatively, the union of hepatic vein risk territories and portal vein risk territories. Besides the risk measure described by Beller et al. [2009a], there might be additional risk measures that need to be considered when assessing surgical difficulty, e.g., the access paths to tumors because a dorsal located tumor might be more difficult to resect than a ventral located tumor.

Resection Planning

Once the vascular risk analysis for each vessel system is performed, resection plans may be prepared and evaluated. This is particularly interesting for cases exhibiting a high surgical risk, including patients with multiple tumors in both lobes and tumors that are close to central vessels. Besides the definition of the cut path, a virtual resection plan provides an important physical value: the estimated amount of postoperative liver parenchyma.

Virtual resection planning is now mostly performed with 2D/3D manipulators such as draggers that are applied on a deformable surface within the 3D planning models or the 2D radiologic images. Konrad-Verse et al. [2004] introduced two basic interaction approaches to specify virtual resections. For the first method, the resection is marked by drawing a few slices of the radiologic dataset (Fig. 2.8a). Thus, a resection can be specified as precisely as desired, but is limited to axial slices which might not be appropriate for complex resections. To reduce the interaction time, the approach considers interpolation methods to reduce the number of required slices.

For the second method, the user draws one or more lines onto the virtual 3D liver surface to initialize the resection surface. Both methods can be used simultaneously.

For further deformation in 3D, a deformable cutting plane (cf. Fig. 2.8b) is generated by applying a principal component analysis (PCA) on the point set which forms the lines. The user can define a sphere of influence as well as the amplitude of the deformation to modify the cutting plane interactively. Both functions are controlled with mouse movements at the point being modified. Besides the local modification of the grid, there is also a function to translate the entire mesh. Finally, both techniques apply a volume calculation of the resected and remaining parts of the liver to provide quantitative information for surgical decisions.

To further reduce the required interaction time, Hiller [2008] applies general geometric shapes, such as planes and wedges, that are placed at the beginning of the procedure. Subsequently, the user may manipulate the shapes based on a mass-and-spring system. Reitinger et al. [2006] developed a virtual reality-based system for surgical planning procedures. To plan a resection on the 3D model, the user can choose from three different possibilities and apply those using optical tracked devices for which even haptic feedback is offered. Besides a simple plane for straight resection paths, the application supports more complex scenarios where a deformable plane is applied. For wedge resections, a scalable sphere is placed inside the virtual reality model and can be used to define disc-like resection paths.

To improve the quality of an interactively defined resection surface, Demedts et al. [2010] introduced evaluation methods for virtual resection surfaces. Therefore, risk factors that parameterize the evaluation function have been described [Demedts et al., 2010]. Using an optimized data structure specialized for liver volume data, interactive framerates for the computation of the resulting resection score are achieved. The resection score enables a quantitative comparison of different resection surfaces. Evaluations with clinical users showed that the quality of virtual resection surfaces is increased when using the interactive evaluation tool, however, the total time to define a resection surface increases. This could be attributed to the presentation of additional information, which leads to increased attention and additional effort.

The question arises whether it is possible to calculate a resection proposal automatically. Preparatory work can be found in the field of ablation therapy and biopsy. For the placement of needles in the liver, automatic path proposal techniques are proposed [Baegert et al., 2007; Schumann et al., 2010]. These techniques use multiple clinical parameters such as tumor coverage, distance to risk structures and penetration depth to calculate an optimal insertion path. However, techniques for automatic generation of liver resection proposals exist only in rudimentary form Preim et al. [2002]; Thorn [2004]; Beller et al. [2008]. A first software prototype for automatic generation of resection proposals was developed in the context of this dissertation and is presented in Chapter 4 on page 87.

2.2.3 Intraoperative Decision Pipeline

Tumor resections in the liver are among the most difficult surgical interventions in the human body. In complex surgical cases, e.g., centrally located tumors, only specialized centers accept patients for resection. Preoperative resection plans as well

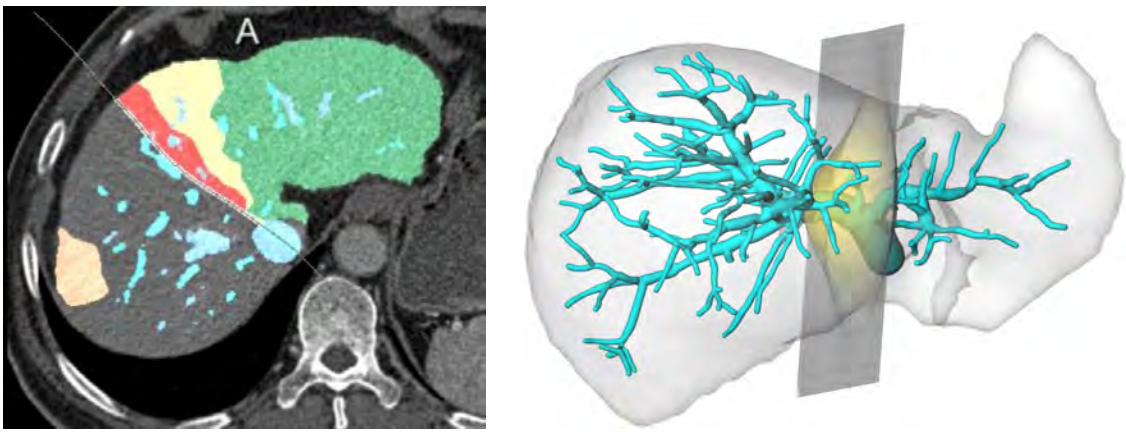

(a) (b)

Figure 2.8: (a) Resection planning by drawing into slices with visualized impaired blood flow (green = HV at risk, yellow = PV at risk, red = PV + HV at risk) [Demedts et al., 2010]. (b) Deformable cutting plane to modify a virtual resection surface [Konrad-Verse et al., 2004]. The yellow part of the mesh indicates the influence range of the deformation.

as the surgical experience are prerequisites for the success of such an intervention. During liver surgery, a lot of decisions must be made by the surgeons during each step. According to Lang et al. [2005], an anatomical liver resection can be divided in the following steps:

(1) Access

(2) Mobilization of the liver

(3) Intraoperative sonography

(4) Liver hilum dissection

(5) Vena cava and hepatic vein dissection

(6) Parenchyma transection

(7) Care of resection surface

(8) Final stage

Each work step calls for special surgical decisions. The **parenchyma transection** (6) is often the most critical and difficult step because risk structures within the parenchyma are not directly visible by surgeons. Therefore, much research is performed to support the parenchyma transection using computational models. The parenchyma transection includes the following surgical subtasks:

(6-1) Mark the planned resection surface on the liver surface (cf. Fig. 2.9a)

(6-2) Follow the planned resection course (cf. Fig. 2.9b)

(6-3) Avoid cutting risk structures such as central vessels

(6-4) Keep an adequate distance to the tumor (safety margin)

(6-5) Adapt the resection strategy in case of intraoperative findings

(6-6) Control bleeding

Navigational support during transection is currently provided by utilizing IOUS or by mentally comparing the intraoperative situation with the planning data. In recent years, **navigation systems** for liver surgery have been proposed [Cash et al., 2007; Beller et al., 2007; Hildebrand et al., 2007; Peterhans et al., 2010]. These systems intraoperatively align preoperative planning data with the patient's liver by using registration techniques.

With the introduction of navigation systems in the clinical workflow, additional workflow steps were introduced, including:

(6-0a) Transfer of planning data to the intraoperative site

(6-0b) Calibration of tracked surgical instruments and tracking devices

(6-0c) Intraoperative registration of preoperative and intraoperative data

(6-0d) Navigated transfer of the resection plan

Furthermore, a method for intraoperative adaptation of planning data in case of additionally detected findings is necessary. All of these new working steps introduced with the utilization of navigated liver surgery demand additional intraoperative decisions, illustrated in Fig. 2.10.

2.2.4 Navigated Liver Surgery

According to the definition of Beller et al. [2010], navigation support can be divided in the following categories:

(1) **Mental** navigation based on preoperative images without the use of tracking technology

(2) Navigation support through **intraoperative imaging** (such as IOUS)

(3) Navigation support through **registration** between preoperative images and patient anatomy (with or without the use of intraoperative imaging)

(4) Navigation support through registration and **continuous tracking** of organ motion

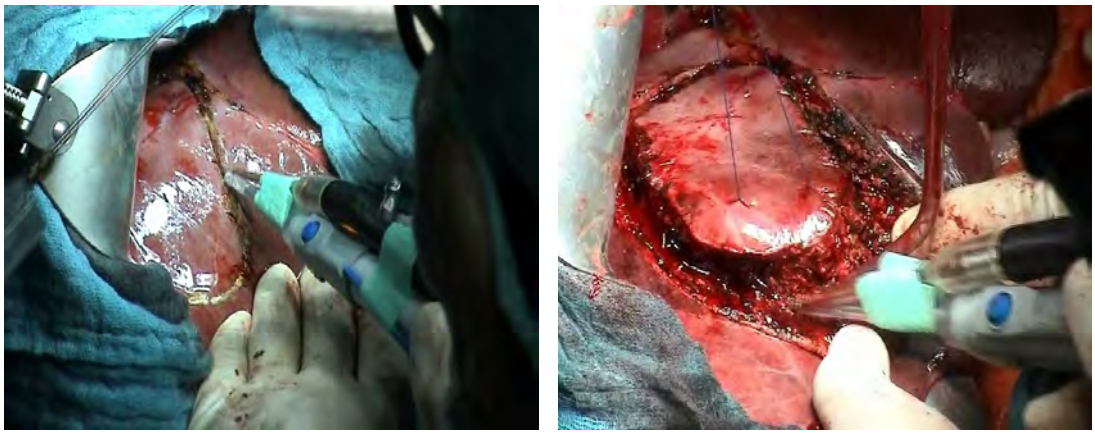

(a) (b)

Figure 2.9: Workflow steps in oncologic liver surgery: (a) Mark a planned resection surface on the liver surface and (b) following the planned resection course. Image courtesy General Hospital Celle, Germany.

Nowadays, mental navigation (1) and intraoperative imaging (2) are widely used for navigation support in liver surgery. For (1), surgeons use a representation of planning data in the operating room, e.g., in print or on a video monitor. Alternatively, mental navigation is often based solely on the surgeon's memory. For (2), intraoperative imaging builds the basis for surgical navigation. IOUS is now a standard procedure in liver surgery because it exhibits several advantages over other image modalities: It provides real-time images of the liver, it is widely available in operating rooms, and surgeons are very familiar with this device. Mental navigation based on preoperative images (1) is often combined with navigation support through intraoperative imaging (2).

One of the first navigated resections based on intraoperative imaging was performed many years ago right after the discovery of x-rays. Cox et al. [1896] applied x-ray imaging to guide the surgical resection of a bullet in a human leg. The introduction of CT imaging for humans in 1971 opened the door for precise 3D operation planning. Now, 3D planning models and associated risk analyses are essential parts of modern planning software. However, transferring the preoperative planning information to the intraoperative situs only by memory represents a great cognitive challenge, because the liver surface shows only a few clear anatomical landmarks [Beller et al., 2010]. Thus, visual and tactile information have to be aligned with the 3D planning models mentally and continuously [Beller et al., 2010]. The amount of planning information that can be transferred is limited in this context.

Thanks to the introduction of clinical tracking devices, it has been possible to track the position of surgical instruments. The use of registration methods allows visualizing the instruments relative to preoperative planning models (3). Recent commercial navigation systems use only rigid registration approaches, whereas non-

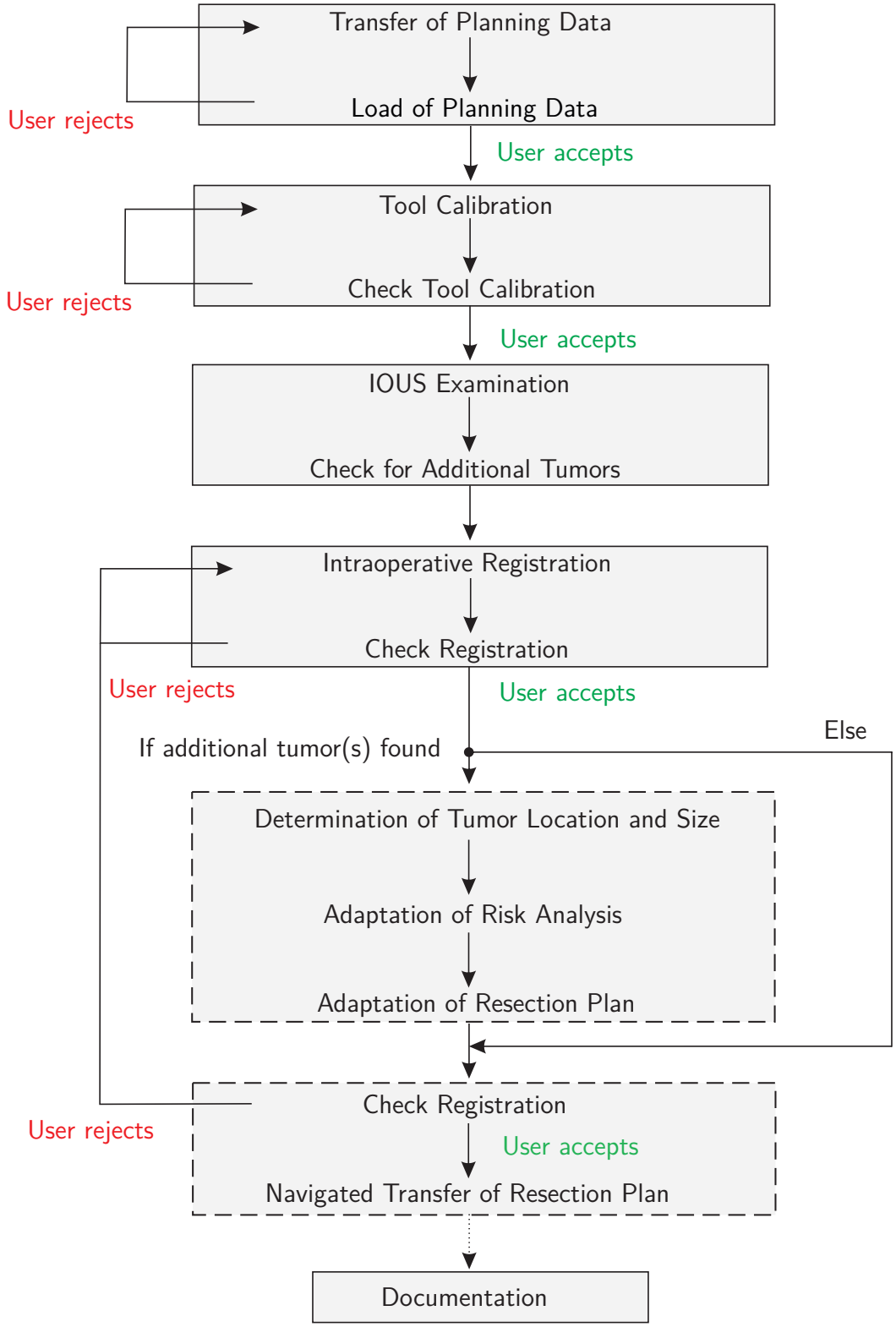

Figure 2.10: Part of intraoperative decision pipeline for navigated liver surgery from a technical viewpoint. The dashed boxes represent workflow steps addressed in this thesis.

rigid registration has been applied in several research systems [Cleary et al., 2010]. However, the value of a registration is limited in case of organ movement, which is common in liver surgery. Therefore, techniques for continuously tracking organ movement (4) are part of current research. Intraoperative registration is a key component of surgical navigation systems and is discussed in the next subsections.

The question arises why surgeons request this new technology. Kleemann et al. [2005] described the aim of navigated liver surgery as the precise transfer of a preoperatively planned resection surface to the patient's liver and the consideration of adequate distance to tumors and central liver vessels. They defined the following **reasons** for using navigation systems in liver surgery:

- Increased surgical accuracy
- Achievement of smaller access paths
- Transfer of preoperative planning data
- Semi-automation of steps in the surgical workflow
- Surgical training

Navigation support has been requested for both laparoscopic (minimally invasive surgery) and open liver surgery. Open liver surgery is widely applied and the standard resection technique for tumors in the liver. Laparoscopic liver surgery is relatively new, however, with recent advances of laparoscopic devices the number of laparoscopic liver interventions increased rapidly. Advantages of laparoscopy are the reduced pain due to smaller incisions and a shorter recovery time. However, due to the absence of tactile feedback, there is a great need for navigation support in this field [Kleemann et al., 2005].

Besides the aforementioned reasons for navigated liver surgery, possible medical **indications** for surgical navigation are described. According to Vetter et al. [2002], navigation support would be desirable for centrally located tumors. For tumors which are palpable and located peripherally, navigation support might not be necessary. Beller et al. [2010] assume that the field of molecular imaging opens a new kind of diagnostics with which early staged, small tumors can be identified. These tumors may not be palpable or visible using conventional imaging such as CT, MRI, or IOUS. The same effect can be observed for tumors that were treated with preoperative chemotherapy. Within a case study on a patient who had undergone preoperative chemotherapy, Oldhafer et al. [2009] showed that the resection of non-palpable, invisible tumors using a surgical navigation system is feasible.

Navigated liver surgery is a promising technique to support surgical decisions and to increase patient safety in the operating room. According to Cleary et al. [2010], key components of surgical navigation systems are:

(1) Tool tracking and calibration

(2) Registration and organ tracking

(3) Visualization

In the following, these key components are described.

Tool Tracking and Calibration

Tracking systems (localization systems) are the core of a modern surgical navigation system. They provide spatial information about the objects to be tracked. Such objects are, for example, surgical instruments or a human organ. The following types of tracking systems can be distinguished:

- Optical tracking systems
- Electromagnetic tracking systems

Optical tracking systems can be further divided into passive and active systems. The objects to be tracked are provided with markers. Markers of active systems emit light, e.g., using an LED. Passive markers are illuminated by a light source and reflect this light. **Infrared**-based optical tracking systems are widely used in clinical applications [Cleary et al., 2010]. The bases of this technology are infrared markers (active or passive) tracked by optical CCD sensors. Three (or sometimes four) infrared markers are arranged in a so-called marker shield. Thus, markers have a fixed spatial relation to each other, which allows calculating the position and orientation of the marker shield. Another group of optical tracking systems are optical **videometric** systems that identity marker patterns (e.g., checkerboards or stripes) on video image sequences obtained using one or more calibrated video cameras [Cleary et al., 2010].

Electromagnetic tracking systems determine position of objects that are located in a pulsed electromagnetic field. The objects are equipped with electromagnetic field sensors. The data received by these field sensors permit a reliable assessment of the sensor location. Electromagnetic trackers can be made much smaller than optical trackers (0.5 mm in diameter and 8mm in length [Cleary et al., 2010]) but are less accurate and are affected by nearby ferromagnetic materials [Glossop, 2009]. The main advantage over optical tracking systems is that there is no line-of-sight constraint. This makes electromagnetic tracking applicable for many kinds of minimally invasive interventions, e.g., laparoscopic surgery. In open liver surgery, both electromagnetic and optical tracking systems are suitable [Beller et al., 2010]. Several groups [Khan et al., 2006; Nakamoto et al., 2008; Feuerstein et al., 2009] proposed hybrid tracking systems that combine optical and electromagnetic tracking in order to compensate the drawbacks of optical tracking (line of sight, size of marker shields) and electromagnetic tracking (ferromagnetic materials, less accuracy).

Surgical dissectors and ultrasound probes are instruments that need to be tracked during navigated liver surgery. In order to receive tracking information that is valid

and reproducible within a defined world coordinate system, a **calibration** of these instruments needs to be performed. This is done by comparing the measurements with a second object with known correctness. If the tracker (marker shield, electromagnetic sensor) is in a fixed spatial constellation to the surgical instrument, the calibration has to be performed only once. Otherwise, the calibration needs to be repeated whenever this spatial constellation changes.

A sophisticated task in navigated liver surgery is the calibration of the ultrasound probe. Thereby, the relation between pixels in the ultrasound image and the 3D coordinate system needs to be found. In most cases, the ultrasound calibration is performed by placing an object with known geometry in a water bath. For a review of existing ultrasound calibration techniques, refer to Mercier et al. [2005].

Intraoperative Registration and Organ Tracking

Navigated liver surgery allows visualizing tracked surgical instruments in spatial relation to 3D planning models. Therefore, the 3D models have to be mapped to the liver. This mapping is called intraoperative registration and requires a determination of corresponding features in the preoperative dataset and on the intraoperative situs. An intraoperative registration is only valid as long as no movement of the liver occurs. Therefore, respiratory gating techniques [Clifford et al., 2002] are applied, and the liver is immobilized with surgical sheets. Although the liver is immobilized, it is frequently squeezed, pulled, and even partly removed by the surgeons during parenchyma transection. Without a continuous tracking of the liver, the registration needs to be frequently repeated in order to stay valid.

In commercial navigation systems for liver surgery, only rigid registration techniques are applied [Cleary et al., 2010]. However, a study by Heizmann et al. [2010] showed that there is no rigid alignment of the pre- and intraoperative organ positions due to overall deflection of the liver. Using local registration, a rigid alignment of the anatomical structure can be achieved with less than 5 mm discrepancy relative to a segmental unit of the liver [Heizmann et al., 2010]. A surface deformation measurement study performed by Clements et al. [2011] indicates that the shape change that occurs from preoperative image acquisition to intraoperative presentation involves a fattening of the liver. They measured surface displacements with magnitudes between 5 and 20 mm. However, how these surface errors translate into errors observed with respect to deep tissue structures remains unclear.

Many registration methods for navigated liver surgery are described in literature. These methods can be classified depending on the kind of features used for registration:

- Surface features of the liver
- Anatomical features within the liver parenchyma

Furthermore, the methods differ in the techniques used to acquire the features intraoperatively:

- Intraoperative imaging, e.g. IOUS, MRI, CT
- Digitization, e.g., using a tracked pointer

Just as CT or MRI are standard modalities for preoperative imaging, IOUS is the standard modality for intraoperative imaging in liver surgery. Vascular structures of the liver proved to be a good feature because they traverse the whole liver and are detectable in pre- and intraoperative images. The main challenges are that IOUS images are perturbed by noise and artifacts (which results, for example, in segmentation errors) and that surgeons require a method that is robust with low computation time.

Papenberg et al. [2008] proposed methods that require the definition of intrahepatic landmarks in both pre- and intraoperative images. On the basis of this definition, the landmarks are aligned using thin plate splines or, alternatively, an image-based term based on normalized gradient fields. Both approaches showed acceptable results for selected clinical datasets. However, the results depend on the amount and accuracy of the defined landmarks. In case a vessel segmentation is available in both image modalities, graph analysis can be applied to find reasonable landmarks for registration [Metzen et al., 2007; Lohe et al., 2008; Metzen et al., 2009]. Penney et al. [2004] proposed a rigid registration method based on probability maps of corresponding vessel features in ultrasound and MRI. The intensity values of the probability maps represent the probability of a voxel containing a vascular structure and are generated using training data sets. Another technique proposed by Wein et al. [2010] performs a direct image-based registration. The technique aligns both image modalities non-rigidly using similarity measures. A simulation of ultrasound based on CT data [Wein et al., 2007] builds the basis.

Other groups use anatomical landmarks on the liver surface as a registration feature. Peterhans et al. [2010] proposed to define anatomical landmarks in the planning data (before or during surgery) and assign these points with the tip of a tracked surgical dissector during surgery. Although reasonably intuitive, the accuracy of this method is limited (median accuracy $\approx 6.3\ mm$) and the method depends on the availability of appropriate surface landmarks. An ongoing clinical study verifies if a combination of surface landmarks and sub-surface landmarks using IOUS increases registration accuracy.

[Clements et al., 2011] evaluated methods using a laser range scanner to measure the intraoperative liver surface and align it with the liver surface extracted from preoperative image data. A signed closest-distance algorithm is applied to calculate a rigid transformation between the acquired surface scan and the intraoperative liver. To estimate the liver deformation, FEM-based liver models are applied [Cash et al., 2005].

Besides laser range scanning, several other surface acquisition techniques such as stereo vision and time-of-flight (TOF) are proposed for the field of image-guided liver surgery. Maier-Hein et al. [2010] presented methods for rigid registration of TOF data with 3D planning models of the liver. The work mainly focuses on error

and noise reduction in TOF data. With recent developments in the automotive and game industries, it can be expected that surface acquisition devices become more accurate and robust in coming years. However, a substantial problem of laser range scanning and TOF is the line-of-sight constraint. Another challenge is that surface acquisition techniques deliver reliable data about the surface of the liver only. The location and spatial relations of structures within the liver parenchyma (which is the main interest for surgeons) needs to be estimated by computational models, which may introduce additional inaccuracies in particular for deep regions.

According to the review of Clifford et al. [2002], intraoperative liver motion is greatest in the cranio-caudal direction, with translation ranging from 10 to 26 mm in quiet respiration. To avoid a repeated re-registration, **organ tracking** techniques have been introduced for liver surgery. Organ tracking using laser range scanning or TOF cameras may be possible in the future, although line-of-sight constrains have to be considered for open liver surgery. Markert et al. [2010] proposed to fix reflective fiducials localizable by an optical tracking system on the liver surface. The methods were evaluated in laboratory settings. Again, line-of-sight problems may hamper continuous tracking in an actual surgical situation. Other groups propose to fix navigation aids localizable by an electromagnetic tracking system on the liver surface or within the liver parenchyma [Vetter et al., 2003; Beller et al., 2009b]. Evaluations of these methods have been performed on phantoms and pig livers [Vetter et al., 2003; Lei et al., 2011] and on five patients undergoing oncologic liver surgery [Beller et al., 2009b].

Intraoperative Visualization

Lightboxes dominated operating rooms for almost the entire 20th century. Dozens of radiologic images were hung next to one another in order to allow the surgeon to view the preoperative information during surgery. Because the lightboxes were located outside the sterile area, surgeons had to leave the operating table, walk to the light box, and return to the patient again. 3D planning models of the liver were not available at this time.

With the introduction of computer-assisted liver surgery planning and the increasing complexity of such interventions, intraoperative visualization is becoming an important part of liver surgery. Currently, there are three different ways to visualize planning data in the operating room. A common practice is to use preoperative 3D planning models as a **printout** (cf. Fig. 2.11). Multiple views of the 3D planning data can be prepared beforehand, annotated if necessary, and easily positioned close to the operating field. However, such static visualizations are not appropriate for navigated surgery, for which planning data is visualized along with tracked surgical instruments.

Another common way to visualize planning data in the operating room is the **presentation on a display**, e.g., ceiling-mounted monitors installed in modern operating rooms. Unlike a printout, a monitor representation enables interaction between surgeon and preoperative data (cf. Fig. 2.12). Preoperative data can be visualized in

Figure 2.11: Visualization of preoperative planning data in the operating room by using printouts of relevant planning models. Image Courtesy University Hospital Essen, Germany.

different ways. Most viewers provide at least the means to slice through the stack of radiologic images. In addition, a 3D visualization of the data is sometimes provided, which is presented either as a direct volume rendering or an isosurface rendering (indirect volume rendering). In contrast to direct volume rendering, isosurface rendering requires a reliable segmentation step beforehand. For a technical description of these visualization techniques refer to the book of Preim et al. [2007].

Monitor-based visualizations are used in many research prototypes, e.g., [Nowatschin et al., 2007; Hildebrand et al., 2007; Beller et al., 2009b; Peterhans et al., 2010], and dominate commercial available navigation systems. During navigated liver surgery, 3D visualization of planning models is currently used for guiding tracked surgical instruments. One important aspect is that these planning models were not developed to provide information in complex workspaces like the operating room. They often portray complex geometries and demand cognitive effort and user interaction. Because appropriate interaction devices are nowadays not widely available in operating rooms, surgeon-computer interaction in the sterile area is difficult and needs often to be performed by a medical assistant outside of the sterile area.

Effective visualizations for liver surgery are rarely described in literature. To the knowledge of the author, only Lamata et al. [2008] developed a system that provides an effective monitor-based visualization for liver surgery. Based on a surgical requirement analysis, they propose to visualize planar resection surfaces in two different views. While a coronal view shows the resection surface, liver surface, nearby vessels, and tumors from the surgical view, a sagittal view presents these planning models perpendicular to the surgeon's line of sight. Subjective assessments

Figure 2.12: Monitor-based visualization of planning data on the CAS-One navigation system. One surgeons (middle) interacts with the 3D visualization using a touchscreen interface. Image Courtesy Asklepios Hospital Hamburg Barmbek, Germany.

gathered in a user study indicate that the provided visualization increases the confidence and the orientation ability of surgeons [Lamata et al., 2010].

Another problem with monitor-based visualizations is that the display location is often not optimal with regard to ergonomic and cognitive aspects [Hanna et al., 1998]. This makes it very hard for surgeons to focus on the monitor while concentrating on the operating field. Especially in critical situations (where information from the navigation system would be helpful), it would be not applicable to avert one's gaze from the patient.

To allow a direct transfer of planning information, such as risk analyses and resection plans, to the operation field, navigation systems that use **AR techniques** are part of current research. Instead of looking on the screen, planning information is directly mixed with the surgical view. The basic approach to employ AR during liver interventions is described by Ayache [2003]. The work proposes to augment intraoperative video images with an associated 3D-reconstruction of the liver surface using alpha compositing (semi-transparent overlay). Samset et al. [2008] use AR to educate surgeons in radiofrequency ablations of liver tumors. Using a head-mounted display (HMD), interventional procedures are trained on phantoms without the risk of performing an invasive intervention in reality. Nicolau et al. [2009] introduced a guidance system for liver percutaneous punctures that superimposes planning models on video images of the interventional view. Alpha compositing is used to achieve semi-transparent planning models. However, if AR applications apply transparency to superimpose planning models on the surgical view, visual depth cues can be

degraded through lower contrast.

Feuerstein et al. [2008] apply direct volume visualization of intraoperatively retrieved CT data to superimpose laparoscopic video images for trocar placement in liver surgery. A drawback therein is its limitation to the intraoperative processed segmentation result, which does not provide an accentuation of risk structures and spatial relations. Several groups [Scheuering et al., 2003; Marescaux et al., 2004] in the field of laparoscopy guidance apply transparency-based superimpositions, similar to [Ayache, 2003; Samset et al., 2008; Nicolau et al., 2009], in order to achieve a superimposition of laparoscopic video images with planning information, which could also lead to misinterpretations.

Projector-based AR represents an interesting way to support surgical decisions: Krempien et al. [2008] and Riechmann [2006] showed that a projector can not only be used for intraoperative visualization, but also for the registration of the patient's organ using structured light techniques. Gavaghan et al. [2011] presented a handheld-navigated laser projector (wrapped in a sterile plastic hull) to visualize 3-D planning models directly onto the organ surface (cf. Fig. 2.13).

Although it is becoming more common for commercial navigations systems to make AR visualizations available (e.g., BrainLab , Medtronic , da Vinci), it is not common to see them used in the clinical routine [Kersten-Oertel et al., 2011]. According to Kersten-Oertel et al. [2011] there are plausible reasons for that: First, the systems are often developed as proof-of-concept prototypes and therefore may not consider clinical needs or constraints imposed by the operation and the surgeon. Second, the added benefit is mainly for less experienced surgeons or surgical residents. Third, the systems are not sufficiently evaluated and therefore are not convincing in proving their value for given surgical tasks.

2.3 Concluding Remarks

With the introduction of personal computers, the era of computer-assisted surgery began. Research in this field was driven by the availability of improved hardware, i.e., graphic units, microprocessors, and large data storage devices. For liver surgery planning, 3D planning models were derived from radiologic data, enabling a model-based assessment of risk. Recent developments in computer-assisted liver surgery focus on the automation and improvement of surgical planning and the transfer of planning information in the operating room.

The decision pipeline for liver surgery described in this chapter illustrates where computer assistance supports and attempts to support surgical decision making in clinical routine. With the emergence of surgical navigation systems into operating rooms, the requirements for surgical planning data have changed. Planning data needs to be displayed in the operating room according to surgical needs. This includes a reduction of complexity and a focus on critical areas. In addition, planning data needs to be updated according to the movement and deformation of the liver and in case of intraoperative findings. At the same time, preoperative planning needs to be

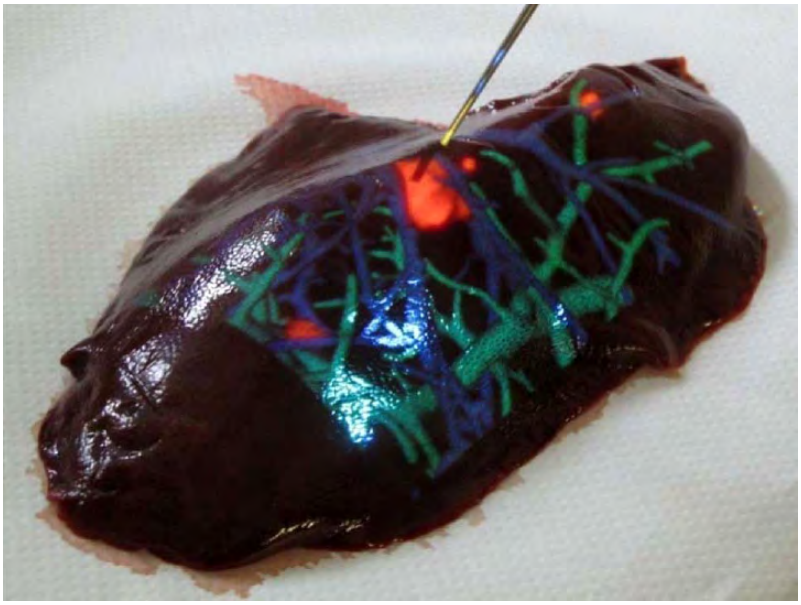

Figure 2.13: Projection of portal vein (green), hepatic vein (blue) and metastasis (red) on a pig liver using a handheld-navigated laser projector. Image Courtesy Kate Gavaghan, University of Bern, Switzerland.

more accurate to minimize resection inaccuracy. This includes steps such as phase registration, segmentation, determination of safety margins, and the generation of resection proposals. Finally, a quick, optimally automated processing of all these steps is desirable because of limited time, staff, and financial resources.

3 Interactive Determination of Safety Margins around Tumors

The oldest, shortest words - 'yes' and 'no' - are those which require the most thought.

(Pythagoras of Samos)

This chapter presents and discusses new methods for supporting preoperative decision making and assessing risk in the context of liver surgery planning. The surgical risk of a tumor resection depends, among other factors, on the width of safety margins around tumors. Therefore, new methods for determination of optimal safety margins are presented in this chapter. Besides an interactive exploration of risk sensitivity and robustness, the combination of risk from different vascular systems is addressed.

3.1 Clinical Background: Safety Margins

The term **safety margin** is often incorrectly used as another expression for **resection margin**. Whereas safety margins are predetermined and constitute a part of a surgical plan, resection margins (or surgical margins) are subsequently verified by the pathologist when the surgical piece is examined [Kopke et al., 2005]. One surgical goal during a tumor resection is to achieve a resection margin as if it was preoperatively planned in terms of a safety margin.

The main factor for a good patient outcome in oncologic liver surgery is the complete excision of all tumors, including a tumor-free resection margin (R0-resection). Histologically unclear resection margins (R1-resection) have been described as disadvantageous with regard to recurrence [Ooijen et al., 2003; Pawlik et al., 2005]. However, when removing a tumor and its margin, adjacent vessels must be transected. These vessels may supply or drain a specific liver region and thus define a **territory at risk**. Therefore, the number of vessels that can be preserved correlates with the postoperative residual liver volume. According to [Pawlik et al., 2008], the postoperative residual liver volume should be at least 20 % of the total estimated liver volume for normal parenchyma, 30-60% if the liver is injured by chemotherapy, steatosis, or hepatitis, or even 40-70% in the presence of cirrhosis.

Due to better outcomes in liver metastasis treatment using modern chemotherapy the surgical trend recently changed from large anatomical resection to non-anatomical resections [Lang et al., 2010]. In this context, the determination of optimal safety margins around liver tumors became increasingly important in recent years.

A wider saftey margin theoretically gives a higher potential for cure, whereas a smaller margin (e.g. < 1 cm for colorectal metastases) should not be an exclusion criterion for resection [Salloum et al., 2008]. Recent studies report that the width of resection margins does not affect recurrence or survival rate, as long as the margin is histologically clear [Pawlik et al., 2008; Muratore et al., 2010]. However, optimal margin width has been (and is still) uncertain because of contradicting results from recent studies [Muratore et al., 2010; Lordan et al., 2010].

3.2 Purpose

The determination of optimal safety margin widths around liver tumors is a challenging surgical task. Type, number, volume, and location of tumors and their relation to vessels are all important factors when deciding whether a R0 resection can be achieved. Thereby, surgeons have to find a compromise between safety margin width and the estimated postoperative liver volume.

Vascular territories at risk may be sensitive to small changes in the width of the safety margin. However, safety margins may exist with a robust risk where changes to the width of the margin only alter the territories at risk to a limited extent.

The purpose of this work is to provide physicians with a computer-aided planning tool with which different safety margins can be evaluated concerning risk sensitivity

and robustness in an adequate time period. Risk analyses from different vascular systems (portal vein and hepatic vein) are considered in this context. In addition, definition of non-uniform safety margins is addressed to allow precise resection planning for patients with insufficient estimated postoperative liver volume.

3.3 Related Work

Methods for model-based risk analysis based on preoperative images are proposed in different surgical fields. The methods are adapted to clinical needs, because anatomical complexity and function varies depending on the treated organ. A variety of methods for risk analysis in liver surgery planning has already been reported in Sect. 2.2.2 on page 20. In addition, model-based risk analyses for tumor resections are also utilized in the context of neuro- and lung surgery.

Rieder et al. [2008] introduced interaction and visualization techniques to explore virtual access paths for resection planning in **neurosurgery**. Therefore, functional areas of the brain are detected from multi-modal datasets (fMRI and DTI) and presented along an interactively definable path towards the tumor. By modifying the incision point or changing size and orientation of the access path, the observer can explore the associated surgical risk and difficulty. Joshi et al. [2008] enhances the techniques described by Rieder et al. [2008] by presenting different shapes of access paths (spherical, cubical, and ellipsoidal) and visualizing SPECT activation regions and the position of electrodes. Another considerable work in the field of interactive risk exploration that is focused on the analysis of fiber tracks (DTI) and functional areas around a tumor is described in Blaas et al. [2007]. Fiber bundles that pass through a region around a tumor are detected and can be filtered and color-enhanced depending on the tumor distance or the distance to a functional area.

Welter et al. [2011] introduced a tool for computer-assisted **lung surgery** planning to define safety margins around lung tumors in order to analyze the distance between tumors and segmental borders. They conclude that adequate margins are an additional factor to prevent recurrence after lung surgery. According to Welter et al. [2011], even larger tumors up to 6 cm could be candidates for segmentectomy in case adequate safety margins with enough distance to the segmental borders can be determined. This creates new possibilities for patients affected with large lung tumors, because nowadays only tumor diameter $\leq 20mm$ is generally accepted for segmentectomies [Okada et al., 2005].

Rieder et al. [2009] introduced methods to visualize risk structures to interactively plan **radiofrequency ablations** in the liver. A numerical simulation of the heat distribution [Kröger et al., 2006] considers heat-sink effects caused by the cooling blood flow. Depending on the orientation and position of a virtual applicator needle, the affected liver tissue is highlighted and the colors of tumors and vessels are adapted according to a color table. In a subsequent publication [Rieder et al., 2010a], a pseudo-cylindrical mapping of a tumor surface onto a 2D image, called the tumor map, is presented (refer also to page Sect. 5.2 on page 97). In combination with a

3D viewer, the tumor map serves as an interactive tool to quickly explore risk. The proposed methods may assist physicians in planning needle placement while ensuring a complete destruction of tumor cells and preserving anatomical risk structures.

3.4 Interactive Determination of Safety Margins

Standard widths for safety margins, as proposed in Preim et al. [2002], may be computed automatically in order to assess surgical difficulty, but they do not allow for detailed exploration of surgical feasibility. Two computational bottlenecks exist in their pipeline which make an interactive exploration of arbitrary safety margins impossible:

(1) Calculation of territories at risk for specific safety margins in image space

(2) Update of the 3D visualization

The computation time for these steps is approximately 10 seconds on a standard medical workstation (compare specified test framework in the appendix on page 155). In order to allow an interactive exploration of territories at risk, safety maps for each vessel system are introduced.

3.4.1 Safety Maps

Safety maps encode the margin at which each voxel of the liver parenchyma will be affected by the tumor. They are calculated in a preprocessing step. For their calculation, one central question has to be answered for each liver voxel: Which vessel branches (that are visible in the radiologic data) are responsible for the perfusion of the liver parenchyma at the position of the liver voxel? This is not easy to determine, because the capillary vessels which perfuse the liver cells are too small to be detectable in radiologic images.

Model assumptions have to be made. In this work, a nearest-neighbor distance model is utilized. The model was evaluated by Selle et al. [2002] on human corrosion casts of the human liver. The evaluation indicated that the assumption of a nearest-neighbor distance model provides sufficient accuracy for liver surgery planning.

Following the nearest-neighbor distance model, a 3D Voronoi decomposition of the liver volume according to the centerline voxels of the segmented vascular structures approximates the perfusion or drainage areas. Combining this information with a Euclidean distance transformation of the tumor segmentation mask and taking the hierarchical dependencies of the vascular tree into account, the safety map for a specific vascular tree of the liver is calculated. The map can be used as a 3D look-up table (cf. Fig. 3.1), with which affected voxels for a specific safety margin can be found . The following sections focus on the efficient and effective visualization of safety maps.

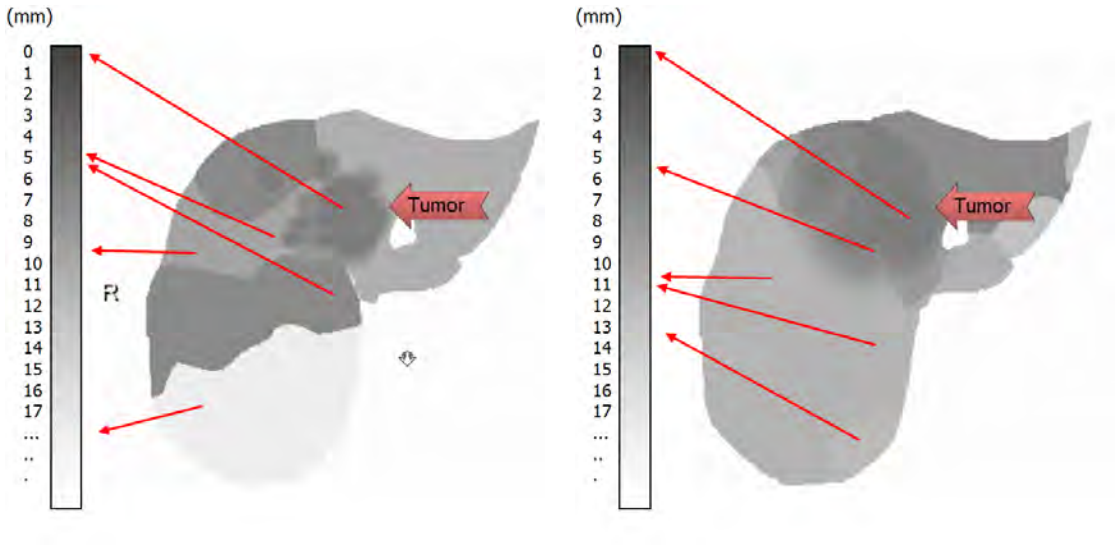

(a) (b)

Figure 3.1: Single axial slices from a safety map for a hepatic vein (a) and a portal vein (b). The grey values encode the width of the safety margin at which each liver voxel will be affected.

3.4.2 Interactive Visualization of Vascular Risk

For the visualization of vascular risk, representations in 2D and 3D are proposed. A 2D diagram shows the relation between affected liver volume and safety margin width. In addition, a 3D view visualizes the vessels and territories that are affected when interactively defining a specific safety margin in the 2D diagram.

2D Visualization of Safety Maps

The quantification of territories at risk as a function of the safety margin is extracted from the safety maps by histogram analysis. To highlight safety margins that are sensitive to small changes, a cumulative histogram is calculated (cf. Fig. 3.2), which visualizes the amount of voxels (y-axis) that are affected for a specific safety margin width (x-axis). However, physicians are not interested in the number of remnant liver voxels, but rather in the fraction of remnant liver volume in relation to the overall liver volume of the patient. Therefore, the **volume-margin function** that visualizes the remaining functional liver volume as a function of the safety margin width is introduced. As distinguished from the cumulative histogram, the volume-margin function is scaled and flipped in the y-direction. Volume-margin functions are calculated for each hepatic vessel of a patient dataset and combined in a **2D risk graph** (cf. Fig. 3.3). A horizontal slider in the risk graph is used to modify the width of a specific safety margin interactively.

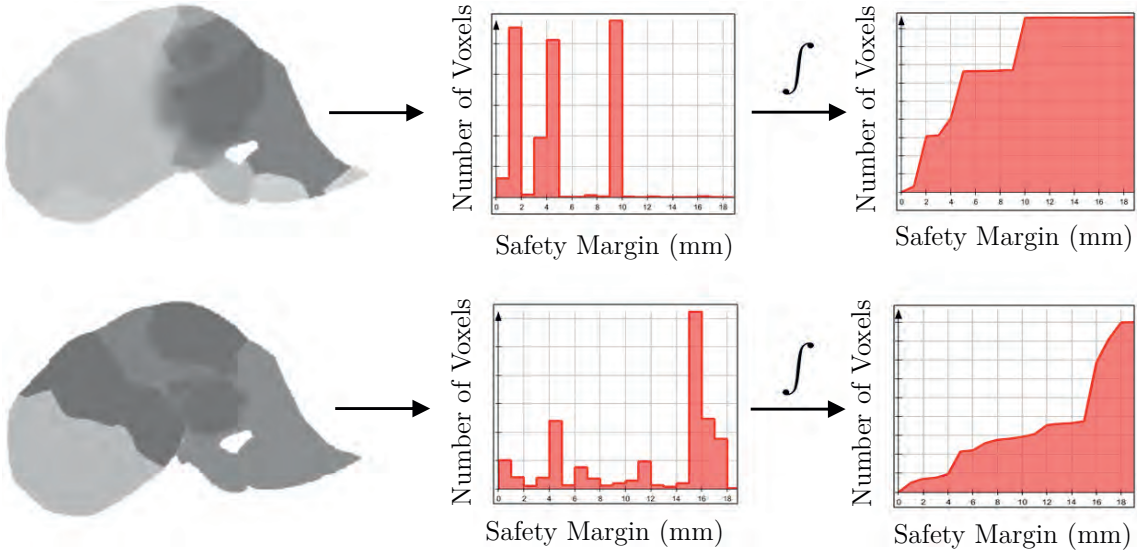

Figure 3.2: Safety maps (left), histograms (center), and corresponding cumulated histograms (right) for portal vein (bottom) and hepatic vein (top)

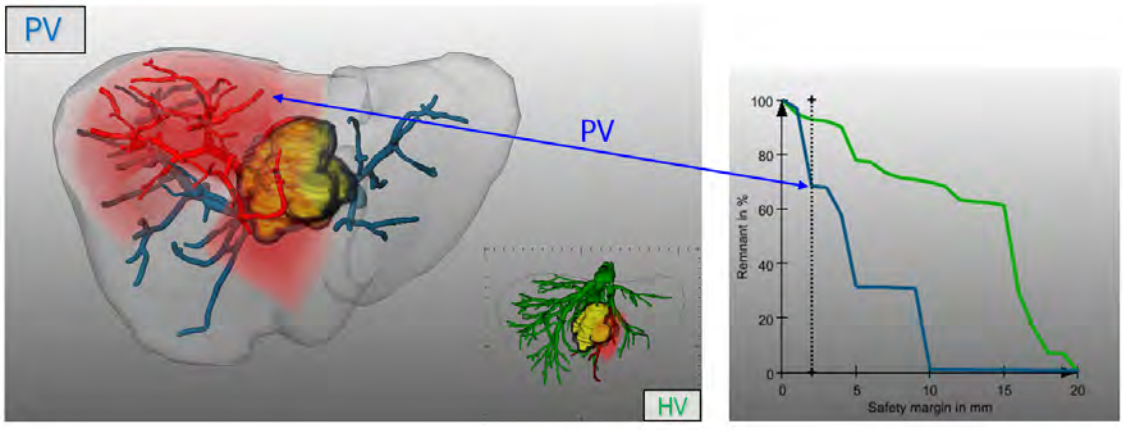

Figure 3.3: Territories at risk of the portal vein (right) that correspond to a discontinuity in the volume-margin function (left). In this case, the discontinuity represents a safety margin of $2mm$, while the affected supply volume adds up to 32% of the total liver volume (same case as Fig. 3.2).

3D Visualization of Safety Maps

The discontinuities in the compromised volume-margin function correspond to the transection of major vessels, setting the dependent territories at risk (cf. Fig. 3.3). Hence, these curve discontinuities directly correspond to sensitive parameters for the surgical planning. Given that the corresponding safety margin is required to guarantee an R0-resection, the surgeon has to decide whether the loss of functional volume in this magnitude can be tolerated.

A fast, interactive 3D visualization of surgical risk with respect to a selected safety margin is essential to evaluate surgical feasibility and to prepare a resection plan. In order to facilitate a quick exploration of risk, the visualization must be rendered with interactive framerates. This update mainly concerns the vessels at risk and territories at risk.

To update the visualization of **vessels at risk** upon modifications of the safety margin, a texture lookup from each vertex of the vascular model into the safety map is performed. A fragment program is used for this purpose. Traversing the graph representations of each vessel is avoided; instead, precomputed safety maps are utilized.

To update the visualization **of territories at risk** upon modifications of the safety margin, a fast, direct volume renderer [Rieder et al., 2011] that applies a transfer function on the precomputed safety map is utilized. Compared to previous approaches, the visualization of territories at risk can be adapted in real-time, which allows fast and detailed exploration of individual anatomic datasets. The volume rendering is mixed with the model-based representation of vascular trees, while affected vessels are labeled in red to highlight the relation between territories at risk and the supplying or draining vessels at risk. Quantitative information, mainly the amount of affected liver volume, enhances the visualization. The described update process is illustrated in Fig. 3.4.

To assess the validity of territories at risk, it is essential that the result can also be displayed in a 2D slice view. For this purpose, the territories at risk are superimposed with the original radiologic data. In addition, the user can generate iso-surfaces of the territories at risk for arbitrary margins to allow platform-independent utilization, e.g., in the operating room.

3.4.3 Combination of Vascular Risk

The combination of risk analyses (consideration of each vascular system) are important to optimize a preoperative resection plan [Lang et al., 2005; Endo et al., 2007]. For the exploration of combined risk, the 2D risk graph is enhanced by volume-margin functions of intersection volume and union volume (cf. Fig. 3.5). The **union** of territories at risk from different vascular systems can be computed by assigning to each liver voxel the minimum value of the both safety maps, while the maximum value is assigned when calculating the **intersection** of territories at risk. This allows for fast comparison of volume-margin functions and their mutual sensitivity of risk.

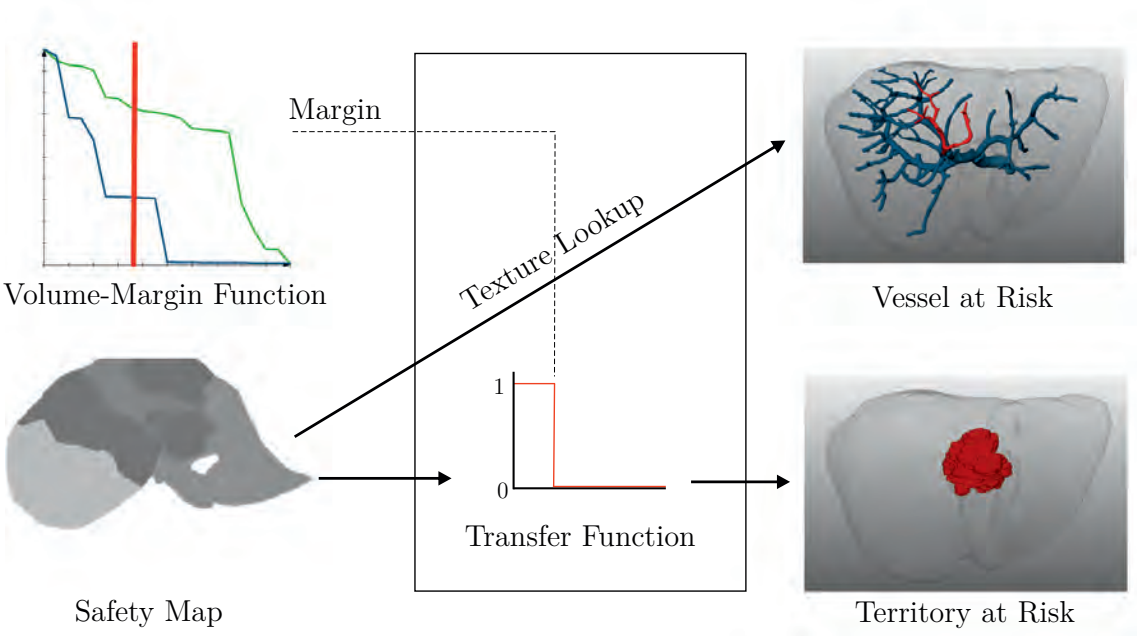

Figure 3.4: Update of vessels at risk and territories at risk upon modifications of the safety margin.

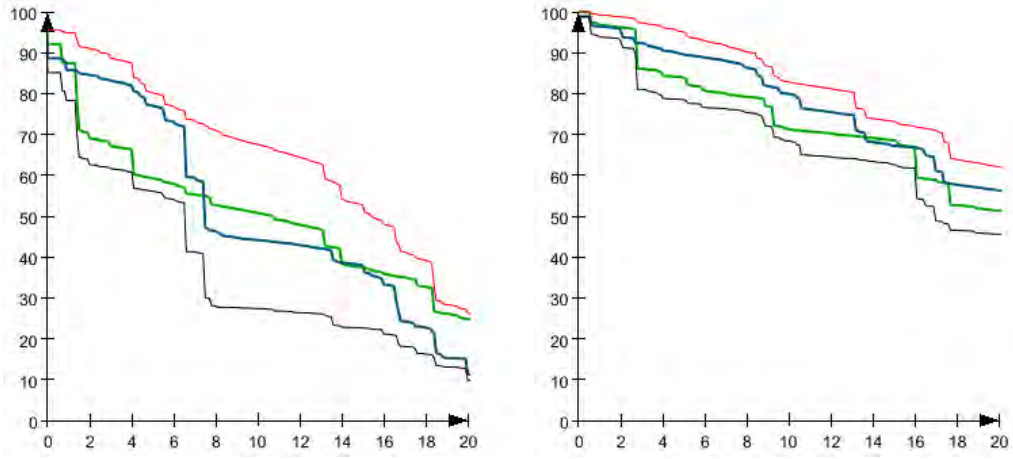

(a) (b)

Figure 3.5: Risk graph containing volume-margin functions of the hepatic vein (green), portal vein (blue), union (black), and intersection (red) for a centrally located lesion (left) and a peripherical tumor (right).

Whereas the combination of vessels at risk in one viewport only requires a simultaneous visualization of all risk-labeled vessel systems, the combination of territories at risk is difficult to visualize, because the risk territories of each vessel system overlap with each other. In order to visualize vascular risk analyses from different vessel systems in a single viewport simultaneously, an integrated **close-up view** with synchronized cameras is applied. Thus, one risk analysis can be focused by the user while providing information about additional risk analyses as context information inside a specified viewport subregion (cf. Fig. 3.6).

To support the definition of virtual resection surfaces trough the liver, a combined visualization of different territories at risk within a single liver model was requested by clinical partners. Therefore, the affected liver volume is classified in segments of:

(1) impaired outflow,

(2) impaired inflow, and;

(3) impaired in- and outflow.

Thus, vascular territories with impaired in- and outflow are visually enhanced, and spatial overlaps of different territories which may result in visual clutter are prevented (cf. Fig. 3.7). Size and location of these three kinds of vascular territories may have an influence on the choice of the safety margin width. In addition, a surgeon could take this additional information into account when defining a virtual resection surface in order to minimize vascular congestion and the formation of necrotic liver tissue.

3.5 Evaluation

To prove whether and how the proposed methods for vascular risk analyses facilitate the process of liver surgery planning, an explorative user study was conducted. The purpose of this study was to compare and analyze the decision making of liver surgeons and radiologic technicians.

This section is structured as follows. First, reference criteria are defined, and the choice of the reference system is discussed. Second, the performed experiments are reported. Third, the used medical datasets and the recruited participants are described.

Evaluation Criteria

To generate evaluable data during the experiments, meaningful evaluation criteria need to be defined. These criteria should provide the basis for an objective comparison between the proposed method and the reference system. Four evaluation criteria were derived from questions that typically arise during the planning of surgical liver interventions.

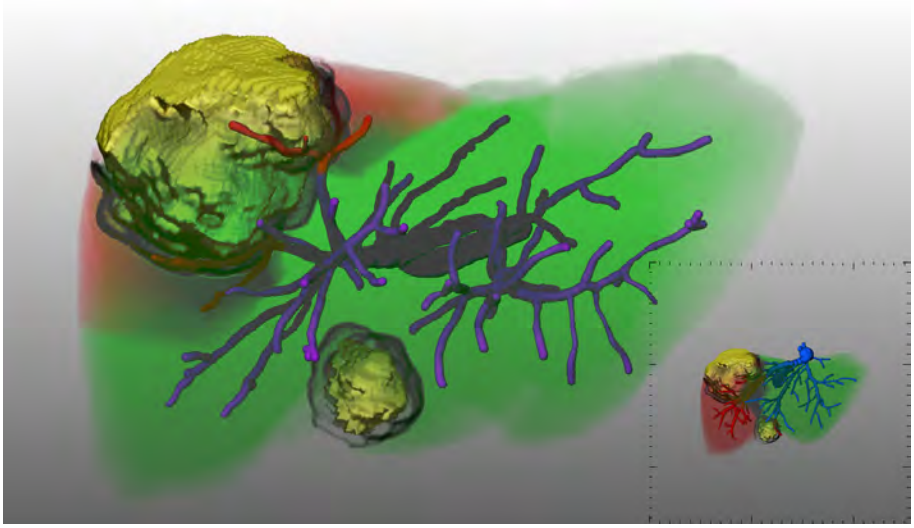

(a)

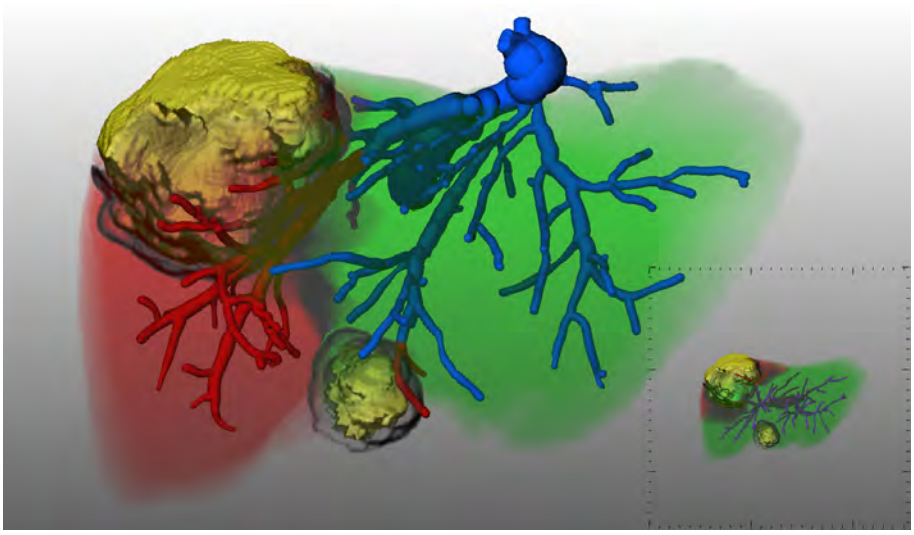

(b)

Figure 3.6: Combination of territories at risk using an integrated close-up view. Affected parenchyma supplied by the portal vein is magnified while the interruption of vascular drainage (hepatic vein) is presented as context information in (a), and vice versa in (b). The width of the safety margin is set to 4 mm.

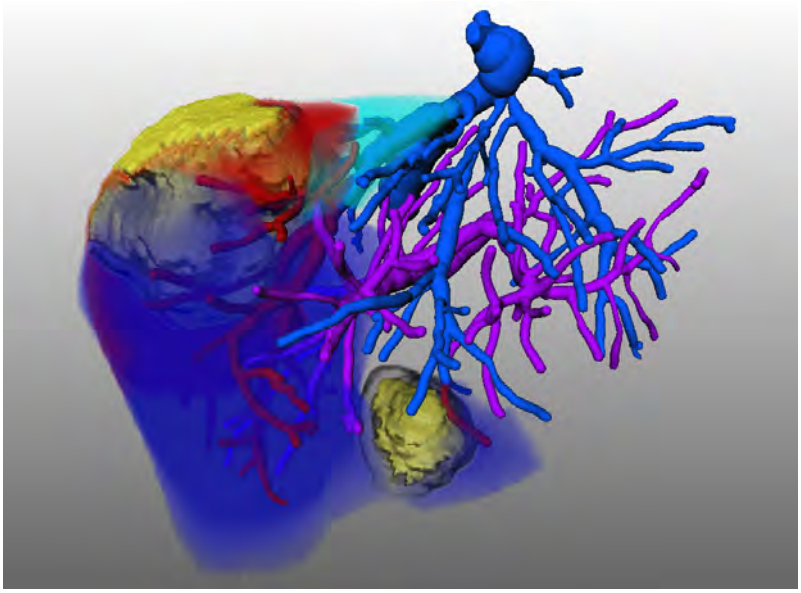

Figure 3.7: Visualization of combined territories at risk, divided into impaired outflow (dark blue), impaired inflow (light blue), and impaired inflow and outflow (red). The width of the safety margin and the underlying patient data are the same as in Fig. 3.6

(R-1) Assessment of **resectability**

(R-2) Choice of **resection strategy**

(R-3) Assessment of **safety margins widths** around tumors

(R-4) Assessment of risk concerning potential postoperative impairment of **inflow and outflow**

These criteria are based on subjective assessments by study participants. In addition, reference criteria which can be derived from this decision-making process are defined:

(R-5) Degree of subjective **confidence** in decision-making

(R-6) Total **time** to analyze a case

(R-7) Amount of **user interaction** per case

Reference System

The choice of a reference system turned out to be non-trivial. It seems obvious to use the methods for vascular risk analysis described by Preim et al. [2002] (cf. Sect. 2.2.2 on page 20). These methods have been frequently used to support planning of liver interventions at MeVis Distance Service (MDS) for more than 10 years [Schenk et al.,

2008]. To test whether the methods represents a good reference system, more than 100 risk analyses generated for clinical use by MDS were compared with the new methods proposed in this work. The comparison of results from both risk analyses showed that the results (territories of risk, vessels at risk, safety margins) differ in most cases only to a limited extent. An interview of radiological technicians working at MDS revealed that much human-computer interaction and experience are required to achieve risk analysis results that are suitable for planning. Many different safety margins often need to be tested to generate an expressive visualization of risk.

In addition, the impact of the risk analyses of Preim et al. [2002] has not yet been thoroughly evaluated. Previous studies [Lamade et al., 2000; Lang et al., 2005] focused on the analysis of surgical decision-making when 3D visualizations of planning data are presented in addition to the 2D radiologic images. Indeed, 3D visualization proved to have an impact on the surgical strategy in selected clinical cases [Lang et al., 2005]. To the knowledge of the author, no study exists which solely evaluated the impact of vascular risk analyses for liver surgery.

Therefore, the risk analysis by Preim et al. [2002] is not taken as a reference system. Instead, a conventional **2D/3D viewer** application for planning data is utilized (cf. Fig. 3.8). While the 2D viewer visualizes the radiologic slice data, the 3D viewer visualizes the 3D models of vascular structures (hepatic vein, portal vein), the liver surface, and tumors. In addition, the application provides **measurement tools** for the assessment of distances within the dataset.

Experiment Design

The study consisted of two separate experiments, called experiment A and experiment B. Each participant completed both experiments. In **experiment A**, the reference system as described above was presented. In **experiment B**, the utilized software application contained all functionalities that were included in the reference system. In addition, a volume-margin function of the dataset was visualized together with an interactive visualization of vessels at risk and territories at risk (cf. Fig. 3.9).

In each experiment, participants were asked to analyze six CT datasets of the liver. The same six dataset were used in each experiment. For each dataset, surgeons had to perform specific planning tasks by using the software assistant described above. These **planning tasks** consisted of:

- Determination of a virtual resection surface
- Selection of critical vessel structures which should be preserved
- Selection of potential areas of impaired inflow and outflow

In addition, participants completed a **questionnaire** for each dataset. The questionnaire directly addresses the comparison criteria defined above and can be found in the appendix (page 157). In the header of each questionnaire, a report on diagnostic findings was given and the desired postoperative liver volume was specified ($> 35\%$).

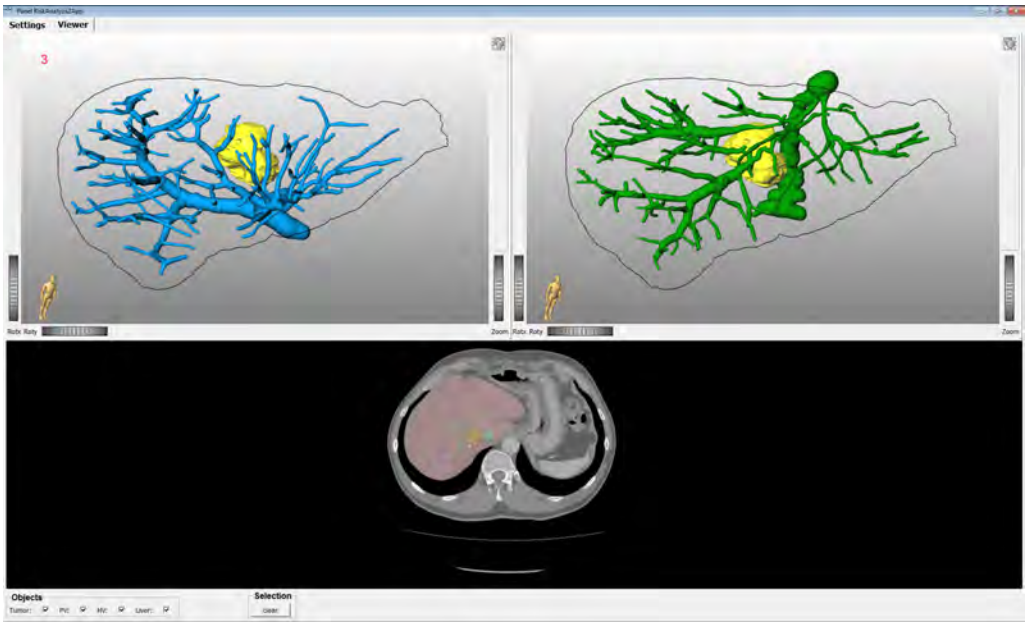

Figure 3.8: Screenshot of the reference system used in experiment A. The 3D viewers on the upper part show the portal vein (left) and hepatic vein (right). The 2D viewer below enables the exploration of the radiologic data.

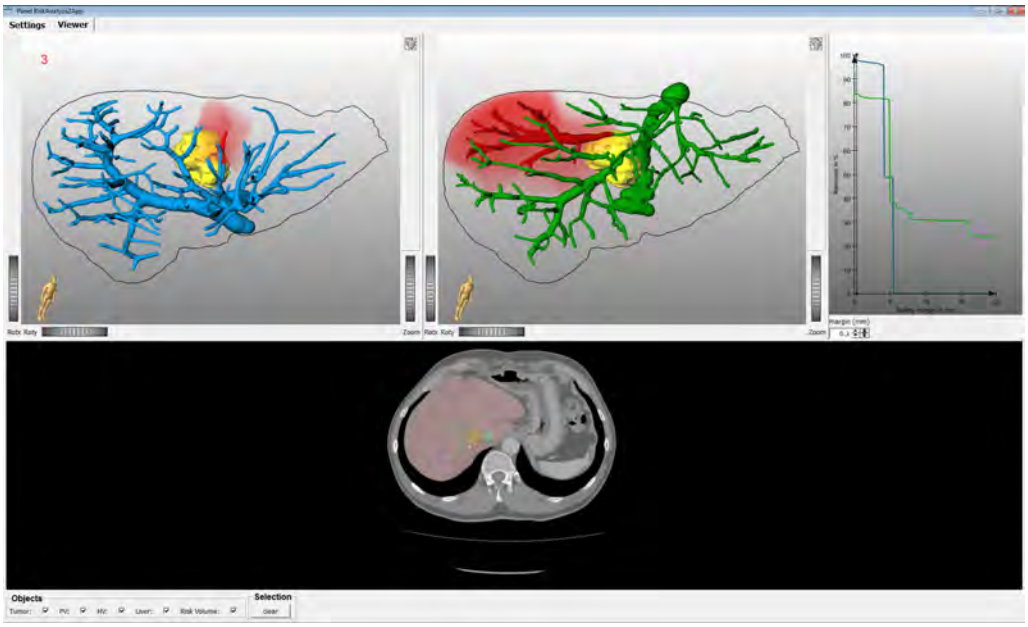

Figure 3.9: Screenshot of the software application used in experiment B. The graphical user interface is identical, except that it contains the proposed risk analysis. The volume-margin function is presented in the upper right viewport, territories at risk in the upper left and upper middle viewport, and the radiologic data can be accessed in the lower viewport.

Each experiment was conducted as follows. First, participants were informed that the experiment takes between 60 and 90 minutes and that the time is measured during the experiment. Second, the software application was presented and its graphical user interface was explained. Third, a training dataset was loaded and participants conducted the planning tasks for this dataset and filled out a questionnaire. The test supervisor ensured that all questions and planning tasks were understood. Finally, five test datasets were loaded in random order. Participants were informed that the experiment starts and that time is measured from now on. Analogous to the training phase, participants performed surgical planning tasks and filled out a questionnaire for each dataset. Verbal comments were transcribed during the experiment.

The experiments were performed in the context of two clinical workshops at Asklepios Clinic Barmbek, Hamburg, Germany (cf. Fig 3.10). Because not all surgeons could take part at both workshops, several separate meetings took place. The distance between experiment A and B was always at least 3 weeks in order to minimize memory effects.

Medical Datasets

The case database consisted of six abdominal CT datasets (1 training dataset, 5 test datasets). For each dataset, 3D models of the liver, hepatic vein, portal vein, and intrahepatic tumors were generated. The test datasets were selected according to the following criteria:

- Presence of colorectal liver cancer
- Solitary metastases that are located adjacent to mayor hepatic vessels
- No presence of cirrhosis

Screenshots of the 3D models that were used in the context of the study are shown Fig. 3.11.

Participants

Medical knowledge and experience in liver surgery planning are necessary to perform the planning tasks and to give meaningful answers in the questionnaire. For that reason, the subject pool consisted of 10 liver experts (3 females, 7 males), including 4 chief physicians, 1 senior physicians, 2 assistant physicians, 3 radiology technicians. The mean age of the participants was 41.45 years ($\pm$ 4.7). The mean number of years of surgical experience were 15.6 ($\pm$ 5.3), excluding the radiology technicians.

3.6 Results

Comparison of given assessments concerning patient **resectability** (Question 2) revealed that participants showed better agreement of answers in experiment B (cf.

Figure 3.10: Workshop with liver surgeons at Asklepios Clinic Barmbek, Hamburg, Germany. The photo shows four participants and four test supervisors.

Fig. 3.12). In addition, the results show that participant's decisions were much more cautious and less optimistic when using the risk analysis. For example, in case 1, two surgeons who rated a patient as "resectable" in experiment A changed their decision to "non-resectable" in experiment B. Furthermore, all participants who rated a patient as "resectable with a large safety margin" ($> 5mm$) in case 1, 3 and 5 changed their decision to "resectable with a small safety margin" ($< 5mm$). Although there exist no significant differences between experiment A and B ($p > 0.05$, Wilcoxon test), the results indicate that the proposed vascular risk analysis enhances the awareness of surgical risk during in the planning stage.

Figures 3.13 - 3.17 illustrate the changes in the **resection strategy** that were made in the study. The amount and direction of changes reveal that the risk analysis has different magnitudes of influence on surgical decision-making that depend, among other factors, on the selected medical dataset. For cases 1 and 2, the changes show a clear trend towards the choice of smaller resections when using the risk analysis. The same trend, to a lesser extent, can also be observed for cases 4 and 5. For case 3, the majority of subjects did not change their resection strategy when using the risk analysis.

The analysis shows that subjects changed their resection strategy in many cases. This is unsurprising, because it can be expected that when repeating experiment A (or B) several times with the same participants, the preferred resection strategy will not be constant (test-retest variability). However, the changes observed in this study follow a clear trend towards the choice of smaller resection volumes in case the risk analysis is available. This supports the above statement that the proposed methods enhance the awareness of surgical risk.

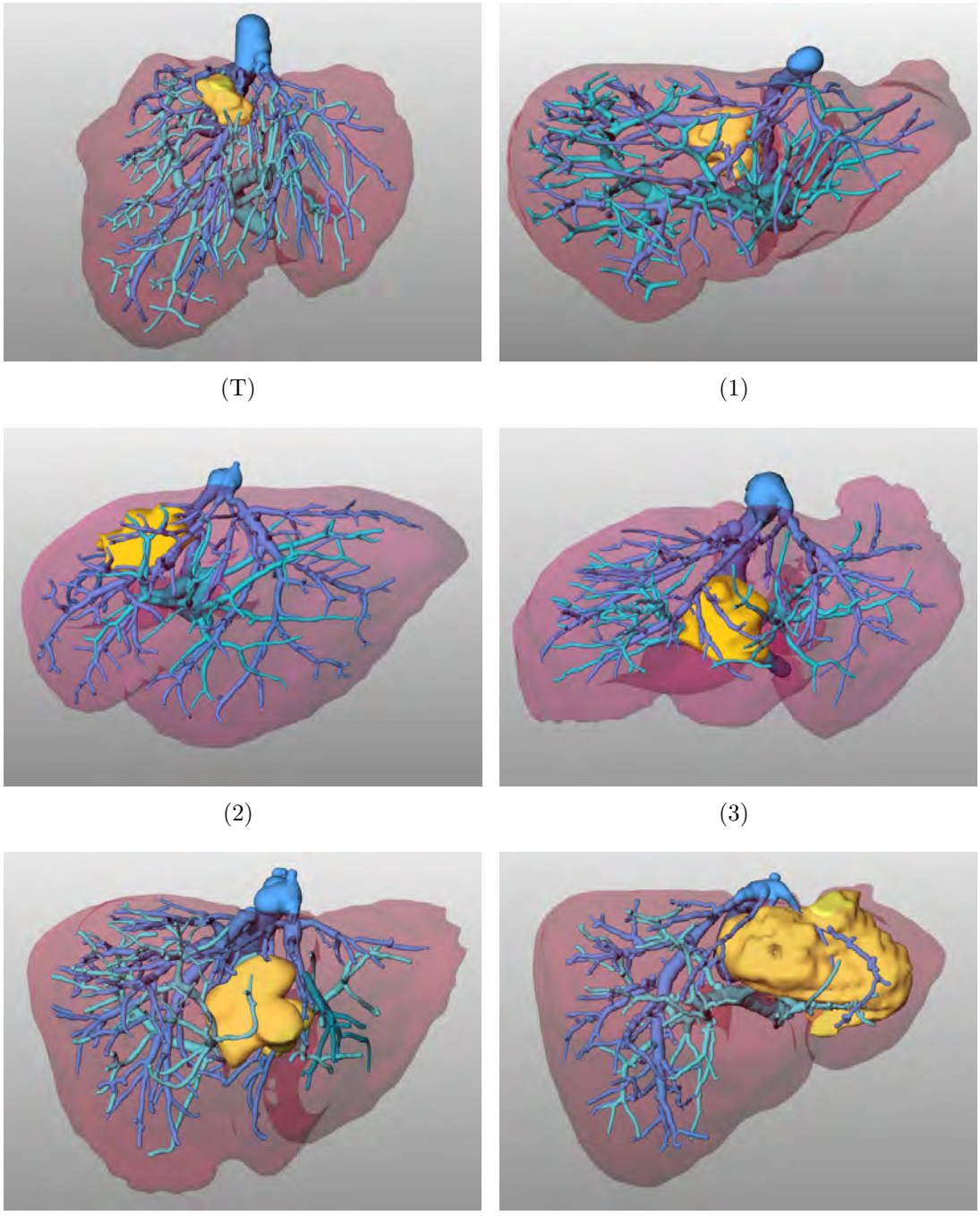

Figure 3.11: Selected datasets: Case T shows a visualization of the training dataset with a peripherally located metastasis close to the MHV. Case 1, 3, and 4 show datasets with centrally located liver metastases (yellow). In case 2, the metastasis is located in the right liver lobe, while in case 5 it is located in the left liver lobe.

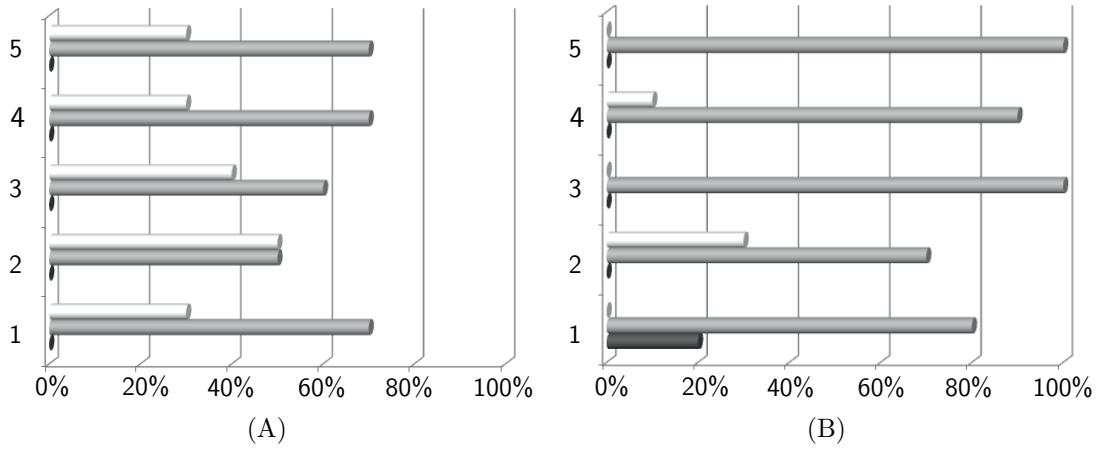

Figure 3.12: Assessed respectability for cases 1-5 in experiments A and B (white = "resectable with a large safety margin ($> 5mm$)", light grey = "resectable with a small safety margin ($< 5mm$)", dark grey = "not resectable").

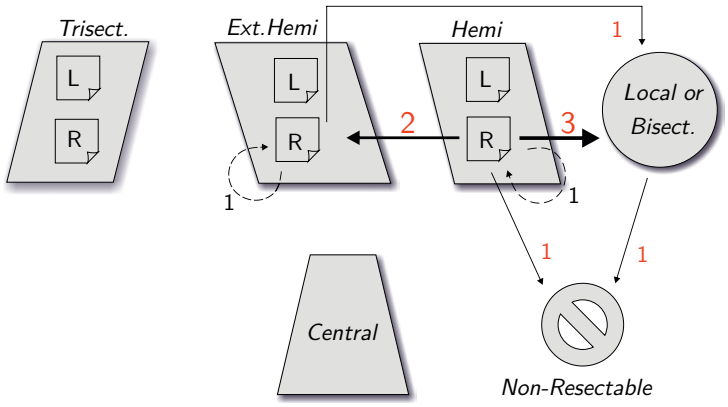

Figure 3.13: Changes in resection strategy for **case 1**. While a right hemihepatectomy was the most frequently chosen resection strategy in experiment A, 6 participants changed their strategy in experiment B. The trend favors local resections (0/4) and rejecting surgical resection (0/2). These changes indicate that participants underestimated risk in experiment A and prefer a smaller resection volume in experiment B.

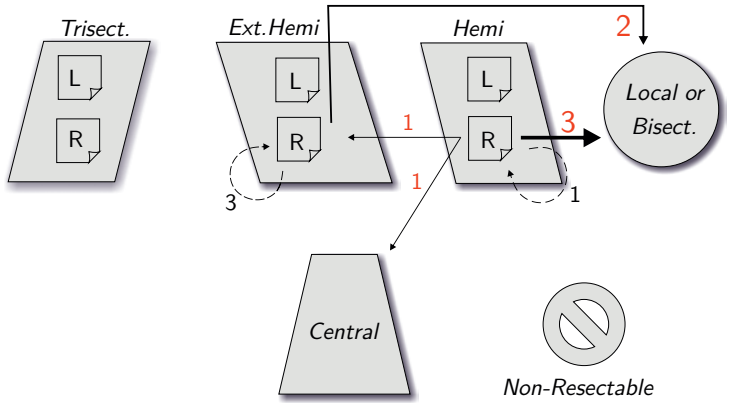

Figure 3.14: Changes in resection strategy for **case 2**. Participants show a similar trend such as in case 1. Right hemihepatectomy and extended right hemihepatectomy were found to be the most appropriate resection strategies in experiment A. However, whereas local resections were not taken into account in experiment A, five subjects chose a local resection. Analogously to case 1, these changes indicate that participants underestimated risk in experiment A and prefer a smaller resection volume in experiment B.

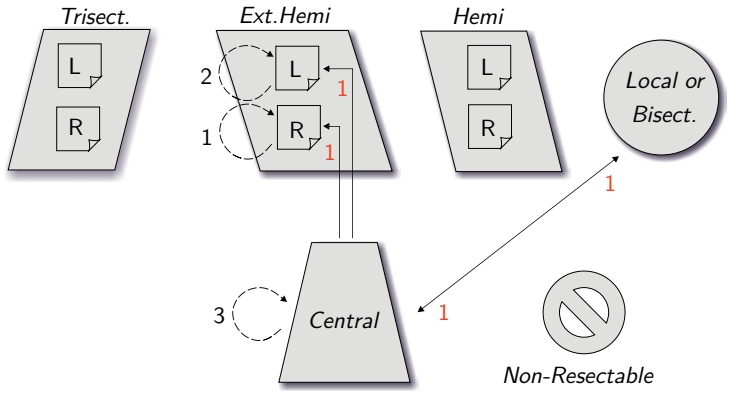

Figure 3.15: Changes in resection strategy for **case 3**. The majority of subjects did not change their resection strategy. No significant trend can be observed for this case.

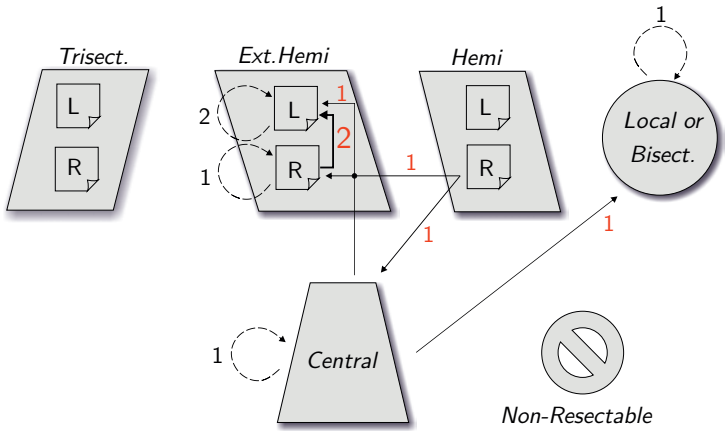

Figure 3.16: Changes in resection strategy for **case 4**. Several trends can be observed. First, the extended left hemihepatectomy (2/5) is the strategy most subjects preferred in experiment B, in contrast to experiment A. Second, all subjects who chose a right hemihepatectomy in experiment A changed their opinion in B. Overall, the changes indicate a trend towards smaller resection (right lobe → left lobe , central → local) when using the risk analysis.

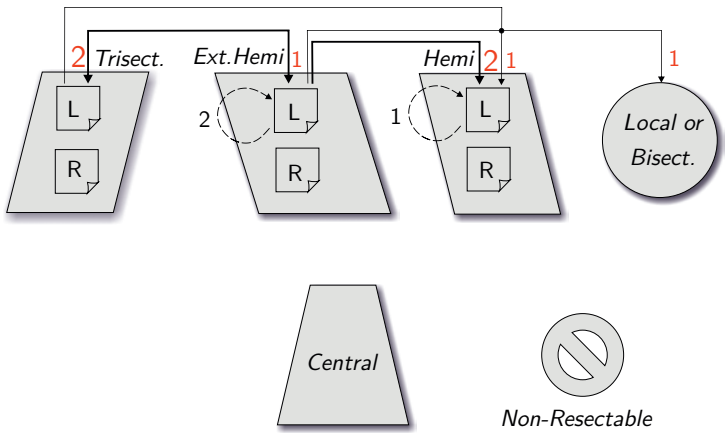

Figure 3.17: Changes in resection strategy for **case 5**. Although the strategy selections and changes of subjects seem to be inconsistent at first glance, there is a clear trend towards smaller resection volumes. 5 subjects choose a resection with a smaller resection volume than in experiment B.

The analysis of selected **safety margins widths** showed that the variation of values was lower for all cases in experiment B (cf. Fig. 3.18). Thus, subjects agree more when the safety margin is chosen with the proposed risk analysis (experiment B) than with 3D measurement tools (experiment A). A selected safety margin width depends on the chosen resection strategy. Thus, the measured trend to choose smaller resection volumes in experiment B seems to have an influence on the width of safety margins, or vice versa. Statistically significant differences were not found ($p > 0.05$, Wilcoxon test).

The comparison of **times** taken to complete the test tasks (cf. Fig. 3.19) revealed that there are no significant differences between experiments A and B ($p > 0.05$, Wilcoxon test). However, the way surgeons used the provided 2D/3D visualization techniques was different in each experiment. In experiment A, the CT slices were more often accessed than in experiment B (cf. Fig. 3.21). The numbers are many times higher in experiment A, especially for cases 1 and 2. An analysis of user interaction during the experiments also showed that the amount of interaction with the volume margin function was highest in cases 1 and 2 (cf. Fig. 3.20). This relation indicates that interaction with the 2D slice data is required less when the risk analyses is extensively used.

Several surgeons stated verbally that the risk analysis is especially helpful in case 1 (five surgeons), case 2 (three surgeons), and case 5 (two surgeons), because the potential areas of risk are hard to identify with 3D planning models or 2D slices. However, three surgeons noted that the territories of risk visualized for the first branching of the left portal vein in case 5 is misleading, because this part of the vessel could be saved intraoperatively by applying a special cutting approach and would therefore not represent a risk for the patient. Similar comments were also made for the inferior vena cava (extrahepatic vein with inflow of the hepatic vein). Participants suggested integrating a function that allows excluding specific vessels from the risk analyses.

During the experiments, participants were asked to select potential areas of postoperatively **impaired inflow and outflow** and to rank the potential risk in the questionnaire on an ordinal scale from 1 to 5. The analysis showed that the mean assessed risk for potential impaired outflow was higher for all cases in experiment B (cf. Table 3.1). The mean assessed risk for potentially impaired inflow was higher in three cases, equal in one case, and lower in one case (cf. Table 3.2). In addition, the standard deviation of given answers was smaller in the majority of cases for experiment B. Statistically significant differences were not found ($p > 0.05$, Wilcoxon test).

There are several reasons why these subjective assessments are of limited validity. First, the areas of inflow and outflow strongly depend on the selected resection strategy. Because the selection of resection strategies was not homogeneous within each experiment, the potentially impaired perfusion correlates with the selected resection strategy. Second, an analysis of user interaction revealed that the risk analysis has received relatively little attention when answering this question. Thus, most participants estimated risk of impaired inflow and outflow without directly

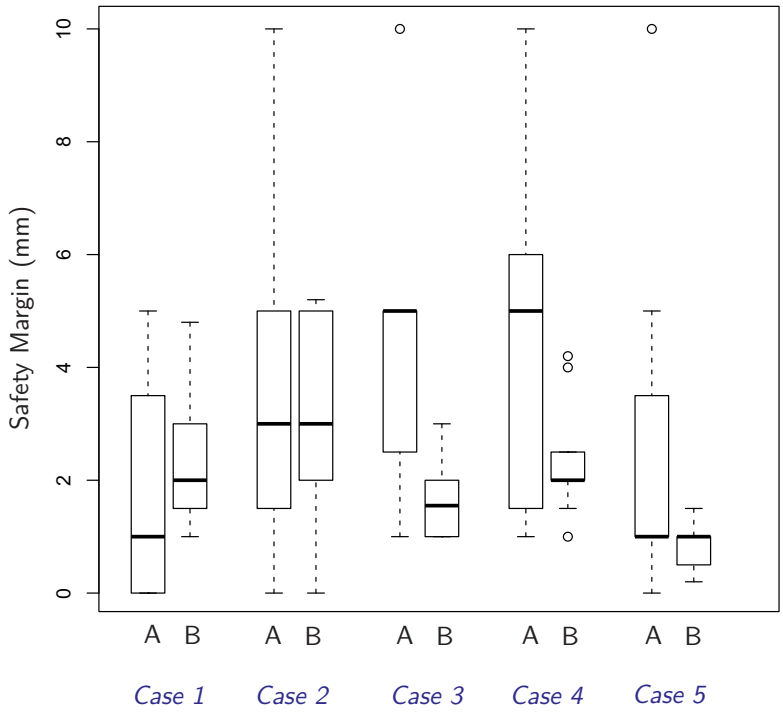

Figure 3.18: Selected **safety margin** widths for cases 1-5 in experiments A and B.

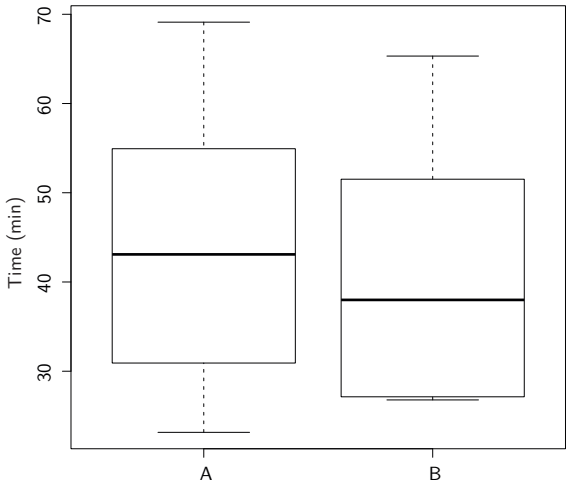

Figure 3.19: **Time** needed by participants for the completion of test tasks in experiment A and experiment B. The antennas in the box plot visualize maximum and minimum values. Data points that exceed the interquartile range more than one and a half time are defined as outliers.

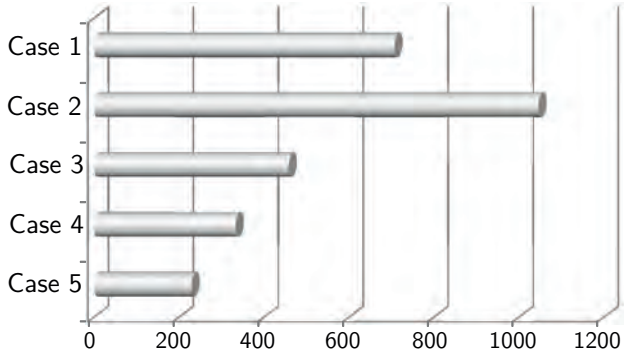

Figure 3.20: Number of values from the volume-margin function that were accessed in experiment B.

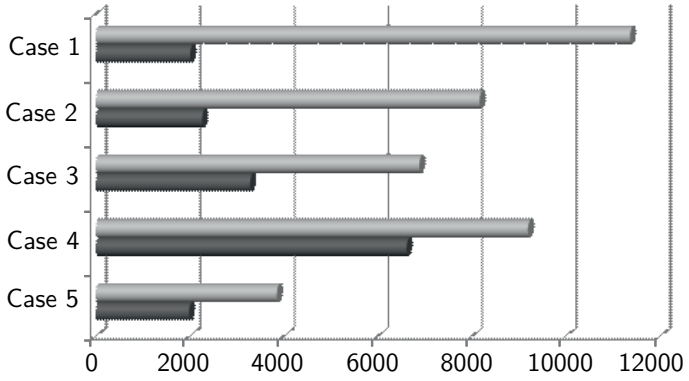

Figure 3.21: Total number of CT slices that were accessed by participants in experiment A (light grey) and experiment B (dark grey) for datasets 1-5.

using a visualization of territories of risk. Third, the question was unambiguous. Participants had a different understanding of "potential" risk. Therefore, the results concerning this question need to be handled with care.

The questionnaire asked participants to rank their **confidence** in decision-making concerning questions 2, 3, 5, and 6 on an ordinal scale from 1 to 4 (1 = very sure, 2 sure, 3 = less sure, 4 = not sure). An analysis of the data revealed that there exist no significant differences between experiment A and B ($p > 0.05$, Wilcoxon test). However, the mean values indicate that participants felt more confidence in experiment A (cf. Table 3.3). An interesting observation in this context was that several participants mentioned that it is even more difficult to make a final decision when considering the additional information provided by the risk analysis. Two surgeons mentioned that they selected "less sure" or "not sure" in experiment B because they would prefer to discuss the resection strategy with colleagues before making a final decision. Such verbal comments were not made in experiment A.
The results of the user study can be summarized as follows:

- The risk analysis enhances the **awareness** of surgical risk in the planning stage (assessment of resectability, determination of resection strategy)
- Subjects prefer **smaller resection volumes** in case the risk analysis is available.
- Subjects agree more on the **safety margins** width in case the risk analysis is utilized.
- Subjects do not take more **time** when analyzing a dataset using the risk analysis. In this context, 2D slices were less accessed in case the risk analyses were available.
- A reliable statement on risk assessment of postoperative **inflow and outflow** could not be made for this study.
- **Confidence** in decision-making is not higher when using the risk analyses.

Case	A	B
1	3.9 (±1.30)	3.5 (±1.13)
2	4.6 (±0.67)	3.4 (±1.64)
3	3.5 (±1.57)	2.3 (±0.82)
4	2.9 (±1.51)	2.6 (±1.07)
5	4.0 (±1.41)	3.1 (±1.10)

Table 3.1: Assessed risk regarding impaired **outflow** in experiment A and B (mean, σ). The assessments were made on a scale from 1 to 5, where 1 = "high risk" and 5 = "no risk".

Case	A	B
1	3.5 ($\pm 1,36$)	3.5 ($\pm 1,01$)
2	3.4 ($\pm 1,57$)	3.9 ($\pm 1,44$)
3	4.0 ($\pm 1,26$)	3.7 ($\pm 1,41$)
4	4.0 ($\pm 1,37$)	3.0 ($\pm 1,24$)
5	3.4 ($\pm 1,69$)	2.6 ($\pm 1,07$)

Table 3.2: Assessed risk regarding impaired **inflow** in experiment A and B (mean, σ). The assessments were made on a scale from 1 to 5, where 1 = "high risk" and 5 = "no risk".

Question	A	B
2 (Resectability)	1.9 (± 0.63)	2.2 (± 0.75)
3 (Resection Surface)	2.0 (± 0.68)	2.3 (± 0.62)
5 (Resection Strategy)	2.0 (± 0.71)	2.2 (± 0.77)
6 (Safety Margin)	2.3 (± 0.63)	2.4 (± 0.63)

Table 3.3: Subjective **confidence** of participants based on a scale from 1 to 4 (1 = very sure, 2 sure, 3 = less sure, 4 = not sure). The confidence assessment was given after participants answered questions 2, 3, 5, and 6 in the questionnaire.

In conclusion, the results show that the methods proposed in this work facilitate the process of liver surgery planning.

3.7 Discussion and Conclusion

New methods for risk analysis in liver surgery planning have been presented and evaluated in the context of this work. The methods enhance approved methods for oncologic risk analysis [Preim et al., 2002] by allowing interactive feedback about the effect on the associated disruption of vascular perfusion. Previous studies in the field of liver surgery planning evaluated only the impact of 3D visualization [Lamade et al., 2000] and virtual resection planning [Lang et al., 2005]. Thereby, the planning data was always evaluated against a presentation of 2D CT images. The study performed in this work investigated the **usefulness** of model-based risk analysis for liver surgery planning. The results of the study show that the proposed risk analysis influences important planning decisions for liver surgery.

An interesting result of the study is that **confidence in decision-making** was not significantly higher when using the risk analysis. The mean confidence values are even higher without the risk analysis. There are several reasons for this result. First, all participants were quite familiar with the 3D planning models and the exploration

of 2D slice data available in experiment A. Thus, the level of trust in the new risk analyses was probably lower than in the established 2D/3D exploration techniques. This might have had an effect on the level of confidence. It is expected that the level of confidence will increase after subjects are more familiar with the approach. Second, the additional information in experiment B enhanced the awareness of surgical risk and could explain why participants rated this as less confident. Thus, the subjective confidence in decision-making might correlate with risk awareness of subjects.

The mean **time** to complete the planning tasks was not significantly lower when using the risk analysis. It would be interesting to measure if this were also true if participants received more training. Another reason for this could be the increase in risk awareness that opened up new questions during the planning process. Thus, additional time was required. It is also assumed that the high difficulty of the selected cases influenced the confidence of participants and the measured time.

The methods have been evaluated under controlled conditions within two separate experiments. For the future, it would be desirable to prove the benefit of the proposed risk analysis by evaluating them in clinical routine. This would require a **clinical study** with a randomized decision regarding the utilization of the results of the risk analysis and the subsequent evaluation of clinical criteria, such as complication rate, tumor recurrence, and blood loss [Schenk et al., 2008]. In addition, evaluation criteria concerning the surgical decision making, as addressed in this chapter, could be utilized. In this context, factors, such as the anamnesis of the patient, degree of liver disease, experience of the surgeon, and surgical technique need to be carefully considered [Schenk et al., 2008]. In addition, such evaluation study could shed light on the transfer of surgical plans to the actual patient. To achieve this, the preoperative made decisions and the final preoperative resection plan could be compared with the intraoperatively performed resection surface. Therefore, the performed resection needs to be measured intraoperatively, e.g., by using a surgical navigation system, or acquired using postoperative imaging such as proposed in Beller et al. [2008].

The question about the **accuracy** of the risk analysis arises in the context of this work and needs to be addressed. The safety map, which represents the basis of the proposed methods, assigns liver voxels to certain sections of the vascular trees in the liver. Anatomically, a scaling problem exists because sections of the vessel trees that actually drain or supply a liver territory are usually not traceable in the image data because they are too small. Choosing a model-based approximation is difficult because the inflow and outflow is realized by complex branching structures whose formation process is not fully understood. A nearest-neighbor distance model to approximate liver territories was chosen in this work; studies on human corrosion casts revealed that this model assumption provided sufficient accuracy for liver surgery planning [Selle et al., 2002]. A challenging future task would be to the further evaluate this model assumption in clinical studies.

Because the accuracy correlates significantly with the quality of the underlying image data, reliable predication of liver tissue at risk must consider the quality of the vessel segmentation (branching generation). Therefore, a visualization of data uncertainty would represent a valuable extension of the proposed risk analysis.

The **liver function** of territories at risk is not considered in this work. It mainly depends on the status of the liver parenchyma. This status varies within the parenchyma and is related to clinical parameters, such as the actual stage of liver damage by chemotherapy or the stage of chronic liver disease. To make a more precise and reliable statement about the potential risk of liver failure, the visualization of territories at risk should include functional information. This information could be estimated on the basis of functional liver tests [Asakuma et al., 2007; Stockmann et al., 2010; Graaf et al., 2010] or by applying MR imaging in combination with liver specific contrast agents [Yamada et al., 2011; Cho et al., 2011]. Therefore, the functional information needs to be integrated in computational models for vascular risk analysis and virtual liver resection planning. This would provide more reliable decision support, especially for patients with impaired liver function.

In conclusion, this work contributes to computer-assisted liver surgery planning. It lays a basis for further evaluations in the context of vascular risk analyses and indicates promising fields for further research.

3.8 Outlook: Non-Uniform Safety Margins

The methods presented so far are based on the assumption that the safety margin around tumors always has a uniform width. This issue was criticized by several participants of the performed evaluation study (cf. Sect. 3.6). They mentioned that safety margins cannot be assumed to be uniform in all cases. According to their comments, the theoretical assumption that the distances between tumor and vessel are static could not be transfered into surgical reality. They suggested a separate analysis of specific vessels in the planning phase.

A method to determine safety margins with non-uniform widths is introduced in the following. Therefore, critical sections within the vascular trees of the liver are detected automatically. By arranging these critical sections in a sorted table, the surgeon may choose whether sections should be included or excluded from resection.

Detection and Analyses of Critical Vessel Sections

The detection and analysis of critical vessel sections is based on a directed, acyclic vessel graph $G = (N, E)$, where nodes N represent furcations and edges E represent branches. Assuming that a safety margin with a uniform width w is already defined with existing methods, this work proposes to analyze the vascular structures within this safety margin in detail.

The result of the vascular analysis described here provides detailed information about hepatic vessels that "collide" with safety margins with uniform widths $\leq w$. Within the range $[0, w]$ safety margins are analyzed in discrete steps using the stepsize s that can be defined by the user or set depending on the voxel size of the image dataset. In each iteration, vessels at risk are calculated for the current safety margin width d. The affected liver volume V_d for a safety margin d is approximated on the

basis of a Voronoi decomposition (nearest-neighbor distance model) as described in [Selle et al., 2002]. In addition, V_{d-s} is defined as the affected liver volume for a safety margin width $d-s$. To identify critical vessel sections, the intersection volume V_{diff} between V_d and its predecessor V_{d-s} is calculated. Thus, vessel sections that may cause a loss of liver volume can be located and quantified.

In case V_{diff} is larger than a given volume threshold t_{Vol}, the first skeleton voxel (starting from root of G) of the affected subtree is labeled as the **start point** of the critical vessel section. The **end point** of the critical vessel section is defined by the next skeleton in the subtree that shows a minimal distance to the tumor $> d$ (or the last skeleton if no skeleton fulfilling this requirement is found). Note that a critical vessel section can contain multiple end points. By this means, vessel sections whose transection causes significant loss of functional liver volume are detected. Quantitative information about critical vessel sections, such as V_{diff} and d are stored in a table for further processing (described in the next subsection).

If the affected subtree contains more than one critical vessel section, it may be important to know if a detected critical vessel section depends on other critical vessel sections. Two special cases are considered. First, a critical section on a lower tree level C_{low} may show a larger distance d to the tumor than a critical section C_{up} on an upper tree level (cf. Fig. 3.22a). In that case, the surgeon may want to choose different distances or want to preserve C_{up}. In addition, the algorithm must consider the dependency between these critical sections, for example, by forcing the user to preserve C_{low} while discarding C_{up}. In the second case, a critical section C_{low} may show a smaller minimal distance d to the tumor than a critical position C_{up} (cf. Fig. 3.22b). In that case, the surgeon may preserve both critical sections using different distances or, alternatively, decide to preserve only C_{up}.

Algorithmically, the subtree is traversed in level order, beginning at the root. Thereby, critical vessel sections located in the highest tree level are labeled as first order sections, while dependent critical sections are labeled as second, third, and fourth order sections, and so on. The algorithm for the detection and analysis of critical vessel sections can be summarized as follows:

```
d = s
While (d ≤ w)
        For (all affected subtrees)
            Compute V_d, V_{d-s}
            V_diff = V_d − V_{d-s}
            If (V_diff > t_Vol)
                Label start and end position of section
                If (additional critical section)
                    Label all sections depending on tree hierarchy
        d = d + s
```

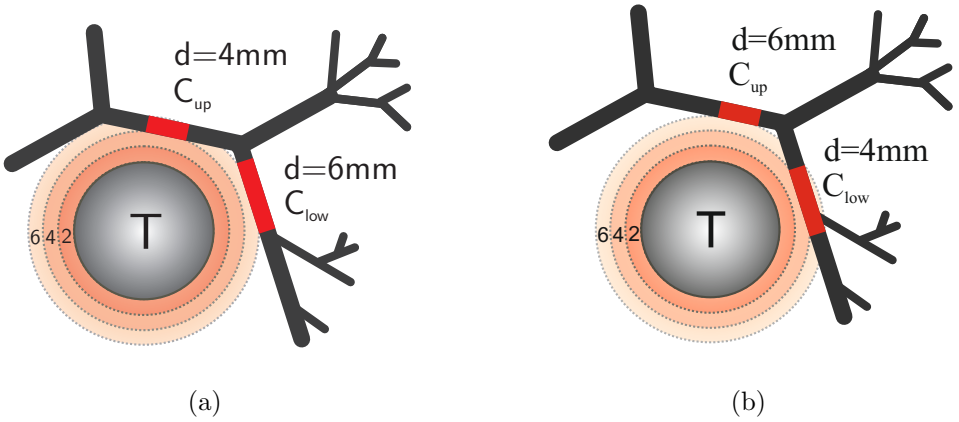

Figure 3.22: Special cases that have to be considered if the affected subtree contains more than one critical vessel.

From Uniform to Non-Uniform Safety Margins

The algorithm described above provides a set of critical vessel sections along with important attributes such as the amount of affected liver volume, distance to the tumor, and type of vessel. To define a non-uniform safety margin, planning either preservation or resection must be decided for each critical section. Because this decision may be significant for the patient prognosis and depends on many medical factors such as anamnesis of the patient and surgical technique, this work proposes to allow the surgeon to make these important decisions. Therefore, each critical section is arranged in a **risk table** as shown in Fig. 3.23a. Each row of the risk table represents a critical vessel section that was identified with the methods described above. The checkboxes in the first column allow selecting or deselecting the vessel section from resection. The second column visualizes the minimal distance of this vessel section to the tumor, i.e., the possible margin width at this location. The third column shows the vessel type (also visualized through the small icon in the first column), and the fourth column represents the amount of affected liver volume. The volume is given in *ml* and percentage of the total functional liver volume.

The user chooses which critical section to preserve by activating the associated check box in the risk table. Therefore, visualization and interaction techniques that allow quick assessment of vessel sections are provided (cf. Fig. 3.24). By selecting a critical section in the risk table following the 3D position of the vessel section is highlighted in the 3D visualization using contrasting color, and the associated liver volume at risk is calculated and visualized . To allow a fast update of the affected liver volume for a selected vessel section, a precomputed 3D texture (similar to the safety map introduced in Sect. 3.4.2) is exploited. This 3D texture assigns a unique vessel section ID to each liver voxel. Thus the affected liver voxels for a specific vessel section can be accessed using a transfer function on the 3D texture, and interactive framerates can be achieved.

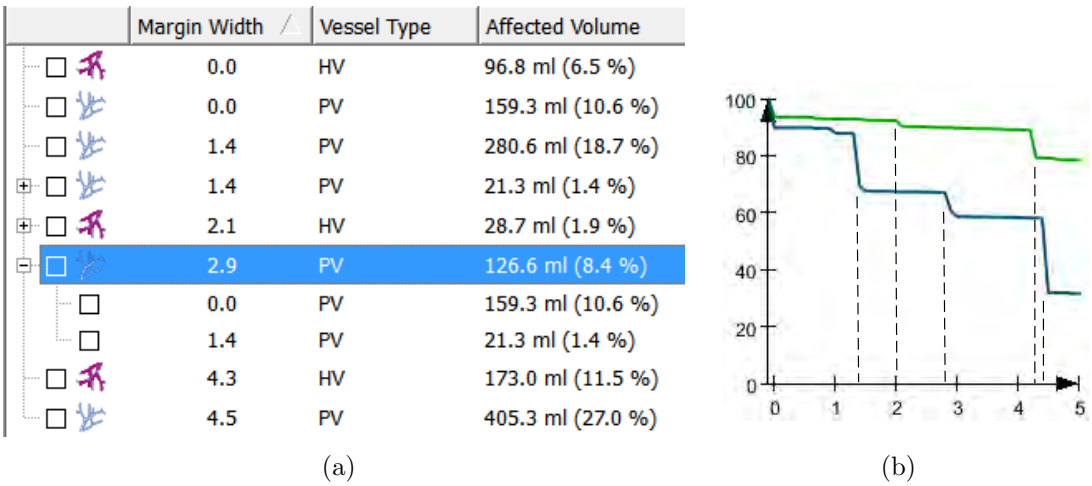

Margin Width	Vessel Type	Affected Volume
0.0	HV	96.8 ml (6.5 %)
0.0	PV	159.3 ml (10.6 %)
1.4	PV	280.6 ml (18.7 %)
1.4	PV	21.3 ml (1.4 %)
2.1	HV	28.7 ml (1.9 %)
2.9	PV	126.6 ml (8.4 %)
0.0	PV	159.3 ml (10.6 %)
1.4	PV	21.3 ml (1.4 %)
4.3	HV	173.0 ml (11.5 %)
4.5	PV	405.3 ml (27.0 %)

(a) (b)

Figure 3.23: (a) Risk table for the determination of non-uniform safety margins and (b) corresponding risk graph. The discontinuities of the volume-margin functions in the risk graph directly correspond to entries in the risk table. Note that the risk table enables a more detailed visualization of the risk distribution, e.g., two portal venous risk volumes are presented at a safety margin of 1.4 mm. In addition, a hierarchical dependency is indicated, e.g., for the fourth critical vessel section with safety margin 2.9 mm.

Besides using the set of automatically calculated critical sections, arbitrary vessel sections can be labeled in the 3D visualization. These positions are subsequently analyzed in a similar fashion, described in the previous subsection, and are inserted into the risk table.

Concluding Remarks

Non-uniform margins, as introduced in this work, support the decision of excluding vessels within a uniform margin from transection. This opportunity may increase the amount of postoperative residual liver volume. Theoretically, non-uniform margins could also increase the probability of histologically unclear margins. However, this issue has been controversially discussed in recent years. Recent studies report that expected narrow surgical margins should not exclude patients from potentially curative surgery [Pawlik et al., 2005; Salloum et al., 2008; Muratore et al., 2010]. Thus, patients not thought to be candidates for resection due to insufficient residual liver volume may indeed become eligible for curative surgery. The definition of resection plans based on non-uniform safety margins could be a valuable tool in this context.

The new method allows a planning of safety margins by considering sub-centimeter widths. The question of whether this accuracy is necessary for preoperative planning arises, because it can generally not be realized during common liver interventions.

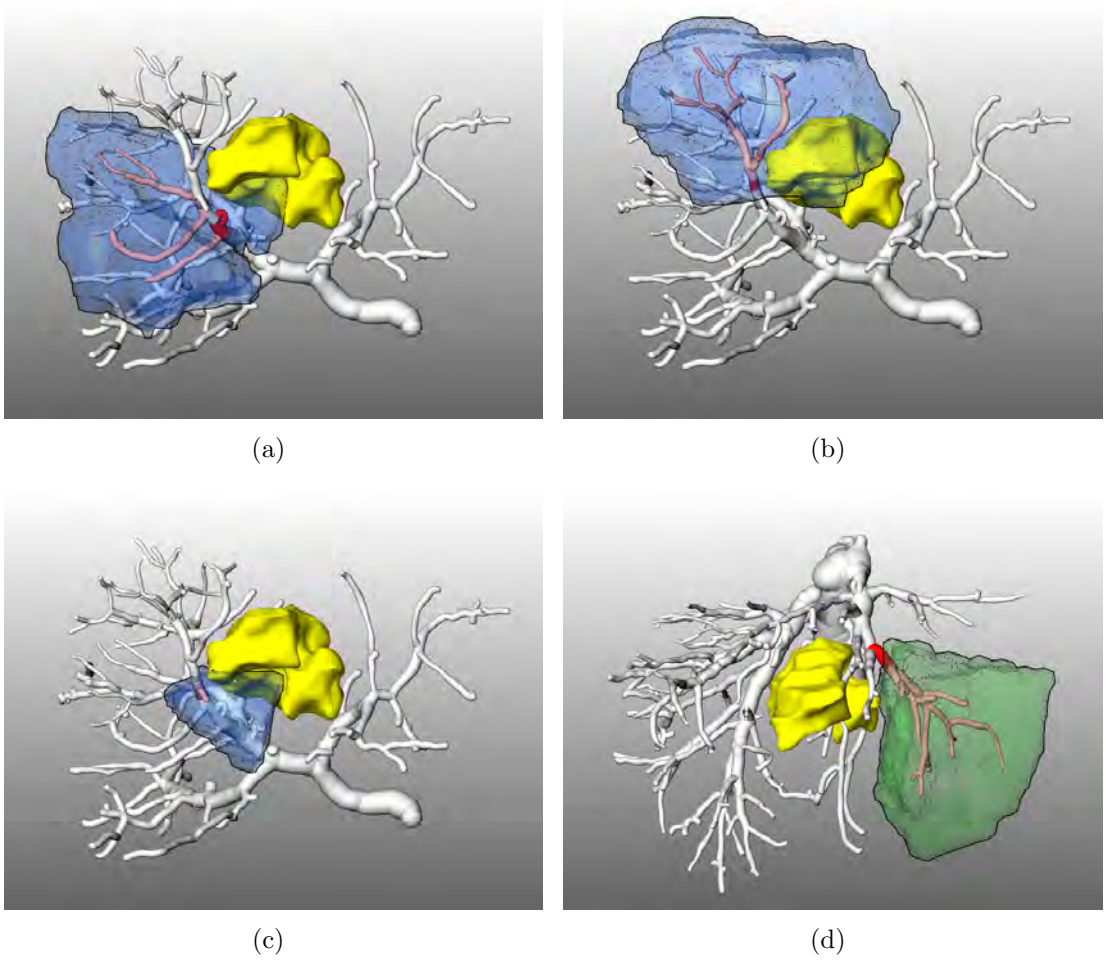

(a) (b)

(c) (d)

Figure 3.24: Risk visualizations that correspond to different selected items of the risk table shown in Fig 3.23a. (a) shows the corresponding visualization for the selected item with distance 2.9 mm (portal vein), while (b) and (c) show the risk visualization for its subitems with distances 0 mm and 1.4 mm. Note that the critical vessel sections shown in (b) and (c) depend on the preservation of (a) as indicated in the risk table. (d) shows the risk visualization for the hepatic vein by selecting the item with distance 4.3 mm. The critical vessel section is highlighted in red. The associated liver volume is visualized as a transparent isosurface. The isosurface is colored blue for areas that are supplied by the portal vein and green for areas that are drained by the hepatic vein.

However, recent developments in navigated liver surgery show that a precise transfer of planning data in the operating room is feasible (cf. Sect. 2.2.4). It can be anticipated that navigation accuracy for liver resection surgery will further increase in the next years. Together with a precise surgical planning such as the one proposed in this work, borderline patients that are treated palliatively with the techniques available today may be selected as candidates for curative surgery in the future.

In conclusion, non-uniform safety margins represent a valuable extension to the established concept of uniform safety margins. In combination with navigated liver surgery the concept has the potential to improve the treatment of liver tumors.

Publications *The first part of this chapter which describes the determination of uniform safety margins (Sect. 3.4.1-3.4.3) was published as an abstract and presentation at the 22th Congress for Computer Assisted Radiology and Surgery (CARS), Berlin, Germany [Hansen et al., 2009a]. In addition, an extended version was published in the International Journal of Computer Assisted Radiology and Surgery [Hansen et al., 2009b]. The method for the determination of non-uniform safety margins and the performed evaluation were not published at the time of submission of this thesis.*

4 Intraoperative Adaptation of Planning Data

There is nothing more constant than change.

(Charles Darwin)

The more complex and dangerous a procedure, the more effort is often invested in planning [Zachow et al., 2010]. However, to achieve the best possible result, almost every plan needs to be adapted during execution because of events that were unexpected at the time of initial planning. An illustrative example of such an event is a little car accident on a highway that causes a big, unexpected traffic jam. Car navigation systems take such events into account and calculate an adapted route plan.

4.1 Clinical Background and Purpose

Computer-assisted risk analyses support surgeons in the planning phase. Based upon safety margins around each tumor, disturbances of blood supply and drainage within the remaining liver parenchyma can be computed, quantified, and visualized preoperatively (cf. Chapter 3).

Using IOUS during oncological liver interventions, between 19% and 33% of patients show additional tumors [Ellsmere et al., 2007; Sietses et al., 2010; Shah et al., 2010]. Although the diameter of these intraoperative findings is smaller than 1 cm in the majority of cases [Hata et al., 2011], changes to the resection strategy are reported in 18 % to 90 % of these cases [Zacherl et al., 2002; Conlon et al., 2003; Wildi et al., 2008; Mazzoni et al., 2008]. A tool to intraoperatively adapt risk analyses and resection proposals (including volumetric information) would be beneficial in case the resection strategy needs to be updated.

Closely related to the adaptation of planning data is the control of intraoperative planning software. Interfaces for surgeon-computer interaction need to consider specific requirements such as the cognitive load, workflow, sterility, and workspace of surgeons. Besides the adaptation of risk analyses and resection proposals, appropriate interfaces could also enable intraoperative adaptation of the planning model's visual representation.

This chapter presents methods for the adaptation of surgical planning data in case of intraoperative findings. Thereby, oncologic risk analyses and resection proposals are addressed. In addition, the chapter provides first results and an outlook of techniques for automatic generation of oncologic resection proposals.

4.2 Related Work

Several groups developed sophisticated planning applications for liver surgery [Meinzer et al., 2002; Bourquain et al., 2002; Ayache, 2003; Reitinger et al., 2006]. However, these applications were restricted to the preoperative planning stage. Appropriate user interfaces for the adaptation of planning data in operating rooms (risk analyses and resection proposals) are not available. This section reviews two approaches in the field of computer-assisted surgery that aim to adapt surgical planning data in the operating room. Furthermore, related methods for surgeon-computer interaction are reported.

Adaptation of Planning Data

An initial concept for the adaptation of risk analyses in case of newly found tumors was presented by Ritter et al. [2005]. They proposed to determine tumor attributes by means of mouse interactions on a notebook inside the operating room. With this method, location and radius of a newly found tumor are marked within a single slice of the original CT data by mouse clicks and dragging. Thus, the result of the risk

analyses depends on the mental ability of a surgeon to transfer location and radius of tumors into the planning dataset. The approach is not designed for sterile areas, but rather for a second physician who controls the application away from the operating table.

Other groups have developed methods to estimate organ deformation using intraoperative registration methods in order to adapt preoperative imaging to the intraoperative situation. For an overview refer to Sect. 2.2.4. Thereof, a promising approach by Feuerstein et al. [2008] is described, where an optically tracked mobile C-arm is applied during laparoscopic liver surgery. Instead of using preoperative planning data, they work directly with the intraoperatively acquired CT images. Thus, vessel positions can be updated and directly superimposed onto the laparoscopic video stream. Assuming that new tumors are visible in the intraoperative CT data, their approach could be enhanced to consider these additional tumors.

Surgeon-Computer Interaction

Commercially available interaction devices have been used in the sterile area of operating rooms for years. In many cases, touchscreens are used, e.g. in laparoscopic liver surgery [Schlichting, 2008] or in open liver surgery [Peterhans et al., 2010]. A disadvantage of touchscreen is that they need to be wrapped in a sterile plastic sheath during surgery. According to observations by the author, the plastic sheath considerably reduces the image quality and leads to interaction errors. In addition, touchscreen interaction is only possible if the surgeons' hand can reach the display. During liver surgery, this is often hard to achieve because of limited space around the examination table.

Nowatschin et al. [2007] proposed to install a 3D mouse close to the surgeon in order to allow the interaction with a surgical navigation system. 3D mice are appropriate to support a precise rotation of 3D models, however, they are inappropriate for simple (but essential) interaction tasks such as the selection of objects.

Other systems attempt to detect finger positions using stereo cameras [Chojecki et al., 2009] or TOF cameras [Penne et al., 2009] to control a mouse cursor. Ritter et al. [2009] track the movements of hands to allow simple interaction tasks such as rotating geometric planning models or triggering of events via buttons.

Several groups use surgical navigation systems (intended to localize surgical instruments) to track a sterilizable pointer in the operating room [Fischer et al., 2005; Reitinger et al., 2006]. In addition, Fischer et al. [2005] introduced a sterile sticker with distinct patterns that can be tracked optically. Being fixes on an appropriate surgical instrument, the instrument is used to interact with the navigation system. According to the literature, none of these approaches has been systematically evaluated under intraoperative working conditions.

4.3 The Intraoperative Planning Assistant

A new application for intraoperative adaptation of planning data, termed the Intraoperative Planning Assistant (IPA), is proposed. In order to provide surgeons with an interface to the IPA, appropriate interaction devices and methods for the intraoperative inspection of surgical planning data are presented.

Several methods introduced in this section employ an ultrasound-based navigation system, and their benefit depends on proper alignment of preoperative data to the intraoperative situation. Hence, the navigation system's setup and the applied registration technique are reported. Subsequently, novel methods for intraoperative adaptation of planning data are introduced. First, a method for intraoperative adaptation of oncologic **risk analyses** is described. Second, methods for the intraoperative adaptation of **resection proposals** through the modification of a preoperatively defined virtual resection surface are presented. The probe of an ultrasound-based navigation system and, alternatively, the Wii Remote pointing device are proposed as intraoperative interaction devices. Third, techniques for the intraoperative adaptation of the **visual representation** of planning data are proposed. All described methods are implemented within the IPA.

Navigation System

In this work, a prototypical ultrasound-based navigation system for laparoscopic liver surgery with electromagnetic tracking is utilized (cf. Fig. 4.1). The system is developed by the Institute for Robotics and Cognitive Systems at University of Lübeck, Germany. A detailed description can be found in [Hildebrand et al., 2007]. The system is equipped with a touchscreen that can be used as a device for simple interaction tasks during surgery. An important feature of the ultrasound-based navigation system is its ability to act as service provider and consumer in a service-oriented architecture (SOA) [Strähle et al., 2007], which allows registered computer systems in the operating room to grab the current navigation data, including the corresponding ultrasound image, via a network connection. This architecture, together with a well-defined exchange protocol, is the basis for the communication between the IPA and the navigation system.

Intraoperative Registration

In order to calculate the relative position of surgical instruments to preoperative planning data, a registration between the IOUS images and the preoperative planning data is necessary. The registration algorithm is developed by the Institute of Mathematics and Image Computing at University of Lübeck, Germany.

The algorithm requires the definition of a small set of corresponding landmarks in both the preoperative radiological data (before surgery) and the IOUS images (during surgery). For this purpose, bifurcations of hepatic vessels are used because they are relatively good to detect in IOUS. Intraoperative landmarks are acquired

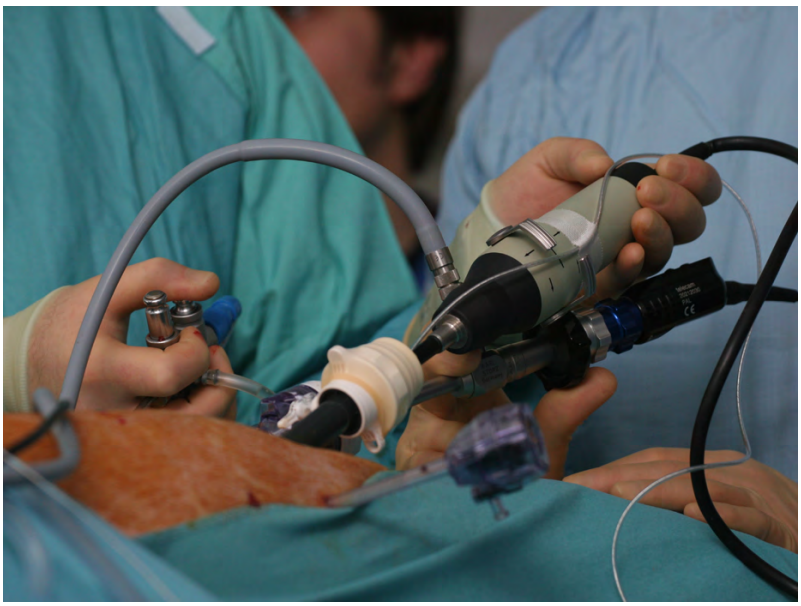

Figure 4.1: Ultrasound-based navigation system for laparoscopic liver surgery [Hildebrand et al., 2007] using electromagnetic tracking.

using a respiratory gating technique that permits the approximation of a motionless liver during the respiratory cycle [Clifford et al., 2002]. The end-exhalation plateau is chosen as the time point for acquisition because it is the longest phase during which nearly no motion occurs. Afterwards, a rigid registration is computed based solely on the alignment of the acquired landmarks as described by Papenberg et al. [2008].

4.3.1 Adaptation of Oncologic Risk Analyses

In this subsection, computational steps to adapt risk analyses intraoperatively are described. First, the underlying **preprocessing** pipeline is presented. Second, a method for the intraoperative **determination of tumor attributes** is introduced. This methods allows to transfer intraoperatively made findings into a preoperative planning dataset. Third, new methods for the intraoperative adaptation of risk analyses, i.e., **vessels at risk** and **territories at risk**, are presented.

Preprocessing of Planning Adaptation

The preoperative planning results are based on contrast-enhanced CT or MRI data acquired with standard examination protocols. Relevant intrahepatic structures are segmented semi-automatically by a radiology assistant in the preprocessing step. Affected vascular branches, as well as affected vascular territories, are computed, and their geometric representation is saved. The IPA stores the generated planning datasets. The datasets can be accessed from a navigation system by sending a request to the IPA. The IPA responds by sending a message which includes the location of

relevant data files, providing quantitative information (XML) and geometric objects (VRML), which can be downloaded via FTP (see exchange protocol in Fig. 4.6 on page 80). This data exchange allows a simultaneous visualization of 3D planning models and navigated 2D ultrasound on the screen of the ultrasound-based navigation system.

Intraoperative Determination of Tumor Location and Size

As discussed above, the result of oncologic risk analyses in the liver depends on the position and dimension of tumors and their safety margins. If additional tumors are discovered during surgery, risk analyses (vessels at risk and territories at risk) are incomplete and thus no longer valid. It is assumed that intraoperatively detected tumors are relatively small (diameter $\leq$ 1cm) [Hata et al., 2011] and approximately spherical in shape.

To define position and size of new tumors, the navigation system's touchscreen is used. Therefore, the surgeon labels the tumor inside the 2D ultrasound view by defining the tumor center with a single click and determining the size of the tumor by dragging a finger towards the tumor's border. Thus, a circle is defined in the 2D ultrasound image (cf. Fig. 4.8). Subsequently, center position and circle radius are transformed from ultrasound image coordinates into world coordinates of the preoperative planning dataset by considering registration and calibration matrices as described in Schlichting [2008]. This transformation is calculated by the ultrasound-based navigation system. To achieve reliable results, it should be noted that the definition of the sphere should happen in the same respiratory phase as the performed intraoperative registration.

After tumor attributes have been determined, the navigation system sends a request to the IPA containing the new tumor size and position. In case the IPA is available in the network, the coordinates of the circle and the radius are transferred to the IPA using a communication protocol that was designed together with medical device vendors (Siemens Healthcare and Dräger Medical). The IPA checks if the patient ID from the currently loaded dataset in the IPA corresponds to the patient ID sent by the navigation system. If this comparison is successful, the request is confirmed. Otherwise, the IPA sends the confirmation after loading the corresponding dataset or sends an error message to the navigation system if loading was unsuccessful.

Adaptation of Vessels at Risk

If the request is accepted by the IPA, the position and radius provided by the navigation system are used to raster a sphere inside a tumor segmentation mask S_{Tum}. S_{Tum} contains all preoperative segmented and intraoperatively acquired tumors of the patient dataset. To create a visualization of vessels at risk, a Euclidean distance transformation is applied to S_{Tum}. The Euclidean distance transformation is used to query the minimum distance from each vessel voxel to S_{Tum} in constant computation time. Thus, vessels at risk are identified and relabeled inside the vessel

graph G depending on standard safety margins widths (5 mm, 10 mm, and 15 mm) around tumors (cf. Fig. 4.2). After the computation has finished, the updated planning models are loaded onto an FTP server. Subsequently, the IPA sends a request to the navigation system, informing about the availability and location of new planning data. The new planning models are thereafter automatically downloaded by the navigation system via FTP (cf. Figure 4.6 on page 80 for the exchange protocol defined between IPA and navigation system).

Adaptation of Territories at Risk

The visualization of vessels at risk provides information about the vessels which are additionally affected when applying a certain safety margin around the detected tumors. According to involved clinical partners, updated quantitative information about the amount of liver volume with probable impaired inflow and outflow could be an intraoperative benefit. Therefore, the option to adapt the affected territories at risk is provided.

In order to calculate territories at risk, a 3D Voronoi decomposition (nearest-neighbor distance model) with respect to G is calculated to approximate the impaired liver volume for each safety margin width (cf. Fig. 4.3). This procedure has to be applied for each vascular system provided by the IPA. However, during the clinical tests described below, the adaptation was constrained to the two main vessel systems, i.e., hepatic vein and portal vein. Finally, the 3D representation of the territories at risk and corresponding volume information are calculated. The updated volume information is arranged in an XML file, while all 3D models are saved in a standard file format (VRML).

The updated 3D planning models of territories at risk as well as the XML file are uploaded to an FTP server. Subsequently, the IPA sends a request to the navigation system that new territories at risk are available by providing information about the location of the data.

4.3.2 Adaptation of Resection Proposals

Once a risk analysis has been adapted intraoperatively, the preoperative resection proposal should be adapted. This includes the definition of a new resection surface that divides the liver in the intended remaining and resection volumes. The **amount of remaining volume** is of utmost importance because it determines if a patient is resectable or not. In contrast to the preoperative planning stage, there is a lack of computer-assisted tools to support this decision intraopertively.

In this subsection, two interaction methods for the intraoperative adaptation of resection proposals are presented. The first method is based on position data from a tracked ultrasound probe; the second method uses the interaction device *Wii Remote*.

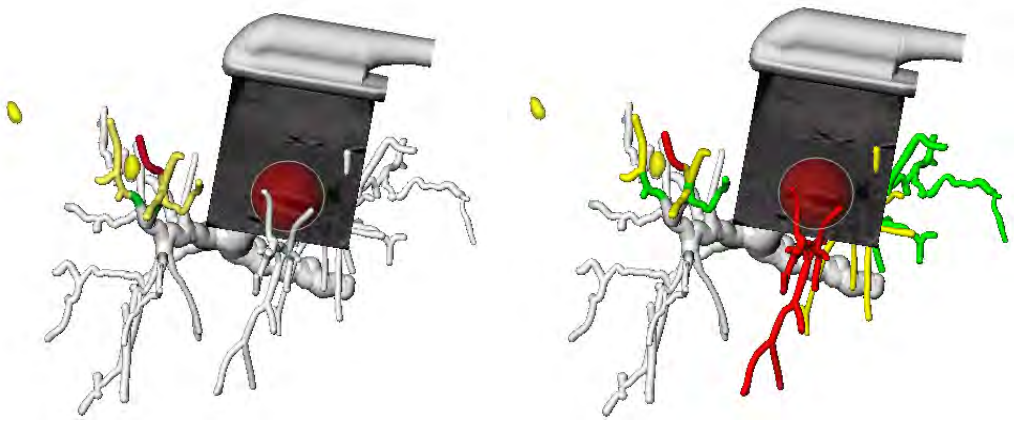

(a) (b)

Figure 4.2: (a) Preoperative risk analysis for the portal vein using different safety margins around the tumors. Three standard safety margins are chosen and the affected vessels are displayed in red (5 mm), yellow (10 mm), and green (15 mm). The sphere on the ultrasound plane shows an additionally detected tumor before adapting the risk analysis. (b) Adapted risk analysis including relabeled vessels.

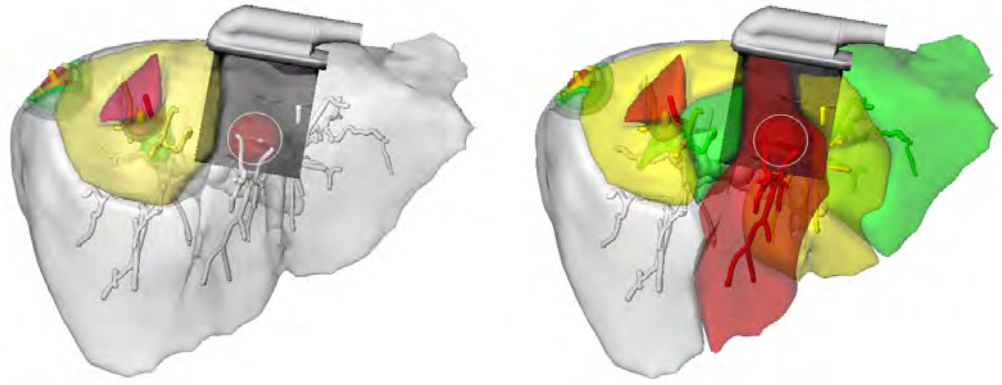

(a) (b)

Figure 4.3: (a) Preoperatively determined portal vein territories at risk that are supplied by the affected vessels shown in Fig. 4.2. The sphere on the ultrasound plane shows an additionally detected tumor before adaptation. (b) Adapted territories at risk. The safety margins are the same as in Fig. 4.2.

Intraoperative Adaptation based on Tracking Information

A method that uses a tracked probe of an ultrasound imaging system as an intraoperative interaction device is presented. The interaction method can be used to redefine a preoperatively defined resection proposal intraoperatively or alternatively to define a completely new resection proposal.

The surgeon determines the desired position and orientation of the resection surface on the patient's liver using a tracked ultrasound probe. While taking the information on the ultrasound image into account, risk structures such as important vessels can be considered. The procedure is divided in three steps:

(1) Preprocessing

(2) Plane definition

(3) Update of planning data, return to step (2) if necessary

Let us take a look at these steps in detail:

(1) **Preprocessing:** The preprocessing is the same as the preprocessing steps described for the update of oncologic risk analyses in subsection 4.3.1. In addition, all 3D mask images that were used to define the selected resection proposal are cached.

(2) **Plane definition:** The plane definition is performed with the navigation system. Therefore, a simultaneous visualization of ultrasound probe and the resection proposal is provided on the screen of the navigation system. To define a new resection surface, a method to save the geometric representation of a current ultrasound plane in the planning dataset is provided. The plane is confirmed using a button on the navigation system's touch screen. The plane's normal determines the part of the liver to be resected. It is displayed as an arrow widget in the center of the plane and can be swapped using the touch screen. When the definition of the plane is completed, the navigation system sends an update request to the IPA that contains information about the plane position and normal.

(3) **Update of planning data:** When the IPA receives a request from the navigation system, the halfspaces of the defined plane are voxelized into a binary mask HS. This is performed by a raster function algorithm that takes the plane position and normal as input. Let S_{Liv} be the preoperative segmentation mask of the liver, the resection volume RS ($RS \subset S_{Liv}$) and the remnant volume RM are provided from the preoperative planning phase. The new resection liver volume RS_{new} and the new remnant volume RM_{new} are calculated as follows:

$$RS_{new} = RS_{old} \vee HS \tag{4.1}$$

$$RM_{new} = RM_{old} \wedge \neg HS \tag{4.2}$$

Thus, the result considers both, the preoperative defined volumes RS_{old} and RM_{old} and the intraoperative defined volume HS (cf. Fig. 4.4a). In addition, an option to exclude the preoperative resection mask from the calculation is provided:

$$RS_{new} = HS \tag{4.3}$$

$$RM_{new} = \neg HS \tag{4.4}$$

This allows defining a new resection surface independent from the preoperatively defined one. Finally, the virtual resection surface that borders RS_{new} and RM_{new} is calculated. Therefore, a dilation D is applied on RS_{new}. Subsequently, RS_{new} is subtracted from $D(RS_{new})$ to calculate the hull of RS_{new}. A logical conjunction between S_{Liv} and this hull delivers the adapted resection surface.

In some cases, preoperatively segmented tumors lie closely to the virtual resection surface. To avoid that the tumor (or parts thereof) are counted as RM_{new}, pre-computed safety margins of the tumors are accessed and used to change the shape of a virtual resection surface. This ensures that tumors and their safety margins are automatically labeled as RM_{new}. Finally, the volumes of RM_{new} and RM_{new} are calculated and geometric surface representations of the updated volumes are generated (cf. Fig. 4.5b).

After computation of all surface representations, the IPA sends a response to the navigation system including the location of relevant data files. These files provide updated volumetric information (XML) and geometric objects (VRML) which can be downloaded via FTP (cf. Fig. 4.6). This data exchange allows a simultaneous visualization of updated planning data and tracked surgical instruments on the navigation system's screen. To sculpt non-planar resection surface the surgeon can return to step (2) and define an additional plane (cf. Fig. 4.4b).

Intraoperative Adaptation using a 3D Pointing Device

A general interaction device to adapt planning data (without the need of a surgical navigation system) would be beneficial. Preliminary user tests in our institute showed, that a pointing device such as Nintendos *Wii Remote* turned out to be appropriate for intraoperative interaction tasks like modifying and refining a virtual resection surface or basic user interactions in 3D such as the rotation of planning models.

The *Wii Remote* is a wireless pointing device for Nintendo's gaming console *Wii* [Nintendo, 2011]. Its motion-sensing capability, based an optical sensor and an accelerometer, allows the user to interact with items on a screen. Recent APIs provide data exchange between the *Wii Remote* and an arbitrary operating system

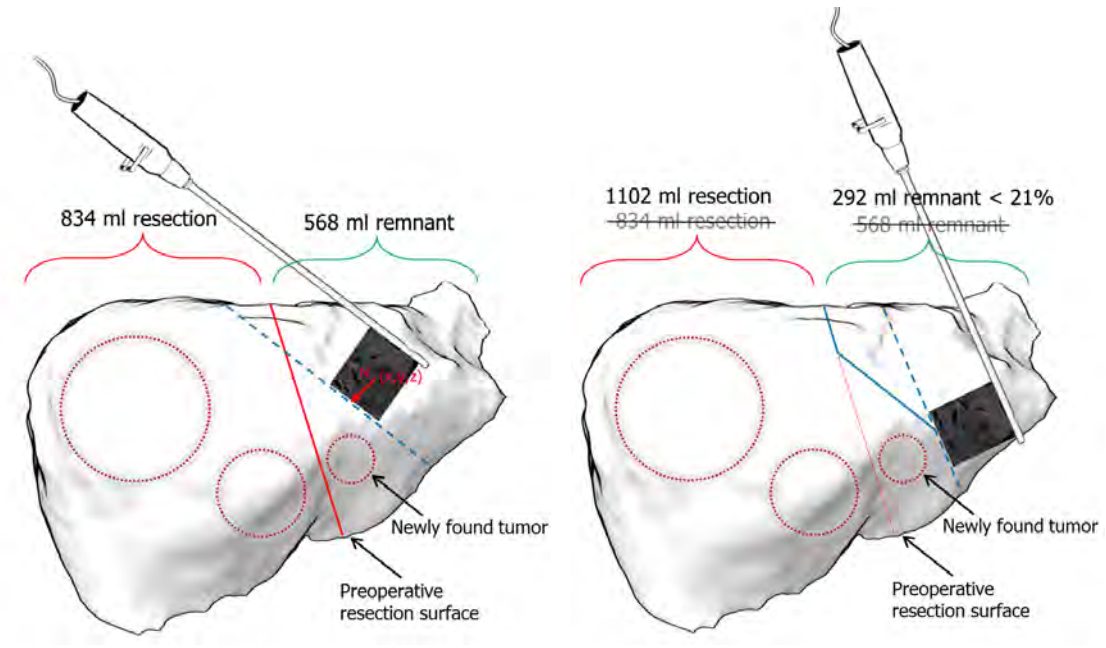

(a) (b)

Figure 4.4: Adaptation of a resection proposal using a tracked ultrasound probe. (a) A new plane within the liver is defined. The displayed plane normal determines the part of the liver to be resected. (b) A second plane is defined in order to optimize the shape of the new resection surface.

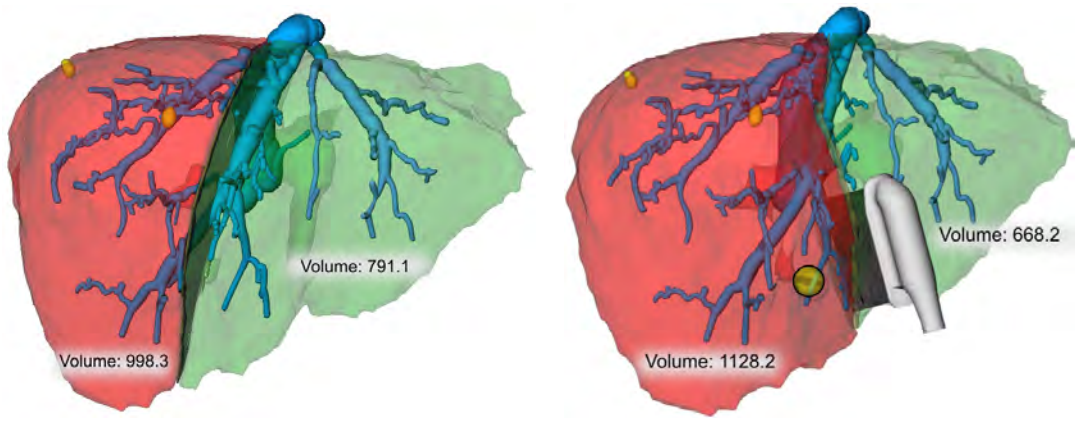

(a) (b)

Figure 4.5: (a) Preoperatively planned right hemihepatectomy with hepatic vein. The left part of the liver model shows the parenchyma to be resected (red), while the right part is intended to remain (green). The small nodules in the left part represent preoperatively segmented metastases. (b) Adapted resection proposal. The added sphere close to the middle hepatic vein represents an intraoperatively determined tumor.

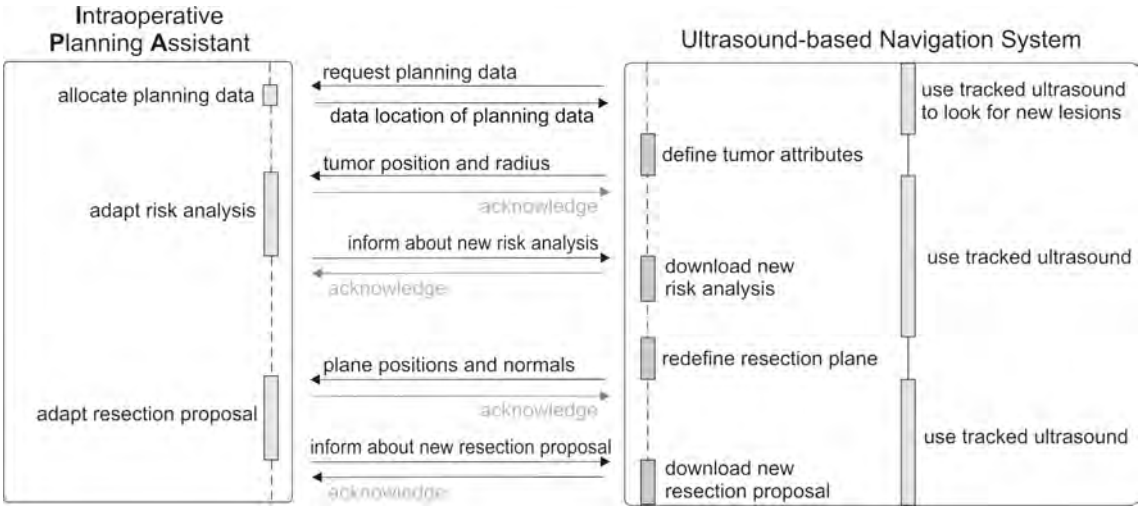

Figure 4.6: Exchange protocol defined between ultrasound-based navigation system and IPA based on a SOA.

using the open Bluetooth standard for data transfer. Thus, the pointing device runs independently of Nintendo's gaming console and can be used in other applications.

To utilize the optical sensor technology of the *Wii Remote*, a sensor bar has to be located near the interaction screen. The sensor bar features ten infrared LEDs with five LEDs being arranged at each end of the bar. The *Wii Remote* can locate the LEDs (i.e., the relative position of the interaction screen) by means of an integrated infrared camera. This allows controlling the mouse pointer by moving the *Wii Remote*. As shown in Fig. 4.7, the device offers several interaction buttons and a directional pad which can be mapped to mouse clicks, keyboard inputs, or even complex instructions. To allow haptic and acoustic feedback, basic audio and rumble functionality is provided.

An open source Bluetooth API [WiiMote API, 2011] for the *Wii Remote* was integrated into the IPA to use the capability of the *Wii Remote*. For the evaluation in the operating room (described below), the device was wrapped in a sterile plastic sheath. To allow an intraoperative adaptation of resection proposals, existing interaction techniques for the modification of virtual resections were extended for the use with the *Wii Remote*, i.e., 'drawing into slices' and 'drawing onto a virtual 3D liver surface' (refer to Sect. 2.2.2 on page 22).

For **drawing into slices**, the *A button* (cf. Fig. 4.7) is reserved to define a resection line in a slice while the *B button* is used to pick and translate these resection lines. The accelerometer and IR tracking data allow for movement direction and speed information to be reported, with which the mouse cursor is controlled. To navigate through a stack of slices, the surgeon moves the *Wii Remote* in the intended direction while pressing the *1 button*. The speed and direction of navigation is also determined through the accelerometer and IR tracking data of *Wii Remote*. For stepwise navigation through a stack of 2D images, e.g. viewing exactly the CT

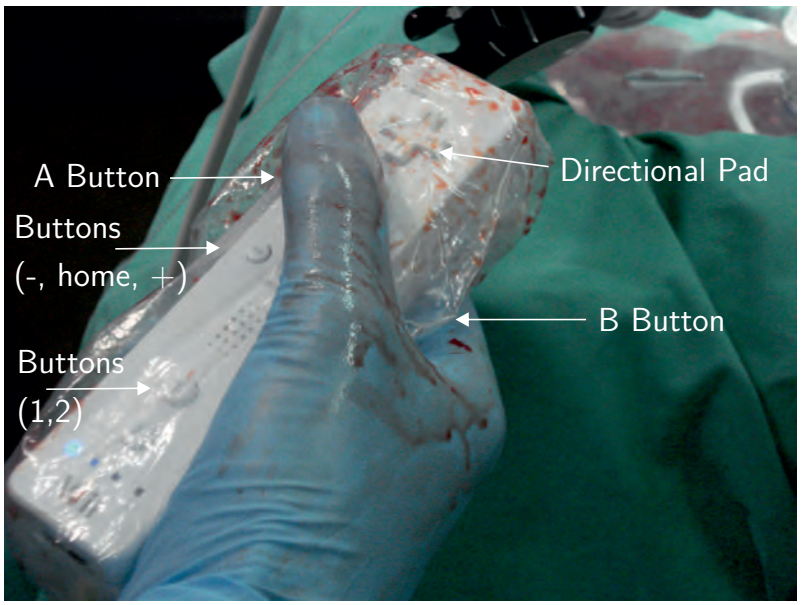

Figure 4.7: *Wii Remote* wrapped in a sterile plastic sheath. The photo was taken during the evaluation of the WiiMote interaction in the experimental operating room of the Institute of Biomedical Optics, University of Lübeck, Germany. The annotations show the positions of interaction buttons on the WiiMote.

image below the currently selected CT image, the user may also employ the + and - *buttons*.

To **draw onto a virtual 3D liver surface**, the *A button* is used to draw an initial line set, while the *B button* is used to deform the cutting plane. View rotation is performed in 22.5° steps around the x and y axes of the camera coordinate system and can be controlled with the directional pad. Pressing the *Home button* resets the view to the standard camera position. Rotating the model by using the optical tracking system was not implemented, as an informal user test preformed under lab conditions showed that participants (two surgeons, two computer scientist, and one student of computer science) spent too much time trying to attain a desired camera position. Another reason for using the directional pad for the rotation tasks was the fact that it can also be used without a line of sight between the *Wii Remote* and the sensor bar.

4.4 Evaluation

To evaluate the IPA, a feasibility study was conducted. The study has been performed in cooperation with technical partners from the Institute for Robotics and Cognitive Systems, University of Lübeck, Germany and clinical partners from the Department of General and Visceral Surgery, University Hospital Lübeck, Germany. The experiments

were conducted in an experimental operating room of the Institute of Biomedical Optics, University of Lübeck, Germany. The feasibility study addressed following aspects:

(1) Technical feasibility

(2) Integration of the IPA in the surgical workflow

(3) Time in that a planning adaptation is achievable

To evaluate the technical feasibility, two experiments on a tumor mimic model of the liver are described. Subsequently, three experiments performed in the context of an animal study with pigs are reported.

Evaluation with a Tumor Mimic Model

To simulate an intervention in the liver, a perfusable ex vivo tumor mimic model of the liver was utilized. Four tumor mimics were injected (a mixture consisting of 3% agarose, 3% cellulose, 7% glycerol, and 0.05% methylene blue) creating hyperechoic lesions in ultrasound and CT [Schlichting, 2008]. Afterwards, CT images were acquired and vascular risk analyses and a resection proposal for the model were prepared.

To prove the technical feasibility of the adaptation of planning data, one additional tumor mimic was injected into the model after performing the CT scan. The planning model was registered to the IOUS using a landmark-based registration approach [Papenberg et al., 2008]. Subsequently, the tumor mimic model was completely scanned with the tracked IOUS and the additional tumor mimic was searched and detected. The position and extension of the finding were determined (cf. Fig. 4.8) and transferred to the IPA. New vessels at risk and territories at risk were calculated as described in Sect. 4.3.1 and provided at the navigation systems display (cf. Fig. 4.9). In a second experiment with the tumor mimic model, risk analyses as well as the adaptation of the resection plan were tested.

The planning adaptation was performed by two scientist who were familiar with the use of the ultrasound-based navigation system.

Evaluation within an Animal Study

In order to verify the described concepts within a surgical environment, the techniques were applied in an animal study with pigs that was conducted in the context of the FUSION project. The goal of the study was to evaluate usability and navigation accuracy of the navigation system for laparoscopic liver surgery as described in [Hildebrand et al., 2008]. In the context of this study, the adaptation of risk analyses and resection proposals was evaluated during laparoscopic liver resection in two surgical cases.

The detailed protocol of the animal study has already been described in the thesis of Schlichting [2008]. In summary, two to three sterile gold fiducials (IZI Medical

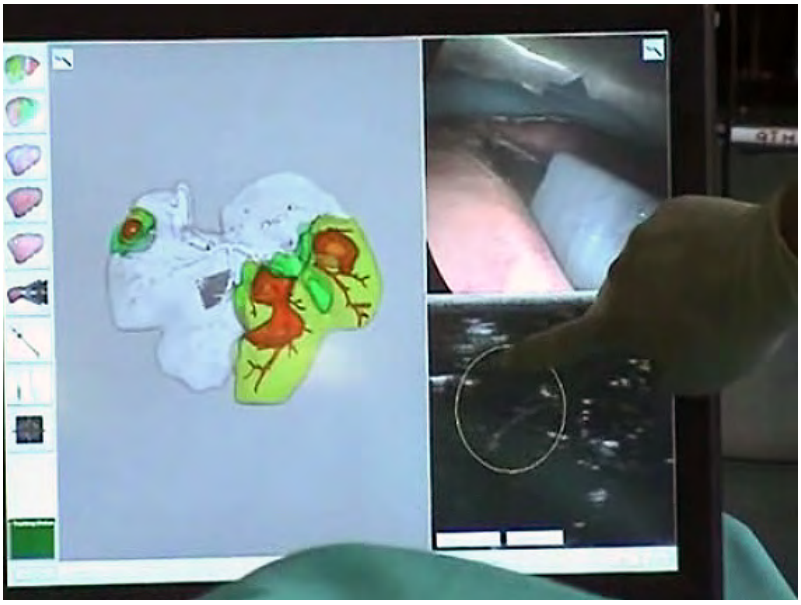

Figure 4.8: Touchscreen of the utilized navigation system [Hildebrand et al., 2007]. The lower right part shows an IOUS image where a tumor mimic is currently detected. The upper right part of the screen shows the laparoscopic video image. The left viewport visualizes the detected tumor mimics and the territories at risk of a porcine liver.

Figure 4.9: Evaluation of the IPA within an experimental operating room (Institute of Biomedical Optics, University of Lübeck, Germany) using a tumor mimic model. The left screen belongs to the IPA; the right screen belongs to the navigation system.

Products, Baltimore, MD, USA) were inserted in the liver under ultrasound guidance. These fiducials simulated small tumors inside the liver. Subsequently, a contrast-enhanced CT scan was acquired, and the fiducials and relevant anatomical structures were segmented and 3D planning data (including risk analyses and a resection plan) was prepared. The surgical resection was performed approximately one week later.

During surgery, a landmark-based registration between IOUS and preoperative planning models was performed. Furthermore, two additional gold fiducials were placed in the liver in order to simulate the detection of new tumors. The intraoperatively placed fiducials were detected by the surgeons using the tracked IOUS and marked on the ultrasound display of the navigation system. Subsequently, the IPA provided updated risk analyses and resection proposals which were defined by the surgeons (using the tracked ultrasound plane) to guide the laparoscopic instruments.

In a third experiment (cf. Fig. 4.11), the surgeons were asked to define a new resection surface using the *Wii Remote*. Therefore, the planning models, including the preoperatively planned resection surface, were visualized on the display of the IPA. In addition, the tumor mimic captured with the ultrasound-based navigation system was inserted in the model. The *Wii Remote* was inserted in a sterile plastic sheath and given to the surgeon.

4.5 Results

The experiments with the tumor mimic model showed that the concepts for intraoperative planning adaptation described in Sect. 4.3.1-4.3.2 are technically feasible. The implemented communication protocol between navigation system and IPA turned out to be an appropriate way for platform independent data exchange. The communication allowed a distributed development and combined the strengths of both systems.

The experiments within the animal study showed that the participated surgeons were able to determine the location and size of intraoperatively detected gold markers. The touchscreen of the navigation system was found to be an appropriate interaction interface for this task. In contrast, the determination of resection proposals using the tracked ultrasound device turned out to be relatively inconvenient. Defining a complex shape, like a curved surface (approximation the shape by a set of planes) lead to a lengthy interaction task.

The *Wii Remote* is a intuitively manageable interaction device for the IPA, especially for the adaptation of resection proposals. To allow precise user interaction, the location of the interaction screen, its size, and the distance between user and screen must be adequate. Assuming a 19" display, a distance of $0.5 - 3.0\ m$ between user and screen turned out to be adequate for the intended interaction tasks. The sterile plastic sheath influenced the control of the *Wii Remote* only marginally. Only the activation of the *B button*, which is located on the bottom side of the *Wii Remote*, was more difficult than without the plastic sheath. Therefore, it is proposed to use this button for less important functions. The plastic sheath did not influence the

(a)

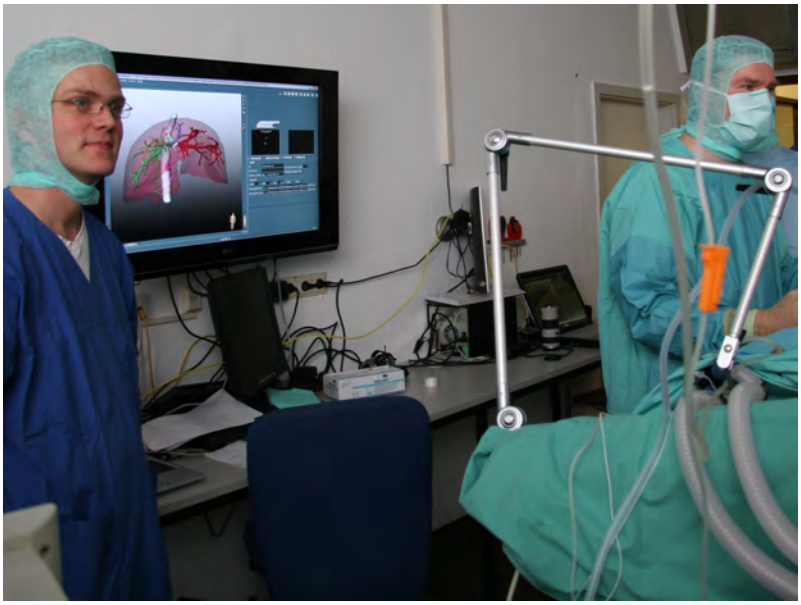

(b)

Figure 4.10: Animal study in the experimental operating room of the Institute of Biomedical Optics, University Lübeck, Germany. While the ultrasound-based navigation system (a) is located in the sterile area of the operating room, the IPA (b) runs on a workstation outside of the sterile area.

Figure 4.11: Interaction with the *Wii Remote* in an experimental operating room (Institute of Biomedical Optics, University of Lübeck, Germany).

performance of the infrared camera.

Within the animal study, the adaptation of risk analyses was performed in less than one minute (see hardware specification for test system at Sect. 8), which is an acceptable time frame in clinical routine. Thereby, only one plane was defined using the tracked ultrasound device to get a rough estimation of the remaining liver volume. Because the calculations for the planning adaptation were performed independently from the surgical navigation system on a peripherical computation unit (IPA), the ultrasound-based navigation system could be used for further exploration of the liver without performance losses.

4.6 Discussion and Conclusion

So far, preoperative risk analyses and resection proposals for liver surgery were of limited value during interventions if resection strategies needed to be updated. In this work, a software assistant for intraoperative adaptation of planning data, i.e., the IPA, is presented and evaluated. The performed experiments confirm that the described concept for intraoperative adaptation of planning data is technically feasible. In addition, the new computer-assisted planning adaptation integrated well in the surgical workflow of navigated liver interventions. The underlying interaction concepts allows an intuitive and quick determination of additional findings.

The **accuracy** of the proposed methods is an important point for discussion. The success of an intraoperative adaptation of planning data correlates with inaccuracies in tracking and the applied registration technique. It is important to measure how

inaccuracies in tracking and registration influence the adaptation of planning data. In experiments described in this chapter, registration landmarks are acquired at equal respiration time points. As a result, the registration is only valid on the same point in the respiratory cycle and only as long as no further mobilization or repositioning of the patient occurs. Besides the registration inaccuracy, the accuracy of the tracking system and the calibration of the ultrasound probe to the tracking system is another critical point. The root-mean-square error of both calibration and tracking sums up to a landmark localization error of approximately 4 mm [Hildebrand et al., 2008], neglecting the liver movement. Although recent advances in navigated liver surgery indicate a continuous minimization of these errors [Beller et al., 2009b; Peterhans et al., 2010], inaccuracies have always to be taken into account in future applications. Therefore, an analysis and visualization of uncertainty would be a valuable extension of the IPA.

Another important topic for discussion is the **applicability** of the IPA in clinical routine concerning usability and workflow. If an ultrasound-based navigation system is used during surgery, no additional interaction device has to be installed in order to adapt a resection proposal intraoperatively. This is one of the great advantages, because additional interaction devices demand additional space and setup time. However, the level of detail of adapted resection surfaces is limited when using the tracked ultrasound probe as a planar sculpting tool. In addition, it might lead to lengthy interaction tasks as described above. It can be assumed that such interaction is not applicable in clinical routine and would only be used in exceptional cases.

In the case of the *Wii Remote* interaction, the ultrasound information is not used. Consequently, both modification techniques have clear limitations. A combination of both seems to be promising, i.e., to use the tracked ultrasound probe to define a first approximation of the desired resection plane, and subsequently use the *Wii Remote* or alternatively a sterilizable, trackable pointer as described in the patent by Broers [2005] for refinement.

In conclusion, the proposed combination of planning adaptation and intraoperative navigation provides surgeons with an efficient tool for quantitative risk assessment in case of changes in the resection strategy. The IPA has the potential to provide major support for decision-making during oncologic liver surgery and thus may improve the safety of surgical interventions. However, before using the IPA in clinical routine further studies concerning accuracy and usability are necessary.

4.7 Outlook: Automatic Generation of Resection Proposals

The IPA provides valuable tools to adapt resection proposals intraoperatively. The adaptation is performed interactively in that the surgeon defines the orientation and shape of the resection surface. However, this approach has several disadvantages. First, the human-computer interaction needed to define the resection proposal is

prone to error [Demedts, 2010] and **consumes time**. Second, the resulting resection proposal is **not standardized** and varies depending on the experience and endurance of the user (refer to the user study described by Demedts [2010]). Therefore, an automated generation of resection proposals would be of great benefit.

In the following, new methods for automatic generation of resection proposals are presented. The methods extend previous approaches [Preim et al., 2002; Thorn, 2004; Beller et al., 2008] which attempt to generate resection proposals using vascular territories. The evaluation is performed by comparing the automatically generated resection proposals with resection proposals which were manually defined on CT datasets of the liver by radiology technicians.

Recall that there exist two kinds of resection types in oncologic liver surgery (refer to Sect. 2.1.3 on page 7). Whereas resection surfaces for **anatomical** resection are based on the boundaries the liver segments defined by the portal vein (cf. Fig. 2.1), resection surfaces for **non-anatomical** resection, e.g., wedge resections, do not consider these anatomical boundaries. This work addressed both resection types.

Generation of Anatomical Resection Proposals

For anatomical resections, the boundaries of the portal venous territories guide the resection proposal. Therefore, the terminology of anatomical resections described by Lang [2007] is utilized (cf. Fig. 2.1 on page 10). In a pre-computation step, portal venous territories are calculated as described in Selle et al. [2002] and provided as a 3D image T_{PV}. In addition, the segmentation mask of the liver S_{Liv} and the segmentation mask of hepatic tumors S_{Tum} are provided from previous planning steps.

As illustrated in Fig. 4.12 the proposed algorithm is described in five steps: First, portal venous territories affected by the tumors are identified by comparing T_{PV} with S_{Tum}. If the percentage volume overlap between an affected territory and the tumor is above a predefined threshold, the territory is labeled as affected. Second, the set of affected territories is mapped to a set T_{Res} of territories which conform to an anatomical resection volume. Third, help markers are generated at the borders of T_{Res}, fulfilling the condition that the markers are located inside of S_{Liv}. Fourth, a plane is defined by applying a PCA on the help markers and using the two largest eigenvectors. Fifth, the plane is divided into a regular grid and transformed in orthogonal plane direction to fit the set of help markers. As described by Konrad-Verse et al. [2004], this is performed by scanning all grid cells and testing whether any help marker is projected in this cell. Finally, S_{Liv} is divided into two parts by the deformed plane. These two parts are termed the **remnant volume** and the **resection volume**. Volume fractions for this subsets of S_{Liv} are calculated in ml and percentage.

In case the user is not satisfied with the result, the utilization of the deformable cutting plane within this procedure allows for further adaption of the proposal. This is particularly important because main branches of the hepatic vein are often located along anatomical resection surfaces. Thus, additional vessels not directly affected by

the tumor might be part of the resection volume. In case this is not the intention of the user, the resection proposal calculated on the basis of the portal vein territories can be adjusted appropriately.

Generation of Non-Anatomical Resection Proposals

For the generation of non-anatomical resection proposals, two different methods are proposed. The first method considers **geometric constraints** of the tumors and the liver surface (geometric method). The second method attempts to generate a resection proposal based on an estimation of **vascular perfusion** (perfusion-based method). The perfusion is thereby simulated by means of a vascular risk analysis (cf. Chapter 3).

Initially, both methods require the **selection of the tumor** that should be resected non-anatomically. This is required, because non-anatomical resections are often combined with other resections, e.g. for patients with metastasis in both liver lobes. The selection of the tumor is done by picking the tumor in a 3D viewer which visualizes all segmented tumors. This procedure is only applicable in the planning stage after the segmentation result of tumors is available. For generation of resection proposals during surgery, an intraoperative selection and determination of tumor position and extent using IOUS as introduced in Sect. 4.3.1 is proposed.

Both methods require the **determination of a safety margin** around each tumor. Because an evaluation of different safety margins is not applicable intraoperatively, standard safety margins that are determined by the surgeon (e.g. 5 mm for colorectal liver metastases) are proposed for intraoperative applications. S_{Liv} and S_{Les} are provided from previous planning steps.

The geometric method defines the resection surface solely based on the selected tumor, its safety margin, and the 3D models of the liver surface. First, an access path from the tumor to the liver surface is calculated. The access path is defined as a 3D line segment that has its start point in the geometric center of the tumor. The end point is defined as a point on the convex hull of the liver model that shows the shortest Euclidean distance to the tumor center. The convex hull of the liver model is used because otherwise locations on the liver fissures, in particular the porta hepatis, might have the shortest distance to the tumor center though it is not usual to resect a tumor from this direction.

Second, a 3D object is generated and aligned to the line segment. The object consists of a half sphere combined with a truncated cone. The diameter of the half sphere is defined by the maximum diameter of the tumor plus the determined safety margin. The circular base of the truncated cone has the same radius as the sphere. The center point of the sphere is fixed to the tumor center. The axis of the truncated cone is aligned with the 3D line segment.

The perfusion-based method generates a resection proposal based on a vascular risk analyses as presented in Chapter 3. First, the territories at risk regarding the portal vein drainage and the hepatic vein supply are determined. The territories at risk contain the tumor and its safety margin. Recall that the size and shape of

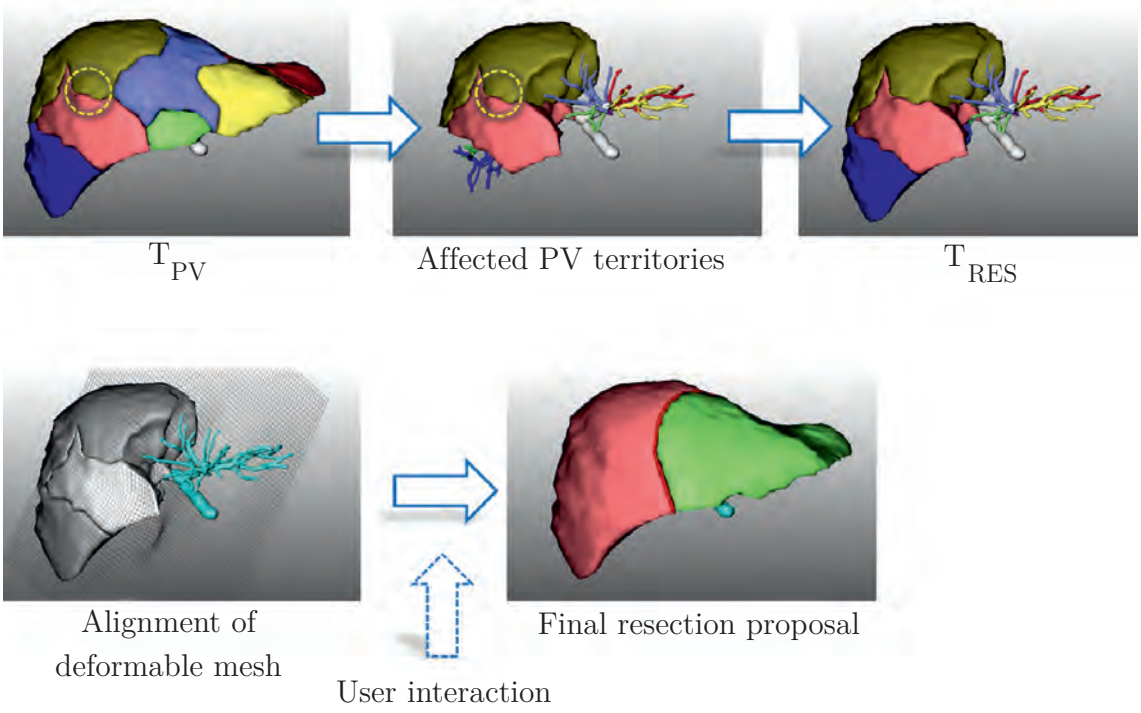

Figure 4.12: Computational steps to calculate anatomical resection proposals.

territories at risk depends on the width of the defined safety margin.

Second, the intersection volume of both territories is calculated (cf. Fig. 4.13). The intersection volume represents a volume that is potentially necrotic tissue after resection because it is neither supplied nor drained according to the vascular risk analysis. Third, an access path is calculated analogous to the geometric method. Instead of the tumor center, the center of the intersection volume is utilized to calculate the access path. Contrary to the geometric approach, the diameter of the half sphere is defined by the maximum diameter of the intersection volume.

For both methods (geometric and perfusion-based) S_{Liv} is divided into two volume fractions and the user can perform quick modifications by dragging the deformable 3D mesh of the proposed resection surface if necessary.

Evaluation

The methods were evaluated by comparing their resection volumes with resection volumes that were manually defined by medical technicians. For the manual definition, a virtual resection tool using a deformable cutting plane [Konrad-Verse et al., 2004] was utilized.

For the evaluation of automatically generated **anatomical** resection proposals, 10 CT liver datasets from LDLT donors were selected. These datasets did not contain any diagnosed malignities. For each CT dataset, a medical technician manually determined five anatomical resection surfaces according to the nomenclature of Lang

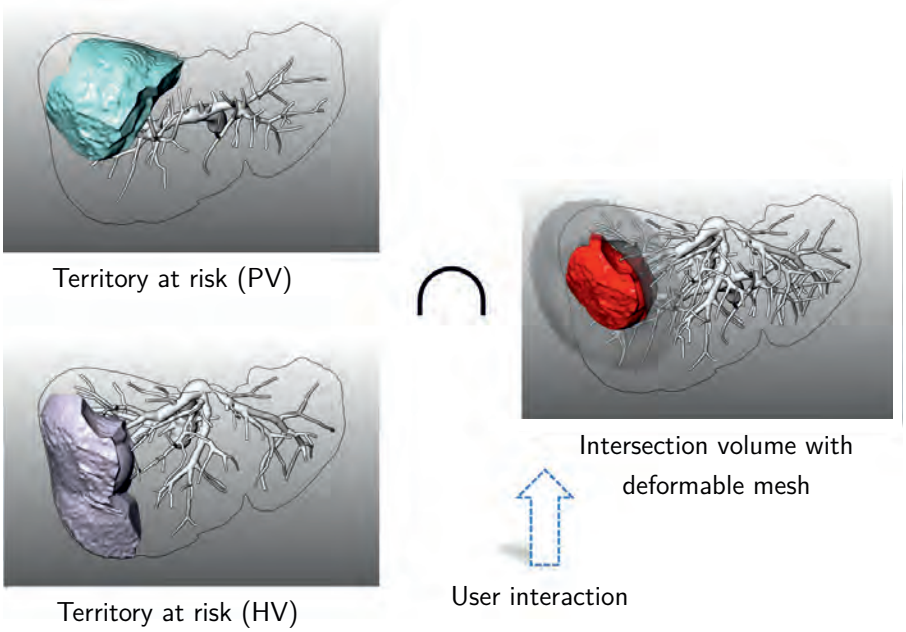

Figure 4.13: The volumes of territories at risks from portal vein and hepatic vein are used to define an intersection volume. Subsequently, a deformable mesh is fitted on the boundaries the intersection volume.

et al. [2005] by considering following five groups of liver resection:

(1) Left Hemihepatectomy and Extended Right Hemihepatectomy

(2) Right Hemihepatectomy and Extended Left Hemihepatectomy

(3) Left Lateral Sectionectomy and Right Trisectionectomy

(4) Right Posterior Sectionectomy and Left Trisectionectomy

(5) Central Resection

Note that an anatomical resection surface may belong to two resection types (the pairs are grouped above). In this cases, the shape of the resection surface is identical but the location of remnant and resection volume are reversed (cf. Fig. 2.1 on page 10). Overall, the test database for the anatomical resections consisted of 45 manually defined resection surfaces (5 resection planes per group, and 10 resection volumes for each resection type, respectively).

For the evaluation of automatically generated **non-anatomical** resection proposals, 44 colorectal liver metastases were selected from 42 CT datasets. For these datasets a computer-assisted resection planning was performed. Analogous to the evaluation of anatomical resections, these resection proposals were defined by medical technicians.

Automatically and manually generated resection proposals were compared pairwise regarding a similarity measure between the resection volumes. As a similarity

measure the **Dice coefficient** (DC) between the resection volumes was used. The DC of two volumes x and y is defined as

$$\frac{2 \cdot |x \cap y|}{|x| + |y|}, \tag{4.5}$$

where x represents the remnant volume and y the resection volume or vice versa.

Results

Post-experiment analysis revealed that several of the automatically generated **anatomical resection** volumes coincide very well with the resection volumes defined manually by medical technicians (cf. Table 4.1). Nevertheless, automatically generated resection surfaces located in the right liver lobe, i.e., *Right Posterior Sectionectomy*, *Left Trisectionectomy* and *Central Resections*, showed comparatively poorer results. A visual comparison with the manually defined resection surface revealed that the manually defined resection surfaces within the right liver lobe do not align with portal venous territories. Instead, parts of the the right hepatic vein are often used as a border for these resections. A subsequent discussion with medical technicians concerning this issue revealed that the consideration of the right hepatic vein would better fit to the needs of most surgeons.

Apart from that, the consideration of the hepatic vein should be important for all resection types. A subsequent analysis of the utilized 3D planning models proved that the borders of the portal vein territories align quite well with the middle and left hepatic vein. This fact was not found to be true for the right hepatic vein.

The analysis of **non-anatomical resections** provided different result depending on the generation methods (geometric-based, perfusion-based) and the selected safety margin (cf. Table 4.2 and 4.3). The best DC was achieved for the perfusion-based methods. Overall, the variation is much higher and the mean DC is considerably lower compared to the anatomical approach. There might be several reasons for these differences. First, the access path calculation used in the proposed method is relatively simple (shortest path between tumor center and the convex hull of the liver). From a surgical point of view, this methods let to non-optimal access paths. Second, the proposed methods for non-anatomical resections are sensitive against changes in the safety margin. This is especially true for the perfusion-based method.

Concluding Remarks

As expected, the outcome of the proposed algorithms is not exactly the same as the manually planned resection proposals. As shown by Demedts [2010], manually defined resection proposals do not provide a gold standard. The chosen safety margin, the access path, and thus the location and extend of virtually planned resection volumes may vary depending on the medical user. A task for future evaluation studies might be to find a more appropriate benchmark. One possible solution could be to ask more than one surgeon to define the best possible resection proposal for

Resection Type	Min DC	Max DC	Mean DC (σ)
Left Hemihepatectomy	0.86	0.95	0.92 ($\pm$0.03)
Extended Right Hemihepatectomy	0.92	0.99	0.96 ($\pm$0.02)
Right Hemihepatectomy	0.89	0.98	0.96 ($\pm$0.03)
Extended Left Hemihepatectomy	0.88	0.95	0.92 ($\pm$0.02)
Left Lateral Sectionectomy	0.89	0.98	0.93 ($\pm$0.03)
Right Trisectionectomy	0.76	0.99	0.96 ($\pm$0.07)
Right Posterior Sectionectomy	0.43	0.74	0.64 ($\pm$0.09)
Left Trisectionectomy	0.22	0.95	0.69 ($\pm$0.24)
Central Resection	0.75	0.86	0.80 ($\pm$0.04)

Table 4.1: Automatically generated anatomical resection proposals compared to manually defined resection proposals (n=10)

Margin Width	Min DC	Max DC	Mean DC (σ)
1 mm	0.23	0.95	0.67 ($\pm$0.19)
5 mm	0.27	0.92	0.64 ($\pm$0.18)
10 mm	0.22	0.91	0.59 ($\pm$0.17)
15 mm	0.16	0.89	0.53 ($\pm$0.17)

Table 4.2: Automatically generated non-anatomical resection proposals (**geometric-based**) compared to manually defined resection proposals (n=44).

Margin Width	Min DC	Max DC	Mean DC (σ)
1 mm	0.18	0.96	0.73 ($\pm$0.18)
5 mm	0.30	0.94	0.72 ($\pm$0.22)
10 mm	0.31	0.94	0.59 ($\pm$0.18)
15 mm	0.17	0.94	0.48 ($\pm$0.19)

Table 4.3: Automatically generated non-anatomical resection proposals (**perfusion-based**) compared to manually defined proposals (n=44).

each dataset. This would increase the information value of the comparison result could lead to a better and more complete evaluation.

For further developments it would be important to know if participants could reliably distinguish between manually and automatically generated method and which parameters influence their decision. An evaluation study similar to a Turing test could provide this information. Therefore, a set of virtual resection proposals could be presented to surgeons separately and in sequence. While not providing information about the underlying generation method, participants could be asked to select the resection proposal they think is most appropriate for the patient.

A valuable extensions of the non-anatomical approach would be the improvement of the access path calculation. Therefore, multiple criteria such as a preferred direction or the spatial relation to adjacent lesions and vessels might be considered. A promising approach would be a combination with sophisticated access path calculations for liver tumor such as presented by Schumann et al. [2010].

It is an ambitious task to automatically create feasible resection proposals and it remains unclear whether this is even possible for all cases. However, in simple anatomical situation, the proposed methods achieve reasonable results, as demonstrated in this work.

Publications *Large parts of this chapter are published in different scientific papers. A preliminary version of the methods for intraoperative adaptation of risk analyses was presented at the 6th Annual Meeting of the German Society of Computer- and Robot-Assisted Surgery, Karlsruhe, Germany [Hansen et al., 2007a]. An improved and extended version including first results of the performed evaluation was presented at the SPIE Medical Imaging conference, San Diego, USA [Hansen et al., 2008b]. The methods for adaptation of resection proposals were presented on the 23th congress for Computer Assisted Radiology and Surgery (CARS), Barcelona, Spain and published in the International Journal of Computer Assisted Radiology and Surgery [Hansen et al., 2008d]. The final version of the IPA was presented on the MICCAI Workshop on Image Guidance and Computer Assistance for Soft-Tissue Interventions, New York, USA [Hansen et al., 2008c]. Work concerning the interaction with the Wii Remote was published together with Felix Ritter in the journal of i-com within a special issue for Human-Computer Interaction in the Operating Room [Ritter et al., 2009].*
A first approach for the automatic generation of resection proposals has been implemented by Björn Lindow within his master's thesis (supervised by the author) [Lindow, 2009]. Longquan Chen implemented a conical raster function within the scope of a student project (supervised by the author). The methods were further evaluated and extended within the context of this dissertation and have been presented on the 24th congress for Computer Assisted Radiology and Surgery (CARS), Genf, Switzerland [Hansen et al., 2010c].

5 Surgical Risk Maps

Less is sometimes more.

(Proverbial saying)

MANY similarities exist between aeronautical navigation and the emerging field of navigated liver surgery. However, few pilots would prefer to navigate their aircraft based on 3D models of virtual buildings, mountains, or clouds. Instead, the information pilots need for navigation is highly specific and abstract. Modern aeronautical cockpits are therefore equipped with displays which show the optimal flight path on distance-encoded maps (cf. Fig. 5.1).

Analogously, the work presented in this chapter aims to strip the superfluous information (the information not needed during surgery) from the preoperative models and only provide information required during surgery (critical structures and navigation aids).

Figure 5.1: Maps in the in the cockpit of an aircraft during the approach of a mountainous island. The topographic map in the upper right visualizes the position of the aircraft and the location and height of surrounding mountains.

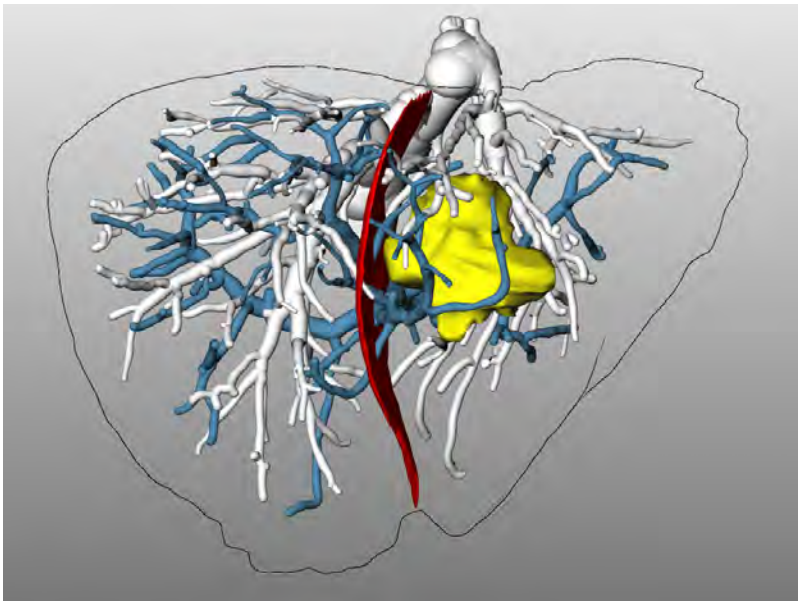

Figure 5.2: Common representation of a 3D planning model for liver surgery in the operation room. In cases in which interaction with the planning model is impossible or inapplicable, critical structures along the resection surface (red) are difficult to perceive.

5.1 Purpose

Optimal display of preoperative planning data in the operating room is challenging. Although advanced navigation systems for liver surgery are currently used in clinical studies, an expressive and effective intraoperative visualization of 3D planning models is still a pressing need.

During navigated liver surgery, visualizations of 3D planning models are currently used for guiding tracked surgical instruments. However, these 3D visualizations were actually intended for the exploration during the preoperative planning stage. As shown in Fig. 5.2, the intraoperative represented models often portray complex geometries and therefore demand cognitive effort and user interaction, especially if the surgeon wants to use them as a navigation aid. However, during surgery it is important that the surgeon focuses on the operating field and not on the navigation display on which the planning models are presented. Therefore, the presentation of information during surgery calls for a context-driven reduction of complexity. Attention should be focused on the preoperatively planned resection surface, adjacent tumors, and vessels at risk.

The objective of this work is to visualize surgically relevant information using a map display. Therefore, a new approach for risk analysis and visualization of planning models is presented that provides relevant information at a glance without the need for user interaction.

5.2 Related Work: Map Displays in Diagnosis and Treatment Planning

Map displays play an important role in diagnosis and medical treatment planning. They are mostly applied to reduce the exploration space from 3D to 2D. This section reviews important work in this field.

The introduction of virtual colonoscopy provided a new, non-invasive way to find pathologies in the colon. Because of the length of the colon, its inspection is time consuming and prone to errors [Hong et al., 2006]. Instead of navigating through the 3D model of the colon, Haker et al. [2000] introduced virtual **colon flattening**. The main challenge in this field is to provide a map that provides minimal distortion and preserves the shape of polyps. Research in this field is described in numerous publications, e.g., [Hong et al., 2006; Yao et al., 2010; Zeng et al., 2011] to name a few.

In neuroscience, cortical **brain flattening** is applied to compare patterns of brain activity across different individuals. The differences are usually hard to compare because of differences in cortical folding and functional foci are often buried within cortical sulci [Hurdal et al., 2009]. Similar to colon flattening, the minimization of distortion is a main challenge in order to provide a meaningful visualization. For a comprehensive overview of mapping techniques in this field refer to Hurdal et al.

[2009]. Apart from comparing brain activity patterns, maps are used for planning of neurosurgical interventions. In order to assist surgeons in selecting an access path to a target by avoiding risk structures, Navkar et al. [2010] proposed access maps for neurosurgery. Therefore, blood vessels are projected on the skin model of the patients head. The depth of the vessels is color-coded. A preliminary evaluation study indicated that the maps provide efficient planning support for procedures such as biopsy, tumor ablation, and deep brain stimulation.

In myocardial imaging, the so-called **bulls eye plot** is a commonly used visualization technique to represent the viability of the left ventricular myocardium. The viability is color-coded in a single 2D map. Therefore, a long-axis mapping of the myocardium is calculated based on late enhanced cardiac MRI images. Termeer et al. [2007] describe several techniques to further enhance conventional bulls eye plots. Particularly, they propose to annotate the map with the locations of coronary arteries. In addition, interaction and visualization techniques are provided to relate a selected area of the bulls eye plot to the 3D anatomy.

In the field of radio-frequency ablation, Rieder et al. [2010b] introduced the **tumor map**. It represents a pseudo-cylindrical mapping of a color-coded tumor surface on a 2D map. Colors encode simulated post-interventional coagulation zones. The tumor map allows for an immediate detection of residual tumor tissue and thus provides an effective way to assess the treatment success. A related approach for cerebral aneurysm surfaces is presented by Neugebauer et al. [2009]. They map the result of a 3D blood flow simulation on a 2D map. This provides an overview visualization as well as a bidirectional link to the 3D data.

5.3 Risk Maps for Liver Surgery

The aim of this work is to reduce the visual complexity of 3D planning models by mapping surgically relevant information onto a risk map. Therefore, methods for the identification and classification of critical anatomical structures in the proximity of a preoperatively planned resection surface are introduced (Sect. 5.3.1). For quick distance assessment during the intervention (without human-computer interaction), it is crucial to provide adequate spatial hints on the risk map. To visualize the distance from the resection surface to the critical structures shadow-like distance indicators are proposed (Sect. 5.3.2). In addition, contour lines are utilized to accentuate shape and spatial depth (Sect. 5.3.3).

5.3.1 Identification of Critical Structures

During a liver resection, the proximities of critical structures (vessels and tumors) to the resection surface need to be determined frequently. However, not all structures adjacent to a preoperatively planned resection surface are critical structures. Their criticality depends on several factors, such as the associated functional volume loss, their spatial relation to other structures, and the distance to the resection plane.

Whereas Lamata et al. [2008] classified all structures close to the resection surface as critical and are thus still confronted with a high number of structures to visualize, this work proposes to analyze the criticality of these structures in detail to reduce the number of visualized items.

To calculate critical regions along a resection surface, it is important to classify anatomical structures with respect to their importance. Potential critical structures include:

- Tumors
- Hepatic vessels

For tumors, the minimal **distance to the resection surface** is the main criterion, because contact with cancer cells must be avoided. Therefore, tumors are classified as critical structures if the minimum distance between a preoperatively defined safety margin around the tumor and the resection surface is smaller than a given threshold. The threshold can be determined by the surgeon.

For hepatic vessels, the identification of critical branches requires a more intensive analysis. Apart from the minimal distance to the resection surface, the associated **functional volume loss** V is a main criterion to define a branch as critical. The criticality analysis is based on an acyclic graph $G = (N, E)$, where nodes N represent vessel furcations and edges E represent branches.

Given a centerline voxel G_I of an edge E_J located inside the resection volume, its distance to the resection surface is irrelevant, because G_I is planned to be resected anyway. The same holds true for vessel sections inside the remnant volume whose parent branches are located inside the resection volume (cf. Fig. 5.3). In these cases, the criticality C of a centerline voxel G_I is set to 0. In all other cases, vessels that are critically close to the resection surface (cf. Fig. 5.4), and whose transection causes significant loss of functional liver volume, are classified as critical, which can be described as:

$$C(G_I) = \begin{cases} 1, & \text{if } (V_{GI} \geq I_V) \wedge (D_{GI} \leq I_D), \\ 0, & \text{else} \end{cases} \tag{5.1}$$

where V_{GI} is the amount of liver volume that is affected when the vessel is transected at G_I, and D_{GI} is the minimal distance between G_I and the resection surface. I_V and I_D are boundary values (margins) that can be adapted by the user, i.e., depending on the surgical strategy. These values have clear physical meaning: I_V represents the minimal affected liver volume (ml) for the associated branch and I_D represents the maximal Euclidean distance to the resection surface (mm).

In order to compute the minimal distance D_{GI} for all centerline voxels G_I, a Euclidean distance transformation of the resection surface D_{SURF} is calculated. To calculate V_{GI}, a Voronoi decomposition (nearest neighbor distance model) of the liver volume according to all centerline voxels of the segmented vascular structure is applied to approximate the perfusion and drainage areas. Combining this information with

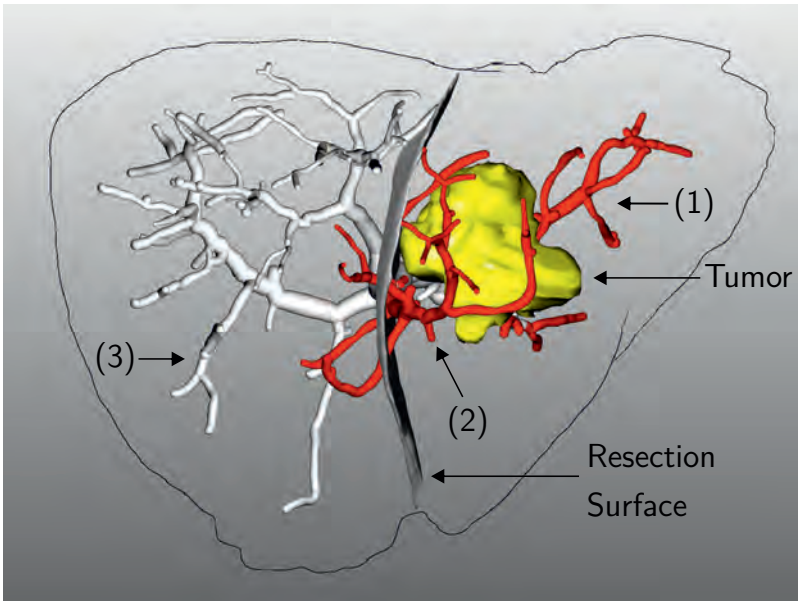

Figure 5.3: Portal venous vessel sections inside the resection volume (1) and vessel sections whose parent branches are located inside the resection volume (2) are defined as non-critical (red), while all other sections (3) are further analyzed in subsequent computation steps. For this, D_{GI} and V_{GI} are considered.

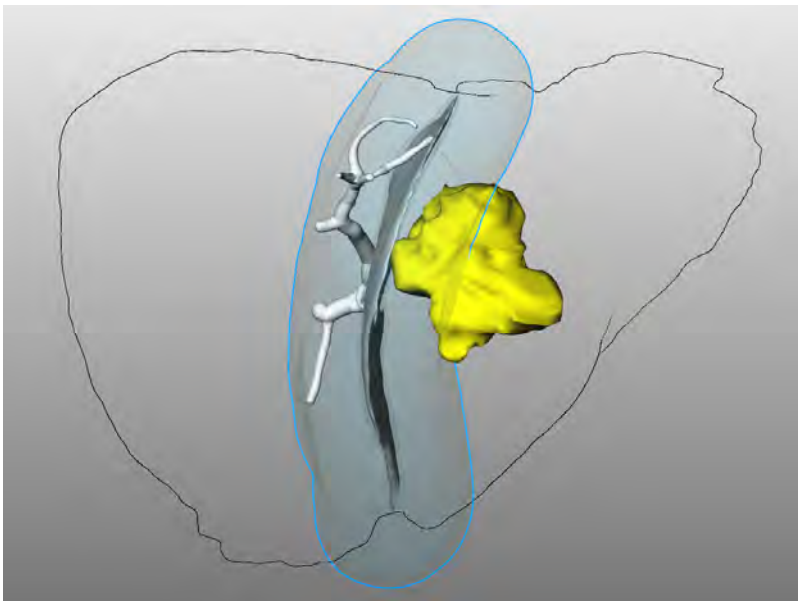

Figure 5.4: Tumor and critical vessel sections (C=1) within a specific margin ($D_{GI} \leq 20mm$) around the resection surface. The patient case is the same as in Fig. 5.3.

D_{SURF} and taking the hierarchical dependencies of the vascular trees into account by traversing G in level order (starting at leaves), a 3D lookup table is generated. This lookup table provides the affected liver volume in ml for each skeleton voxel G_I.

5.3.2 Visualization of Critical Areas and Resection Portals

Instead of enhancing the critical anatomic structures in the 3D model, a risk map is proposed which corresponds to the geometric model of the virtual resection surface and visually encodes the minimal distance to critical structures using shadow-like distance indicators. Therefore, a Euclidean distance transformation applied to anatomical structures that are classified as critical ($C = 1$) is calculated in 3D. Because the critical structures can be categorized into hepatic vessels (portal vein, hepatic vein) and tumors, three separate distance transformations D_{PV}, D_{HV}, D_T are generated. The hepatic artery and bile duct are not considered in the current prototype. In order to assess the distance transformation inside an OpenGL fragment program, D_{PV}, D_{HV}, D_T and D_{SURF} are stored in an 3D RGBA texture. Thereby, each distance map (D_{PV}, D_{HV}, D_T, D_{SURF}) is mapped to one of the four channels (RGBA). A texture lookup into the 3D texture (linear interpolation) returns the current value for each distance map.

To allow a quantitative assessment of distances between the resection surface and critical structures, the range of values on each map is divided into intervals, and colors are assigned to each interval (cf. Fig. 5.5). The colors encode different safety margins to the critical structures. These safety margin widths and colors can be adjusted by the user. By using different color templates for vessels and tumors, it is easy to visually identify so-called portals in which the surgeon must cut between two or more critical structures, e.g., between a tumor on one side and an important vessel on the other side of the resection surface (cf. Fig. 5.5a). In fact, portals are located at areas where intervals from vessels and tumors intersect.

5.3.3 Visualization of Shape and Spatial Depth

In liver surgery, preoperatively planned resection surfaces exhibit different shapes depending on factors such as the location of tumors or the surgical strategy. For quick distance assessment during the intervention (without human-computer interaction), it is crucial to provide adequate shape and depth hints on the risk map.

In this work contour lines as established in cartography are applied to encode different levels of elevation. To this end, a precomputed Euclidean distance map D_B provides the minimum distance from each vertex on the resection surface to the boundary of the resection surface. The current value of D_B on the resection surface is accessed via 3D texture lookup. Equidistant contour lines are mapped onto the resection surface by employing a smooth threshold function which provides stroke antialiasing as described in [Freudenberg, 2003] by evaluating the threshold function for each pixel in a fragment program, the line thickness can be influenced on a pixel-by-pixel basis (cf. Fig. 5.6). Thus, line thickness can be held constant or vary

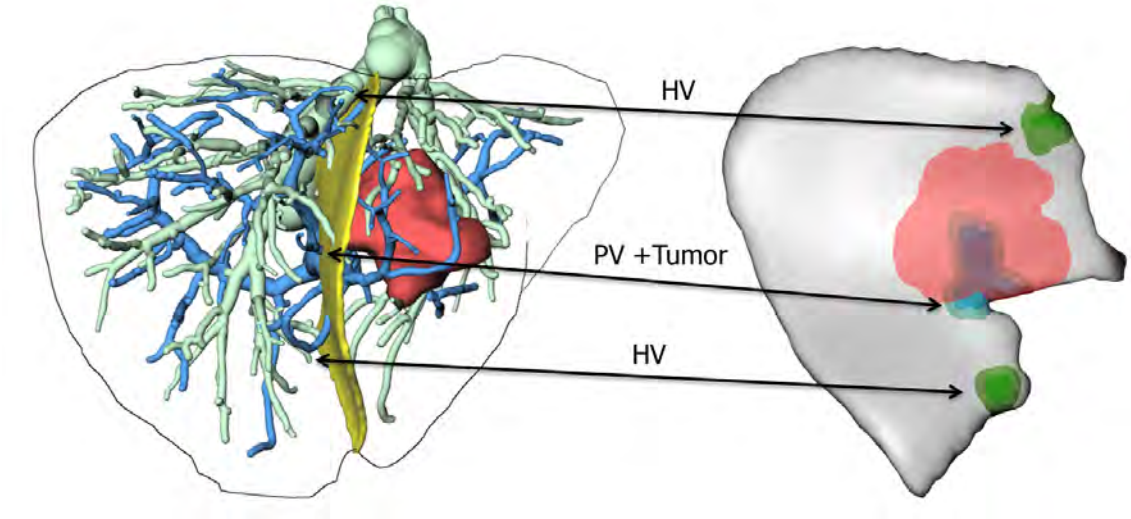

(a)

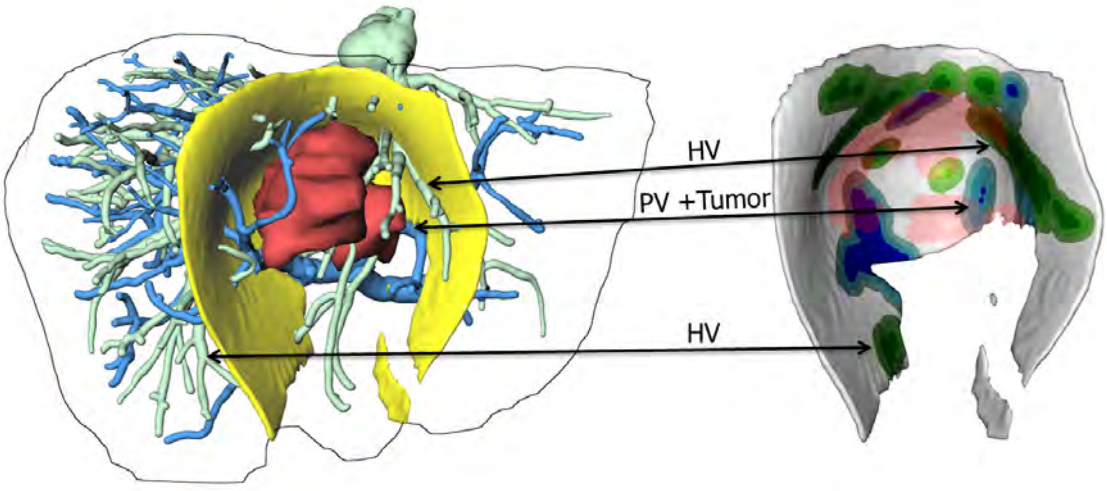

(b)

Figure 5.5: Risk maps ($I_V = 10$ml, $I_D = 10$mm) on the right and associated 3D planning models on the left. The connecting arrows indicate corresponding points in both models. (a) shows a resection proposal for an extended left hemihepatectomy and (b) for a central tumor resection. Shadow-like distance indicators on the risk map encode different safety margins to critical structures such as portal vein (blue contour intervals) and hepatic vein (green contour intervals). The light red area encodes the proximity ($\leq 10mm$) to a tumor.

linearly depending on the current value of D_B. In addition, the distances between lines can be adjusted, e.g., by 5mm, which facilitates a quantitative assessment of spatial depth.

5.4 Evaluation

In order to get clinical feedback about the risk map visualization, the development was accompanied by regular meetings with liver surgeons where the current development progress was presented and discussed. In addition, two formal evaluation studies were conducted that are described in this section. The central aim of these studies is to measure whether and how the visualization of risk maps facilitates the process of surgical risk assessment.

Study I: Experiment Design

Three experienced liver surgeons, not involved in the development of the risk maps, were interviewed. In the beginning, each surgeon was familiarized with the concept of identification of critical structures along a planned resection surface (cf. Sect. 5.3.1) which builds the basis for the risk map. This was done in a short slide presentation and an interactive software demo. All interviewed surgeons agreed that the proposed visualization of the risk map is intuitive and would be beneficial to support surgical planning and the execution of liver resections.

After the training phase, **eight stimuli** were presented separately and in randomized order. Each stimulus consisted of a resection plan (hemihepatectomy or extended hemihepatectomy) including vascular structures, tumors, and resection surface. Overall, four resection plans were presented to the surgeons. Each resection plan was presented twice, once without the risk map and once with risk map. The risk map was thereby displayed within the 3D planning model of the liver as shown in Fig. 5.7. Based on a discussion with a liver surgeon (who did not take part in the evaluation study), the distance values for all color intervals on the risk map were set to 1 mm and 5 mm. I_V was set to 10 ml and I_D to 5 mm.

For each stimulus, surgeons were asked to mark locations on the resection surface at which they would expect risk or difficulties during the actual resection. To accomplish that **task**, each surgeon received three colored pencils and several sheets of papers where different outlines of resection surfaces were printed on („empty“ risk maps). The marking had to be done in specific colors: red for the tumor, green for the hepatic vein, and blue for the portal vein (cf. Fig 5.9). Time and the amount of model rotation were captured. Within an attached questionnaire, surgeons had to rank how much the risk map supported them in assessing the surgical risk.

Study I provided first evaluation results (cf. Sect. 5.5) and facilitated the definition of hypotheses. These hypotheses were evaluated in a subsequent study.

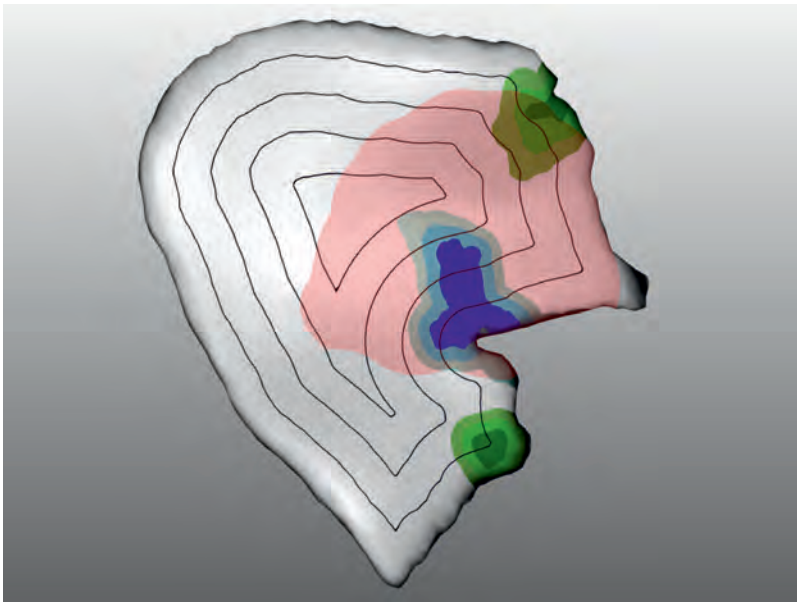

Figure 5.6: Risk map for an extended left hemihepatectomy ($I_V = 10$ml, $I_D = 10$mm). Equidistant contour lines encode the distance to the liver surface.

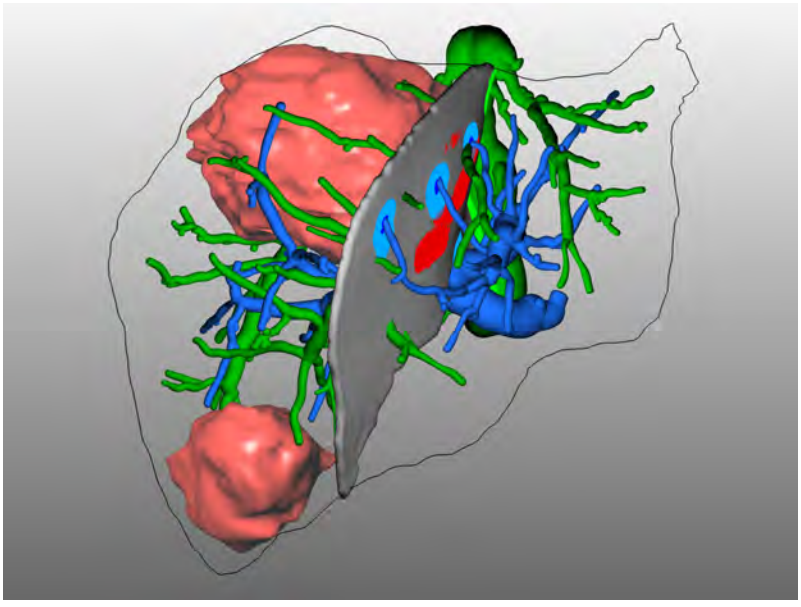

Figure 5.7: 3D model with risk map inside the model as used in study I. Compared to study II, the risk map was not additionally visualized in a second viewport.

Study II: Hypotheses

The improvement of user performance during navigated liver surgery is the main reason why the risk map was developed. Recall that surgical risk for a focused area on the planned resection surface needs to be frequently assessed during liver resection surgery, in particular during the transection of the liver parenchyma. Therefore, aspects of human-computer interaction in risk assessment were evaluated in a larger, second study.

In order to evaluate the risk map, the techniques have to be compared with a comparison system **C** that represents the state of the art in navigated liver surgery. In the context of this study, C is defined as the 3D visualization of planning models such as it is commonly used in navigation systems for liver resection surgery [Cash et al., 2007; Nowatschin et al., 2007; Beller et al., 2009b; Peterhans et al., 2010]. Let **R** be a system that provides a risk map visualization. The following null hypotheses regarding human-computer interaction are evaluated in the context of this study:

(H-1) R requires equal **time** for risk assessment as C, and

(H-2) the same amount of **errors** are made when estimating the surgical risk using R and C,

The hypotheses address the assessment of surgical risk for positions on the planned resection surface.

Study II: Experiment Design

The study consisted of two separate experiments. The two experiments for each participant were no closer than two weeks apart to minimize memory effects. Each participant was asked to evaluate 50 different **positions of a virtual surgical dissector** in 5 datasets (10 positions per dataset). In order to avoid expectation effects, half of the participants started with experiment **C**, while the other half started with experiment **R**. The question to be answered was the same for each position of the surgical dissector: „Which risk structures are located close (5 mm) to the instrument tip?“. The following possible answers were provided and had to be selected in a checkbox list:

- Portal vein
- Hepatic vein
- Tumor
- No risk

Multiple selections were possible. Subsequently, the participant was asked to directly press a next-button which triggers the loading of the next stimuli.

In experiment R, the stimulus consisted of a 3D planning model of the liver, including vascular structures, tumors, resection surface (hemihepatectomy or extended hemihepatectomy), and the 3D model of a surgical dissector. The instrument tip of the dissector was always located on the resection surface (cf. Fig 5.8). In addition, the risk map for the dataset was displayed in a second viewport. The stimulus in **experiment C** was identical except the fact that the risk map for the dataset was not displayed. In order to facilitate distance assessment in experiment C, a half-transparent sphere with a radius of 5 mm was located in the center of the instrument tip.

Before starting each experiment session, participants were informed which structures in the liver model are defined as risk structures. Therefore, a printout of Fig. 5.3 was presented and the concept to identify risk structures was explained (cf. Sect. 5.3.1). In addition, the following instructions were given to participants at the beginning of each experiment:

(1) Please interact with the provided visualization only if this is necessary in order to answer the current question.

(2) Please answer the questions as fast as possible.

(3) Please answer each question correctly.

Subsequently, the participants started the experiment with a training dataset of 10 stimuli. Within this training phase open questions were answered by the test supervisor. After finishing the training phase, every participant confirmed that she or he understood the task. Subsequently, the test phase started with a presentation of 50 test stimuli as described above.

The subject pool consisted of 10 participants, including 7 scientists (engineers, mathematicians, computer scientists) and 3 radiologic technicians. All participants were familiar with the anatomy of the human liver and had experience with 3D planning models of the liver and 3D viewers.

5.5 Results

An analysis of the recorded data from **Study I** revealed that surgeons were faster in risk assessment when the risk maps were presented. In addition, the amount of model rotations (cumulated rotation angle of the viewer camera) was lower. However, these differences did not reach statistical significance (Wilcoxon test with $p > 0.05$), which could be ascribed to the little number of participants. The analysis of the qualitative results from the questionnaire indicated that the risk map supported surgeons in assessing risk. The mean response was 3.06 ($\sigma = 0.4$) on a Likert scale from 1 to 4 (1 = strongly disagree, 2 = disagree, 3 = agree, 4 = strongly agree).

An analysis of the hand-drawn risk maps revealed that the assessment of risk along a planned resection surface varies depending on the observer. Surgeons had

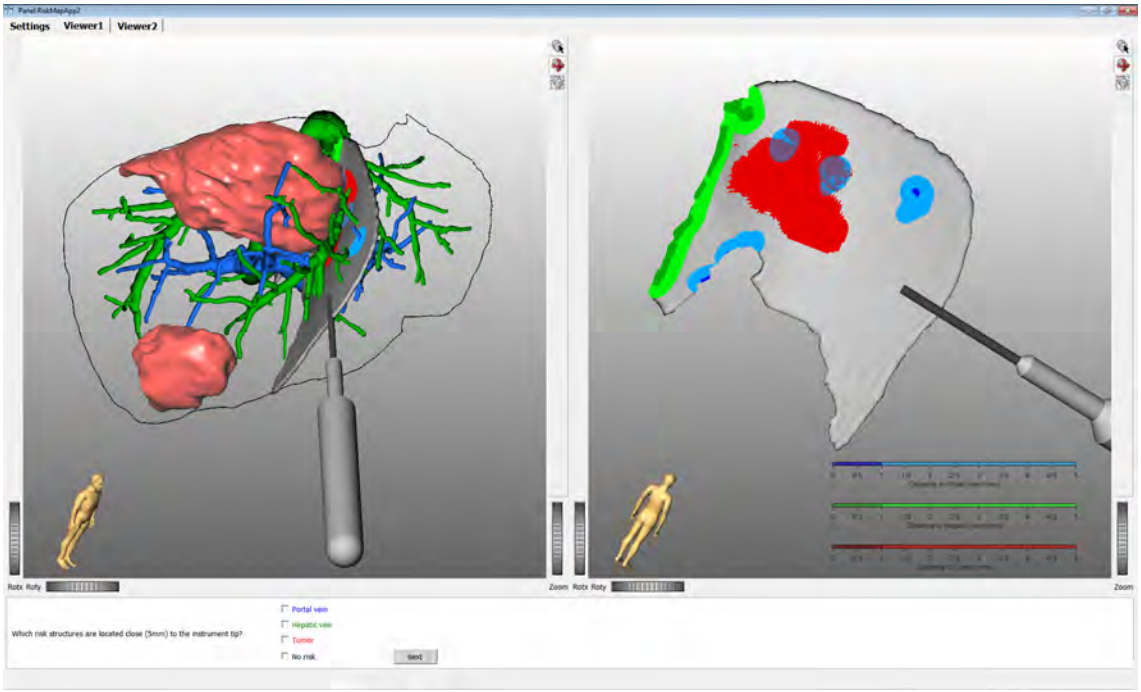

Figure 5.8: Screenshot of the software application that was used in experiment R. The 3D planning model is shown on the left and the risk map on the right. The superimposed legend in the right viewer (lower right corner) maps the used colors of the risk map to distance values. At the bottom part of the screenshot, four checkboxes and a next-button are arranged in order to gather answers from the participants.

differing definitions of what a critical area on a resection surface would be (cf. Fig. 5.9). This might be ascribed to the fact that participants exhibit different levels of experience and thus different kinds of risk awareness. The perceived level of risk can be technically described through the volume threshold I_V, the distance threshold I_D, and the distances used for the color intervals on the risk map. The analysis of the drawings showed that especially changes of I_V simulate different levels of risk (cf. Fig. 5.9). In conclusion, the parameters of the risk map need to adapt not only to the type of intervention but also to surgical preferences and the level of individual experience with this type of intervention.

Study II focused on aspects of human-computer interaction. Statistical analysis consisted of comparisons of the arithmetic means between data from experiment C and experiment R. Differences were tested using the Wilcoxon test and a $p < 0.05$ was defined as statistically significant. Both null hypotheses defined above could be rejected. The measured times for risk assessment (cf. Fig. 5.10) were significantly lower in experiment R. In addition, participants made fewer errors in risk assessment during experiment R than in C (cf. Fig. 5.11). Only 81.4 % of judgments were correct in C, compared to 99.96 % in R. In experiment C, false negative judgments (50.6 %) were approximately as often made as false-positive judgments (49.4 %).

The risk map approach was implemented using the rapid prototyping software MeVisLab [Ritter et al., 2011]. The rendering is performed using GLSL. Because the resultant visualization is solely based on a single OpenGL fragment program and a set of 3D textures, the risk map can be displayed on any system which supports OpenGL 2.0. Only a custom fragment shader needs to be implemented. The calculation of the required 3D textures requires around 10 s, depending on the size of the volume dataset and the hardware setup (compare hardware specification for the planning system in the appendix on page 155). The risk map visualization achieves interactive framerates on the specified graphic hardware.

5.6 Discussion and Conclusion

The first study showed that the parameter I_V is especially important to visualize different risk levels. An interactive manipulation of I_V would be desirable. However, changes in I_V require a re-identification of critical vascular structures as described in Sect. 5.3.1. Although not all calculation steps need to be repeated completely, the update requires at least the re-calculation of the Euclidean distance transformation (which encodes the distance to the critical structures) and an update of the associated 3D texture. A complete implementation on the GPU would probably facilitate faster update processes. Another possibility would be to identify standard parameter settings for I_V. Such standardization would enable better comparison of risk maps from different patients and might introduce a reliable measure for the difficulty of a resection, similar to the approach described by Beller et al. [2009a].

Alternative criticality measures, such as the vessel diameter at the position of G_I or the path length were not considered in this work. The parameter V_{GI} is of

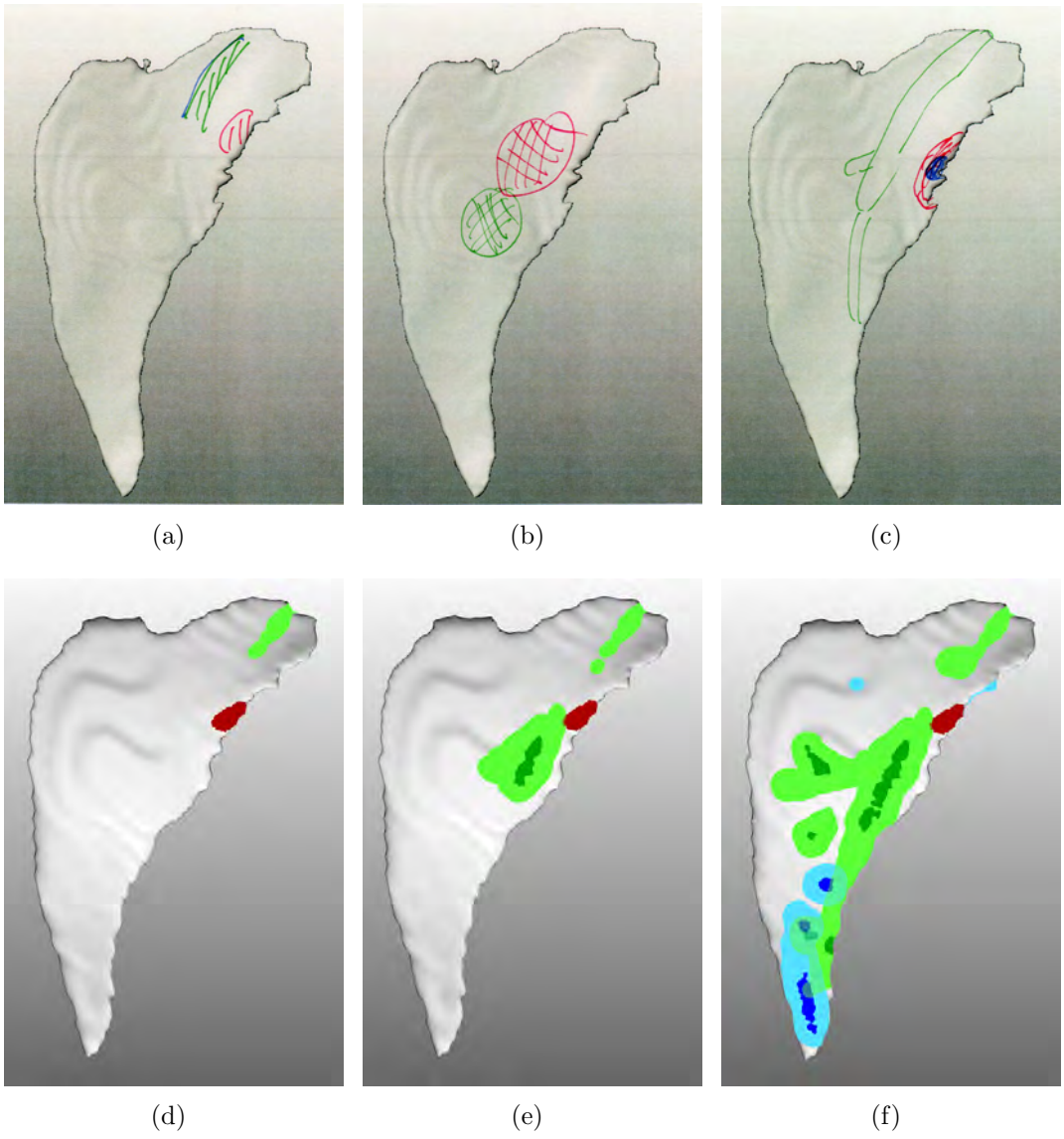

(a) (b) (c)

(d) (e) (f)

Figure 5.9: (a-c) Hand-painted risk maps by three different surgeons based on a presentation of 3D planning models. The drawings show that the level of perceived risk varies depending on the observer. (d-f) Computer-generated risk maps using different values of I_V (500 ml, 100 ml, 10 ml). 1 mm and 5 mm were chosen as distance values for the color intervals.

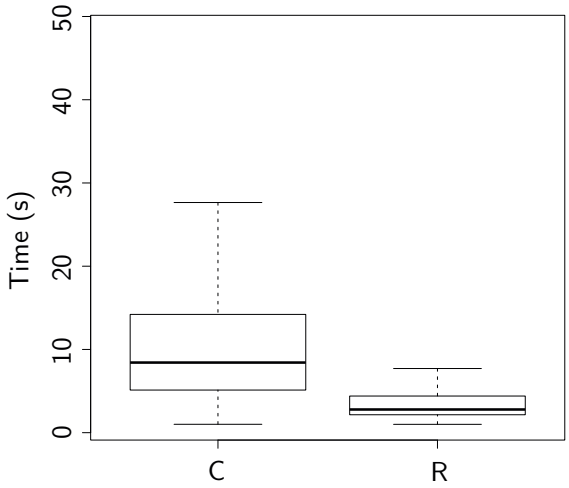

Figure 5.10: Mean **times** per participant for experiment C (Min = 1.0, 1st Qu. = 5.1, Median = 8.4, 3rd Qu. = 14.2, Max = 27.6) and for experiment R (Min = 1.0, 1st Qu. = 2.1, Median = 2.7, 3rd Qu. = 4.4, Max = 7.7).

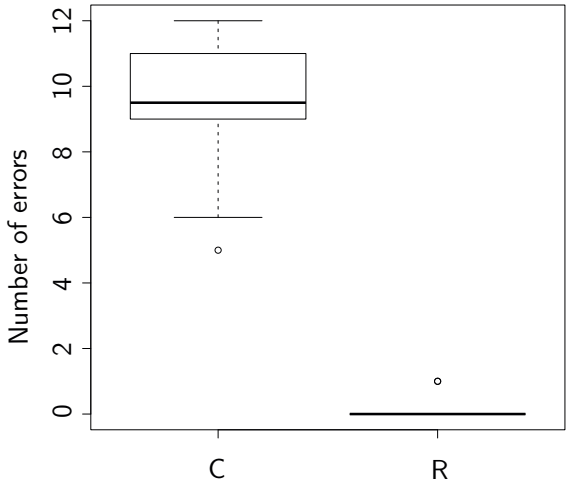

Figure 5.11: Number of **errors** per participant for experiment C (Min = 6.0 , 1st Qu. = 9.0, Median = 9.5, 3rd Qu. = 11.0, Max = 12.0) and experiment R (Min = 0.0 , 1st Qu. = 0.0, Median = 0.0 , 3rd Qu. = 0.0, Max = 1.0).

utmost importance when assessing criticality (particularly for patients with marginal remnant liver volume), because clinical studies report the remnant liver volume as an essential factor for operability [Broek et al., 2008]. Nevertheless, a combination of V_{GI} with risk measures involving an analysis of different safety margins around tumors (cf. Chapter 3) could be a valuable extension to the method.

The second study revealed that risk maps are an effective visualization to assess risk in liver resection surgery. Using the risk map as additional information, participants are faster and make fewer errors. However, the performed experiments did not exactly match the situation of an actual liver resection. Instead of having to concentrate on the operating field, participants could completely focus on the visualized planning data. Assuming a realistic operational setting, it is suspected that the amount of user interaction (model rotation, camera panning) and process time decreases for settings such as those in experiment C. This decrease would probably be accompanied with an increase in assessment errors. In this context, it would be interesting to measure how many errors are made when using the risk map.

A future step will be the application of risk maps in the operating room during liver surgery. Because the liver is a deformable object, the issue of the validity of this distance information during liver surgery arises. It is obvious that the static distance information visualized in the risk map could not be valid during the whole intervention, especially during parenchyma transection. Methods for intraoperative adaptation of the risk map might be necessary to provide reliable support for resection guidance. This requires repeated re-registration or a continuous tracking of liver deformation (refer Sect. 2.2.4 on page 30). Nevertheless, apart from an accurate visualization of distance information, the risk map provides a general overview of potential areas at risk along the planned resection surface. Besides intraoperative application, the risk map could also support resection planning.

In summary, a method for the identification and classification of critical structures along a resection surface is introduced in the context of this work. Critical regions are visualized on a risk map in a clear and intuitive way. Thus, surgeons are provided with additional information that is not directly visible in the radiological data. The approach provides a new and objective basis for the assessment of risks. The performed evaluations indicate that the risk map may prevent possible damage to risk structures and thus has the potential to enhance patient safety during liver surgery. To the knowledge of the author, the presented method is, in addition to the work of Lamata et al. [2008], one of the first approaches towards a simplified and effective visualization of surgical risk in liver surgery. Related methods for risk assessment were primarily designed for the preoperative planning stage and of limited use during liver interventions.

The concept of risk maps was designed for intraoperative guidance in navigated liver surgery. Application during preoperative planning or to other surgical fields, such as neurosurgery, shows great promise and could be part of future research. Even without integration in the surgical navigation system, the risk maps may improve the orientation and the confidence of surgeons while transferring a preoperative resection plan to the operative site.

Publications *The methods described in this chapter have been presented at the SPIE Medical Imaging conference, San Diego, USA [Hansen et al., 2010b]. The presented evaluation studies have not been published at the time of submission of this thesis.*

6 Illustrative Augmented Reality

> We know nothing truly, for the truth lies hidden in the depth.
>
> *(Democritus)*

DURING navigated liver intervention, surgeons need to frequently shift their visual focus to access preoperative planning data (cf. Fig. 6.1). Based on observations from such interventions and many discussions with surgeons, a mental fusion of planning models with the current surgical view is prone to error. Furthermore, it results in frequent distracting comparisons during the intervention that consume an unacceptable amount of time. Therefore, AR approaches that augment planning information with the surgical view obtain increasing acceptance in navigated surgery.

This chapter presents methods for intraoperative visualization of 3D planning models which extend illustrative rendering and AR techniques.

6.1 Purpose

Numerous applications for medical AR apply classical rendering methods (e.g., Gouraud or Phong Shading) for overlaying graphical information [Kersten-Oertel et al., 2011]. However, opaque planning models such as vascular structures, organ surfaces, and tumors can occlude the surgical view in a way that is inappropriate in surgical routine. The use of transparency, on the other hand, complicates the perception of relative depth distances between surfaces [Interrante et al., 1997], particularly if manual rotation of the model is not possible. Moreover, the assessment of spatial relations in static images is difficult even when opaque models are presented (refer to the study described in Ritter et al. [2006]).

A meaningful augmentation of the surgical view with a 3D visualization of planning data which allows reliable comparisons of distances and spatial relations is still an open request. To improve the understanding of spatial relations and depth, illustrative visualization methods for complex 3D planning models that encode relevant distance information are presented in this chapter. The methods reduce visual complexity of 3D planning models and accentuate spatial relations between relevant objects. The main contribution is an advanced silhouette algorithm for 3D planning models (distance-encoding silhouettes) combined with procedural textures (distance-encoding surfaces). In addition, a method for illustrative visualization of resection surfaces is presented. The methods are integrated in an AR application for liver surgery.

6.2 Related Work: Techniques for Improvement of Spatial Perception in Medical AR

Incorrect depth interpretation is the most common perceptional problem in AR applications, interfering with the interpretation of spatial relationships between the first person perspectives, the objects in view, and the overlaid information [Kruijff et al., 2010]. The surgical need to exactly assess spatial information of planning models during an intervention has lead to the development of several techniques which attempt to improve spatial perception in AR applications.

Several AR applications provide depth cues through **motion parallax**. Motion parallax is an important depth cue that is observed when objects with a short distance to the observer move farther across the field of view than objects far away from the observer. This effect occurs when the observer or the objects move. In the context of projector-based AR, Riechmann [2006] proposed to project vascular structures onto an organ surface via projective texture mapping while tracking the surgeons head. However, a permanent tracking via head-attached tracking applicators is necessary to perceive depth cues via motion parallax. This head movement might affect the surgical workflow, e.g. by forcing surgeons to move their head to improve depth perception. Another approach by Sielhorst et al. [2006] that utilizes motion parallax describes a “virtual window” for HMD-based AR which creates the feeling

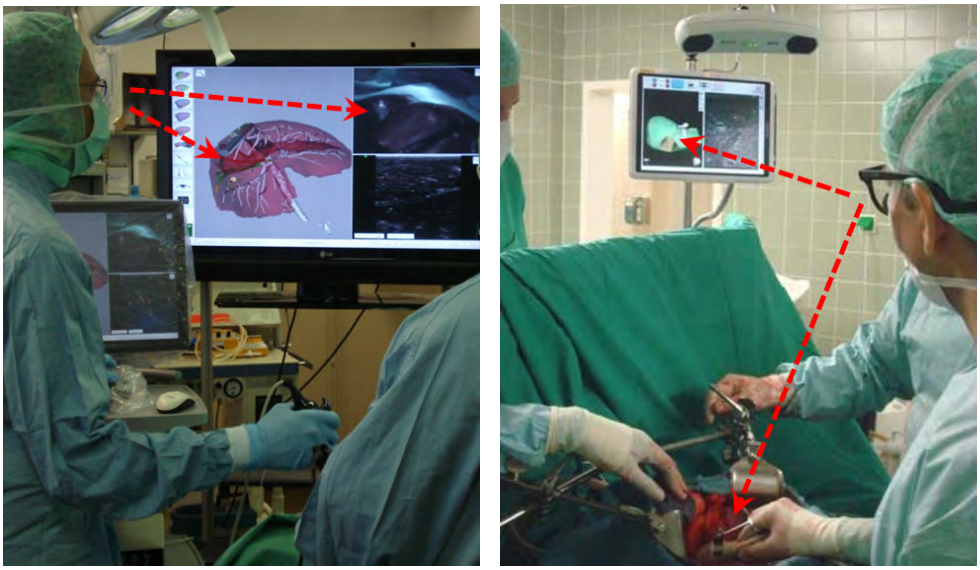

(a) (b)

Figure 6.1: (a) Intraoperative visualization of 3D planning models on the screen of a navigation system for laparoscopic surgery. The screen shows the 3D planning model (left), the laparoscopic video stream (upper right), and the IOUS stream (lower right). (b) Intraoperative visualization of 3D planning models for navigated open liver surgery. Image Courtesy University Hospital Lübeck, Germany and General Hospital Celle, Germany.

of getting a view on the inside of the patient. The window plane is slightly structured with a texture in order to additionally enhance depth perception through partial occlusion when using a tracked HMD. However, HMD's can handicap a surgeon during interventions and need further technological improvement before getting into the operating room.

Multiple viewports have been proposed to enhance depth perception in AR without forcing observers to change their viewing position or to rotate the model. Navab et al. [2007b] presented a render-to-texture approach, termed virtual mirror, for medical AR which provides additional views on the planning model. Particularly, the interpretation of partial self-occlusions inside complex planning models is improved.

The correct display of **occlusion** between virtual models and real objects is a main challenge in AR. In an ideal case, the real object is tracked and its geometry is known, e.g., a surgical instrument that is tracked by a navigation system. Otherwise the position and geometry needs to be captured, e.g. through video analysis. Fischer et al. [2007] use a TOF camera, which provides a 2D distance map of the real scene. By performing a registration between distance map and virtual 3D models, the distance map is used to decide which objects are rendered in front. A common way is to change the rendering style for occluded objects, e.g., using a wireframe presentation [Tsuda et al., 2005], transparency [Elmqvist et al., 2007], or focus and context techniques [Kalkofen et al., 2007].

Based on traditional illustration techniques, a variety of **illustrative visualization** methods have been proposed in order to increase expressiveness of 3D models. Detailed overviews can be found in the theses of Bruckner [2008] and Tietjen [2009]. An interesting approach is described by Lerotic et al. [2007]. They analyze surface features from stereo laparoscopic camera images and derive the orientation of the organ surface. This information is used to generate a translucent contour layer. Surfaces of the real scene that are parallel to the viewing plane are rendered as transparent whilst sloped structures are accentuated using non-photorealistic rendering (strokes). Thereby, surface features are extracted and augmented in correct depth order. An associated user study proved that the proposed visualization led to improved depth assessment.

Bichlmeier et al. [2007] presented an approach that uses surface topology, viewing attributes, and the location of surgical instruments to generate a transparency map that is applied to control the pixel transparency of video images. Thus, a context-preserving focus region is provided that facilitates depth perception. Fischer et al. [2005] developed an illustrative rendering technique that is capable of generating a stylized augmented video stream. Based on an edge-detection algorithm, silhouettes are extracted and applied to both the camera image and the virtual objects. Through this approach, visual realism of the virtual objects and the real camera image is reduced. Both modalities become less distinguishable from each other and thus an improved immersion can be achieved. A similar approach is described in [Kalkofen et al., 2007], however, they apply silhouettes to visualize hidden objects in the area of augmentation (x-ray visualization). Complexity of the superimposed silhouettes is controlled by an importance measure and an interactive, user controlled filter.

Prior Work

The new techniques proposed in the following section are based on prior work [Hansen, 2006; Ritter et al., 2006] in the field of illustrative visualization. The techniques accentuate spatial depth of 3D vascular structures and improve the perceptive separation of important vascular properties such as branching level and supply area. Besides a GPU-based hatching algorithm for tubular structures (distance-encoding surfaces), shadow-like depth indicators (distance-encoding shadows), which enable reliable comparisons of depth distances, are introduced. A user study that was performed in the context of this preliminary work revealed that the developed techniques provide appropriate monoscopic depth cues to assess distances in static representations of 3D liver planning models.

6.3 Illustrative AR for Liver Surgery

This section presents new techniques for illustrative visualization of 3D planning models for liver surgery. Thereby, planning information is either projected onto the liver surface during open liver surgery using a light projector as described in [Glossop, N. 2003; Riechmann et al., 2006; Krempien et al., 2008; Gavaghan et al., 2011], or rather superimposed with the images from a laparoscopic camera [Feuerstein et al., 2008; Scheuering et al., 2003; Marescaux et al., 2004].

First, a requirement analysis is presented. Second, clinical visualization scenarios that guided the development are described. Third, an advanced silhouette algorithm for 3D planning models, termed distance-encoding silhouettes, is introduced. Fourth, several visualization techniques are presented in which distance-encoding silhouettes are applied together with distance-encoding surfaces. Finally, a method for illustrative visualization of resection surfaces is presented.

Requirement Analysis

An augmentation of the surgical view by planning models may result in unacceptable occlusions of the operation field or misinterpretation of spatial relations, colors, and contrast. Therefore, the proposed visualization approach is guided by three requirements:

- Spatial depth of planning models must be perceivable, even in static images,
- occlusion of the surgical view by planning models should be minimal,
- transitions in color and brightness must be avoided in order to ensure a maximal contrast.

Visualization Scenarios

To test the usability of the methods, three visualization scenarios were specified in collaboration with experienced liver surgeons. These scenarios represent surgical situations wherein expressive visualizations are requested:

(1) **Anatomical Overview**: This scenario contains all tumors identified preoperatively and their relations to relevant vascular structures. Besides providing an abstract overview of available planning objects, this visualization scenario allows fast assessment of alignment errors between the real and the virtual world.

(2) **Focusing the current tumor**: During the treatment of a specific tumor, this visualization provides information about surrounding risk structures such as vessels which are invisible for the surgeon.

(3) **Focusing the virtual resection surface**: In case of a precise prepared resection strategy, this scenario provides spatial information of the virtual resection surface, while enhancing its relation to risk structures.

Predefined views for each scenario are generated in advance and provided intraoperatively. In the following subsections the developed illustrative rendering techniques are described.

6.3.1 Distance-Encoding Silhouettes

Silhouettes play an important role in figure-to-ground distinction and can be applied to reduce the visual complexity of geometric models. However, the abstraction of a classical shaded object to its silhouette results in the loss of shading information and consequently in a reduction of depth cues. Therefore, conventional silhouette algorithms are enhanced by two optional rendering settings.

The first extension allows for varying the **stroke thickness** of silhouettes continuously by using the distance to relevant objects (organ surface, adjacent risk structures, or surgical tracked instruments) as input. The distance-dependent scaling of silhouettes is similar to the concept described by Isenberg et al. [2002], however, the algorithm proposed in this work controls the stroke thickness on the GPU using two framebuffer objects. The algorithm is based on a translation of each vertex of the 3D planning model in direction of its normal by a vertex shader. Utilizing multiple render targets, the silhouette is calculated by subtracting the original planning model from the scaled model in a fragment program. The length of the applied vertex translation is defined by calculating a distance value, e.g. the distance between a vertex and the tip of a tracked surgical instrument, via built-in shader functions. Alternatively, it is possible to exploit a precomputed 3D distance map via texture lookup. The algorithm controls stroke thickness within a user-defined interval (minimum and maximum stroke thickness). Irrelevant parts of the model can thus be omitted.

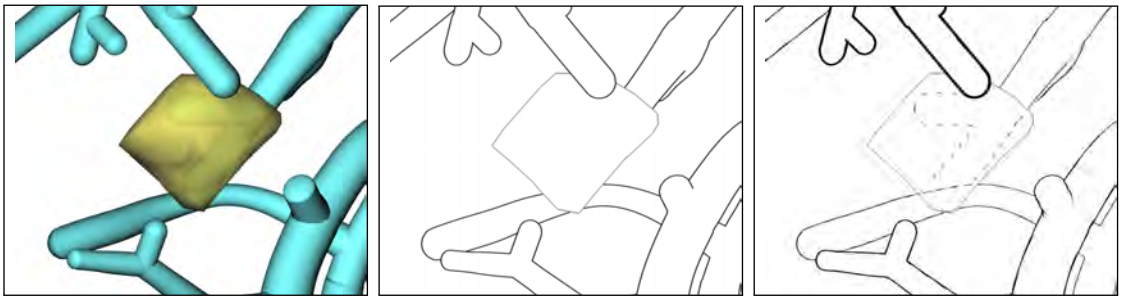

(a) (b) (c)

Figure 6.2: (a) Focusing a tumor using classical rendering techniques. (b) A silhouette representation of the scene results in a loss of depth cues. Occluded vessel branches are not visible. (c) Distance-encoding silhouettes allow for the accentuation of important vessels by applying varying stroke thickness, while occluded vessels are emphasized via varying stroke styles.

The second extension uses **different stroke styles** (solid, dashed, dotted) to accentuate view-dependent spatial relations (in front, within, behind) of interwoven objects. The developed rendering styles are particularly important for vessels that intersect other planning models such as resection volumes, territories at risk, or tumors. The stroke styles are varied by means of a sawtooth function in a fragment program. Occluded objects are detected using the depth buffer, while overlapping objects are identified by a texture look-up in the underlying 3D segmentation masks of planning models. Figure 6.2a shows an example for a close-up view of a tumor with surrounding vessels rendered with classical shading (cf. Fig. 6.2a), conventional silhouettes (cf. Fig. 6.2b), and the proposed techniques termed distance-encoding silhouettes (cf. Fig. 6.2c).

6.3.2 Distance-Encoding Surfaces

Distance-encoding surfaces provide the observer with distance information displayed on the surface of geometric objects. This technique was introduced in [Ritter et al., 2006] to visualize the distance of vascular structures to the observer by using texture gradients as additional depth cues. A procedural stroke texture with varying stroke thickness is used for this purpose.

Instead of applying a hatching texture on the whole vessel system, a distance-based transfer function is exploited to limit the use of texture to a specific scope. Thus, distances between arbitrary planning objects can be visualized, e.g. vessels at risk can be accentuated while their spatial relation to other objects (organ surface, vascular territories, and tracked surgical instruments) is encoded by distance-encoding silhouettes. In addition, this enables the combination of distance-encoding surfaces with distance-encoding silhouettes. Figure 6.4 shows an example for the combination of both techniques: vessels at risk are emphasized using a distance-encoding surface

while a distance-encoding silhouette highlights branches close to the organ surface.

Regarding the tumor scenario, spatial relations between a tumor and surrounding risk structures have to be visualized. Besides the distance between tumors and vessels, the location of a vessel (in front, inside, or behind a specific tumor) has to be clearly perceivable in order to support surgical decisions. Inspired by standardized conventions in technical drawings, spatial relations are encoded as follows: Vessels in front of the volume are encoded by the union of the distance-encoding surface and the distance-encoding silhouette. Vessels within the volume are rendered as solid silhouette, while occluded vessels are rendered as dotted or dashed silhouette (cf. Fig. 6.3). In order to achieve corresponding stroke- and texture-frequencies, the silhouette style for occluded vessels is controlled by the same sawtooth function as the distance-encoding surface.

6.3.3 Contour Lines for Resection Surfaces

If a resection plan has been created before surgery, the aim of an intervention is to execute the preoperatively planned resection as accurately as possible. If a 3D model of the resection surface is used for this purpose, it is important to provide the surgeon with reliable information about distances of the virtual resection surface to other relevant objects like the liver surface, vessels, or surgical instruments. Contour lines (also named isolines) were found to be appropriate for this purpose. They provide an efficient representation of data changing continuously which is often used on topographic maps to represent points of equal value.

For the visualization of virtual resection surfaces, contour lines are projected onto the outer shape of resection volumes. The distance between contour lines is controlled by exploiting a precomputed Euclidian distance map. This distance map encodes the shortest distance of each liver voxel to the liver surface. Thus, line thickness can be kept constant or varied linear depending on a distance function in a fragment program. In addition, the distances between lines can be adjusted, e.g. 5 mm, which facilitates quantitative assessment of spatial depth. As illustrated in Fig. 6.5, the proposed contour lines can also be combined with distance-encoding silhouettes and distance encoding-surfaces.

6.4 Evaluation

To verify the expressiveness of our illustration methods, we performed a user study under controlled conditions. In addition, a preliminary test in the operating room was preformed.

User Study

As part of a user study with liver experts, design considerations presented in Sect. 6.3 were verified under controlled lab conditions using verbal comments as data accord-

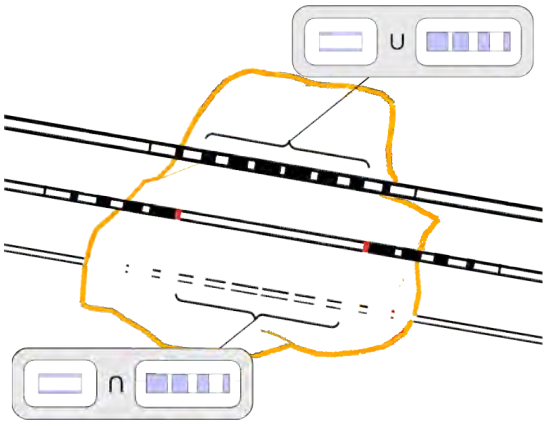

Figure 6.3: Combination of distance-encoding silhouettes and distance-encoding surfaces to visualize spatial relations between vessels and a tumor (tumor scenario).

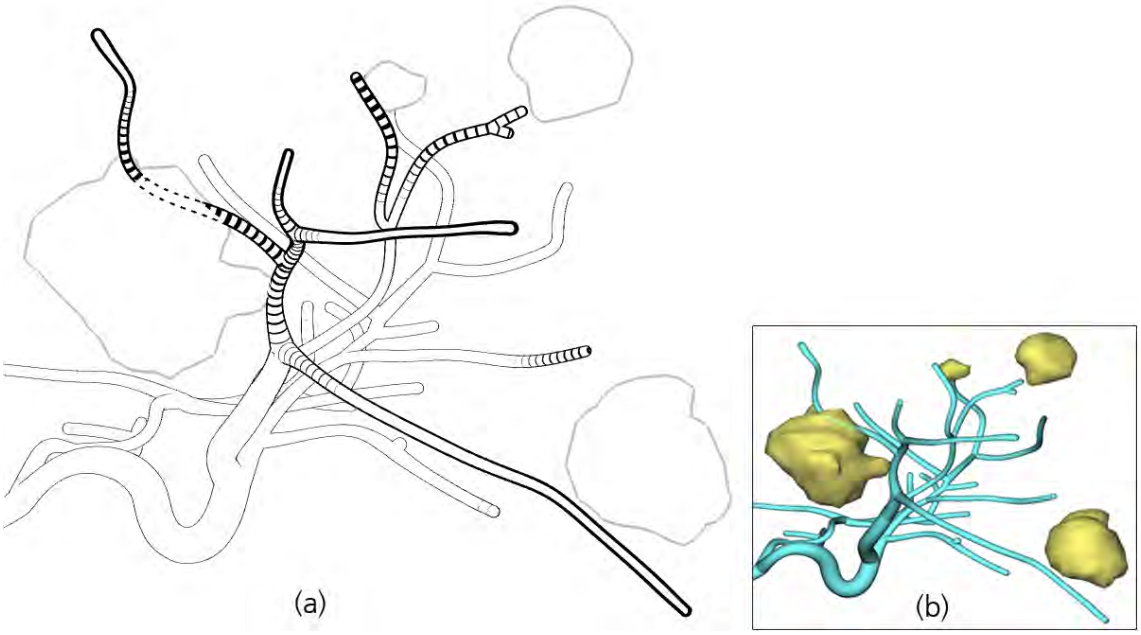

Figure 6.4: Illustrative visualization approach (a) in comparison to the classical rendering (b). While the spatial relations between vessels and tumors are difficult to perceive in (a), vessels at risk are accentuated in (b) using a varying stroke texture, termed distance-encoding surface. The distance-encoding silhouette enhances branches close to the organ surface (varying silhouette thickness). The part of the vessel behind the left tumor is accentuated with dashed strokes.

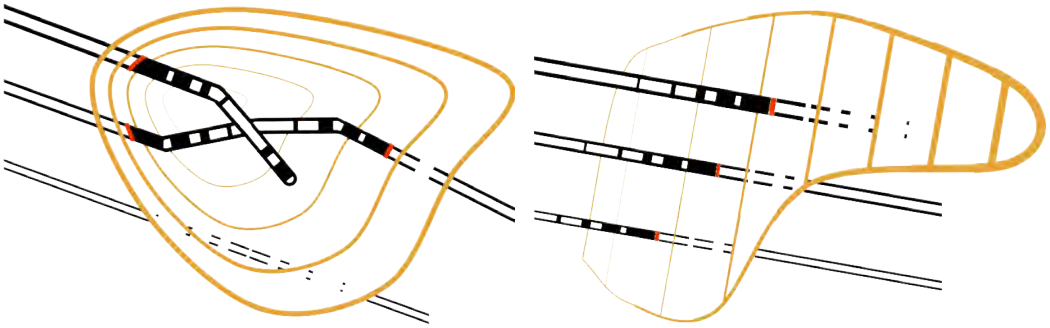

(a) (b)

Figure 6.5: (a) Illustration of a wedge-shaped resection via contour lines. Line thickness depends on the distance to the organ's surface and is reduced with increasing distance. Contour lines are equidistant which allows a quantitative assessment of distance. (b) Illustration of a planar resection. Spatial depth is encoded via the thickness of silhouettes and contour lines.

ing to the Think-Aloud protocol [Ericsson et al., 1993]. Therefore, an electronic questionnaire was created that contained single video frames from laparoscopic and open liver interventions with overlayed planning models as well as photos from a projector-based AR visualization using a cadaver liver of a pig. In order to probe the subjects' perception of spatial relations, tasks that require a precise judgment of distances were designed. Three vessel positions in each image were labeled with markers, while each task started with a question about the distance of these markers to a second object (e.g. tumor, resection surface, organ surface). Participants were asked to determine the correct order of marks. Because the effect of the new techniques should be assessed, a visualization of the planning model using one of the new techniques had to be compared with a second visualization of the same model identical in every aspect, except for the rendering algorithms. This requirement has been met by using the same model and viewpoint. Each visualization scenario was evaluated using three paired tests in different sequences: Fig. 6.6 shows an example for a paired test for scenario 1 (overview scenario), Fig. 6.7 for scenario 2 (focusing the current tumor), and Fig. 6.8 for scenario 3 (focusing the resection surface). The first paired test for each scenario was conducted with video images from open liver surgery, the second paired test with video images from laparoscopic liver surgery, and the third paired test with images from planning models projected on a pig's liver using a light projector. Six liver specialists participated in the study: two surgeons, two radiologist, and two medical software engineers. Before performing the test, participants were informed about the underlying principles for visual distance encoding.

Clinical Test

To evaluate the clinical applicability of the new methods, a test in the operating room was preformed. Therefore, the images from a video camera focusing the patient's liver during an open liver intervention were captured. A rigid registration of the planning model to one video frame was carried out while the liver was immobilized. Subsequently, associated planning models were superimposed onto the video stream which itself was presented on a display in front of the surgeon.

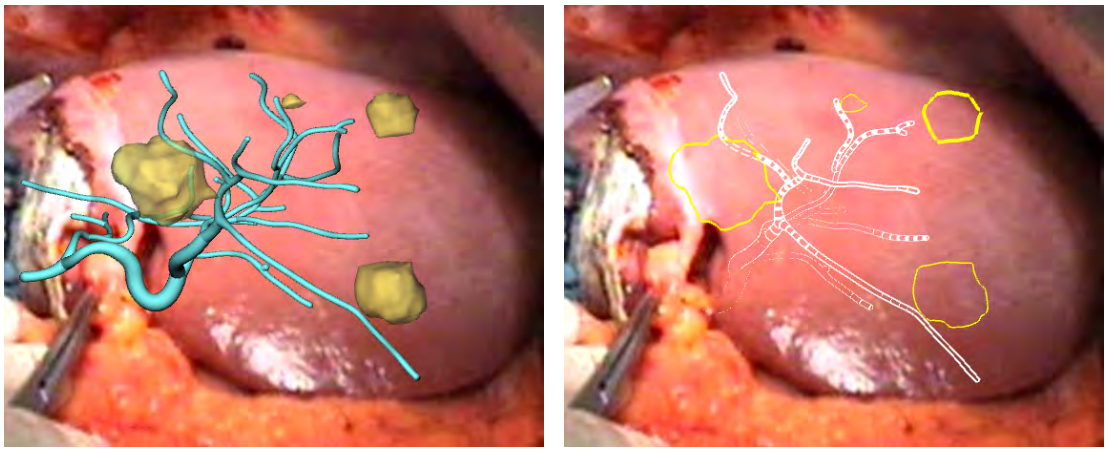

(a) (b)

Figure 6.6: Scenario 1 for open liver surgery: Superimposition using classical rendering techniques (a) and the proposed illustrative approach (b). Distance-encoding silhouettes are applied to visualize the distance between vessels and liver surface, while a distance-encoding surface emphasizes vessels that are located close to tumors.

6.5 Results

User Study

The user study confirmed the results of our previous study [Ritter et al., 2006] in the field of explicit distance encoding: Compared to classical rendering methods, all six participants were better and faster in judging distances. Because the advantage of explicit distance encoding had already been stated in the previous study, the recent study focused on a collection of qualitative data. Liver experts have been asked to express their thoughts on the application while executing the tasks using a Think-Aloud protocol. In case of a wrong distance judgment, participants were informed and asked to describe their decision in detail. Thus, a number of constructive suggestions were made:

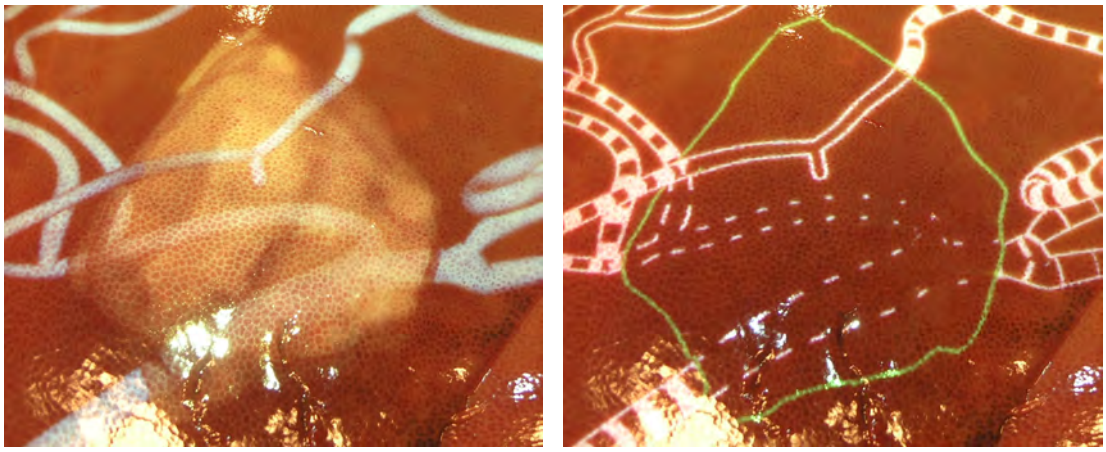

(a) (b)

Figure 6.7: Scenario 2 for projector-based AR: (a) Classical rendering that shows a transparent tumor and adjacent vessels. (b) A distance-encoding surface is applied to vessels at risk, while their spatial relation is accentuated using a distance-encoding silhouette.

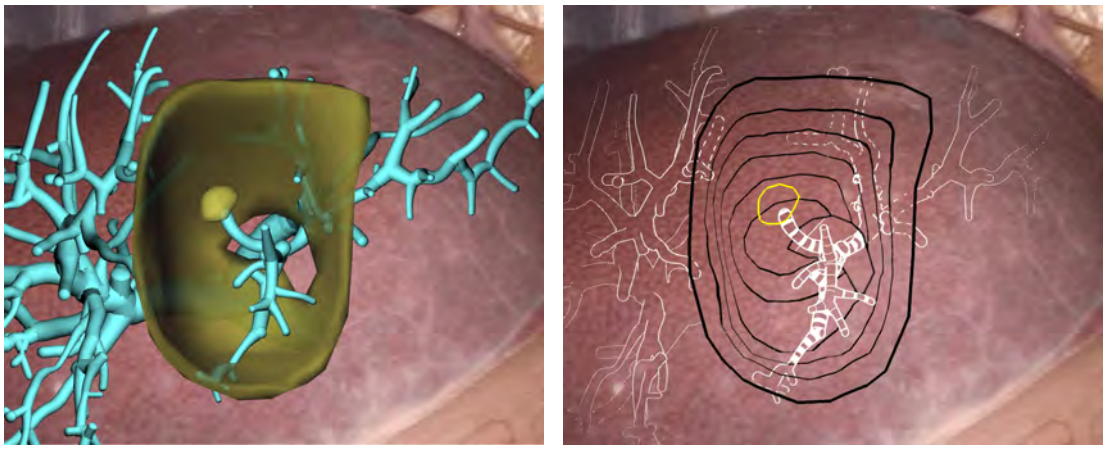

(a) (b)

Figure 6.8: Scenario 3 for a laparoscopic camera view: Classical rendering (a) causes occlusions of the surgical view while depth of the wedge-resection surface is difficult to perceive. The illustrative visualization technique (b) uses equidistant contour lines for a better assessment of spatial depth. Inside the resection volume, the distance between vessels and resection surface is visualized using distance-encoding surfaces. In addition, a distance-encoded silhouette is applied to illustrate the spatial relation between vessels and resection surface.

(1) Although the proposed visualization methods aim at reducing the complexity of planning models, participants reported that too much information was presented in scenario 3. One surgeon proposed to use the position of a tracked surgical instrument to select a specific depth layer of the resection surface. In addition, vessels that do not supply or drain healthy parenchyma could be omitted.

(2) When presenting scenario 3, several experts asked for a better emphasis of intersections between vessels and resection surface in order to judge depth. Similar requests were made for scenario 2, where the intersections between tumor and vessels are important.

(3) In several tests, two independent parameters were presented. One parameter was encoded using distance-encoding surfaces, while the second parameter was visualized using distance-encoding silhouettes. However, a few participants mixed up the parameters. After being informed about the mistake, subjects proposed to enhance the visualization with appropriate labels.

(4) Concerning the projector-based AR approach, the assessment of distance of an object from varying stroke styles (dashed, dotted) was not successful in all cases. Participants noted that the variation in style and frequency is not always perceivable on the liver surface.

(5) To assess the spatial relation of tumors and vessels in scenario 2, participants asked for an improved visualization of tumors. Particularly, quantitative distance information and additional shape hints would be necessary.

Clinical Test

The developed algorithms have been embedded into a clinical prototype that has been tested in the operating room for a preliminary evaluation. Because the movement of the liver surface was not tracked during the test, the performed registration was only valid as long as the liver was immobilized. This situation occurred before the marking of the resection line on the liver surface (before parenchyma transaction). Thus, a registration was preformed prior to this step. The superimposition of the planned resection surface (scenario 3) on the video image revealed that the marking of the resection line on the patients liver surface could be supported with the proposed visualization method. Subsequent discussions indicated that the presented visualization has considerable advantages, compared to traditional intraoperative visualization methods. However, during the cutting phase, the surgeons could not make reliable statements about the surgical benefit of the augmentation.

6.6 Discussion and Conclusion

The performed user study revealed that the applied double-encoding of distances may be misleading, especially if users are not familiar with the encoding scheme. A similar effect is described by Kruijff et al. [2010] who argue that perceptional incorrect augmentations are often a result of conflicting cues. Because the usability of the visualization correlates with the surgeon's familiarity with these concepts it could be reasonable to integrate the illustrative techniques in software assistants for liver surgery training such as proposed in [Cordes et al., 2009]. In order to prevent that surgeons take a wrong decision, the encoding of distances should be limited to one distance parameter. In addition, information about the visualized distance has to be included in the visualization, e.g., in the form of a legend.

Nevertheless, the possibility to visualize distances using different illustrative rendering styles could be important: The encoding of one distance parameter using two distance visualizations techniques (redundant representation) may lead to a clearer visualization compared to a visualization that uses only one distance visualization technique. In addition, a combination with color-based distance encoding could be considered. However, as mentioned in the requirement analysis, transitions in color and brightness should be avoided in order to ensure a maximal contrast.

An important requirement on intraoperative AR applications is that the occlusion of the surgical view by planning models should be minimal. Therefore, three visualization scenarios have been proposed in this work. The visualization scenarios reduced the set of available planning models to a set that is necessary to answer a specific surgical question. In addition, illustrative rendering techniques were applied to reduce model complexity. The limitation to a small number of planning models and the scenario-based reduction of model complexity reduce visual clutter. However, according to feedback that was collected in the context of the user study a further reduction of model complexity is desirable. A systematic workflow analysis such as proposed in [Navab et al., 2007a] could be a good basis for a definition of more specific and effective visualization scenarios. The choice of relevant information has to be made in collaboration with liver surgeons. As an alternative to predefined visualization scenarios, interactive AR would allow surgeons to interact with an augmented image, e.g., by using tracked surgical instruments. Examples for interactive AR in medicine are presented in [Fischer et al., 2005; Navab et al., 2007a; Kocev et al., 2011].

While expectations of surgeons on accuracy and stability in AR settings are high [Kruijff et al., 2010], an accurate and time-stable registration is hard to achieve. With commercially available navigation systems for liver surgery, a reliable registration can only be calculated for immobilized organs. Thus, the augmentation is only accurate if the liver is immobilized. To alleviate this limitation, surface-based organ tracking methods as proposed in [Cash et al., 2007; Schwaiger et al., 2011] need to be integrated into surgical navigation systems to adapt intraoperative registrations. However, inaccuracies in camera calibration, tracking and registration have always to

be taken into account in liver surgery. Another computational problem is the latency of the augmentation. From today's perspective, an intraoperative augmentation of planning data on a patient's liver without any alignment errors is technically not feasible. Therefore, a visualization of uncertainty (quality of the alignment between virtual and real world) could be important for clinical acceptance.

A general problem of AR that was experienced during the test in the operating room is the visual blocking of the liver during surgery, e.g., when a surgeon moves a surgical instrument between the line of sight of projector-camera system and liver surface. This is quite often the case during a liver intervention. As a result, projected planning models look like they do not belong to the scene. One pragmatic solution could be to limit the augmentation to the visible part of the liver. The visible part could be determined by an analysis of video images. Another way to visualize objects that are occluded by another object is to use a different rendering style, e.g., some form of x-ray rendering as proposed in Kalkofen et al. [2007].

Technically and methodologically, there is room for improvement. First of all, existing methods for tracking of liver movement need to be transferred from academic research to clinical applicability. In addition, work is required to further evaluate the proposed visualization techniques during surgical interventions in order to understand how the techniques would influence surgical decisions. In addition, perceptional studies are required to better understand the effects of illustrative augmentation.

As shown in this work, illustrative AR has a high potential to improve spatial perception, an essential problem in medical AR. The proposed visualization methods reduce the amount of superimposed information by applying focus and context visualization techniques. The selection of important planning objects is also given by predefined visualization scenarios. Occlusions of the surgical view by planning models are thus kept minimal. Depth cues are encoded using texture gradients and varying silhouette thickness which provides strong monocular depth cues without the requirement of a medium able to display color.

Publications *An AR application with the illustrative visualization techniques presented in this chapter was implemented together with Jan Wieferich as a part of his bachelor thesis at Fraunhofer MEVIS (supervised by the author) [Wieferich, 2008]. The prototype was presented at the 7th Annual Meeting of the German Society of Computer and Robot-assisted Surgery (CURAC), Leipzig, Germany [Hansen et al., 2008a]. Based on a ranked result of the review, the paper was selected for an invited publication in the International Journal of Computer Assisted Radiology and Surgery (IJCARS) [Hansen et al., 2010a]. This chapter contains large parts of the journal publication.*

7 Auditory Resection Guidance

> We can't solve problems by using the same kind of thinking we used when we created them.
>
> *(Albert Einstein)*

VISUALIZATION is a powerful way to present planning data. A route with a car, for example, can be explored with route planners of navigation systems concerning parameters such as journey time, estimated fuel consumption, or sightseeing opportunities along the route. However, the execution of the plan often takes place under completly different conditions. Because the driver has to concentrate on the surrounding traffic, only quick glances at the navigations system's display are appropriate. This means that the visualization can only be used to a limited extent. To this end, car navigations systems make uses of auditory display to notify and guide the driver when important landmarks are approached. Additional information is visualized on the navigation's system screen and can be accessed by the driver if necessary.

In this chapter, an auditory display system for open liver surgery is introduced by providing support for guiding the tracked instrument towards and remaining on a predefined resection line.

7.1 Purpose

Navigated resection of tumors in the liver enable a higher degree of precision and could lead to smaller resection volumes, more frequent tumor-free margins, and thus, improved outcomes [Oldhafer et al., 2009]. However, surgeons frequently need to consult the navigation system, which leads to increased mental load and time pressure during surgery [Manzey et al., 2009]. Viewing the navigation system's screen interrupts the surgical workflow.

The purpose of this work is to integrate concepts from the field of auditory display to enhance intraoperative visualizations for navigated liver surgery. Auditory display is applied as an additional information channel. It might reduce the dependence on the visual display. Thereby, it frees the eyes for other tasks, and provides high temporal resolution and fast processing [Jovanov et al., 1999].

Although auditory alarms and monitoring devices are commonplace in operating rooms, audio has been a neglected modality in navigated surgery. During liver resection, the auditory channel is relatively unused by the surgeon, and thus is more open to provide information that supplements or complements the visual display.

This work presents a solution for a primary problem in navigated liver surgery: the excessive dependence on the visual display during resection guidance. This work focuses on marking the resection path on the liver surface. The resection marks help determine the subsequent cut path through the liver parenchyma. Until now, resection guidance has been supported solely by visual displays.

7.2 Related Work

Despite research in the field of alarms and auditory status monitoring [Sanderson et al., 2005; Wee et al., 2008], only a few publications describe auditory display to support navigated surgical tasks. To the knowledge of the authors, only two groups have developed auditory displays for this field.

Wegner et al. [Wegner et al., 1997; Wegner, 1998] introduced a navigation system for the blind placement of a biopsy needle. Based on an electromagnetic tracked needle, surgeons attempted to follow a planned trajectory inside a custom gelatin phantom with an embedded target (tumor mimic). Three relevant methods are described in their papers: The first method applies a beat interference method, for which two sinus waves (one with fixed, the other with varying frequency) are mapped to the positional error in one spatial dimension. By bringing the frequencies in harmony, the user can guide the needle. However, to guide the needle in 3D, three wave pairs are needed which can be misleading if the sinus waves of one spatial dimension are in harmony with the sinus wave of another dimension. The second method is used to perform intraoperative distance measurements. Therefore, the user determines a start point with the tracked needle. As the user moves the needle away from the start point, short sound events are triggered in equidistant distances. For example, at each millimeter an audible click is triggered and at each centimeter

a speech sample that indicates the distance in centimeter is triggered. The third method aims to explore surface characteristics of anatomical 3D models. The angle between the needle and the surface of the 3D models is measured. Based on a 2D wave table, a homogeneous tone is produced when the needle is located in a homogeneous surface region. The sound frequency varies when the user passes the needle across an uneven surface. These changes in sound frequency are intended to guide the operator. Although the proposed methods by Wegner et al. showed great potential, formal evaluations were not reported in literature.

A group from the University Medical Center in Utrecht, Netherlands presented a method for auditory display for neurosurgery. In this case, auditory display was applied to resect a floral foam phantom meant to simulate brain tissue [Willems et al., 2005] and later for operation on six patients [Woerdeman et al., 2009]. When the tracked instrument approached the tumor, the system produced a pure tone with a duration of 0.1 seconds emitted approximately 3 times per second. Frequency and amplitude of the tone increased when approaching the target. Directional information was not encoded. The task involving the phantom consisted of removing a target volume from a block of floral foam. The resection using auditory display was compared to resection with visual-based navigation (using a computer monitor for display) and with a heads-up display (for which contours of segmented structures were superimposed onto real-time microscopic images) [Willems et al., 2005]. Resection quality (similarity of actual and planned resection volume) and resection time did not significantly differ when comparing the results between interaction with auditory display and visual display. In clinical tests, the auditory display was employed on 6 patients and evaluated on instrument handling during the course of surgery. The study results showed that the speed of the instrument tip was not significantly faster when using auditory support. However, in both studies participants felt that they performed better when auditory feedback was added because they could focus more on the working area.

7.3 Materials and Methods

This section describes an auditory display for image-guided liver surgery. First, the applied navigation system, the underlying planning data, and the auditory feedback engine are described. Second, a novel method for auditory resection guidance is introduced. Third, the performed evaluation of the developed auditory display is described.

7.3.1 Navigation System: CAS-One

Surgical navigation systems are intended to assist surgeons when placing or moving surgical instruments. Generally based on visual display, the position of tracked surgical instruments such as dissectors, ultrasound probes, and needles, can be viewed in relation to 3D planning models.

The planning models are generated based on CT or MR scans acquired from the patient's liver using planning software for liver surgery [Bourquain et al., 2002]. Besides anatomical 3D models of the liver, the planning model includes relevant functional information such as a virtual resection surface [Konrad-Verse et al., 2004]. One element of the virtual resection surface is the resection line (on the organ surface), which is used within the evaluation study of this work.

The surgical navigation system CAS-One (CAScination AG, Switzerland) is used within this project to visualize planning models relatively to tracked surgical instruments. CAS-One provides visual support during liver resection and has been evaluated in the context of clinical trials [Peterhans et al., 2010]. The system consists of an infrared-based optical tracking system (Vicra®, Northern Digital Inc., Canada), an ultrasound device, a touchscreen, and a computer unit. A rigid body with passive markers is mounted on surgical instruments (ultrasound and dissector) intraoperatively, or on a pointer for laboratory experiments. Landmark-based registration is applied during the first phase of the procedure, so that the modalities of the physical patient and 3D planning model align.

7.3.2 The Auditory Feedback Engine

As development platforms the medical image processing framework MeVisLab [Ritter et al., 2011] and the audio synthesis environment SuperCollider [McCartney, 2002] were chosen. The developed prototype application was independently implemented from the certified navigation software provided by the manufacturer of the navigation system. All necessary visualizations for navigation support including the representation of tracked instruments and 3D planning models were provided by a customized MeVisLab application installed on the navigation system. In addition, the application continuously sends distances and information about associated object entities to the SuperCollider engine using the OSC (Open Sound Control) protocol. In the following subsection, a novel method for auditory resection guidance is presented.

7.3.3 Auditory Resection Guidance

For complex liver operations, resection surfaces are preoperatively defined using surgical planning software. Intraoperatively, surgeons aim to resect according to these plans by means of surgical navigation systems. Before cutting the liver, the resection path is marked on the organ surface. An accurate marking of the resection path is a decisive factor for the quality of the whole resection. The marks provide orientation aid during the relatively long cutting phase ($\approx$ 1-2 hours) and thus impact the subsequent cut path through the liver parenchyma.

The proposed auditory feedback for resection guidance is a function of δ, where δ describes the distance between surgical instrument tip and the nearest point on the planned resection line. A precomputed Euclidean distance transformation provides δ for each position in the patient dataset. Thus, the auditory feedback can access δ in constant computation time.

The distance from the instrument tip on either side of the resection line is divided into three margins:

- safe
- warning
- outside

The first margin, called safe, is located on both sides of the resection line. When the instrument tip is in this margin, it is permissible for the surgeon to resect or mark. The second margin, the warning range, is located outside of the safe margin and reaches from the outer border of the safe range to the warning-range width. When the instrument tip is located in this margin, the surgeon is roughly near the planned resection line but not close enough for a safe resection marking. Finally, the outside margin includes all distances that are further from the resection line than the outside width of the warning margin. The distances for the safe and warning margins can be set by the surgeon or planning staff depending on the surgical situation.

To communicate the presence of these different margins and to direct the surgeon towards the resection line, two tones for auditory resection guidance are proposed which correspond to both the safe and warning margins. When the instrument tip is in the safe margin ($0 \leq \delta \leq$ safe width), signifying that it is permissible to mark the resection line, the safe tone is produced. When the tip is in the warning range (safe width $< \delta \leq$ warning width), the warning tone aids the surgeon in directing the instrument tip to enter the in-range margin. When the instrument tip is in the outside margin (warning width $< \delta$), no tone is produced. The combination of both warning and confirmation tones provides the user with a way of both locating and remaining on the planned resection line.

Prior Work

Based on our prior work in the field of auditory display [Black et al., 2010; Black, 2010] a refined **resection guidance model** is introduced. Within this prior work, different auditory display models for resection guidance have been developed. These first models ranged from very simple using only a single sine wave, to more complex featuring banks of digital resonating bodies, to ones that modeled real-life sounds such as ringing bells. A preliminary user study was carried out, first to provide a general consensus on whether or not auditory display would be beneficial for navigated liver surgery, and thereafter to gather clinicians' opinions regarding the functions and aesthetics of a range of exploratory auditory display models. The study revealed that auditory display was recognized by a majority of surgeons to be a useful addition to the visual interaction with the navigation system. A systematic analysis of user comments confirmed that the auditory feedback combated main limitations of the current navigation system, i.e., the dependence on the visual display and the lack of notification when approaching risk structures. In addition, the meaning

of the sound and the interaction with the systems was easily learned within less than two minutes of training. The second aim of these preliminary studies was to gather comments about a selection of different auditory display models for resection guidance. Comments regarding these first models were used in the development of the refined resection guidance model.

A Refined Resection Guidance Model

As part of the process of continual evaluation and refinement, the most popular elements of the exploratory resection guidance sound models were used to create a single model that could be used for the quantitative evaluation described in this paper. The concept of this model is broadly similar to a Geiger counter in that the inter-onset interval of a series of very short auditory events is one parameter that is mapped to the urgency of a situation. In the case of resection guidance, an increase in distance from the planned resection line causes an increase in urgency.

Safe Margin Tone When the instrument tip is in the safe margin, a "safe margin tone" is produced to guide the surgeon to $\delta = 0$ and to inform that it permissible to mark the resection at that point. The safe tone consist of two elements. First, a two-pole resonant filter with a frequency of 698.5 Hz (corresponding to MIDI note 77) and a 60 dB decay time of 1.0 second is triggered at a variable inter-onset interval. At a distance of $\delta = 0$, this inter-onset interval is 1.5 Hz, and at the edge of the safe margin, the interval is 5.5 Hz. By moving the instrument tip so that the inter-onset interval is longer, the surgeon is guided towards the planned resection line. Second, a bank of sine oscillators with frequencies of 220.0, 261.6, 349.2, 440.0, and 523.3 Hz (corresponding to MIDI notes 57, 60, 65, 69, and 72) is produced when $\delta = 0$ and muted at all other distances. Thus, this confirmation element informs the surgeon when it is optimal to mark the line.

Warning Margin Tone When the instrument tip is outside the safe margin, a warning margin tone helps guide the surgeon towards the safe margin. Similar to the safe tone, a series of repeating two-pole resonant filters are employed. In this model, three primary auditory characteristics are used to relay distance information and thus convey a sense of urgency (see [Edworthy et al., 1991]) when approaching the outside of the warning margin and a sense of calm when approaching the safe margin. Each of these variables varies linearly over δ.

The sound settings for the resection guidance model (inter-onset interval, tone length and pitch) are described in [Hansen et al., 2012]. The combination of onset frequency, tone length, and rising and falling pitch relay to the surgeon both the distance to the resection line and which side of the resection line the tracked instrument occupies. By moving the instrument back and forth across the safe and warning margins, the surgeon should be able to use these auditory cues to place the instrument tip directly on the planned resection line and be aware when the instrument deviates from the optimal line.

7.4 Evaluation

The objective of this work is to evaluate the suitability of auditory display as an enhancement to visual display in navigated liver surgery. Therefore, a clinically oriented study was conducted in which participants were asked to accomplish surgical tasks on a special manufactured 3D liver phantom. User performance was evaluated quantitatively by analyzing instrument movement and aspects of human-computer interaction.

Liver Phantom

Because an evaluation of the new interaction techniques would not be fruitful unless a physical representation of a human liver were present, a CT liver dataset with segmented anatomical structures was used to create a stereolithographical model of the liver. This liver phantom only includes an outer shell with a cuboid cavity in the front to enable access to the interior with the tracked instrument. A piece of floral foam (®mosy colorfoam) was trimmed to fit inside this cavity to provide tactile resistance to the tracked instrument during testing (Fig. 7.1a). The phantom was mounted on a wooden board together with a trackable marker shield, which allowed for easy calibration with the navigation system's camera.

Evaluation Criteria

Appropriate evaluation criteria for the evaluation were found by an analysis of which characteristics of the auditory display could potentially improve the surgical workflow of open liver interventions. The dependence on the visual display, which is a primary problem, was observed during the study. In addition, the movement of the instrument tip was compared. The following evaluation criteria were defined:

- Total time participants looked at the screen relative to looking at the phantom
- Time needed to draw the resection line
- Mean distance between planned resection line and subject-drawn resection line

Experiment Design

The tests were performed in a clinical environment with 12 surgeons from the Robert-Bosch Hospital in Stuttgart, Germany. The liver phantom was affixed to an examination table. Participants were asked to stand next to the liver phantom. The navigation systems display was placed on the opposite side of the table, as common during clinical interventions that employ video displays (see Fig. 7.2).

First, two **training tasks** had to be performed by the participants. Therefore, a red resection line and a 3D model of the liver phantom were displayed on the

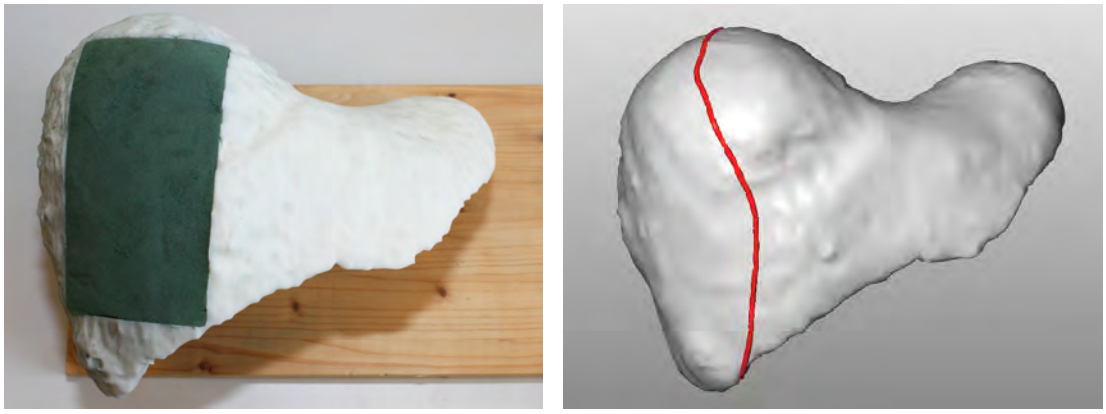

(a) (b)

Figure 7.1: (a) Liver phantom with floral foam (green) inside and (b) virtual 3D model of the liver and planned resection line (red) visualized on the navigation system's display.

(a) (b)

Figure 7.2: Setup of the navigation system and the liver phantom within the user study. The participating surgeon uses the tracked instrument to mark the planned resection line on the liver phantom. (a) shows the surgeon observing the liver phantom, and (b) shows him glance at the navigation systems screen.

navigation system's display (see Fig. 7.1b). Participants were asked to transfer the resection line visualized on the video monitor to the liver phantom by lightly marking the path on the floral foam using a pointer whose position was tracked by the navigation system. Participants were instructed to look at the video monitor only if necessary and to concentrate on the surgical instrument and the liver phantom. One training task was to be performed without auditory support (visual only) and the other training task with auditory support (combined condition).

Second, eight **test tasks** had to be performed by the participants. Thereby, four resection lines (with the 3D model of the liver phantom) were separately presented two times on the screen of the navigation system. The test tasks were divided into two groups: While four tasks ($V_1 - V_4$) did not make use of auditory display (visual only), the other four tasks ($A_1 - A_4$) presented both visual and auditory displays (combined condition). The presentation of these test tasks occurred in random order. In order to reduce the memory effect, a randomization algorithm was chosen which prohibited two test tasks with the same resection line to be performed in succession.

Before starting each test, participants were informed of the group to which the upcoming test belonged. Participants were further asked to look at the video monitor only when necessary. After marking the resection line on the foam, participants were asked to draw the final resection line a second time. The position and orientation of the pointer were recorded during the whole experiment. In addition, all tests were recorded with a video camera.

Third, each participant completed a questionnaire consisting of personal questions (regarding age, gender, handedness, surgical experience, etc.) and statements for which the participants chose the degree to which they agreed or disagreed.

Analysis

A post-experiment video analysis provided the timing data for subjects' looks at the screen or the phantom, respectively. These data were used to construct the time budget data and the mean times between changes of looks between phantom and screen.

Data for marking accuracy was sampled using the tracking mechanisms of the navigation system. The distance δ between the pointer tip position and the nearest point on the resection line was calculated for each sample. Because these samples were taken in equal temporal distance, arithmetic means of δ would be skewed by different drawing speeds. When, for example, a subject did not move the tracked pointer at all, remaining in a position with low δ, the data with low δ would accumulate over time and thus overrepresent a low δ in the mean. Therefore, the mean distance between planned resection line I_p and subject-drawn resection line I_d was introduced as a benchmark for marking quality. Given the arclength s on I_d, the mean distance is defined in the continuum as:

$$\frac{1}{L} \cdot \int_{I_d} \delta(s)\, ds, \text{ where } L = \int_{I_d} ds \text{ is the total length of } I_d. \tag{7.1}$$

Statistical analysis consisted of comparisons of the arithmetic means between data for the auditory and visual conditions. Differences were tested using the Wilcoxon test and $p < 0.05$ was defined as statistically significant.

7.5 Results

For all evaluation criteria, differences between the visual and combined conditions were found. For the visual only condition, subjects looked nearly 100 % of the time at the screen. This time was reduced to around 10 % for the condition where the auditory signal was additionally available (Fig. 7.3).

When the additional auditory information was available to the subjects, deviation from the planned resection line was smaller than with the visual information alone (Fig. 7.4). However, subjects could not mark the resection line as fast as when relying on the auditory information as opposed to the visual display only (Fig. 7.5).

Qualitative data for this evaluation was gathered from both voluntary comments from the participants as well as a questionnaire filled out by each participant. From this data, the direction of future development may be guided. Table 7.1 lists each statement and the average response and standard deviation.

Statement	Average Response (σ)
The sounds could be heard well	3.92 ($\pm$0.29)
The sounds were appropriate for the operating situation	3.25 ($\pm$0.75)
The meaning of the sounds was clear	3.67 ($\pm$0.65)
The system was intuitive	3.58 ($\pm$0.67)
The audio feedback matched the visual feedback	3.42 ($\pm$0.67)
The interaction was fun to use	3.58 ($\pm$0.90)
The sounds helped me concentrate on the resection task	3.58 ($\pm$0.90)
The sounds reduced my dependence on the visual display	3.17 ($\pm$0.83)
I would use the sound feedback in my surgical task	3.33 ($\pm$0.65)
I would recommend this to a colleague	3.33 ($\pm$0.65)

Table 7.1: Results of the questionnaire with chart showing average responses and standard deviation σ, with a response of 1 corresponding to “strongly disagree” and a response of 4 corresponding to “strongly agree”.

7.6 Discussion and Conclusion

The clinically oriented tests performed in the context of this work revealed that auditory feedback could be a beneficial extension to surgical navigation systems. However, tests during surgical interventions have to still be performed in order to further adapt the proposed sound model for clinical routine. Specifically, the effects

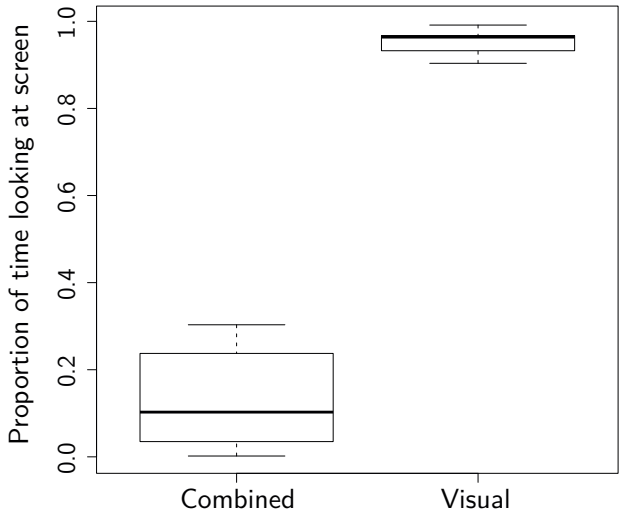

Figure 7.3: Proportion of time looking at screen for combined condition (Min = 0.00, 1st Qu. = 0.03, Median = 0.10, 3rd Qu. = 0.23, Max = 0.30) and visual condition (Min = 0.90, 1st Qu. = 0.93, Median = 0.96, 3rd Qu. = 0.96, Max = 0.99).

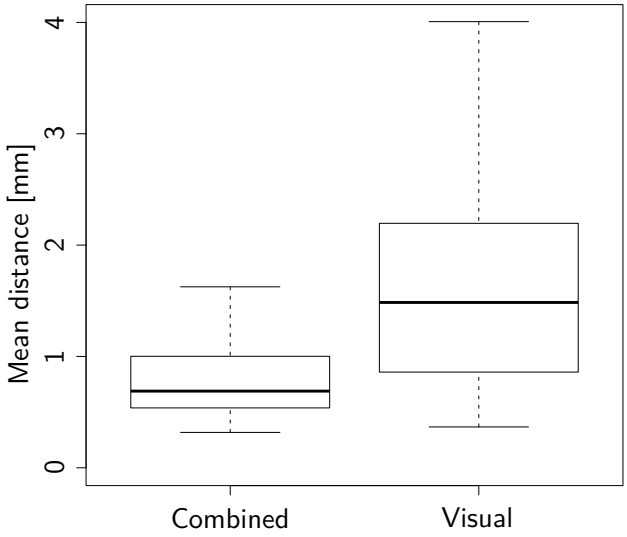

Figure 7.4: Mean distance between planned resection line and subject-drawn resection line for combined condition (Min = 0.31, 1st Qu. = 0.53, Median = 0.68, 3rd Qu. = 1.00, Max = 1.62) and visual condition (Min = 0.36 , 1st Qu. = 0.85, Median = 1.48, 3rd Qu. = 2.19, Max = 4.00).

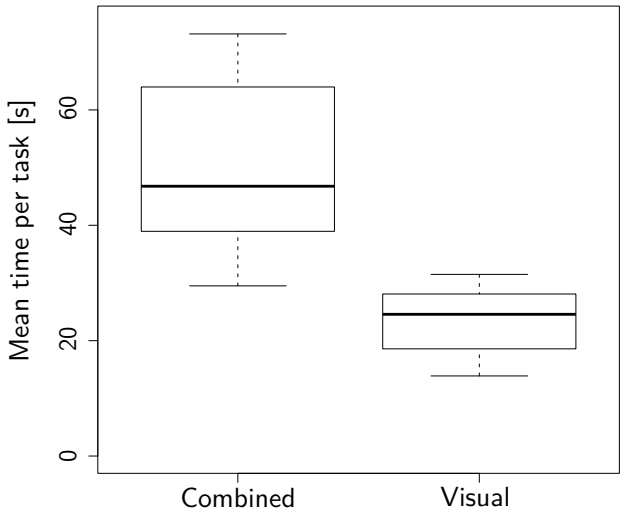

Figure 7.5: Mean time per task for combined condition (Min = 29.49, 1st Qu. = 38.95, Median = 46.76, 3rd Qu. = 63.97, Max = 73.17) and visual condition (Min = 13.88, 1st Qu. = 18.58, Median = 24.56, 3rd Qu. = 28.09, Max = 31.49).

of environmental sounds such as speech, cutting device noise, or warning signals from anesthesia devices on the surgeons' interaction and recognition of the auditory display must be evaluated.

Overall, the qualitative questionnaire showed that the subjects found the approach of using auditory display for resection marking as promising and well suited for the task. Surgeons requested aesthetically pleasing sounds that could be tolerated to hear over a time range long enough for surgical tasks. However, it is difficult to discover sound models that meet these requirements as well as providing the required resection guidance support in a clear way. An adequate variety of sound models might be provided to give surgeons a choice of equally functional sound models. In addition, these sound models might be made easily configurable for surgeons or assistants to improve acceptance and reduce possible annoyance. Moreover, industrial standards such as IEC 60601-1-8 for alarms in medical equipment [IEC, 2006] have to be taken into account in order to meet legal requirements for audio in operating environments.

In the evaluation, the auditory display significantly reduced the time that surgeons looked on the navigation system screen. Simultaneously, the auditory display reduced the mean distance to the planned resection line. However, the mean time needed for each task was almost doubled. Thus, the proposed auditory display reduces the dependency on the visual display and increases accuracy, albeit at the cost of task completion time.

One contributing factor for this increase in task completion time could be that the auditory display alerted the surgeon when leaving the safe margin. This auditory notification may have caused a more cautious (but also more accurate) marking of

the resection line than without having this information. A second contributing factor could be the new introduction of the auditory display to the subjects, many with experience working with visual navigation systems but none with auditory displays. When using the visual display alone, the interaction with the system was similar to using a computer mouse, because the position and movements of the on-screen instrument directly corresponded to those of the physically tracked instrument. Due to the novelty of the method, a longer and more intense training period would likely reduce the task completion time. Conversations with test surgeons revealed that longer task times are not necessarily a negative effect if these longer times accompany an increase in concentration. In the qualitative questionnaire, most subjects agreed that the auditory display helped to concentrate on the resection task.

A third contributing factor to increased task completion time could be the study conditions, which did not exactly match the situation of an actual liver resection. Although the task to mark a resection line on a liver phantom is similar to resection marking on a real human liver, one important difference is that during real liver surgery it would be irresponsible to mark a resection line on the liver by looking nearly 100% of the time at the screen, as several subjects did during the tests. It could be assumed that during actual liver surgery, the time looking at the screen decreases, while the time to mark a resection line increases. For further laboratory studies, the study design should consider conditions that stimulate participants to look more often at the liver phantom, e.g., by showing essential information on the phantom that needs to be perceived by the participant to pass the test.

The work proposed in this chapter builds upon work by Wegner [1998] and Woerdeman et al. [2009], who provided a groundwork for applying auditory display to navigated surgery tasks. However, this work aims to go beyond basic approaches, such as those of Woerdeman et al., and more deeply explore the ability of alternative modalities like auditory display can have to reduce stress and increase concentration and accuracy in navigated surgery.

Because the auditory display system has shown promise in helping to improve the accuracy of resection marking and reducing the amount of time looking on the screen, it may also improve other aspects of navigated liver surgery, and by extension, other types of navigated surgery as well. In the domain of liver surgery, auditory display has also been explored [Black, 2010] for notifying the surgeon of potential risk structures in the vicinity of the tracked instrument, such as veins and tumors that should not be damaged. By emitting warning signals when the instrument tip enters predefined distances to the risk structures, the surgeon could be notified of presence of such a risk without having to look at the visual display and taking concentration away from the patient. However, when considering clinical applicability of available navigation systems for liver surgery, it is important to mention that currently only the marking step is supported with adequate registration accuracy. An accurate, continuous tracking of liver movement during the cutting phase is still under research [Vetter et al., 2003; Cash et al., 2007; Beller et al., 2009b]. The method proposed in this paper intends to support the marking step, but could also be applied for the cutting phase in the future.

In addition to navigated liver surgery, auditory display methods could be useful additions to other types of surgery for which visual contact to the situs is important or for which there is a strong dependence on a visual display, including neurosurgery, laparoscopic surgery, and radio-frequency ablation. Further work must discover for which cases auditory display is beneficial and the optimal means of implementing such displays.

Publications *The content of this chapter contains work that is accepted for publication in the International Journal of Medical Robotics and Computer Assisted Surgery [Hansen et al., 2012] at the time point of submission of this thesis. In addition, preliminary work was presented at the 24th Congress for Computer Assisted Radiology and Surgery (CARS), Genf, Switerland [Black et al., 2010]. The research has been performed in strong collaboration with David Black (Fraunhofer MEVIS), who implemented parts of the proposed sound model within his masters thesis [Black, 2010].*

8 Conclusion

> The solution to every problem is yet another problem.
>
> *(Johann Wolfgang von Goethe)*

Probably no one in 1895 could foresee that the discovery of radiologic imaging by Wilhelm Conrad Röntgen would have such an impact and would revolutionize medicine over the following decades. With the later development of scanner technologies, it was possible to provide 3D visualization of body regions, like those of complex organs such as the liver. Due to continuous research, the radiation load was reduced over the years while image quality was improved. In addition, other image modalities such as MR imaging and ultrasound were introduced in the clinical routine.

Challenges

The increasing advance of imaging technology in hospitals during the last decades has led to large amounts of data for each patient. The development of software assistants that support physicians in extracting the essential information from this data is challenging.

This thesis focuses on computer-assisted liver surgery. Thereby, following clinical problems are addressed:

- Preoperative risk assessment for complex tumor resections
- Adaptation of surgical planning data in case of intraoperative findings
- Appropriate presentation of surgical planning data in the operating room

In this context, it is important to keep in mind that medical images and the derived surgical planning data represent only a part of reality. For this reason, software assistance should provide decision support rather than dictating final surgical decisions.

Contributions of this Thesis

An overall objective of this work is the separation of the essential information from the nonessential information. This required a closer look at the dedicated surgical workflow steps and the clinical questions that need to be answered.

This work introduces a software assistant to explore the dependency of vascular territories from safety margins around tumors. Robustness and sensitivity of vascular risk in the liver is visualized within a volume-margin function and in interactive 3D renderings. The results of the performed user study showed that the proposed risk analysis represents additional information that influences surgeons' decisions. Besides a method to evaluate the effect of safety margins with uniform width, tools for the exploration of non-uniform safety margins are proposed. Non-uniform safety margins take into account that the minimal distance to the resection surface varies. This concept expands planning possibilities and reflects the reality better than established methods that utilize uniform safety margins.

Another central contribution of this work are tools for the intraoperative adaptation of risk analyses and resection plans in case of intraoperative findings. So far, preoperative planning data for liver surgery has had limited value during interventions when the planning strategy needed to be adapted. An intraoperative planning assistant that can be remotely controlled by surgical navigation systems is introduced. The proposed combination of planning adaptation and intraoperative navigation provides surgeons with a tool for quantitative risk assessment in case changes to the resection strategy are necessary. A clinically oriented study proved the feasibility of the concept and showed how the proposed methods can be integrated in the workflow of navigated liver interventions.

New methods for intraoperative visualization of surgical planning data are introduced. A main contribution is the risk map, which enhances difficult locations on a planned resection surface and visualizes the information in one single view. Difficult locations are determined through detailed analysis of critical structures in the proximity of the resection surface. The resulting visualization is clear and intuitive, allowing for a fast mental mapping of the current resection surface to the risk map.

In addition, illustrative visualization methods for 3D planning models are presented. The methods aim to enhance spatial relations and allow reliable distance assessment in medical AR applications. To minimize occlusion of the surgical view, the geometric complexity of planning models is reduced through focus and context visualization techniques. The selection of important structures (focus) is guided by visualization scenarios which address workflow steps in navigated liver surgery. As shown in this work, illustrative AR has great potential to improve spatial perception, an essential problem in medical AR.

Finally, methods for auditory resection guidance in open liver surgery are introduced. The methods supports guiding the tracked instrument towards and remaining on a predefined resection line. The performed user study revealed that surgeons spent less time looking on the screen and more time looking at the working area when marking a resection line. Auditory display in combination with a visualization of planning data shows great promise to become an important part of navigation systems for liver surgery.

Proposal for Future Work

To provide a reliable software assistant for preoperative risk analysis, previous and subsequent steps in the planning pipeline need to be adapted according to the needs of the proposed risk analysis. A measure of the accuracy of segmentation results would be a great benefit to indicate the level of risk analysis reliability. In addition, it is promising to combine the proposed risk analysis with advanced tools for liver resection planning, such as methods for the evaluation of resection surfaces as presented by Demedts et al. [2010]. A selected margin width for a tumor and associated volumes at risk could be directly integrated in the evaluation function of a virtual resection surface.

Future developments in surgical planning adaptation should further automate the update of planning data, particularly the definition of new resection plans. A method that delivers meaningful results from radiologic data in a completely automated way is desirable but not currently technically feasible. The decision of a specific resection strategy often depends on individual parameters, such as anamnesis of the patient, status of the liver, and the experience of the surgeon. A future application for automatic adaptation of resection plans needs to take these individual parameters into account to generate meaningful results.

Intraoperative visualization for liver surgery needs to be further investigated and evaluated in clinical settings. The reduction of model complexity enables very

effective visualization of surgical risk. However, the apparent accuracy harbors risks for the observer. An important step for future research represents the analysis and visualization of inaccuracies. This is especially true if the visualization is used as an intraoperative navigation aid.

Accuracy of navigation systems in liver surgery needs to be further increased to provide reliable navigation support. To use a visualization of planning data during navigated liver surgery, the location of critical structures needs to be updated according to the actual deformation of the liver. In order to estimate the deformation, sophisticated intraoperative registration methods might be combined with deformation models of the liver. Furthermore, medical vendors need to integrate AR devices, such as camera-projector systems, in their product portfolio to promote the use of AR techniques and to reduce setup time of required technical equipment.

The proposed method for auditory display opens up completely new possibilities and dangers for navigated liver surgery. While the recent concept of navigated liver surgery is solely based on the visualization of planning models, no explicit navigation commands are provided. Incidentally, this eases the clearance of surgical navigation systems for clinical trials because the navigations systems provide only implicit navigation support. With auditory display, explicit navigation commands or notifications can be provided even if the surgeon does not look on the screen. Future evaluations of such systems during clinical interventions must be carefully prepared with regard to legal and ethical requirements.

To sum up, the methods developed in the context of this dissertation project contribute to the field of computer-assisted liver surgery and have the potential to improve the safety of surgical intervention. Research in computer-assisted liver surgery has not been completed by now. The development needs to be continued in the future in strong collaboration between radiologist, surgeons and scientists.

Appendix

Acknowledgement

This thesis would not have been possible without the support of many people. First, I would like to thank my supervisor Horst Hahn whose understanding and encouraging guidance has been a great value for me. Horst has been a great teacher and his detailed and constructive feedback improved the quality of this work. Similarly, I thank Bernhard Preim for all the discussions from the very early stages of this thesis and for his support in various ways. Many thanks go to Lars Linsen for being part of the dissertation committee and for his constructive comments.

This thesis would not have been possible without the support of my colleagues from Fraunhofer MEVIS in Bremen. Big thanks go to Stephan Zidowitz and Felix Ritter, who supervised my project work at Fraunhofer MEVIS, guided me during the last years and taught me to think out of the box. I would like to thank Heinz-Otto Peitgen, who brought in fundamental ideas into this thesis, founded the MeVis group and is mainly responsible for the outstanding work atmosphere at our institute.

Without the support and advice of Guido Prause and Markus Lang, many things would have been impossible. They motivated me continuously and enabled me to write this dissertation alongside my daily project work. Special thanks go to my office colleague Darko Ojdanic for his advice and encouragement. I also gratefully acknowledge Thomas Eberhardt, Milo Hindennach, Alexander Köhn, Christoph Lange, and Wolf Spindler for answering almost every technical question that arose. A lot of colleagues and friends reviewed the draft versions of this thesis or related publications and provided valuable comments. I would particularly like to thank David Black, Holger Bourquain, Ola Friman, Benjamin Geisler, Frank Heckel, Jan Klein, Hans Meine, Bernd Merkel, Jan Moltz, Christian Rieder, Andrea Schenk, and Christian Schumann. I was also privileged to work with a number of great students, including David Black, Longquan Chen, Daniel Demedts, Benjamin Durth, Björn Lindow, Bojan Kocev, Ursula Marciniac and Jan Wieferich.

I express gratitude to all involved physicians for all the fruitful discussions and clinical advice. Their feedback and ideas led the research in the context of this dissertation project. I particularly acknowledge Marcello Donati, Human Honarpisheh, Karl Oldhafer and Gregor Stavrou from Asklepios Hospital Barmbek, Markus Kleemann from University Hospital Lübeck, Wolfram Lamade and Fabian Rieber from Robert-Bosch Hospital Stuttgart, Nicholas Wendt from Sankt Josef Hospital Bremen, Thomas Jungbluth from Asklepios Hospital Bad Oldesloe, Hauke Lang from University Hospital Mainz, Michael Neipp from Hospital Itzehoe, and Thomas Mansfeld from Asklepios Hospital Wandsbek.

I would like to thank our project partners, especially Stefan Schlichting from Dräger Medical in Lübeck, Armin Besirevic and Volker Martens from the University

of Lübeck, Sylvain Andregg and Matthias Peterhans from CAScination in Bern, Stefan Weber from the University of Bern, Mathias Markert from the Technical University Munich, Konrad Mühler from the University of Magdeburg, Marcus Barann, Christiane Engel, Michaela Jesse, Ulrike Kayser, Olaf Konrad, Uwe Siems and Susanne Zentis from MeVis Medical Solutions in Bremen for productive collaboration in the last years and their contributions.

Lastly, I would like to thank my family for their love and encouragement. My parents, who never suppressed my joy of experimentation, and my wife Daniela, whose support and understanding in the final stages of this thesis was appreciated very much.

List of Abbreviation

API	Application Programming Interface
AR	Augmented Reality
BD	Bile Duct
CCD	Charge-Coupled Device
CRLM	Colorectal Liver Metastasis
CT	Computer Tomography
DTI	Diffusion Tensor Imaging
FDA	Food and Drug Administration (United States of America)
FEM	Finite Element Method
fMRI	Functional Magnetic Resonance Imaging
FTP	File Transfer Protocol
GLSL	OpenGL Shading Language
GPU	Graphics Processing Unit
HA	Hepatic Artery
HCC	Hepatocellular Carcinoma (a primary malignant liver tumor)
HMD	Head-Mounted Display
HV	Hepatic Vein
IOUS	Intraoperative Ultrasound
IPA	Intraoperative Planning Assistant
LDLT	Living Donor Liver Transplantation
LED	Light-Emitting Diode
LHV	Left Hepatic Vein
MDS	MeVis Distance Service
MELD	Model of End Stage Liver Disease
MHV	Middle Hepatic Vein
MPR	Multiplanar Reformation
MR(I)	Magnetic Resonance (Imaging)
PCA	Principal Component Analysis
PV	Portal Vein
RHV	Right Hepatic Vein
SOA	Service-Oriented Architecture
SPECT	Single Photon Emission Computed Tomography
TOF	Time of Flight
VR	Virtual Reality
VRML	Virtual Reality Modeling Language
XML	Extensible Markup Language

List of Symbols

G	Mathematical graph
N	Nodes of graph G
E	Edges of graph G
d	Current width of safety margin (mm)
δ	Distance to the virtual resection surface (mm)
D_B	Distance transformation encoding the distance to resection surface boundary
D_{HV}	Distance transformation coding the distance to hepatic vein
D_{PV}	Distance transformation encoding the distance to portal vein
D_{SURF}	Distance transformation encoding the distance to resection surface
D_T	Distance transformation encoding the distance to tumors
I_p	Planned resection line
I_d	Subject-drawn resection line
L	Total length of subject-drawn resection line I_d
P_{in}	Point set for which each point is located within the liver volume
P_{out}	Point set for which each point is located on the liver surface
σ	Standard deviation
s	Arclength on subject-drawn resection line I_d
S_{Liv}	3D segmentation mask of the liver
S_{Tum}	3D segmentation mask of tumors
RS	3D mask encoding the resection volume of a resection plan
RM	3D mask encoding the remnant volume of a resection plan
T_{PV}	3D mask encoding portal vein territories
T_{HV}	3D mask encoding hepatic vein territories
t_{Vol}	Volume threshold
V_d	Affected volume for a safety margin of width d
V_{d-1}	Affected volume for a safety margin of width $d-1$
w	Width of uniform safety margin (mm)

Specification of used Hardware

Intraoperative Planning Assistant (IPA)

Processor	Intel©Core^{TM} 2 Duo E8500, 3.16GHz
Main memory	8GB RAM
Graphic board	Nvidia GeForce 8800 GTX
Operating system	Windows©Vista Enterprise 64 Bit

Preoperative Planning System

Processor	Intel©Core^{TM} i7-975, 3.33 GHz
Main memory	12GB RAM
Graphic board	NVIDIA GeForce 295 GTX
Operating system	Windows©7 Enterprise 64 Bit

Questionaires

Questionaire 1: Vascular Risk Analysis (Chapter 3)

Klinische Information: Patient mit CRLM. Anzustrebendes Leber-Rest-Volumen > 35 %.

(1) Wie stufen Sie insgesamt die Schwierigkeit dieser Tumorresektion ein?

- ☐ Sehr groß
- ☐ Groß
- ☐ Mittel
- ☐ Mäßig
- ☐ Gering

(2) Ist der vorliegende Tumor Ihrer Meinung nach resektabel?

- ☐ Nein
- ☐ Ja, aber mit kleinem Sicherheitsabstand ($< 5mm$)
- ☐ Ja, mit großem Sicherheitsabstand ($> 5mm$)
- ☐ Keine Aussage möglich

(3) Wie sicher sind Sie sich?

- ☐ Sehr sicher
- ☐ Sicher
- ☐ Weniger sicher
- ☐ Unsicher

(4) An welchen Stellen müssen Ihrer Meinung nach Gefäße durchtrennt werden?

Selektieren Sie die Stellen am Bildschirm.

(5) Wie sicher sind Sie sich?

- ☐ Sehr sicher
- ☐ Sicher
- ☐ Weniger sicher
- ☐ Unsicher

(6) Welche Resektionsstrategie würden Sie vorschlagen?

- **Anatomisch**
  - ☐ Segmentorientierte Resektion (Segment- oder Bisegmentektomie)
  - ☐ Zentrale Leberresektion
  - ☐ Hemihepatektomie rechts
  - ☐ Hemihepatektomie links
  - ☐ Sonstiges: _____

- **Erweitert-Anatomisch**
  - ☐ Erweiterte Hemihepatektomie rechts
  - ☐ Erweiterte Hemihepatektomie links
  - ☐ Hemihepatektomie rechts
  - ☐ Hemihepatektomie links
  - ☐ Sonstiges: _____

- **Nicht-Anatomisch**
  - ☐ Lokale Resektion
  - ☐ Sonstiges: _____

(7) Wie sicher sind Sie sich?

- ☐ Sehr sicher
- ☐ Sicher
- ☐ Weniger sicher
- ☐ Unsicher

(8) Welche Sicherheitsabstände um die Metastase würden Sie anstreben?

Minimaler Sicherheitsabstand: _____ mm

(9) Wie sicher sind Sie sich?

- ☐ Sehr sicher
- ☐ Sicher
- ☐ Weniger sicher
- ☐ Unsicher

(10) Zu welcher/n Struktur/en würden sie den minimalen Abstand wählen?

Selektieren Sie die Strukturen am Bildschirm.

(11) Wie beurteilen Sie das Risiko von relevanten Abflussstörungen (Lebervene)?

- ☐ Hohes Risiko
- ☐
- ☐ Mittleres Risiko
- ☐
- ☐ Kein Risiko
- ☐ Keine Aussage möglich

Selektieren Sie die Bereiche am Bildschirm.

(12) Wie beurteilen Sie das Risiko von relevanten Zuflussstörungen (Portalvene)?

- ☐ Hohes Risiko
- ☐
- ☐ Mittleres Risiko
- ☐
- ☐ Kein Risiko
- ☐ Keine Aussage möglich

Selektieren Sie die Bereiche am Bildschirm.

Questionaire 2: Risk Maps (Chapter 5)

An welchen Stellen der Resektionsfläche würden sie besonders vorsichtig operieren?

Skizzieren und klassifizieren Sie die Areale farblich mit Hilfe der auf dem Tisch befindlichen Buntstifte:

Portalvene = BLAU
Lebervene = GRÜN
Tumor = ROT

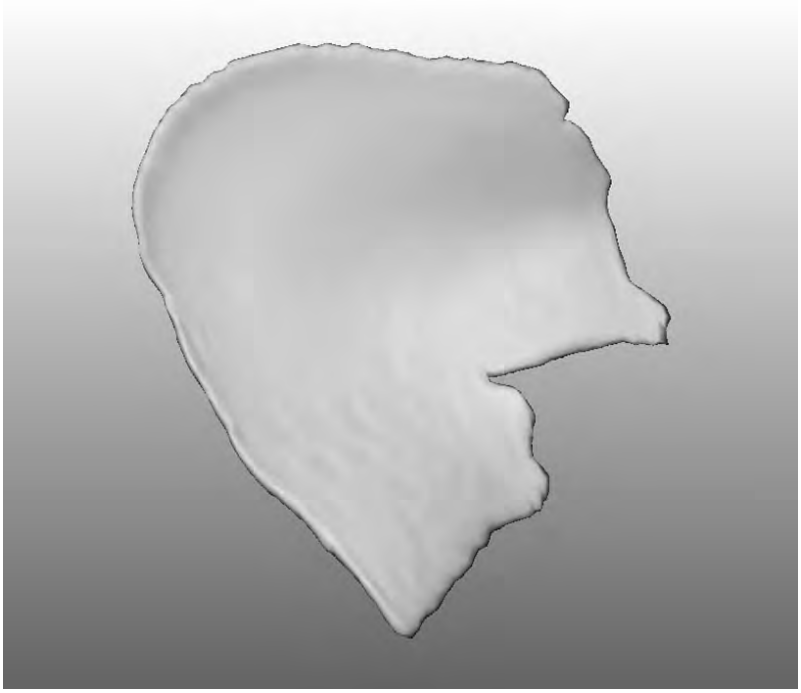

Bitte skizzieren Sie hier

Die im Computer eingefärbte Resektionsfläche hat mich bei der Risikobewertung der Resektion unterstützt?

- ☐ Trifft zu
- ☐ Trifft eher zu
- ☐ Trifft eher nicht zu
- ☐ Trifft nicht zu

Questionaire 3: Auditory Display (Chapter 7)

(1) Ich konnte die Töne gut hören.

- ☐ Trifft zu
- ☐ Trifft eher zu
- ☐ Trifft eher nicht zu
- ☐ Trifft nicht zu

(2) Die Töne waren an die Situation im OP angepasst.

- ☐ Trifft zu
- ☐ Trifft eher zu
- ☐ Trifft eher nicht zu
- ☐ Trifft nicht zu

(3) Die Bedeutung der Töne war mir klar.

- ☐ Trifft zu
- ☐ Trifft eher zu
- ☐ Trifft eher nicht zu
- ☐ Trifft nicht zu

(4) Das Audio-System war intuitiv zu bedienen.

- ☐ Trifft zu
- ☐ Trifft eher zu
- ☐ Trifft eher nicht zu
- ☐ Trifft nicht zu

(5) Die Töne stimmten mit der visuellen Darstellung überein.

- ☐ Trifft zu
- ☐ Trifft eher zu
- ☐ Trifft eher nicht zu
- ☐ Trifft nicht zu

(6) Die Instrumenten-Interaktion mit Hilfe der Töne hat mir Spaß gemacht.

- ☐ Trifft zu
- ☐ Trifft eher zu
- ☐ Trifft eher nicht zu
- ☐ Trifft nicht zu

(**7**) **Die Töne halfen mir mich auf das Markieren der Resektionsfläche zu konzentrieren.**

- ☐ Trifft zu
- ☐ Trifft eher zu
- ☐ Trifft eher nicht zu
- ☐ Trifft nicht zu

(**8**) **Die Töne reduzierten meine Abhängigkeit vom Bildschirm.**

- ☐ Trifft zu
- ☐ Trifft eher zu
- ☐ Trifft eher nicht zu
- ☐ Trifft nicht zu

(**9**) **Ich würde ein solches akustisches Feedback zur Unterstützung chirurgischer Aufgaben nutzen.**

- ☐ Trifft zu
- ☐ Trifft eher zu
- ☐ Trifft eher nicht zu
- ☐ Trifft nicht zu

(**10**) **Ich würde ein solches System an Kollegen weiterempfehlen.**

- ☐ Trifft zu
- ☐ Trifft eher zu
- ☐ Trifft eher nicht zu
- ☐ Trifft nicht zu

List of Own Publications

Black, D., Hansen, C., Loviscach, J., and Peitgen, H.-O. (2010). "Auditory Support for Image-Guided Liver Surgery." In: *Proc. of the 24th International Symposium on Computer Assisted Radiology and Surgery (CARS)*, 5(Supplement 1), pp. 187–188 (cited on pp. 133, 142).

Demedts, D., Schenk, A., Hansen, C., and Peitgen, H.-O. (2010). "Evaluation of Resection Proposals for Liver Surgery Planning." In: *Proc. of the 9th Annual Meeting of the German Society of Computer- and Robot-Assisted Surgery*, pp. 13–16 (cited on pp. 12, 23, 24, 145).

Hansen, C., Schlichting, S., Markert, M., Hindennach, M., Zidowitz, S., and Peitgen, H.-O. (2007a). "Intraoperative Adaptation of Preoperative Risk Analyses for Oncologic Liver Surgery using tracked 2D ultrasound." In: *Proc. of the 6th Annual Meeting of the German Society of Computer- and Robot-Assisted Surgery*, pp. 155–158 (cited on p. 94).

Hansen, C., Koehn, A., Ritter, F., Zidowitz, S., and Peitgen, H.-O. (2007b). "Simultaneous Visualization of Preoperative Planning Models and Intraoperative Ultrasound for Liver Surgery." In: *Proc. of Eurographics (Short Papers and Medical Prize Awards)*, pp. 117–120.

Hansen, C., Wieferich, J., Ritter, F., Rieder, C., and Peitgen, H.-O. (2008a). "Illustrative Visualization of 3D Planning Models for Augmented Reality in Liver Surgery." In: *Proc. of the 7th Annual Meeting of the German Society of Computer- and Robot-Assisted Surgery*, pp. 1–4 (cited on p. 127).

Hansen, C., Zidowitz, S., Schenk, A., Oldhafer, K., Lang, H., and Peitgen, H.-O. (2008b). "Intraoperative Adaptation and Visualization of Preoperative Risk Analyses for Oncologic Liver Surgery." In: *Proc. of SPIE Medical Imaging*. Vol. 6918, pp. 691809–1–10 (cited on p. 94).

Hansen, C., Schlichting, S., Zidowitz, S., Kleemann, M., and Peitgen, H.-O. (2008c). "Intraoperative Adaptation of Planning Data for Oncologic Liver Surgery." In: *Proc. of MICCAI Workshop on Image Guidance and Computer Assistance for Soft-Tissue Interventions*, pp. 36–45 (cited on p. 94).

Hansen, C., Köhn, A., Schlichting, S., Weiler, F., Konrad, O., Zidowitz, S., and Peitgen, H.-O. (2008d). "Intraoperative Modification of Resection Plans for Liver Surgery." In: *Int J Comput Assist Radiol Surg*, 2(3-4), pp. 291–297 (cited on p. 94).

Hansen, C., Zidowitz, S., Hindennach, M., Schenk, A., Hahn, H., and Peitgen, H.-O. (2009a). "Interactive Determination of Robust Safety Margins for Oncologic Liver Surgery." In: *Proc. of the 23rd International Symposium on Computer Assisted Radiology and Surgery (CARS)*, 4(Supplement 1), p. 94 (cited on p. 67).

Hansen, C., Zidowitz, S., Hindennach, M., Schenk, A., Hahn, H., and Peitgen, H.-O. (2009b). "Interactive Determination of Robust Safety Margins for Oncologic Liver Surgery." In: *Int J Comput Assist Radiol Surg*, 4(5), pp. 469–474 (cited on p. 67).

Hansen, C., Wieferich, J., Ritter, F., Rieder, C., and Peitgen, H.-O. (2010a). "Illustrative Visualization of 3D Planning Models for Augmented Reality in Liver Surgery." In: *Int J Comput Assist Radiol Surg*, 5(2), pp. 133–141 (cited on p. 127).

Hansen, C., Zidowitz, S., Schenk, A., Oldhafer, K., Lang, H., and Peitgen, H.-O. (2010b). "Risk maps for navigation in liver surgery." In: *Proc. of SPIE Medical Imaging*. Vol. 7625, pp. 762528–1–8 (cited on p. 112).

Hansen, C., Lindow, B., Zidowitz, S., Schenk, A., and Peitgen, H.-O. (2010c). "Towards Automatic Generation of Resection Surfaces for Liver Surgery Planning." In: *Proc. of the 24th International Symposium on Computer Assisted Radiology and Surgery (CARS)*, 5(Supplement 1), pp. 119–120 (cited on p. 94).

Hansen, C., Black, D., Lange, C., Rieber, F., Lamade, W., Donati, M., Oldhafer, K. J., and Hahn, H. K. (2012). "Auditory Support for Resection Guidance in Navigated Liver Surgery." In: *Int J Med Robot*, in print (cited on pp. 134, 142).

Mühler, K., Hansen, C., Neugebauer, M., and Preim, B. (2008). "Automatische Kamerapositionierung für intra-operative Visualisierungen in der onkologischen Leberchirurgie." In: *Proc. of Bildverarbeitung für die Medizin*. Informatik aktuell, pp. 143–147.

Ritter, F., Hansen, C., Dicken, V., Konrad, O., Preim, B., and Peitgen, H.-O. (2006). "Real-time illustration of vascular structures." In: *IEEE Visualization*, 12(5), pp. 877–884 (cited on pp. 114, 117, 119, 123).

Ritter, F., Hansen, C., Wilkens, K., Köhn, A., and Peitgen, HO (2009). "User Interfaces for Direct Interaction with 3D Planning Data in the Operation Room." In: *Journal of i-com (Zeitschrift für interaktive und kooperative Medien)*, 8(1), pp. 24–31 (cited on pp. 71, 94).

Bibliography

Adams, R. and Bischof, L. (1994). "Seeded Region Growing." In: *IEEE Trans. Pattern Anal. Mach. Intell.* 16 (6), pp. 641–647 (cited on p. 18).

Amenta, P. S. (1997). *Histology: From Normal Microanatomy to Pathology*. Piccin Nuova Libraria, Italy (cited on p. 7).

Asakuma, M., Fujimoto, Y., Bourquain, H., Uryuhara, K., Hayashi, M., Tanigawa, N., Peitgen, H. O., and Tanaka, K. (2007). "Graft selection algorithm based on congestion volume for adult living donor liver transplantation." In: *Am. J. Transplant.* 7, pp. 1788–1796 (cited on pp. 20, 21, 62).

Ayache, N. (2003). "Epidaure: a research project in medical image analysis, simulation, and robotics at INRIA." In: *IEEE Transactions on Medical Imaging*, 22(10), pp. 1185–1201 (cited on pp. 34, 35, 70).

Baegert, C., Villard, C., Schreck, P., Soler, L., and Gangi, A. (2007). "Trajectory optimization for the planning of percutaneous radiofrequency ablation of hepatic tumors." In: *Comput. Aided Surg.* 12, pp. 82–90 (cited on p. 23).

Baek, C. K., Choi, J. Y., Kim, K. A., Park, M. S., Lim, J. S., Chung, Y. E., Kim, M. J., and Kim, K. W. (2011). "Hepatocellular carcinoma in patients with chronic liver disease: A comparison of gadoxetic acid-enhanced MRI and multiphasic MDCT." In: *Clin Radiol* (cited on p. 15).

Bale, R., Widmann, G., and Stoffner, D. I. (2010). "Stereotaxy: breaking the limits of current radiofrequency ablation techniques." In: *Eur J Radiol*, 75, pp. 32–36 (cited on p. 9).

Beller, S., Hünerbein, M., Eulenstein, S., Lange, T., and Schlag, P. M. (2007). "Feasibility of navigated resection of liver tumors using multiplanar visualization of intraoperative 3-dimensional ultrasound data." In: *Annals of Surgery*, 246(2), pp. 288–294 (cited on p. 25).

Beller, S., Lange, T., Eulenstein, S., Beller, L., Chopra, S., Dudeck, O., Schlag, P., and Hünerbein, M. (2008). "3D-Elaboration of postoperative CT data after liver resection: technique and utility." In: *Int J Comput Assist Radiol Surg*, 3(6), pp. 581–589 (cited on pp. 23, 61, 88).

Beller, S., Eulenstein, S., Lange, T., Niederstrasser, M., Hünerbein, M., and Schlag, P. M. (2009a). "A new measure to assess the difficulty of liver resection." In: *European Journal of Surgical Oncology*, 35(1), pp. 59–64 (cited on pp. 21, 22, 108).

Beller, S., Eulenstein, S., Lange, T., Hünerbein, M., and Schlag, P. M. (2009b). "Upgrade of an optical navigation system with a permanent electromagnetic position control: a first step towards ''navigated control'' for liver surgery." In:

Journal of Hepato-Biliary-Pancreatic Surgery, 16(2), pp. 165–170 (cited on pp. 32, 33, 87, 105, 141).

Beller, S., Hünerbein, M., Lange, T., Eulenstein, S., and Schlag, P. M. (2010). "Navigation in der offenen Leberchirurgie." In: *Computerassistierte Chirurgie*. Urban & Fischer Verlag, pp. 525–532 (cited on pp. 25, 26, 28, 29).

Bichlmeier, C., Wimmer, F., Heining, M., and Navab, N. (2007). "Contextual Anatomic Mimesis Hybrid In-Situ Visualization Method for Improving Multi-Sensory Depth Perception in Medical Augmented Reality." In: *Proc. of 6th IEEE and ACM International Symposium on Mixed and Augmented Reality*. IEEE Computer Society, pp. 1–10 (cited on p. 116).

Blaas, J., Botha, C. P., Majoie, C., Nederveen, A., Vos, F. M., and Post, F. H. (2007). "Interactive Visualization of Fused fMRI and DTI for Planning Brain Tumor Resections." In: *Proc. of SPIE Medical Imaging*. Vol. 6509 (cited on p. 39).

Black, D., Hansen, C., Loviscach, J., and Peitgen, H.-O. (2010). "Auditory Support for Image-Guided Liver Surgery." In: *Proc. of the 24th International Symposium on Computer Assisted Radiology and Surgery (CARS)*, 5(Supplement 1), pp. 187–188 (cited on pp. 133, 142).

Black, David (2010). "Auditory Display for Liver Surgery." MA thesis. Department of Computer Science, University of Applied Sciences Bremen, Germany (cited on pp. 133, 141, 142).

Bourquain, H., Schenk, A., Link, F., Preim, B., Prause, G., and Peitgen, H.-O. (2002). "HepaVision2: A software assistant for preoperative planning in living-related liver transplantation and oncologic liver surgery." In: Proc. of Computer Assisted Radiology and Surgery (CARS). Springer, pp. 341–346 (cited on pp. 19, 20, 70, 132).

Brant, W. and Helms, C. (1999). *Fundamentals of Diagnostic Radiology*. 2nd ed. Lippincott Williams and Wilkins (cited on p. 6).

Broek, M. A. J. van den, Olde Damink, S. W. M., Dejong, C. H. C., Lang, H., Malago, M., Jalan, R., and Saner, F. H. (2008). "Liver failure after partial hepatic resection: definition, pathophysiology, risk factors and treatment." In: *Liver International : Official Journal of the International Association for the Study of the Liver*, 28(6), pp. 767–780 (cited on p. 111).

Broers, H. (2005). "Probe and optical measuring system." Pat. EP1498688 (cited on p. 87).

Brouquet, A., Abdalla, E. K., Kopetz, S., Garrett, C. R., Overman, M. J., Eng, C., Andreou, A., et al. (2011). "High survival rate after two-stage resection of advanced colorectal liver metastases: response-based selection and complete resection define outcome." In: *J. Clin. Oncol.* 29, pp. 1083–1090 (cited on p. 7).

Bruckner, S. (2008). "Interactive Illustrative Volume Visualization." PhD thesis. Department of Computer Science, Vienna University of Technology, Austria (cited on p. 116).

Cash, D. M., Miga, M. I., Sinha, T. K., Galloway, R. L., and Chapman, W. C. (2005). "Compensating for intraoperative soft-tissue deformations using incomplete sur-

face data and finite elements." In: *IEEE Trans Med Imaging*, 24, pp. 1479–1491 (cited on p. 31).

Cash, D. M., Miga, M. I., Glasgow, S. C., Dawant, B. M., Clements, L. W., Cao, Z., Galloway, R. L., and Chapman, W. C. (2007). "Concepts and Preliminary Data Toward the Realization of Image-guided Liver Surgery." In: *Journal of Gastrointestinal Surgery*, 11(7), pp. 844–859 (cited on pp. 25, 105, 126, 141).

Chandra, A., Mangam, S., and Marzouk, D. (2009). "A review of risk scoring systems utilised in patients undergoing gastrointestinal surgery." In: *J. Gastrointest. Surg.* 13, pp. 1529–1538 (cited on p. 20).

Cho, S. H., Kang, U. R., Kim, J. D., Han, Y. S., and Choi, D. L. (2011). "The value of gadoxetate disodium-enhanced MR imaging for predicting posthepatectomy liver failure after major hepatic resection: a preliminary study." In: *Eur J Radiol*, 80, pp. 195–200 (cited on p. 62).

Chojecki, P. and Leiner, U. (2009). "Berührungslose Gestik-Interaktion im Operationssaal Touchless Gesture-Interaction in the Operating Room." In: *Journal of i-com (Zeitschrift für interaktive und kooperative Medien)*, 8(1), pp. 13–18 (cited on p. 71).

Cleary, K. and Peters, T. (2010). "Image-guided interventions: technology review and clinical applications." In: *Annual Review of Biomedical Engineering*, 12, pp. 119–142 (cited on pp. 28–30).

Clements, L., Dumpuri, P., Chapman, W., Dawant, B., Galloway, R., and Miga, M. (2011). "Organ surface deformation measurement and analysis in open hepatic surgery: Method and preliminary results from 12 clinical cases." In: *IEEE Trans Biomed Eng* (cited on pp. 30, 31).

Clifford, M. A., Banovac, F., Levy, E., and Cleary, K. (2002). "Assessment of hepatic motion secondary to respiration for computer assisted interventions." In: *Computer Aided Surgery*, 7(5), pp. 291–299 (cited on pp. 30, 32, 73).

Conlon, R., Jacobs, M., Dasgupta, D., and Lodge, J. P. (2003). "The value of intraoperative ultrasound during hepatic resection compared with improved preoperative magnetic resonance imaging." In: *Eur J Ultrasound*, 16, pp. 211–216 (cited on p. 70).

Cordes, J., Dornheim, J., and Preim, B. (2009). "Scenario-Based Design of Surgical Training and Planning Systems." In: *Journal of i-com (Zeitschrift für interaktive und kooperative Medien)*, 8(1), pp. 5–12 (cited on p. 126).

Couinaud, C. (1954). "Lobes et segments hepatiques." In: *La Presse Medicale*, 62(33), pp. 709–712 (cited on pp. 6, 10, 19).

Cox, J. and Kirkpatrick, R. C. (1896). "The new photography, with report of a case in which a bullet was photographed in the leg." In: *Montreal Med*, 24, pp. 661–665 (cited on p. 26).

Demedts, D. (2010). "Bewertung von Resektionvorschlägen für die Leberchirurgie." MA thesis. Institute of Mathematics and Image Computing, University of Lübeck, Germany (cited on pp. 88, 92).

Demedts, D., Schenk, A., Hansen, C., and Peitgen, H.-O. (2010). "Evaluation of Resection Proposals for Liver Surgery Planning." In: *Proc. of the 9th Annual*

Meeting of the German Society of Computer- and Robot-Assisted Surgery, pp. 13–16 (cited on pp. 12, 23, 24, 145).

Edworthy, J., Loxley, S., and Dennis, I. (1991). "Improving auditory warning design: relationship between warning sound parameters and perceived urgency." In: *Hum Factors*, 33, pp. 205–231 (cited on p. 134).

Ellsmere, J., Kane, R., Grinbaum, R., Edwards, M., Schneider, B., and Jones, D. (2007). "Intraoperative ultrasonography during planned liver resections: why are we still performing it?" In: *Surg Endosc.* 34(4), pp. 353–358 (cited on pp. 2, 70).

Elmqvist, N., Assarsson, U., and Tsigas, P. (2007). "Employing dynamic transparency for 3D occlusion management: design issues and evaluation." In: *Proc. of the 11th International Conference on Human-Computer Interaction*. Springer, pp. 532–545 (cited on p. 116).

Endo, I., Shimada, H., Takeda, K., Fujii, Y., Yoshida, K., Morioka, D., Sadatoshi, S., Togo, S., Bourquain, H., and Peitgen, H. O. (2007). "Successful duct-to-duct biliary reconstruction after right hemihepatectomy. Operative planning using virtual 3D reconstructed images." In: *J. Gastrointest. Surg.* 11, pp. 666–670 (cited on p. 43).

Ericsson, K. A. and Simon, H. A. (1993). *Protocol analysis: Verbal Reports as Data*. The MIT Press (cited on p. 122).

Fasel, J. H., Selle, D., Evertsz, C. J., Terrier, F., Peitgen, H.-O., and Gailloud, P. (1998). "Segmental anatomy of the liver: poor correlation with CT." In: *Radiology*, 206(1), pp. 151–6 (cited on pp. 6, 19).

Ferlay, J., Shin, H.-R., Bray, F., Forman, D., Mathers, C., and Parkin, D. M. (2010). "Estimates of worldwide burden of cancer in 2008: GLOBOCAN 2008." In: *Int J Cancer* (cited on p. 7).

Feuerstein, M., Mussack, T., Heining, S. M., and Navab, N. (2008). "Intraoperative laparoscope augmentation for port placement and resection planning in minimally invasive liver resection." In: *IEEE Transactions on Medical Imaging*, 27(3), pp. 355–369 (cited on pp. 35, 71, 117).

Feuerstein, M., Reichl, T., Vogel, J., Traub, J., and Navab, N. (2009). "Magneto-optical tracking of flexible laparoscopic ultrasound: model-based online detection and correction of magnetic tracking errors." In: *IEEE Trans Med Imaging*, 28, pp. 951–967 (cited on p. 29).

Fischer, J., Bartz, D., and Straßer, W. (2005). "Stylized Augmented Reality for Improved Immersion." In: *Proc. of IEEE Virtual Reality*, pp. 195–202 (cited on pp. 71, 116, 126).

Fischer, J., Huhle, B., and Schilling, A. (2007). "Using Time-of-Flight Range Data for Occlusion Handling in Augmented Reality." In: *Proc. of Eurographics Symposium on Virtual Environments (EGVE)*, pp. 109–116 (cited on p. 116).

Fischer, L., Cardenas, C., Thorn, M., Benner, A., Grenacher, L., Vetter, M., Lehnert, T., Klar, E., Meinzer, H.-P., and Lamade, W. (2002). "Limits of Couinauds liver segment classification: a quantitative computer-based three-dimensional analysis." In: *J Comput Assist Tomogr*, 26(6), pp. 962–7 (cited on p. 6).

Freudenberg, B. (2003). "Real-Time Stroke-Based Halftoning." PhD thesis. School of Computer Science, University of Magdeburg, Germany (cited on p. 101).

Friman, O., Hindennach, M., Kuhnel, C., and Peitgen, H. O. (2010). "Multiple hypothesis template tracking of small 3D vessel structures." In: *Med Image Anal*, 14, pp. 160–171 (cited on p. 18).

Gavaghan, K. A., Peterhans, M., Oliveira-Santos, T., and Weber, S. (2011). "A portable image overlay projection device for computer-aided open liver surgery." In: *IEEE Trans Biomed Eng*, 58, pp. 1855–1864 (cited on pp. 35, 117).

Gloger, O., Kuhn, J., Stanski, A., Volzke, H., and Puls, R. (2010). "A fully automatic three-step liver segmentation method on LDA-based probability maps for multiple contrast MR images." In: *Magn Reson Imaging*, 28, pp. 882–897 (cited on p. 16).

Glossop, N. D. (2009). "Advantages of optical compared with electromagnetic tracking." In: *J Bone Joint Surg Am*, 91(Supplement 1), pp. 23–28 (cited on p. 29).

Glossop, N. (2003). "Laser projection augmented reality system for computer-assisted surgery." In: *International Congress Series*, 1256, pp. 65–71 (cited on p. 117).

Graaf, W. de, Lienden, K. P. van, Dinant, S., Roelofs, J. J., Busch, O. R., Gouma, D. J., Bennink, R. J., and Gulik, T. M. van (2010). "Assessment of future remnant liver function using hepatobiliary scintigraphy in patients undergoing major liver resection." In: *J. Gastrointest. Surg.* 14, pp. 369–378 (cited on pp. 20, 62).

Grady, L. and Funka-Lea, G. (2006). "An energy minimization approach to the data driven editing of presegmented images/volumes." In: *Proc. of Medical Image Computing and Computer-Assisted Intervention (MICCAI)*, 9, pp. 888–895 (cited on p. 17).

Grundmann, R. T., Hermanek, P., Merkel, S., Germer, C. T., Grundmann, R. T., Hauss, J., Henne-Bruns, D., et al. (2008). "Diagnosis and treatment of colorectal liver metastases - workflow." In: *Zentralbl Chir*, 133, pp. 267–284 (cited on p. 11).

Hahn, H.K., Preim, B., Selle, D., and Peitgen, H.-O. (2001). "Visualization and Interaction Techniques for the Exploration of Vascular Structures." In: *IEEE Visualization*, pp. 395–402 (cited on p. 18).

Haker, S., Angenent, S., Tannenbaum, A., and Kikinis, R. (2000). "Nondistorting flattening maps and the 3-D visualization of colon CT images." In: *IEEE Trans Med Imaging*, 19, pp. 665–670 (cited on p. 97).

Hammerstingl, R., Huppertz, A., Breuer, J., Balzer, T., Blakeborough, A., Carter, R., Fuste, L. C., et al. (2008). "Diagnostic efficacy of gadoxetic acid (Primovist)-enhanced MRI and spiral CT for a therapeutic strategy: comparison with intraoperative and histopathologic findings in focal liver lesions." In: *Eur Radiol*, 18, pp. 457–467 (cited on p. 15).

Hanna, G. B., Shimi, S. M., and Cuschieri, A. (1998). "Task performance in endoscopic surgery is influenced by location of the image display." In: *Ann. Surg.* 227, pp. 481–484 (cited on p. 34).

Hansen, C. (2006). "Verwendung von Textur in der Gefäßvisualisierung." MA thesis. School of Computer Science, University of Magdeburg, Germany (cited on p. 117).

Hansen, C., Schlichting, S., Markert, M., Hindennach, M., Zidowitz, S., and Peitgen, H.-O. (2007a). "Intraoperative Adaptation of Preoperative Risk Analyses for

Oncologic Liver Surgery using tracked 2D ultrasound." In: *Proc. of the 6th Annual Meeting of the German Society of Computer- and Robot-Assisted Surgery*, pp. 155–158 (cited on p. 94).

Hansen, C., Koehn, A., Ritter, F., Zidowitz, S., and Peitgen, H.-O. (2007b). "Simultaneous Visualization of Preoperative Planning Models and Intraoperative Ultrasound for Liver Surgery." In: *Proc. of Eurographics (Short Papers and Medical Prize Awards)*, pp. 117–120.

Hansen, C., Wieferich, J., Ritter, F., Rieder, C., and Peitgen, H.-O. (2008a). "Illustrative Visualization of 3D Planning Models for Augmented Reality in Liver Surgery." In: *Proc. of the 7th Annual Meeting of the German Society of Computer- and Robot-Assisted Surgery*, pp. 1–4 (cited on p. 127).

Hansen, C., Zidowitz, S., Schenk, A., Oldhafer, K., Lang, H., and Peitgen, H.-O. (2008b). "Intraoperative Adaptation and Visualization of Preoperative Risk Analyses for Oncologic Liver Surgery." In: *Proc. of SPIE Medical Imaging*. Vol. 6918, pp. 691809–1–10 (cited on p. 94).

Hansen, C., Schlichting, S., Zidowitz, S., Kleemann, M., and Peitgen, H.-O. (2008c). "Intraoperative Adaptation of Planning Data for Oncologic Liver Surgery." In: *Proc. of MICCAI Workshop on Image Guidance and Computer Assistance for Soft-Tissue Interventions*, pp. 36–45 (cited on p. 94).

Hansen, C., Köhn, A., Schlichting, S., Weiler, F., Konrad, O., Zidowitz, S., and Peitgen, H.-O. (2008d). "Intraoperative Modification of Resection Plans for Liver Surgery." In: *Int J Comput Assist Radiol Surg*, 2(3-4), pp. 291–297 (cited on p. 94).

Hansen, C., Zidowitz, S., Hindennach, M., Schenk, A., Hahn, H., and Peitgen, H.-O. (2009a). "Interactive Determination of Robust Safety Margins for Oncologic Liver Surgery." In: *Proc. of the 23rd International Symposium on Computer Assisted Radiology and Surgery (CARS)*, 4(Supplement 1), p. 94 (cited on p. 67).

Hansen, C., Zidowitz, S., Hindennach, M., Schenk, A., Hahn, H., and Peitgen, H.-O. (2009b). "Interactive Determination of Robust Safety Margins for Oncologic Liver Surgery." In: *Int J Comput Assist Radiol Surg*, 4(5), pp. 469–474 (cited on p. 67).

Hansen, C., Wieferich, J., Ritter, F., Rieder, C., and Peitgen, H.-O. (2010a). "Illustrative Visualization of 3D Planning Models for Augmented Reality in Liver Surgery." In: *Int J Comput Assist Radiol Surg*, 5(2), pp. 133–141 (cited on p. 127).

Hansen, C., Zidowitz, S., Schenk, A., Oldhafer, K., Lang, H., and Peitgen, H.-O. (2010b). "Risk maps for navigation in liver surgery." In: *Proc. of SPIE Medical Imaging*. Vol. 7625, pp. 762528–1–8 (cited on p. 112).

Hansen, C., Lindow, B., Zidowitz, S., Schenk, A., and Peitgen, H.-O. (2010c). "Towards Automatic Generation of Resection Surfaces for Liver Surgery Planning." In: *Proc. of the 24th International Symposium on Computer Assisted Radiology and Surgery (CARS)*, 5(Supplement 1), pp. 119–120 (cited on p. 94).

Hansen, C., Black, D., Lange, C., Rieber, F., Lamade, W., Donati, M., Oldhafer, K. J., and Hahn, H. K. (2012). "Auditory Support for Resection Guidance in Navigated Liver Surgery." In: *Int J Med Robot*, in print (cited on pp. 134, 142).

Hata, S., Imamura, H., Aoki, T., Hashimoto, T., Akahane, M., Hasegawa, K., Bekku, Y., Sugawara, Y., Makuuchi, M., and Kokudo, N. (2011). "Value of Visual Inspection, Bimanual Palpation, and Intraoperative Ultrasonography During Hepatic Resection for Liver Metastases of Colorectal Carcinoma." In: *World J Surg* (cited on pp. 15, 70, 74).

Heckel, F., Moltz, J. H., Bornemann, L., Dicken, V., Bauknecht, H.-C., Fabel, M., Hittinger, M., et al. (2009). "3D contour based local manual correction of tumor segmentations in CT scans." In: *SPIE Medical Imaging*. Vol. 7259. 1. SPIE, pp. 72593L–1–9 (cited on p. 17).

Heckel, F., Konrad, O., Hahn, H. K., and Peitgen, H.-O. (2011). "Interactive 3D Medical Image Segmentation with Energy-Minimizing Implicit Functions." In: *Computer & Graphics: Special issue on Visual Computing for Biology and Medicine*, 35(2), pp. 275–287 (cited on p. 17).

Heimann, T., Wolf, I., and Meinzer, H. P. (2006). "Active shape models for a fully automated 3D segmentation of the liver–an evaluation on clinical data." In: *Med Image Comput Comput Assist Interv*, 9, pp. 41–48 (cited on p. 16).

Heimann, T., Ginneken, B. van, Styner, M. A., Arzhaeva, Y., Aurich, V., Bauer, C., Beck, A., et al. (2009). "Comparison and evaluation of methods for liver segmentation from CT datasets." In: *IEEE Trans Med Imaging*, 28, pp. 1251–1265 (cited on p. 16).

Heizmann, O., Zidowitz, S., Bourquain, H., Potthast, S., Peitgen, H. O., Oertli, D., and Kettelhack, C. (2010). "Assessment of intraoperative liver deformation during hepatic resection: prospective clinical study." In: *World J Surg*, 34, pp. 1887–1893 (cited on p. 30).

Hildebrand, P., Schlichting, S., Martens, V., Besirevic, A., Kleemann, M., Roblick, U., Mirow, L., Bürk, C., Schweikard, A., and Bruch, H. (2007). "Prototype of an intraoperative navigation- and documentation system for laparoscopic radiofrequency ablation: First Experiences." In: *European Journal of Surgical Oncol.* 34(4), pp. 418–421 (cited on pp. 25, 33, 72, 73, 83).

Hildebrand, P., Schlichting, S., Martens, V., Besirevic, A., Kleemann, M., Roblick, U., Mirow, L., Burk, C., Schweikard, A., and Bruch, H.-P. (2008). "Prototype of an intraoperative navigation and documentation system for laparoscopic radiofrequency ablation: first experiences." In: *European Journal of Surgical Oncology*, 34(4), pp. 418–421 (cited on pp. 82, 87).

Hiller, S. (2008). "Konzeption und Implementierung eines Verfahrens zur Erstellung von Resektionsebenen für die Leberchirurgieplanung." MA thesis. School of Computer Science, University of Magdeburg, Germany (cited on p. 23).

Hong, W., Gu, X., Qiu, F., Jin, M., and Kaufman, A. (2006). "Conformal virtual colon flattening." In: *Proc. of ACM symposium on Solid and physical modeling*. ACM, pp. 85–93 (cited on p. 97).

Huang, X., Wang, W., Wang, X., Liu, R., Ke, S., and Wu, Z. (2009). "A Hybrid Image Registration for Different Phases of Contrast Enhanced Liver CT Data." In: *Computer Science and Information Engineering*, 6, pp. 239–243 (cited on p. 15).

Hurdal, M. K. and Stephenson, K. (2009). "Discrete conformal methods for cortical brain flattening." In: *Neuroimage*, 45, pp. 86–98 (cited on p. 97).

IEC, 60601-1-8 (2006). *Collateral Standard: General Requirements, Tests and Guidance for Alarm Systems in Medical Electrical Equipment and Medical Electrical Systems*. IEC, Geneva, Switzerland (cited on p. 140).

IHPBA, Brisbane (2000). "Terminology of Liver Anatomy and Resections." In: *The Official Journal of the International Hepato Pancreato Biliary Association*, 2, pp. 333–339 (cited on p. 8).

Interrante, V., Fuchs, H., and Pizer, S. M. (1997). "Conveying the 3d shape of smoothly curving transparent surfaces via texture." In: *IEEE Transactions on Visualization and Computer Graphics*, 3, pp. 98–117 (cited on p. 114).

Isenberg, T., Halper, N., and Strothotte, T. (2002). "Stylizing Silhouettes at Interactive Rates: From Silhouette Edges to Silhouette Strokes." In: *Computer Graphics Forum*, 21(3), pp. 249–258 (cited on p. 118).

Jolly, M.P. and Grady, L. (2008). "3D general lesion segmentation in CT." In: *Proc. of 5th IEEE International Symposium on Biomedical Imaging: From Nano to Macro*, pp. 796–799 (cited on p. 17).

Joshi, A., Scheinost, D., Vives, K. P., Spencer, D. D., Staib, L. H., and Papademetris, X. (2008). "Novel interaction techniques for neurosurgical planning and stereotactic navigation." In: *IEEE Trans Vis Comput Graph*, 14, pp. 1587–1594 (cited on p. 39).

Jovanov, E., K., Wegner, V., Radivojevic, D., Starcevic, S., Quinn M., and B., Karron D. (1999). "Tactical audio and acoustic rendering in biomedical applications." In: *IEEE Transactions on Information Technology in Biomedicine*, 3(2), pp. 109–118 (cited on p. 130).

Kainmueller, D., Lange, T., and Lamecker, H. (2007). "Shape constrained automatic segmentation of the liver based on a heuristic intensity model." In: *Proc. of MICCAI Workshop 3D Segmentation in the Clinic: A Grand Challenge*, pp. 109 –116 (cited on p. 16).

Kalkofen, Denis, Mendez, Erick, and Schmalstieg, Dieter (2007). "Interactive Focus and Context Visualization for Augmented Reality." In: *Proc. of the 6th IEEE and ACM International Symposium on Mixed and Augmented Reality*. IEEE Computer Society, pp. 1–10 (cited on pp. 116, 127).

Kang, Y., Engelke, K., and Kalender, W. A. (2004). "Interactive 3D editing tools for image segmentation." In: *Med Image Anal*, 8, pp. 35–46 (cited on p. 17).

Karaliotas, C., E., Broelsch C., and A., Habib N. (2007). *Liver and Biliary Tract Surgery: Embryological Anatomy to 3D-Imaging and Transplant Innovations*. Springer (cited on p. 10).

Kersten-Oertel, M., Jannin, P., and Collins, D. L. (2011). "DVV: A Taxonomy for Mixed Reality Visualization in Image Guided Surgery." In: *IEEE Trans Vis Comput Graph*, in press (cited on pp. 35, 114).

Khan, M. F., Dogan, S., Maataoui, A., Wesarg, S., Gurung, J., Ackermann, H., Schiemann, M., Wimmer-Greinecker, G., and Vogl, T. J. (2006). "Navigation-based needle puncture of a cadaver using a hybrid tracking navigational system." In: *Invest Radiol*, 41, pp. 713–720 (cited on p. 29).

Kirbas, Cemil and Quek, Francis (2004). "A review of vessel extraction techniques and algorithms." In: *ACM Comput. Surv.* 36 (2), pp. 81–121 (cited on p. 18).

Kleemann, M., Hildebrand, P., Mirow, L., Roblick, U., Bürk, C. G., and Bruch, H.-P. (2005). "Navigation in der Vizeralchirurgie." In: *Chir Gastroenterol*, 21(Supplement 2), pp. 1–7 (cited on p. 28).

Kleinman, R., Goulet, O.-J., Mieli-Vergani, G., Sanderson, I., Sherman, P., and Shneider, B. (2008). *Walker's Pediatric Gastrointestinal Disease*. 5th ed. Vol. 2. PMPH, USA (cited on p. 6).

Kocev, B., Ojdanic, D., and Peitgen, H.-O. (2011). "An Approach for Projector-based Surgeon-Computer Interaction using Tracked Instruments." In: *Proc. of GI Workshop: Emerging Technologies for Medical Diagnosis and Therapy*, in press (cited on p. 126).

Konrad-Verse, O., Preim, B., and Littmann, A. (2004). "Virtual Resection with a Deformable Cutting Plane." In: *Proc. of Simulation und Visualisierung*, pp. 203–214 (cited on pp. 22, 24, 88, 90, 132).

Kopke, L. F. F., Bastos, J. C. F., Andrade Filho, J. de S., and Gouvêa, P. S. (2005). "Safety margin: an old and relative concept." In: *Anais Brasileiros de Dermatologia*, 80(3) (cited on p. 38).

Krempien, R., Hoppe, H., Kahrs, L., Daeuber, S., Schorr, O., Eggers, G., Bischof, M., Munter, M., Debus, J., and Harms, W. (2008). "Projector-Based Augmented Reality for Intuitive Intraoperative Guidance in Image-Guided 3D Interstitial Brachytherapy." In: *International Journal of Radiation Oncology*Biology*Physics*, 70(3), pp. 944–952 (cited on pp. 35, 117).

Kröger, T., Altrogge, I., Preusser, T., Pereira, P. L., Schmidt, D., Weihusen, A., and Peitgen, H. O. (2006). "Numerical simulation of radio frequency ablation with state dependent material parameters in three space dimensions." In: *Proc. of Medical Image Computing and Computer-Assisted Intervention (MICCAI)*, 9, pp. 380–388 (cited on p. 39).

Kröger, T., Pätz, T., Altrogge, I., Schenk, A., Lehmann, K. S., Frericks, B. B., Ritz, J. P., Peitgen, H. O., and Preusser, T. (2010). "Fast Estimation of the Vascular Cooling in RFA Based on Numerical Simulation." In: *Open Biomed Eng J*, 4, pp. 16–26 (cited on p. 9).

Kruijff, E., Swan II, J. E., and Feiner, S. (2010). "Perceptual Issues in Augmented Reality Revisited." In: *Proc. of IEEE International Symposium on Mixed and Augmented Reality*. IEEE Computer Society, pp. 3–12 (cited on pp. 114, 126).

Kunzli, B. M., Abitabile, P., and Maurer, C. A. (2011). "Radiofrequency ablation of liver tumors: Actual limitations and potential solutions in the future." In: *World J Hepatol*, 3, pp. 8–14 (cited on p. 9).

Lamade, W., Glombitza, G., Fischer, L., Chiu, P., Cardenas, C. E., Thorn, M., Meinzer, H. P., et al. (2000). "The impact of 3-dimensional reconstructions on operation planning in liver surgery." In: *Arch Surg*, 135, pp. 1256–1261 (cited on pp. 48, 60).

Lamata, P., Jalote-Parmar, A., Lamata, F., and Declerck, J. (2008). "The Resection Map, a proposal for intraoperative hepatectomy guidance." In: *Int J Comput Assist Radiol Surg*, 3(3-4), pp. 299–306 (cited on pp. 33, 99, 111).

Lamata, P., Lamata, F., Sojar, V., Makowski, P., Massoptier, L., Casciaro, S., Ali, W., et al. (2010). "Use of the Resection Map system as guidance during hepatectomy." In: *Surgical Endoscopy*, 24(9), 2327–2337 (cited on p. 34).

Lang, H. (2007). "Technik der Leberresektion: Teil II. Operationsdurchführung." In: *Der Chirurg*, 78, 849–866(18) (cited on p. 88).

Lang, H., Radtke, A., Hindennach, M., Schroeder, T., Fruhauf, N. R., Malago, M., Bourquain, H., Peitgen, H.-O., Oldhafer, K. J., and Broelsch, C. E. (2005). "Impact of virtual tumor resection and computer-assisted risk analysis on operation planning and intraoperative strategy in major hepatic resection." In: *Archives of Surgery*, 140(7), pp. 629–38 (cited on pp. 2, 8, 21, 24, 43, 48, 60, 90).

Lang, H. and Schenk, A. (2010). "Planung von Leberresektionen." In: *Computerassistierte Chirurgie*. Urban & Fischer Verlag, pp. 515–524 (cited on pp. 2, 14, 38).

Lange, T., Wenckebach, T., Lamecker, H., Seebaß, M., Hünerbein, M., Eulenstein, S., and M., Schlag P. (2005). "Registration of different phases of contrast-enhanced CT/MRI data for computer-assisted liver surgery planning: Evaluation of state-of-the-art methods." In: *Int. J. Medical Robotics and Computer Assisted Surgery*. Vol. 1 (3), pp. 6 –20 (cited on p. 15).

Lei, P., Moeslein, F., Wood, B. J., and Shekhar, R. (2011). "Real-time tracking of liver motion and deformation using a flexible needle." In: *Int J Comput Assist Radiol Surg*, 6, pp. 435–446 (cited on p. 32).

Lerotic, M., Chung, A. J., Mylonas, G., and Yang, G.-Z. (2007). "Pq-space based non-photorealistic rendering for augmented reality." In: *Medical Image Computing and Computer-Assisted Intervention (MICCAI)*, 10(Pt 2), pp. 102–109 (cited on p. 116).

Lesage, D., Angelini, E. D., Bloch, I., and Funka-Lea, G. (2009). "A review of 3D vessel lumen segmentation techniques: models, features and extraction schemes." In: *Med Image Anal*, 13, pp. 819–845 (cited on p. 18).

Li, K. and Jolly, M. (2008). "Simultaneous detection of multiple elastic surfaces with application to tumor segmentation in CT images." In: *Proc. of SPIE Medical Imaging*. Vol. 6914. 2, 69143S_1–11 (cited on p. 17).

Lindow, B. (2009). "Automatic Generation of Resection Surfaces for Liver Surgery Planning." MA thesis. School of Computer Science, University of Rostock, Germany (cited on p. 94).

Lohe, T., Kröger, T., Zidowitz, S., Peitgen, H.-O., and Jiang, X. (2008). "Hierarchical Matching of Anatomical Trees for Medical Image Registration." In: *ICMB*, pp. 224–231 (cited on p. 31).

Lordan, J. T. and Karanjia, N. D. (2010). "'Close shave' in liver resection for colorectal liver metastases." In: *European Journal of Surgical Oncology*, 36(1), pp. 47–51 (cited on p. 38).

Lu, R., Marziliano, P., and Hua Thng, C. (2005). "Liver tumor volume estimation by semi-automatic segmentation method." In: *Proc. of IEEE Eng Med Biol Soc*, 3, pp. 3296–3299 (cited on p. 17).

Maier-Hein, L., Schmidt, M., Franz, A. M., Santos, T. R. dos, Seitel, A., Jahne, B., Fitzpatrick, J. M., and Meinzer, H. P. (2010). "Accounting for anisotropic noise in fine registration of time-of-flight range data with high-resolution surface data." In: *Med Image Comput Comput Assist Interv*, 13, pp. 251–258 (cited on p. 31).

Manzey, D., Rottger, S., Bahner-Heyne, J. E., Schulze-Kissing, D., Dietz, A., Meixensberger, J., and Strauss, G. (2009). "Image-guided navigation: the surgeon's perspective on performance consequences and human factors issues." In: *Int. J. Medical Robotics and Computer Assisted Surgery*, 5, pp. 297–308 (cited on p. 130).

Marescaux, J., Rubino, F., Arenas, M., Mutter, D., and Soler, L. (2004). "Augmented-Reality-Assisted Laparoscopic Adrenalectomy." In: *JAMA: The Journal of the American Medical Association*, 292(18), pp. 2214–2215 (cited on pp. 35, 117).

Markert, M., Koschany, A., and Lueth, T. (2010). "Tracking of the liver for navigation in open surgery." In: *Int J Comput Assist Radiol Surg*, 5, pp. 229–235 (cited on p. 32).

Massoptier, L. and Casciaro, S. (2008). "A new fully automatic and robust algorithm for fast segmentation of liver tissue and tumors from CT scans." In: *European Radiology*, 18(8), pp. 1658–1665 (cited on p. 17).

Maurel, P. (2010). *Hepatocytes: Methods and Protocols*. Methods in Molecular Biology. Springer Verlag (cited on p. 7).

Mazzoni, G., Napoli, A., Mandetta, S., Miccini, M., Cassini, D., Gregori, M., Colace, L., and Tocchi, A. (2008). "Intra-operative ultrasound for detection of liver metastases from colorectal cancer." In: *Liver Int.* 28, pp. 88–94 (cited on p. 70).

McCartney, J. (2002). "Rethinking the Computer Music Language: SuperCollider." In: *Computer Music Journal*, 26(4), pp. 61–68 (cited on p. 132).

Meinzer, H. P., Thorn, M., and Cárdenas, C. E. (2002). "Computerized planning of liver surgery—an overview." In: *Computers & Graphics*, 26(4), pp. 569 –576 (cited on p. 70).

Mercier, L., Lang? T., Lindseth, F., and Collins, D. L. (2005). "A review of calibration techniques for freehand 3-D ultrasound systems." In: *Ultrasound Med Biol*, 31, pp. 449–471 (cited on p. 30).

Metzen, J. H., Kröger, T., Schenk, A., Zidowitz, S., H.-O., Peitgen, and Jiang, X. (2007). "Matching of Tree Structures for Registration of Medical Images." In: vol. 4538. Lecture Notes in Computer Science. Springer, pp. 13–24 (cited on p. 31).

Metzen, J. H., Kröger, T., Schenk, A., Zidowitz, S., Peitgen, H.-O., and Jiang, X. (2009). "Matching of anatomical tree structures for registration of medical images." In: *Image Vision Comput.* 27 (7), pp. 923–933 (cited on p. 31).

Mühler, K., Hansen, C., Neugebauer, M., and Preim, B. (2008). "Automatische Kamerapositionierung für intra-operative Visualisierungen in der onkologischen Leberchirurgie." In: *Proc. of Bildverarbeitung für die Medizin*. Informatik aktuell, pp. 143–147.

Militzer, A., Hager, T., Jager, F., Tietjen, C., and Hornegger, J. (2010). "Automatic Detection and Segmentation of Focal Liver Lesions in Contrast Enhanced CT Images." In: *Proc. of the 20th International Conference on Pattern Recognition*. IEEE Computer Society, pp. 2524–2527 (cited on p. 17).

Moltz, J. H., Bornemann, L., Kuhnigk, J. M., Dicken, V., Peitgen, E., Meier, S., Bolte, H., et al. (2009). "Advanced Segmentation Techniques for Lung Nodules, Liver Metastases, and Enlarged Lymph Nodes in CT Scans." In: *IEEE Journal of Selected Topics in Signal Processing*, 3(1), pp. 122–134 (cited on p. 17).

Motosugi, U., Ichikawa, T., Morisaka, H., Sou, H., Muhi, A., Kimura, K., Sano, K., and Araki, T. (2011). "Detection of pancreatic carcinoma and liver metastases with gadoxetic acid-enhanced MR imaging: comparison with contrast-enhanced multi-detector row CT." In: *Radiology*, 260, pp. 446–453 (cited on p. 15).

Muratore, A., Ribero, D., Zimmitti, G., Mellano, A., Langella, S., and Capussotti, L. (2010). "Resection margin and recurrence-free survival after liver resection of colorectal metastases." In: *Annals of Surgical Oncology*, 17(5), pp. 1324–1329 (cited on pp. 38, 65).

Nakamoto, M., Nakada, K., Sato, Y., Konishi, K., Hashizume, M., and Tamura, S. (2008). "Intraoperative magnetic tracker calibration using a magneto-optic hybrid tracker for 3-D ultrasound-based navigation in laparoscopic surgery." In: *IEEE Trans Med Imaging*, 27, pp. 255–270 (cited on p. 29).

Nathan, H., Bridges, J. F., Schulick, R. D., Cameron, A. M., Hirose, K., Edil, B. H., Wolfgang, C. L., Segev, D. L., Choti, M. A., and Pawlik, T. M. (2011). "Understanding Surgical Decision Making in Early Hepatocellular Carcinoma." In: *J Clin Oncol*, in print (cited on p. 9).

Navab, N., Traub, J., Sielhorst, T., Feuerstein, M., and Bichlmeier, C. (2007a). "Action- and workflow-driven augmented reality for computer-aided medical procedures." In: *IEEE Computer Graphics and Applications*, 27(5), pp. 10–14 (cited on p. 126).

Navab, N., Feuerstein, M., and Bichlmeier, C. (2007b). "Laparoscopic Virtual Mirror New Interaction Paradigm for Monitor Based Augmented Reality." In: *Virtual Reality Conference, IEEE*, pp. 43–50 (cited on p. 116).

Navkar, N. V., Tsekos, N. V., Stafford, J. R., Weinberg, J. S., and Deng, Z. (2010). "Visualization and planning of neurosurgical interventions with straight access." In: *Proc. of the First International Conference on Information Processing in Computer-Assisted Interventions*. Springer-Verlag, pp. 1–11 (cited on p. 98).

Neugebauer, M., Gasteiger, R., Beuing, O., Diehl, V., Skalej, M., and Preim, B. (2009). "Map Displays for the Analysis of Scalar Data on Cerebral Aneurysm

Surfaces." In: *Computer Graphics Forum (EuroVis)*. Vol. 28 (3), pp. 895–902 (cited on p. 98).

Neumann, U. P., Seehofer, D., and Neuhaus, P. (2010). "The Surgical Treatment of Hepatic Metastases in Colorectal Carcinoma." In: *Deutsches Ärzteblatt International*, 107(19), pp. 335–342 (cited on pp. 7, 8, 11).

Nicolau, S. A., Pennec, X., Soler, L., Buy, X., Gangi, A., Ayache, N., and Marescaux, J. (2009). "An augmented reality system for liver thermal ablation: Design and evaluation on clinical cases." In: *Medical Image Analysis*, 13(3), pp. 494–506 (cited on pp. 34, 35).

Nintendo (Jan. 2011). Internet source: www.nintendo.com/wii/what/controllers, visited: 2011, October 15 (cited on p. 78).

Nowatschin, S., Markert, M., Weber, S., and Lüth, T. C. (2007). "A system for analyzing intraoperative B-Mode ultrasound scans of the liver." In: *Proc. IEEE Eng Med Biol Soc*, pp. 1346–1349 (cited on pp. 33, 71, 105).

Oeltze, S. and Preim, B. (2005). "Visualization of vasculature with convolution surfaces: method, validation and evaluation." In: *IEEE Trans Med Imaging*, 24, pp. 540–548 (cited on p. 18).

Okada, M., Nishio, W., Sakamoto, T., Uchino, K., Yuki, T., Nakagawa, A., and Tsubota, N. (2005). "Effect of tumor size on prognosis in patients with non-small cell lung cancer: the role of segmentectomy as a type of lesser resection." In: *J. Thorac. Cardiovasc. Surg.* 129, pp. 87–93 (cited on p. 39).

Olabarriaga, S. D. and Smeulders, A. W. (2001). "Interaction in the segmentation of medical images: a survey." In: *Med Image Anal*, 5, pp. 127–142 (cited on p. 17).

Oldhafer, K. J., Preim, B., Dorge, C., Peitgen, H. O., and Broelsch, C. E. (2002). "[Acceptance of computer-assisted surgery planning in visceral (abdominal) surgery]." In: *Zentralbl Chir*, 127, pp. 128–133 (cited on p. 14).

Oldhafer, K. J., Stavrou, G. A., Prause, G., Peitgen, H.-O., Lueth, T. C., and Weber, S. (2009). "How to operate a liver tumor you cannot see." In: *Langenbeck's Archives of Surgery*, 394(3), pp. 489–494 (cited on pp. 28, 130).

Ooijen, P. M. A. van, Wolf, R., Schenk, A., Rouw, D. B., Slooff, M., Peitgen, H.-O., and Oudkerk, M. (2003). "Recent Developments in Organ-Selective Reconstruction and Analysis of Multiphase Liver CT." In: *Imaging Decisions MRI*, 7(1), pp. 37–43 (cited on p. 38).

Papenberg, N., Lange, T., Modersitzki, J., Schlag, P. M., and Fischer, B. (2008). "Image registration for CT and intraoperative ultrasound data of the liver." In: *Proc. of SPIE Medical Imaging*. Vol. 6918, pp. 691808–1–8 (cited on pp. 31, 73, 82).

Pawlik, T. M., Scoggins, C. R., Zorzi, D., Abdalla, E. K., Andres, A., Eng, C., Curley, S. A., et al. (2005). "Effect of surgical margin status on survival and site of recurrence after hepatic resection for colorectal metastases." In: *Ann. Surg.* 241, pp. 715–722 (cited on pp. 38, 65).

Pawlik, T. M., Schulick, R. D., and Choti, M. A. (2008). "Expanding criteria for resectability of colorectal liver metastases." In: *The Oncologist*, 13(1), pp. 51–64 (cited on pp. 8, 38).

Penne, J., Soutschek, S., Stürmer, M., Schaller, C., Placht, S., Kornhuber, J., and Hornegger, J. (2009). "Touchless 3D Gesture Interaction for the Operation Room." In: *Journal of i-com (Zeitschrift für interaktive und kooperative Medien)*, 8(1), pp. 19–23 (cited on p. 71).

Penney, G. P., Blackall, J. M., Hamady, M. S., Sabharwal, T., Adam, A., and Hawkes, D. J. (2004). "Registration of freehand 3D ultrasound and magnetic resonance liver images." In: *Med Image Anal*, 8, pp. 81–91 (cited on p. 31).

Pescia, D., Paragios, N., and Chemouny, S. (2008). "Automatic detection of liver tumors." In: *ISBI*, pp. 672–675 (cited on p. 17).

Peterhans, M., Vom Berg, A., Dagon, B., Inderbitzin, D., Baur, C., Candinas, D., and Weber, S. (2010). "A navigation system for open liver surgery: Design, workflow and first clinical applications." In: *Int. J. Medical Robotics and Computer Assisted Surgery*, 7(1), pp. 7–16 (cited on pp. 25, 31, 33, 71, 87, 105, 132).

Preim, B., Bourqain, H., Selle, D., Peitgen, H.-O., and Oldhafer, K. (2002). "Resection Proposals for Oncologic Liver Surgery based on Vascular Territories." In: Proc. of the 17th International Symposium on Computer Assisted Radiology and Surgery (CARS). Elsevier, pp. 353–358 (cited on pp. 12, 21–23, 40, 47, 48, 60, 88).

Preim, B. and Bartz, D. (2007). *Visualization in Medicine. Theory, Algorithms, and Applications*. Morgan Kaufmann (cited on pp. 19, 33).

Pulitano, C., Castillo, F., Aldrighetti, L., Bodingbauer, M., Parks, R. W., Ferla, G., Wigmore, S. J., and Garden, O. J. (2010). "What defines 'cure' after liver resection for colorectal metastases? Results after 10 years of follow-up." In: *The Official Journal of the International Hepato Pancreato Biliary Association*, 12, pp. 244–249 (cited on p. 7).

Radtke, A., Nadalin, S., Sotiropoulos, G. C., Molmenti, E. P., Schroeder, T., Valentin-Gamazo, C., Lang, H., et al. (2007). "Computer-assisted operative planning in adult living donor liver transplantation: a new way to resolve the dilemma of the middle hepatic vein." In: *World J Surg*, 31, pp. 175–185 (cited on p. 21).

Reitinger, B., Bornik, A., Beichel, R., and Schmalstieg, D. (2006). "Liver surgery planning using virtual reality." In: *IEEE Computer Graphics and Applications*, 26(6), pp. 36–47 (cited on pp. 23, 70, 71).

Riechmann, M. (2006). "Visualisierungskonzept für die Projektorbasierte Erweiterte Realität in der Leberchirurgie." MA thesis. Institute for Process Control and Robotics, University of Karlsruhe, Germany (cited on pp. 35, 114).

Riechmann, M., Kahrs, L. A., Ulmer, C., Raczkowsky, J., Lamadé, W., and Wörn, H. (2006). "Visualisierungskonzept für die projektorbasierte Erweiterte Realität in der Leberchirurgie." In: *Proc. of Gemeinsame Jahrestagung der Deutschen, Österreichischen und Schweizerischen Gesellschaft für Biomedizinische Technik*, p. 209 (cited on p. 117).

Rieder, C., Ritter, F., Raspe, M., and Peitgen, H.-O (2008). "Interactive Visualization of Multimodal Volume Data for Neurosurgical Tumor Treatment." In: *Computer Graphics Forum (Special Issue on Eurographics Symposium on Visualization)*, 27(3), pp. 1055–1062 (cited on p. 39).

Rieder, C., Schwier, M., Weihusen, A., Zidowitz, S., and Peitgen, H.-O. (2009). "Visualization of Risk Structures for Interactive Planning of Image Guided Radiofrequency Ablation of Liver Tumors." In: *Medical Imaging 2009: Visualization, Image-Guided Procedures, and Modeling*. Vol. 7261. Proc. of the SPIE Medical Imaging, pp. 726134.1–726134.9 (cited on p. 39).

Rieder, C., Altrogge, I., Kröger, T., Zidowitz, S., and Preusser, T. (2010a). "Interactive Approximation of the Ablation Zone incorporating Heatsink Effects for Radiofrequency Ablation." In: *Proc. of 9th Annual Meeting of the German Society of Computer- and Robot-Assisted Surgery*, pp. 9–12 (cited on p. 39).

Rieder, C., Weihusen, A., Schumann, C., Zidowitz, S., and Peitgen, H.-O. (2010b). "Visual Support for Interactive Post-Interventional Assessment of Radiofrequency Ablation Therapy." In: *Computer Graphics Forum (Special Issue on Eurographics Symposium on Visualization)*, 29(3), pp. 1093–1102 (cited on p. 98).

Rieder, C., Palmer, S., Link, F., and K., Hahn H. (2011). "A Shader Framework for Rapid Prototyping of GPU-Based Volume Rendering." In: *Computer Graphics Forum (Special Issue on Eurographics Symposium on Visualization)*, 30(3), pp. 1031–1040 (cited on p. 43).

Ritter, F., Hindennach, M., Lamade, W., Oldhafer, K., and Peitgen, H.-O. (2005). "Intraoperative Adaptation of Preoperative Risk Analysis in Oncological Liver Surgery." In: *Proc. of the 4th Annual Meeting of the German Society of Computer- and Robot-Assisted Surgery* (cited on p. 70).

Ritter, F., Hansen, C., Dicken, V., Konrad, O., Preim, B., and Peitgen, H.-O. (2006). "Real-time illustration of vascular structures." In: *IEEE Visualization*, 12(5), pp. 877–884 (cited on pp. 114, 117, 119, 123).

Ritter, F., Hansen, C., Wilkens, K., Köhn, A., and Peitgen, HO (2009). "User Interfaces for Direct Interaction with 3D Planning Data in the Operation Room." In: *Journal of i-com (Zeitschrift für interaktive und kooperative Medien)*, 8(1), pp. 24–31 (cited on pp. 71, 94).

Ritter, F., Boskamp, T., Homeyer, A., Laue, H., Schwier, M., Link, F., and Peitgen, H. O. (2011). "Medical image analysis." In: *IEEE Pulse*, 2, pp. 60–70 (cited on pp. 108, 132).

Rusko, L. and Bekes, G. (2011). "Liver segmentation for contrast-enhanced MR images using partitioned probabilistic model." In: *Int J Comput Assist Radiol Surg*, 6, pp. 13–20 (cited on p. 16).

Salloum, C. and Castaing, D. (2008). "Surgical margin status in hepatectomy for liver tumors." In: *Bulletin du Cancer*, 95(12), pp. 1183–1191 (cited on pp. 38, 65).

Samset, E., Schmalstieg, D., Vander Sloten, J., Freudenthal, A., Declerck, J., Casciaro, S., Rideng, Ø., and Gersak, B. (2008). "Augmented reality in surgical procedures." In: *Proc. of SPIE Medical Imaging*. Vol. 6806, 68060K–1–12 (cited on pp. 34, 35).

Sanderson, P. M., Watson, M. O., and Russell, W. J. (2005). "Advanced patient monitoring displays: tools for continuous informing." In: *Anesth. Analg.* 101, pp. 161–168 (cited on p. 130).

Scheele, J., Stangl, and Altendorf-Hofmann, A. (1990). "Hepatic metastases from colorectal carcinoma: impact of surgical resection on the natural history." In: *Br J Surg*, 77(11), pp. 1241–1246 (cited on p. 7).

Schenk, A., Prause, G., and Peitgen, H.-O. (2000). "Efficient Semiautomatic Segmentation of 3D Objects in Medical Images." In: *Proc. of Medical Image Computing and Computer-Assisted Intervention (MICCAI)*, pp. 186–195 (cited on p. 16).

Schenk, A., Zidowitz, S., Bourquain, H., Hindennach, M., Hansen, C., Hahn, H. K., and Peitgen, H.-O. (2008). "Clinical relevance of model based computer-assisted diagnosis and therapy." In: *Proc. of SPIE Medical Imaging*. Vol. 6915, 691502_1–19 (cited on pp. 20, 47, 61).

Scheuering, M., Schenk, A., Schneider, A., Preim, B., and Greiner, G. (2003). "Intraoperative Augmented Reality for Minimally Invasive Liver Interventions." In: *Proc. of SPIE Medical Imaging*. Vol. 5029, pp. 407–417 (cited on pp. 35, 117).

Schlichting, S. (2008). "Konzeption und Entwicklung eines klinisch einsetzbaren Navigationsystem für die laparoskopische Leberchirurgie." PhD thesis. Institute for Medical Informatics, University of Lübeck, Germany (cited on pp. 71, 74, 82).

Schumann, C., Bieberstein, J., Trumm, C., Schmidt, D., Bruners, P., Niethammer, M., Hoffmann, R. T., Mahnken, A. H., Pereira, P. L., and Peitgen, H.-O. (2010). "Fast Automatic Path Proposal Computation for Hepatic Needle Placement." In: *Proc. of SPIE Medical Imaging*. Vol. 7625, 76251J–1 –76251J–10 (cited on pp. 23, 94).

Schwaiger, J., Markert, M., Seidl, B., Shevchenko, N., Doerfler, N., and Lueth, T. C. (2010). "Risk analysis for intraoperative liver surgery." In: *Proceeding of IEEE Eng Med Biol Soc*, 2010, pp. 410–413 (cited on p. 21).

Schwaiger, J., Markert, M., Shevchenko, N., and Lueth, T. C. (2011). "The effects of real-time image navigation in operative liver surgery." In: *Int J Comput Assist Radiol Surg* (cited on p. 126).

Schwier, M., Moltz, J. H., and Peitgen, H. O. (2011). "Object-based analysis of CT images for automatic detection and segmentation of hypodense liver lesions." In: *Int J Comput Assist Radiol Surg*, in press (cited on p. 17).

Selle, D. (1999). "Analyse von Gefäßstrukturen in medizinischen Schichtdatensätzen für die computergestützte Operationsplanung." PhD thesis. School of Mathematics and Computer Science, University of Bremen, Germany (cited on p. 19).

Selle, D., Preim, B., Schenk, A., and Peitgen, H.-O. (2002). "Analysis of vasculature for liver surgical planning." In: *IEEE Transactions on Medical Imaging*, 21(11), pp. 1344–1357 (cited on pp. 18–21, 40, 61, 63, 88).

Shah, A. J., Callaway, M., Thomas, M. G., and Finch-Jones, M. D. (2010). "Contrast-enhanced intraoperative ultrasound improves detection of liver metastases during surgery for primary colorectal cancer." In: *The Official Journal of the International Hepato Pancreato Biliary Association*, 12, pp. 181–187 (cited on pp. 2, 70).

Sielhorst, T., Bichlmeier, C., Heining, S. M., and Navab, N. (2006). "Depth perception–a major issue in medical AR: evaluation study by twenty surgeons." In: *Proc.*

of Medical Image Computing and Computer-Assisted Intervention (MICCAI), 9, pp. 364–372 (cited on p. 114).

Sietses, C., Meijerink, M. R., Meijer, S., and Tol, M. P. van den (2010). "The impact of intraoperative ultrasonography on the surgical treatment of patients with colorectal liver metastases." In: *Surg Endosc*, 24, pp. 1917–1922 (cited on pp. 2, 70).

Smeets, D., Loeckx, D., Stijnen, B., De Dobbelaer, B., Vandermeulen, D., and Suetens, P. (2010). "Semi-automatic level set segmentation of liver tumors combining a spiral-scanning technique with supervised fuzzy pixel classification." In: *Med Image Anal*, 14, pp. 13–20 (cited on p. 17).

Stawiaski, J., Decenciere, E., and F., Bidault (2008). *Interactive liver tumor segmentation using graph cuts and watershed, Workshop on 3D Segmentation in the Clinic: A Grand Challenge II. Liver Tumor Segmentation Challenge*. Liver Tumor Segmentation Challenge. MICCAI, New York, USA., Internet source: http://hdl.handle.net/10380/1416 (cited on p. 17).

Stockmann, M., Lock, J. F., Malinowski, M., Niehues, S. M., Seehofer, D., and Neuhaus, P. (2010). "The LiMAx test: a new liver function test for predicting postoperative outcome in liver surgery." In: *The Official Journal of the International Hepato Pancreato Biliary Association*, 12, pp. 139–146 (cited on pp. 20, 62).

Strähle, M., Ehlbeck, M., Prapavat, V., Kuck, K., Franz, F., and Meyer, J. U. (2007). "Towards a Service-Oriented Architecture for Interconnecting Medical Devices and Applications." In: *Proc. of Joint Workshop on High Confidence Medical Devices, Software, and Systems and Medical Device Plug-and-Play Interoperability*, pp. 153–155 (cited on p. 72).

Swan, P. J., Welsh, F. K., Chandrakumaran, K., and Rees, M. (2011). "Long-term survival following delayed presentation and resection of colorectal liver metastases." In: *Br J Surg* (cited on p. 7).

Termeer, M., Olivan Bescos, J., Breeuwer, M., Vilanova, A., Gerritsen, F., and Groller, E. (2007). "CoViCAD: comprehensive visualization of coronary artery disease." In: *IEEE Trans Vis Comput Graph*, 13, pp. 1632–1639 (cited on p. 98).

Thorn, M., Sonntag, S., Glombitza, G.-P., Lamadé, W., and Meinzer, H.-P. (1999). "Ein interaktives Tool für die Segmenteinteilung der Leber in der chirurgischen Operationsplanung." In: *Proc. of Bildverarbeitung für die Medizin*, pp. 155–159 (cited on p. 19).

Thorn, M. S. (2004). "Konzeption, Integration und Evaluierung unterstützender Softwaremodule in der konventionellen Chirurgie der Leber und Niere. Analyse von Gefäßstrukturen in medizinischen Schichtdatensätzen für die computergestützte Operationsplanung." PhD thesis. School of Medicine, Ruprecht-Karls-Universität Heidelberg, Germany (cited on pp. 23, 88).

Tietjen, C. (2009). "Illustrative Visualisierungstechniken zur Unterstützung der präoperativen Planung von chirurgischen Eingriffen." PhD thesis. Otto-von-Guericke University Magdeburg, School of Computer Science, Germany (cited on p. 116).

Tsuda, T., Yamamoto, H., Kameda, Y., and Ohta, Y. (2005). "Visualization methods for outdoor see-through vision." In: *Proc. of the Iinternational Conference on Augmented Tele-Existence*. ACM, pp. 62–69 (cited on p. 116).

Vetter, M., Hassenpflug, P., Cardenas, C., Thorn, M., Glombitza, G., and Meinzer, H. P. (2002). "Navigation in der Leberchirurgie - Ergebnisse einer Anforderungsanalyse." In: *Proc. of Bildverarbeitung für die Medizin*, pp. 49–53 (cited on p. 28).

Vetter, M., Wolf, I., Hassenpflug, P., Hastenteufel, M., Ludwig, R., Grenacher, L., Richter, G. M., Uhl, W., Büchler, M. W., and Meinzer, H. P. (2003). "Navigation aids and real-time deformation modeling for open liver surgery." In: *Proc. of SPIE Medical Imaging*. Vol. 5029, pp. 58–68 (cited on pp. 32, 141).

Vigano, L., Ferrero, A., Lo Tesoriere, R., and Capussotti, L. (2008). "Liver surgery for colorectal metastases: results after 10 years of follow-up. Long-term survivors, late recurrences, and prognostic role of morbidity." In: *Ann. Surg. Oncol.* 15, pp. 2458–2464 (cited on p. 7).

Walsh, M. and Crumbie, A. (2007). *Watson's Clinical Nursing and Related Sciences*. 7th ed. Bailliere Tindall, USA (cited on p. 7).

Wee, A. N. and Sanderson, P. M. (2008). "Are melodic medical equipment alarms easily learned?" In: *Anesth. Analg.* 106, pp. 501–508 (cited on p. 130).

Wegner, C. M. and Karron, D. B. (1997). "Surgical navigation using audio feedback." In: *Stud Health Technol Inform*, 39, pp. 450–458 (cited on p. 130).

Wegner, K. (1998). "Surgical navigation system and method using audio feedback." In: British Computer Society (cited on pp. 130, 141).

Wein, W., Khamene, A., Clevert, D.-A., Kutter, O., and Navab, N. (2007). "Simulation and fully automatic multimodal registration of medical ultrasound." In: *Medical Image Computing and Computer-Assisted Intervention (MICCAI)*, 10(Pt 1), pp. 136–143 (cited on p. 31).

Wein, W., Kutter, O., Aichert, A., Zikic, D., Kamen, A., and Navab, N. (2010). "Automatic non-linear mapping of pre-procedure CT volumes to 3D ultrasound." In: *Proc. IEEE International Symposium on Biomedical Imaging*, pp. 1225 –1228 (cited on p. 31).

Welter, S., Stöcker, C., Dicken, V., Kühl, H., Kraß, S., and Stamatis, G. (2011). "Lung segment geometry study: Simulation of largest possible tumours that fit into bronchopulmonary segments." In: *The Thoracic and Cardiovascular Surgeon)*, in press (cited on p. 39).

Wendt, N. (2011). *Based on an oral discussion with Dr. Nicholas Wendt, St. Josef Hospital, Bremen, Germany* (cited on p. 8).

Wieferich, J. (2008). "Visualisierungskonzept zur intraopertiven Unterstützung in der Leberchirurgie." MA thesis. Department of Computer Science, University of Applied Sciences Bremen, Germany (cited on p. 127).

WiiMote API (2011). Internet source: code.google.com/p/wiimote-api/, visited: 2011, October 15 (cited on p. 80).

Wildi, S. M., Gubler, C., Hany, T., Petrowsky, H., Clavien, P. A., Jochum, W., Gerlach, T., Fried, M., and Mullhaupt, B. (2008). "Intraoperative sonography in

patients with colorectal cancer and resectable liver metastases on preoperative FDG-PET-CT." In: *J Clin Ultrasound*, 36, pp. 20–26 (cited on p. 70).

Willems, P. W., Noordmans, H. J., Overbeeke, J. J. van, Viergever, M. A., Tulleken, C. A., and Sprenkel, J. W. van der (2005). "The impact of auditory feedback on neuronavigation." In: *Acta Neurochir*, 147, pp. 167–173 (cited on p. 131).

Wimmer, A., Soza, G., and Hornegger, J. (2009). "A generic probabilistic active shape model for organ segmentation." In: *Proc. of Medical Image Computing and Computer-Assisted Intervention (MICCAI)*, 12, pp. 26–33 (cited on p. 16).

Woerdeman, P. A., Willems, P. W. A., Noordmans, H. J., and Sprenkel, J. W. B. van der (2009). "Auditory feedback during frameless image-guided surgery in a phantom model and initial clinical experience." In: *J Neurosurg*, 110, pp. 157–262 (cited on pp. 131, 141).

Yamada, A., Hara, T., Li, F., Fujinaga, Y., Ueda, K., Kadoya, M., and Doi, K. (2011). "Quantitative evaluation of liver function with use of gadoxetate disodium-enhanced MR imaging." In: *Radiology*, 260, pp. 727–733 (cited on p. 62).

Yao, J., Chowdhury, A. S., Aman, J., and Summers, R. M. (2010). "Reversible projection technique for colon unfolding." In: *IEEE Trans Biomed Eng*, 57, pp. 2861–2869 (cited on p. 97).

Zacherl, J., Scheuba, C., Imhof, M., Zacherl, M., Langle, F., Pokieser, P., Wrba, F., et al. (2002). "Current value of intraoperative sonography during surgery for hepatic neoplasms." In: *World J Surg*, 26, pp. 550–554 (cited on p. 70).

Zachow, S., Hahn, H., and Lange, T. (2010). "Computerassistierte Chirurgieplanung." In: *Computerassistierte Chirurgie*. Urban & Fischer Verlag, pp. 119–149 (cited on pp. 14, 69).

Zeng, W., Marino, J., Kaufman, A., and Gu, X. D. (2011). "Volumetric Colon Wall Unfolding Using Harmonic Differentials." In: *Comput Graph*, 35, pp. 726–732 (cited on p. 97).

Zhou, J. Y., Wong, D. W., Ding, F., Venkatesh, S. K., Tian, Q., Qi, Y. Y., Xiong, W., Liu, J. J., and Leow, W. K. (2010). "Liver tumour segmentation using contrast-enhanced multi-detector CT data: performance benchmarking of three semiautomated methods." In: *Eur Radiol*, 20, pp. 1738–1748 (cited on p. 17).